CONFERENCE ON ARTIFICIAL SATELLITES

PART B

VIRGINIA POLYTECHNIC INSTITUTE
BLACKSBURG, VIRGINIA

AUGUST 1963

BULLETIN

OF THE

VIRGINIA POLYTECHNIC

INSTITUTE

Engineering Experiment Station Series No. 156

(In three parts: A, B, C)

PART B

PROCEEDINGS OF THE CONFERENCE

ON ARTIFICIAL SATELLITES

August 12 through August 16, 1963

Supported by a Grant
from the
NATIONAL SCIENCE FOUNDATION

and

Cosponsored by the
LANGLEY RESEARCH CENTER

of the

NATIONAL AERONAUTICS AND SPACE
ADMINISTRATION

TABLE OF CONTENTS

PART B

SOLAR SPACE ENVIRONMENT

METEOROLOGICAL AND COMMUNICATION SATELLITES

SOLAR SPACE ENVIRONMENT

THE ORBITING ASTRONOMICAL OBSERVATORY AND THE ORBITING SOLAR OBSERVATORY

BY

NANCY G. ROMAN

NATIONAL AERONAUTICS AND SPACE ADMINISTRATION

WASHINGTON, D. C.

THE ORBITING ASTRONOMICAL OBSERVATORY AND THE ORBITING SOLAR OBSERVATORY

by

Nancy G. Roman

National Aeronautics and Space Administration

The Orbiting Astronomical and the Orbiting Solar Observatories are designed to permit astronomers to observe the sun, planets, stars, and galaxies from outside the disturbing influences of the earth's atmosphere. To understand why such observations are important, let us review the ways in which the atmosphere hinders our observations.

The first slide gives a schematic map of the transmission of the atmosphere. You notice the large and clear radio window which has been so important to astronomy in the past two decades, and the much smaller and less clear window through which the wave lengths to which our eyes are sensitive are transmitted and in which all observations of astronomical bodies have been made until recently. As you see, much of the atmosphere is completely opaque, but this does not mean that astronomical objects are not interesting to study in these regions of the atmosphere. Not only are some objects brighter in the ultraviolet or the infrared regions of the spectrum, but even those objects which can be studied in the normal visual or photographic region present a changed appearance when observed in other wave length regions.

The second slide shows three photographs of the surface of the sun. The first is a so-called "White light" picture which shows the sun as one would see it if he projected its image on a moderately active day on a piece of white cardboard. The next picture is taken in the light of the hydrogen-alpha line in the red region of the spectrum. The third picture is taken in the light of the resonance line of ionized calcium in the violet region of the spectrum. As you can see, the sun of each of these pictures presents a strikingly different appearance. Actually, in going from the first picture to the third, you are observing the sun at increasingly higher levels in the atmosphere. By going into the ultraviolet it is possible to study the sun at still higher levels and, thus, to build up a three dimensional picture of the sun and particularly of solar activity.

The third slide illustrates another reason for observing the sun from beyond the earth's atmosphere. This picture of a sunspot was taken with the Stratoscope I telescope, a twelve-inch telescope carried above most of the disturbing effects of the atmosphere. You can see the enormous amount of detail, not only in the sunspot itself, but also in the mottled background. Only once or twice since the sun has been observed photographically has detail as clear as this ever been obtained from the surface of the ground. The use of balloons and satellites will make it possible to obtain such detail on a routine basis

The fourth slide illustrates the third disturbing influence of the atmosphere. This is a picture of the sun taken during a solar eclipse at a time when the moon hides most of the sun and allows us to study the corona or outer atmosphere of the sun. At other times the bright light from the portion of the sun which the moon now covers is so

scattered by the atmospher of the earth that it is impossible to observe this outer atmosphere. In the Orbiting Solar Observatory to be launched later this year we are flying a coronograph--an instrument specially designed to produce an artificial eclipse of the sun. A disk blocks the light from the body of the sun just as the moon blocks the light of the earth and permits us to explore, on a day-to-day basis, the outer atmosphere of the sun which has previously been observable only during solar eclipses. This experiment is being prepared by the Naval Research Laboratory.

So much for why we wish to study the sun. The next question is how do we go about it. To do this we have designed the Orbiting Solar Observatory. This satellite consists of three major portions: a wheel which rotates at the rate of thirty revolutions per minute to provide a gyroscopic stabilization to the satellite; a sail which is driven against the wheel so that it is always pointed at the sun; and two instrument compartments, each eight by four by thirty-two inches in size, which are rotated with the sail and can be moved in elevation a short distance to point to the sun with an accuracy of approximately two minutes of arc. The axis of rotation of the satellite is maintained perpendicular to the sun by means of gas jets and thus it is possible for the solar cell from the sail always to see the sun with nearly maximum efficiency. The wheel of the satellite contains additional experiments so that, in all, approximately 150 pounds of experiments can be carried on this 450 pound spacecraft.

Slides six and seven show the spacecraft under construction. In the first of these the arms holding the gas bottles are folded down as they are during launch so that they fit around the top of the third stage of the Delta launch vehicle and within the Delta

shroud. The next slide shows the spacecraft from the top while under construction. In it you can see the construction not only of the solar sail but also of the instrument section in the wheel.

After the satellite is launched it goes through the sequence illustrated in slide eight. The rocket's third stage is spun for stabilization and thus, when the shroud and the booster are ejected, the Orbiting Solar Observatory itself is also spinning. The arms containing the nitrogen bottles are then extended, slowing the spin rate appreciably and gas jets are used to slow the spin rate down to 30 rpm. Solar sensors and gas jets are then used to point the axis of rotation of the satellite to a direction perpendicular to the sun and the solar sail and instrument section to the sun itself. The observatory is then ready to operate. An indication of the accuracy with which the pointing was maintained on the first of the Orbiting Solar Observatories is illustrated in slide nine.

The first of the Orbiting Solar Observatories contained a number of instruments. Of particular interest are the results obtained with an x-ray spectrometer—one of the instruments in the pointed section and the most sophisticated of the instruments carried by the satellite. This x-ray spectrometer was built by the Solar Physics Branch of the Goddard Space Flight Center. The entrance slit allows the light from the sun to fall on a grazing incidence grating which forms a spectral image along the Rowland circle. Also on the Rowland circle an exit slit allows the light from a narrow spectral region to fall on an open window photomultiplier. By means of a chain drive, the exit slit and photocell together are moved back and forth along the Rowland circle to scan the spectrum. With this instrument, it was possible to study the solar spectrum, in a number

of wave lengths, the behavior of two of which is illustrated in slide eleven, together with the behavior of some more of the more common indices of solar activity. These are the Zurich sunspot numbers, the area of the calcium plage regions; that is, the regions that were bright in the light of the ionized calcium line, and the emission of the sun in the high frequency radio region. As you see, the lines of the highly ionized iron follow the behavior of the more common solar activity indices quite well. Notice, however, that the brightness of the regions in the iron 15 line holds up from cycle to cycle while the calcium plage area decreases. A similar effect is observed at the birth of such active regions. In the early stages they are brighter in the calcium line than they are in the iron line relative to their strength later in the cycle. Thus it appears that higher in the atmosphere, where the iron lines are formed, the intensity of the activity somewhat lags behind that farther in.

Other interesting results were also obtained by GSFC by means of an x-ray ion chamber. In slide twelve we see illustrations of the intensity observed with these chambers. It is to be noted that during solar activity not only is the total intensity of the x-ray emission higher but there are marked changes in this intensity during very short intervals of time. Another interesting observation in the x-ray region is that small micro-flares seemed to occur in series with increasing or decreasing strength and with a predictable relation between both the intensity and the time lag of each succeeding flare. If this holds up during further information, it will be the first time that we have been successfully able to predict any facet of flare activity.

We will continue to use the Orbiting Solar Observatory type of satellites for some time for a number of observations of the sun and related activity. However, it is not

the ideal solar observatory. For that we would like to have a spacecraft which can carry an instrument with a much longer optical path. Such instruments are needed for high resolution spectrographs and high resolution images. To make use of the imaging possibilities we should have accurate pointing and the ability to scan both the entire sun and small areas of the sun. Further, we should have the storage capacity to store the information obtained from the high resolution images and from the scans. Finally, we would like to get away from the present situation where almost two-thirds of the scientific payload is located in the wheel and sees the sun only briefly once every two seconds.

Slide 14 illustrates the need of higher pointing accuracy. Although the picture of the sun is schematic, the size of the features is approximately correct. The larger square illustrates the pointing accuracy of the present Orbiting Solar Observatory. The small square represents the pointing accuracy of an improved version for which we are now undertaking design studies. Preliminary thoughts on such an instrument are illustrated in slide 15. The spacecraft will be approximately 8 to 10 feet long and will contain instruments up to about 13 inches in diameter. These instruments can be pointed anywhere within 10 solar radii and scan either the entire solar image or a small region on the surface of the sun or in the solar corona. Design studies for this satellite are presently being conducted by Republic Aviation. We hope to have the Advanced Orbiting Solar Observatory in orbit in time to study the next solar maximum.

So much for the sun, our reasons for studying, and the spacecraft which we intend to use for this purpose.

We are also interested in studying the stars and other celestial objects from beyond the disturbing atmosphere of the earth. Slide 16 illustrates the Orion nebula, with which I am sure you are all familiar. In this region we see several of the reasons for studying the universe in other wave lengths. The dark area is due to the absorption by interstellar dust which becomes increasingly transparent as we move to the red and infrared region of the spectrum. The bright region is emission nebulosity, excited by the light of the very hot stars in this region. Not only should this emission itself be more easily studied in lines in the presently inaccessible region of the spectrum, but the hot stars illuminating it have most of their emission energy in this spectrum region. Thus, to understand the processes in the nebula itself, we must extrapolate from the relatively faint red tail of the stellar energy distribution to predict the energy exciting the nebulosity. Preliminary results from our early rocket flights indicate that the extrapolations we have made in the past are in error. Extensive observations from both rockets and satellites will be needed to learn the true nature of this energy distribution. Finally, in this region of space, there are apparently stars which are forming, probably from the interstellar dust. These stars should be very red objects early in their lifetimes and thus most readily visible in the presently inaccessible infrared region of the spectrum.

Slide 17 shows the Crab Nebula. You see here sharp red filaments in a general green background glow. The red is the emission of highly ionized forms of well-known atoms. The green light is highly polarized and has been attributed to the synchroton radiation from high velocity electrons moving in a magnetic field. This object is exceedingly bright in a radio region also and it has been proposed that it is the source of

cosmic rays, in which case it should be bright in the gamma ray region; the synchroton radiation may well be bright in the x-ray region. Again, observations from the surface of the earth are impossible and are presently sadly lacking.

Another interesting possibility in the study of astronomical objects from beyond the atmosphere is illustrated in slide 18, which shows the well-known red shift of galaxies. The spectrum of the distant galaxies is shifted to the red by increasingly greater amounts at greater distances. Thus, the region of the nearby galaxies which we can study easily is in the spectra of the most distant galaxies and is shifted to the red where photographic plates and other detectors are insensitive. Conversely, that portion of the spectra of the distant galaxies which can be observed easily is in the inaccessible ultraviolet in the nearby galaxies. Observations from satellite telescopes will permit us for the first time to compare nearby and distant galaxies and thus to determine whether the universe as a whole has aged since its creation.

To answer questions such as those I have raised we have designed an Orbiting Astronomical Observatory, as shown here in slide 19. As the name implies, this spacecraft has been designed to make a large variety of astronomical observations and to carry a variety of astronomical instruments in different versions of the same basic structure. Experiments for three of these have already been selected. The first satellite will carry two major experiments --four 12" telescopes to map the sky in the ultraviolet. The second Orbiting Astronomical Observatory will have a 36" mirror feeding light into a spectrograph for moderate dispersion studies of stars and nebulae. The third spacecraft will also contain a telescope and spectrograph for ultraviolet studies. However, the mirror will

be only 32" in diameter and much higher dispersion will be used to permit the study of the narrow, weak interstellar absorption lines.

Slide 20 shows the construction of the spacecraft. An inner tube 40" in diameter contains the basic optical system. Around the outside of this tube which is well-insulated from the remainder of the spacecraft, is a series of bays holding the spacecraft equipment and those portions of the scientific equipment which do not need to be in the optical section of the spacecraft. Heat produced by electronics will be radiated to space through the outer shell of the spacecraft which is not illustrated on this slide.

After the telescope is in orbit, it will determine its direction by means of six star trackers which can track any star brighter than second magnitude. Before these star trackers can pick up the stars on which they point, however, the spacecraft must go through a series of maneuvers which are illustrated on slide 21. Immediately after launch, the solar paddles will be extended. Rate gyros will command gas jets to obtain the preliminary stabilization of the satellite. It will be permitted to roll until the solar sensor picks up the sun. Then gas jets will be used to point the solar sensors to the sun and to roll the observatory around the satellite sun line. Incidentally, the slide is incorrect; sunlight will not be permitted to enter the main tube of the observatory during this maneuver. On the contrary, if this happens, it may well permanently damage the delicate and sensitive equipment designed for nighttime operation. The observatory will rotate around the earth's sun line until the star trackers which have been preset to specific angles pick three stars on which they can track. The observatory will then be entirely oriented. When we wish to go to a new object, the star trackers will be told

to move to new gimbal angles. The command will be given to the coarse inertia wheel to move the satellite so that the star trackers pick up tracking stars in these new positions. The star trackers themselves actuate the fine inertia wheels which provide pointing to about one minute of arc. If still more accurate pointing is necessary, an error signal will be obtained from the primary experiment. Equipment is being designed to provide tracking up to a tenth of a second of accuracy.

As I have implied, pointing of the telescope will be under ground command. The astronomer will state the right ascension and declination of the object or objects he wishes to study. This information will be fed into a computing machine together with the current status of the observatory and the machine will tell both whether it is possible to go to this right ascension and declination without coming too close to the sun or making any other illegal maneuvers and, if so, will tell the satellite operator the commands which should be given to the satellite to send it to the new position. All of this programming will be done through the tracking station which NASA is erecting in Rosman, North Carolina. The computer and primary control station will be at the GSFC. At the other tracking stations, Quito and Santiago, it will be possible to receive information from the satellite, both from stored data and from the real-time system. It will not, however, be possible to program the satellite other than for diagnostic operations. It is possible to store commands in the satellite to tell it to go to a new position and/or perform new operations at any minute during the orbit, whether or not it is in sight of a ground station at that time.

The next set of slides illustrates the instrumental layout of the first three satellites. In slide 22 we see the four vidicon cameras of the Smithsonian to be used to map the sky between Lyman-alpha and 3000 A, and the mirrors for the photometers to be used by the University of Wisconsin. A 16" mirror is used for nebulae with a wider acceptance angle, because, in general, the nebulae will be fainter than stars. In addition to the five nebular cameras, there are two objective grating spectrometers to obtain low resolution objective grating spectra of the brighter stars which the satellite scans. Slightly more detail of the Smithsonian camera is given in slide 23.

Slide 24 shows the layout of the GSFC experiment on the second Orbiting Astronomical Observatory. By tilting the grating, the spectrum of the star is scanned across six photocells. The rate of the scan and the size of the entrance slit can both be altered to provide resolutions ranging from 2 A to 64 A.

It is hoped with this instrument to be able to reach stars as faint as 11th magnitude.

The third instrument is illustrated in slide 25. In this case, the photocell will be moved along the Rowland circle to provide the spectral scan. A second photocell will be used to monitor the total light coming through the slit and allow for any inaccuracies in guidance. Two detectors can be used to provide different resolutions in the spectra. It will be possible not only to scan the entire spectrum but also to spend the observing time scanning individual lines in detail.

So far experiments for only three of the Orbiting Astronomical Observatories have been selected but it is fully expected that the series will continue. In addition to further observations in the ultraviolet it will be desirable to observe objects in the

infrared, to observe them with high resolution, and to study them in the x-ray and gamma-ray region of the spectrum. The importance of the latter observations are illustrated in slide 26, where we see a 200" photograph of the radio souce, Cygnas A. Even with the best of our terrestrial telescopes, image is blurred. High resolution photographs obtained outside the atmosphere of this object would be very interesting. In addition, we would expect this object to be a major emitter of both x-rays and gamma rays. Only time will tell whether this is the case.

SOLAR AND STELLAR RADIATIONS ABOVE THE EARTH'S ATMOSPHERE

BY

TALBOT A. CHUBB

E. O. HULBURT CENTER FOR SPACE RESEARCH

U. S. NAVAL RESEARCH LABORATORY

WASHINGTON, D. C.

SOLAR AND STELLAR RADIATIONS ABOVE THE EARTH'S ATMOSPHERE

by

Talbot A. Chubb

U. S. Naval Research Laboratory

During the past 15 years considerable new knowledge has been gained concerning solar and stellar radiations striking the earth's atmosphere. This new knowledge has come from a series of rocket and satellite experiments designed to measure ultraviolet and x-ray radiations unable to penetrate the air ocean in which we live. This paper summarizes some of this new knowledge and explains how the measured radiation fluxes confirm and add to our conception of the nature of the sun and stars.

The early rocket radiation studies were concerned only with the sun. A photograph of the sun is shown in Figure 1. This photograph was made in white light. It shows us a disk image of the only star close enough to show up as anything other than a dimensionless point in space. Let us now ask ourselves what such a photograph really means. From how deep below the surface of the sun does the light we observe come? Why does the sun appear slightly darker near its edge than at its center?

These questions can be answered if we pause a moment to consider what the sun really is. The sun is essentially nothing more than a giant nuclear furnace, in which the inner fires are protected from the frigid cold of space

by extensive blanketing layers of protective gas. Heat energy flows steadily upward out of the intensely hot core. It flows through the blanketing gas layers, and finally it bursts forth into space. When we look at the sun our vision penetrates only into high-up levels of the insulating gas. The depth of our vision is determined by the amount of haziness or absorption that is present in the solar gas. For all practical purposes we look down into the sun to the same depth that an observer in the sun would be able to see out.

We can now answer the question as to why the sun looks darker at the solar limb. The answer is this: We see less deeply into the sun when we look near the limb, than we do when we look at the disk's center. Consider our imaginary observer inside the sun. An observer in the sun looking at earth would have to position himself higher in the sun's atmosphere if he were near the solar limb, since he would be looking out horizontally through the solar haze. Since heat flows from a hotter to a cooler object, and since heat is flowing outward through the sun's atmosphere, this higher layer should be cooler, and since cooler objects appear darker than hot objects, we have a good explanation of solar limb darkening.

Looking near the edge of the solar disk is not the only way of viewing the higher layers of the solar blanket. We have another way of varying our depth of vision. We can look at the sun in colors of light that are absorbed much more strongly by the solar gas than visible light. If we look at the sun in ultraviolet radiation below 3000 Å, we find that the sun looks like a much cooler incandescent ball than it does in the visible. In Figure 2,

we show how the brightness of the ultraviolet sun compares with incandescent objects of various temperatures. Seen in ultraviolet light of 2000 Å wavelength, the sun looks like an object at a temperature of 5000 degrees K. In contrast the sun seen in the visible appears like an object at roughly 6000 degrees K. Fluctuations in solar brightness temperature reflect fluctuations in absorption coefficient as one proceeds to shorter wavelength.

The spectral energy distribution shown in Figure 2 was measured from rockets. Radiation of wavelengths less than 3000 Å cannot penetrate the earth's atmosphere. Between 2000 Å and 3000 Å ozone in the upper stratosphere is opaque to incident radiation; below 2000 Å molecular oxygen itself becomes a strong absorber. Hence rocket or satellite vehicles provide the only means of obtaining information about the shorter wavelengths.

A photographic spectrum of the sun at still shorter wavelengths is shown in Figure 3. In this portion of the spectrum, the solar emission curve no longer resembles the continuum character of emission seen in the visible and near ultraviolet. Instead Figure 3 shows us a very peculiar phenomenon. The very wavelengths for which solar material is most absorbent and which must, therefore, come from the highest levels, stand out as bright emission lines. This emission line spectrum is characteristic of the topmost levels of the sun. The existence of such emission lines means that the topmost levels of the sun are actually hotter than the levels underneath, despite the outward flow of radiant heat. Such a condition is possible only because the fringing levels are so transparent to visible light that the enormous outflow of light energy from deeper layers passes through them without absorption.

Most of the bright emission lines shown in Figure 3 are formed in a thin layer called the solar chromosphere. This thin colored layer can be seen briefly at the start and end of a total solar eclipse. It is a region in which temperature increases with altitude. It is too transparent to be considered as part of the sun's gas insulation. Moreover it contributes only about one part in one hundred thousand parts to the outward flow of radiant energy from the sun. Actually, however, this small amount of radiant energy is of very considerable importance to us on earth. It is the only energy capable of ionizing gases in the earth's atmosphere. Combined with the weak short wavelength portion of the photospheric continuum, it is responsible for both the heating and chemical changes occurring in the upper part of the earth's atmosphere. From a scientific point of view this short wave energy is important in that it can tell us much about the outer layers of the sun. In particular it provides a tool for studying phenomena associated with solar activity, the main manifestations of which are confined to the chromospheric layer described and to the sun's corona still higher up.

Let us consider some of the details shown in Figure 3. The strongest feature in the spectrum is the Lyman Alpha line of hydrogen. Lyman Alpha is the emission produced by atomic hydrogen when it changes from its lowest excited state to its ground state. The Lyman Alpha line is greatly over-exposed in the photograph. It is by far the most intense feature in the chromospheric spectrum. The continuum emission near Lyman Alpha is not photospheric continuum; instead it is radiation arising in the wings of the Lyman Alpha line. The dark bands crossing the spectrum are instrumental in

origin; they are caused by water vapor absorption occurring in the spectrographic instrument. The continuum present below 912 Å is the recombination Lyman continuum of atomic hydrogen gas.

By spectrographic techniques it is possible to photograph the sun in Lyman Alpha light. Such a photograph is shown in Figure 4. The image of the sun in Lyman Alpha is very similar to the solar images seen in Calcium K light as shown in Dr. Roman's paper. The Lyman Alpha photograph shows the splotchy character of the photospheric surface. The bright areas are known as plages. They are a very sensitive feature of solar acitvity, and show up on the sun before sunspot groups are seen, and persist after spots have disappeared.

Images of the solar disk can also be made in solar emission lines other than Lyman Alpha. Figure 5 shows focused images of a slice across the center of the sun. In each slice one can see individual plage regions. Slice images of this type promise to tell us information concerning the excitation character of the individual emission lines. Solar emission lines appear to differ in at least two ways. One way in which they differ is in the relative brightness of the resultant solar image at the limb of the sun as compared to the brightness at the center of the disk. For example, two of the images shown in Figure 5 are distinctly brighter at the limb than they are at the center of the disk. This behavior is called limb brightening. These two lines are emitted by oxygen atoms that have lost five electrons. Such oxygen ions are called O^{VI} ions.

The second way in which solar emission lines differ is in their relative brightness in plage regions as compared to their brightness in other parts of

the solar disk. Some lines come almost exclusively from plages. Figure 6 shows some faint and in some cases overlapping circular disk images of the sun which were obtained in the 300 Å region of the far ultraviolet. The darkest disk image is that produced by the 304 Å line emission of ionized helium. This image seems fairly normal as regards plage-disk brightness ratio. On each side of the 304 Å image, and partially overlapping it are two solar images formed in light from Fe^{XV} and Fe^{XVI} ions. These images are hard to spot, because they do not show the circular disk pattern of the sun. Instead the image consists only of five or six bright patches, corresponding to the main emitting plages on the sun. Interestingly these Fe^{XV} and Fe^{XVI} radiations and also the 304 Å helium radiation have been monitored from the OSO-A Satellite. The iron lines showed a high relative variability in contrast to the rather stable helium emission, suggesting the expected relationship that large plage to disk brightness ratio implies a strong time variation with solar activity conditions.

Solar emission lines have been photographed using grating spectrograph techniques well down into the x-ray portion of the spectrum. Figure 7 shows a photographic spectrum which extends at the left down to 44 A. The bright group of lines at the center are a largely unidentified group of lines located at about 170 A. The solar spectrum appears to show a very large drop in intensity below 170 A. It is not known for certain whether this drop is really a characteristic of the sun. The presence of x-ray lines around 50 A is also quite interesting. It indicates that very likely most of the sun's x-ray emission is line emission rather than continuum.

In addition to the ultraviolet photographs of the sun's upper layers, it has been found possible to obtain solar images using the sun's x-ray emission as the source of exposure. These photographs have not been of the same quality as the ultraviolet images, mainly because the long exposure time required has resulted in motion of the camera during image build-up. The x-ray photographs were obtained by mounting the camera on a rocket-borne solar pointing control. The pointing control has succeeded in keeping the camera accurately pointed at the sun; however, in accomplishing this feat it has rotated the camera back and forth during exposure. One of the resultant images is shown in Figure 8. It can be seen that the plage emission regions have been smeared into exposure arcs. It is nevertheless clear that the bulk of the x-ray emission comes from the plage areas. The camera, incidentally, was actually a pin-hole camera. It differed from a true pin-hole camera only in that the small aperture admitting the desired radiation was covered with a thin film which blocked visible and ultraviolet light, but transmitted soft x-ray radiation.

At wavelengths below 25 A, non-photographic techniques become important tools for studying the detailed character of the solar emission spectrum. One device that has been effective in defining the solar x-ray spectrum is the Bragg crystal diffraction spectrometer. Using this device, the solar spectrum was mapped for the first time in the 13-25 A region during the summer of 1963. The wavelengths of about a dozen lines were identified. It was also found possible to learn something about the plage-disk character of the x-ray lines. As we expected, most of the lines came predominantly from the single dominant plage on the sun at the time of the experiment. However, surprisingly there were also several lines which were not so plage dominant; in particular, emission

lines appearing to arise from O^{VII}.

As we have mentioned, some solar emission lines show a significant intensity variation with time. This variability is in distinct contrast to the great stability of the sun as an energy source in the visible portion of the spectrum. The variability encountered in the solar emission spectrum at short wavelengths has been studied for over a decade. Shortly after the start of these studies it became apparent that intensity fluctuations were much more severe in the short wavelength portion of the x-ray spectrum that at longer wavelengths. Figure 9 shows the approximate shape of the solar x-ray emission spectrum at various times during the solar sun spot cycle and during quiet sun and flare sun activity conditions. When sun spots become numerous on the sun, solar x-ray emission becomes much more intense. Comparing the quiet sun emission at sun spot maximum to sun spot minimum emission we see that the solar cycle variation in x-ray emission is of the order of a factor of five at 50 A, eighty at 15 A and three hundred at 8 A. Superposed on this fluctuation is a large increase of emission at shorter wavelengths during solar flares, accompanied with an extension of solar emission to considerably shorter wavelengths than those normally present.

The contrast between the high variability in solar emission at short x-ray wavelengths as compared with the relative constancy of solar ultraviolet emission is strikingly shown in a study of flare activity made from the first successful Solar Radiation Satellite. A portion of the data obtained by this satellite is shown in Figure 10. The figure shows the time variation in solar Lyman emission and in 2-8 A solar x-ray emission during the development of

a small limb flare. Figure 11 is a photographic sequence showing the flare responsible for the radiation outburst. The top curve in Figure 8 shows the response of the ultraviolet ion chamber within the satellite. This detector indicated that total solar Lyman α emission was almost constant during the development of the flare, amounting to possibly a 5% intensity increase. In contrast the second curve shows the very large increase that occurred in solar x-ray output during the event. The 2-8 A x-ray flux increased a factor of five during the two minute period accompanying the most rapid period of flare growth. This x-ray burst was accompanied by a short-lived radio fadeout and other ionospheric disturbances. The event gives a clear demonstration of the important effects sometimes produced in the earth's upper atmosphere by relatively modest solar activity.

A summary of solar events for which x-ray increases were recorded during the SR-1 satellite is shown in Figure 12. X-ray increases were recorded during twelve important disk flares. In each case for which the x-ray flux below 8 A exceeded 2×10^{-3} erg cm^{-2} sec^{-1} of energy, the earth was subjected to a coincident ionospheric disturbance resulting in shortwave fadeout. When the x-ray flux was less, the ionospheric disturbance was either not noticed, or was significantly less severe. The conclusion that solar x-rays were responsible for the radio fadeouts is quite clear. The most interesting result demonstrated by the data, however, is the occurrence of strong x-ray fluxes which did not arise from major disk flares. Two very low class limb flares had strong x-ray emission with accompanying shortwave fadeout. In addition strong x-ray emission accompanied three limb activity events which were not classed as flares at all.

The strikingly similarity in character of the x-ray burst accompanying the limb events and those accompanying important disk flares is strongly suggestive of the equivalence of the two very different appearing phenomena. This similarity constitutes the best present evidence that small limb flares, bright surges on the limb and active prominences are the high altitude portions or effects of major disk flares.

Although it has been the custom of the NRL group to describe solar x-ray emission as a diluted blackbody emission, it has always been recognized that this was merely a very approximate way of describing a complex spectrum. In reality solar x-ray emission at wavelengths longer than 1 A is believed to be made up mainly of a series of emission lines. The relative intensity of these emission lines reflect the relative abundance of elements in the solar corona and the distribution of electron temperatures describing the energy spectrum of coronal electrons. The shortest wavelength x-ray lines expected in the solar emission spectrum are the iron line emissions occurring between 1 and 2 A. All the chemical elements occurring in the sun that have an abundance at all comparable to the abundance of iron atoms are very much lighter than iron, and emit x-ray lines only at much longer wavelength. Because iron has the unique set of characteristics that it is both abundant and heavy, iron x-ray emissions can be expected to play a major role in solar emission from the very hot regions produced during the solar flares. For this reason, and also because iron x-rays penetrate deeply enough into the earth's atmosphere to cause major radio wave absorption, it is especially interesting to look for evidence of such emission during flares.

Evidence for the presence of iron line emission was obtained from proportional counter data obtained in 1959. From the distribution of pulse amplitudes produced by the proportional counters, three crude x-ray spectra of the sun were obtained between 0.7 and 6 A. These three spectra were recorded during supposedly quiet solar conditions; however, some form of microflare or other solar activity was almost continuously present during the summer of 1959, which was during the sun spot maximum period. The results of three flights are shown in Figure 13. One flight showed an energy spectrum distribution compatible with the concept of dilute blackbody radiation from regions of varying temperature. Two flights, however, showed an emission spectrum peaking in x-ray emission in the 1.1 A region. This wavelength does not correspond to the known wavelengths of the iron lines. However, it seems difficult to explain the occurrence of the emission peaking other than by the assumption that iron line radiation was present and that the calibration of the pulse amplitude spectrometer was slightly in error.

Probably the most important wavelengths to study in order to determine the physical processes occurring during solar flares are the shortest wavelengths. These shortest wavelength photons are x-rays in the 20 to 100 kev medical x-ray region. They can only be produced in the most highly excited regions of a solar flare. The total amount of emission from the sun in the medical x-ray region is quite small, containing much less energy than is present in the x-ray line spectrum at longer wavelengths. Emission in the 20 to 100 kev region is due to electrons being scattered in a very hot gas, similar to the emission that one gets in high temperature plasma machines, such as are being built to produce thermonuclear power.

Figure 14 shows how the sun's emission varied with wavelength in the medical x-ray regi during a particular flare event. The type of a curve shown in Figure 13 is interpretable physically as indicating that on the sun there existed for a short time a region of very hot gas, a plasma at a temperature of about 120 million degrees. Such a region was apparently produced by the flare process. The change in slope between the two curves means that in the sun the hot gas cooled during the three minute interval between rocket measurements. By studying data of this type it is possible to study the temperature history of such very hot flare-produced regions, and also to determine their source strength (the square of the electron density times the volume on the sun of the emitting region) and the manner in which they grow. From such studies one should be able to learn a great deal about this most interesting phenomenon of solar physics.

Let us now leave the sun and consider radiations observable in the night sky. The remainder of this discussion will be concerned with what has been learned from rocket-borne experiments about high energy emission from stars and from the night airglow.

If you fly a rocket at night and look out into space in the ultraviolet there is one radiation which dominates your sight. The whole sky glows in a uniform glow of 1216 Angstrom radiation. This radiation is the familiar Lyman α line. If you are at 130 kilometers, you see this radiation all above you; you also see it looking down with almost half the brightness that you see looking up. Figure 15 is a plot of the intensities of this Lyman α radiation as measured in 1957. The data show a slight local minimum in intensity, not very deep, looking directly away from the sun. Most of this night Lyman α

glow is believed to be really sunlight which has been scattered back to the dark side of earth by atomic hydrogen in the earth's own atmosphere. This scattered sunlight is a real problem in certain astronomical studies. The intensity of this Lyman α glow is five times as great as that of all the visible light emitted by the stars. So it is quite an intense glow.

Despite the brightness of the night Lyman α glow we can still carry out studies on stars in the vacuum ultraviolet by using simple telescopes in rockets. The Lyman α problem is usually avoided by restricting the spectral band under study to wavelengths which exclude the Lyman α line. In Figure 16 is shown the bottom portion of a rocket instrumentation which contains a set of 6-inch reflecting telescopes. At the focus of each of these 6-inch reflecting telescopes is mounted a small ultraviolet detector of high sensitivity which has a very narrow spectral response band. The detector is sensitive only to a very narrow range of far ultraviolet color. The experiment is carried out by firing the rocket, typically from White Sands, New Mexico, up above the atmosphere. The carrier rocket is completely unguided; it rolls very slowly and tumbles or precesses about a large cone, as a rigid body in space will do. As a result of the rocket's roll and tumble the telescopes repeatedly sweep across the sky. In a single flight they can map almost 2/3's of the accessible sky with a typical 2.5 degree field of view. The information telling us what the telescopes see is sent down by radio and we get telemetry records which show the time response of the detectors throughout the flight.

The detectors used in the rocket astronomy program are quite unusual. Figure 17 shows the sensitivity curve of one of the detectors. The detectors

are called gas gain ion chambers. They are characterized by small size and very high sensitivity. The reader will note that Figure 16 indicates a sensitivity of over 10^{-17} coulombs per quantum. Now to get some feeling for what that means let us suppose a detector produced within it one free electron every time a light quantum hit the window. If the detector was that sensitive, the sensitivity would be 1.6×10^{-19} coulombs per quantum. Thus a sensitivity of 1.6×10^{-17} coulombs per quantum means that there are 100 electrons produced in the detector for every quantum which hits the window. Actually such a sensitivity is achieved by having a detector which is basically 10 per cent efficient, but which has within it means of getting amplification of a factor of 1000. This type of operation is achieved by having within the detector a gas which is ionized by incident far ultraviolet light. The resulting free electrons are then accelerated toward an anode collector. Sufficient voltage is impressed across the detector so that a large gas amplification is achieved in the region near the anode.

Figure 18 is a photograph of a portion of the telemetry response recorded when one of the mirror telescopes scanned across the Milky Way. The star signals are seen to show up as single pulses whose width is determined by the rocket roll rate and the telescope field of view. Scans of this type have shown that the sky is quite simple in the far ultraviolet. The stars which you see are much less in number than when you look with your eyes in the visible. Also the ultraviolet stars are highly concentrated along the Milky Way. The main problem is carrying out this type of rocket astronomy is that of determining which stars caused each of the recorded star signals. The

solution of this problem is achieved by a detailed analysis of the rocket motion occurring in each flight. The motion analysis is made possible by means of magnetometers and horizon sensors carried in the rocket. Once such an analysis is complete, the ultraviolet brightness of each star seen can be determined from the amplitude of the recorded star signals.

The results of two rocket astronomy flights of this type are shown in Figures 19 and 20. These figures show the relative brightness of various stars in the far ultraviolet as compared to their brightness in the visible. As Dr. Nancy Roman of the National Aeronautics and Space Administration has pointed out, the stars which emit in the far ultraviolet are the very blue stars, which are the B and O stars. As we examine bluer and bluer stars, we find as one would expect, that the far ultraviolet brightness, compared to the visible brightness, increases.

These pioneering rocket astronomy experiments have done a moderately good job in defining the relative far ultraviolet brightness of bright stars. It is not so certain that they have achieved highly reliable absolute energy measurements of the ultraviolet stellar fluxes. Nevertheless, it is interesting that all of the early measurements have indicated that the absolute energy received from the B stars is considerably less than stellar models would predict. This discrepancy provides a real problem. The very hot stars are believed to be simpler than stars like the sun, because they are so hot that most of the metals and light elements in their atmospheres are ionized and do not contribute much to light absorption in their outer layers. Therefore, it should be possible to analyze the outward flow of energy through their upper layers in a more

quantitative fashion than can be done for cooler stars. Thus we find, if it continues to be confirmed by future work, that we really do have an ultraviolet deficiency, then this poses a series problem for stellar theory. Study of these very hot stars is also of considerable interest in analysis of galactic energy output since these same hot stars are the dominant energy producers in the newer portions of the galaxy.

Let us now consider the story of the far ultraviolet nebular glow. The story illustrates some of the pitfalls into which it is possible to fall in pioneering studies. Sometimes early exploratory studies lead to preliminary conclusions which are not always confirmed by subsequent investigation. Let us now consider one such story and show the evidence which now makes us think that the original conclusions of this story were not correct.

Figure 21 shows a type of instrumentation used in an exploratory study of the night sky in 1957. This instrumentation approach preceded the telescope type of instrumentation illustrated in Figure 16. In Figure 21 are shown a set of Geiger counters which are sensitive to ultraviolet light. Their angles of view are restricted not by use of telescopes but by looking through a bunch of collimating nickel tubes. The counter view angles are restricted to about three degrees. This experiment was flown in an Aerobee rocket. As in the telescope experiments the rocket rolled and precessed throughout the flight. Again the detectors scanned large portions of the overhead celestial sphere.

Now what we expected when this experiment was flown was the observation of early type stars like Spica and like the bright blue stars in Orion. This was not what the telemetry response showed however, The telemetry responses showed no localized humps corresponding to the angular width expected for

point sources, but instead showed rather extended regions which seemed to be centered on hot stars. The individual star did not seem to be seen. An analysis was carried out of the extended regions of glow and maps were prepared. Figure 22 is the brightness map which seemed to be suggested by the experiment in the star region centered about the star Spica. A far ultraviolet brightness map of this particular portion of the sky should be particularly easy to interpret because Spica is relatively isolated and is the only bright early type star in its particular neighborhood. In the Spica region there is no way in which the sum of responses of many hot but weaker stars could be confused with a diffuse glow. This broad diffuse glow became known as the far ultraviolet nebular glow.

During the Spring of 1963, the collimated Geiger counter experiment was repeated in essentially the same form as used in the original experiment. The results of the repeat experiment are shown in Figure 23. Our sky explorations with the small telescopes had always shown that the stars radiated at point sources, but we had never succeeded in obtaining good data with detectors that had exactly the same spectral sensitivity band as that used in the original experiment. In contrast the repeat Geiger counter experiment did cover the same spectral band, it had the same detector as the original experiment, it had the same collimating nickel tubes, and the detector scanned across the same star, Spica. The portion of the telemetry record shown in Figure 23 is the response due to the star Spica. The width of the response is exactly the width that would be calculated for a point source on the basis of the geometry of the nickel tube collimator, the total width being 5.8 degrees. All of the

stars seen in the repeat experiment appeared as localized sources. The background counting rate near Spica is very low and has the same value that occurs when the detector looks toward earth. So here we see a clear picture of the fact that that original experiment did not give the right answer. The discrepancy is embarrassing because we really do not know what caused the smeared-out responses in the first experiment. Maybe the answer to that puzzle will never be solved with certainty.

Another rocket flight which was carried out in the Spring of 1963 contained a telescope experiment which also relates to the question of far ultraviolet nebular glow. One argument that has been put forth, by us at NRL as a matter of fact, was that possibly the far ultraviolet glow did exist, but existed only at a wavelength close to the Lyman α line, and that there might have been small differences in detector sensitivity near the Lyman α line which might have permitted the glow to be seen in the first experiment but not in any later experiment. This second 1963 experiment makes such a hypothesis seem untenable. Figure 24 shows a portion of the telemetry response recorded by one of our telescope-ion chamber photometer combinations during a scan directly across the star Spica. This particular telescope photometer combination, however, is sensitive to a broad band of wavelengths (1050 - 1350 A), including Lyman α. Figure 24 shows a generally elevated signal response which is due to the night Lyman α glow, the intense diffuse atmospheric ultraviolet glow which we have previously described. Superimposed on top of this glow background is a point source response caused by the star, Spica. This response rises above the Lyman α glow with no evidence of nebular emission surrounding the star. Notice the Lyman α glow is seen even when one looks toward the earth.

Also shown in Figure 24 are responses from two other telescopes looking in the same direction as the one sensitive to Lyman α. The uppermost response was produced by a telescope which was sensitive in a region of the ultraviolet confined to a spectral band below the Lyman α line. This band is the shortest ultraviolet wavelength band in which non-solar star emissions have yet been recorded. The other photometer response curve was produced by a photometer sensitive at about 1427 Angstroms. In both cases radiation from the star Spica saturates the detectors.

The bottom trace in Figure 24 was produced by a conventional multiplier tube sensitive to visible light. A comparison between the response of the visible light detector and the detector sensitive to the Lyman Alpha glow demonstrates an interesting fact about air glow. The visible light detector sees a strongly peaked response when it looks tangent to the layer producing the night air glow. This phenomenon is called horizon brightening. In contrast the night Lyman Alpha glow never shows any horizon brightening. The reason for the difference is that the night Lyman Alpha glow is produced by multiple scattering from an optically thick layer of atomic hydrogen while the normal air flow is produced chemically in an atmosphere transparent to the produced radiation.

In conclusion let us consider one other somewhat speculative field, namely, the new field of x-ray astronomy. X-ray astronomy really had its birth in an experiment that was carried out by Giacconi, Gursky, Paolini and Rossi in an attempt to look for fluorescent x-rays produced on the moon. It was their hope that discovery of lunar x-rays would eventually permit analysis

of the composition of the surface of the moon. When the lunar x-ray experiment was flown an x-ray signal was seen; however, it turned out that, after they had worked out the details of the orientation solution of the rocket, it was found that the x-ray source did not correspond to the location of the moon. Since the lunar x-ray detector looked out at the sky with quite a broad field of view, it was impossible to pin-point the position of the x-ray source very precisely. Nevertheless, the source of x-rays was clearly not the moon. Analysis of the manner in which the x-ray responses disappeared as the rocket descended into the atmosphere, suggested the conclusion that the x-rays might very possible be coming from the galactic center.

The possibility that there exist x-ray sources in the night sky was very exciting. NRL had looked for such possible soft x-ray sources previously, but with clearly inadequate sensitivity. It was, therefore, decided to fly an experiment with much greater sensitivity, and also with tighter collimation, in order to confirm the existence of a galactic source. In the NRL experiment a proportional counter was used rather than Geiger counters. The NRL detector consisted of a single large tube with 31 windows and 31 anodes and a common gas supply. The detector looked out through a collimator which has an angular field of view of about 10 degrees full width at half maximum. The detector window was made of 0.005 inch beryllium and provided x-ray sensitivity between about 0.5 and 8 A. Now a proportional counter is characterized by producting pulses, the amplitude of which is crudely proportional to the energy of the incident x-ray quantum. The pulses produced by the NRL detector were amplified and sorted into three groups of pulse amplitude. The counting rates of each

amplitude group were individually metered, so as to permit a partial determination of the spectral character of any emitting x-ray source discovered.

The results of this experiment proved quite interesting. The existence of one relatively strong x-ray source seems to be clearly established, and existence of a second weaker source at the Crab Nebula is also relatively certain. The strong source is located in the constellation Scorpio and is a point in the sky with celestial coordinates: 16 hours 15 minutes Right Ascension, -15° Declination. No optical or radio star has been identified with the x-ray object.

One of the telemetry responses showing the Scorpio x-ray source is shown in Figure 25. The source shows up clearly above the general background. The source was scanned about ten times during the flight. Although the data permit pin-pointing the position of the source center, they do not tell us whether the source is a point source or a diffuse source which is excended over as much as 5 degrees of arc. Although the spectral analysis based on pulse amplitudes is of relatively poor quality, the source seems to produce mainly soft x-ray quanta near the 8 A long-wavelength limit of the detector sensitivity curve, rather than higher energy quanta below 2 A. The source delivers to earth a 1-8 A x-ray flux of the order of 2×10^{-7} erg cm^{-2} sec^{-1}; thus as seen at earth it is about 10^4 less intense than the sun. Since the thermal radio brightness of the sun is much less than 10^4 times the brightness of the minimum detectable radio source, it is not entirely surprising that no distinctive radio source clearly corresponds with the x-ray star. Although the location of the strong x-ray source differs by 15 to 20 degrees from the location claimed by Giacconi, et al., it appears probable that the NRL experiment has served to pin-point the previously seen source.

ACKNOWLEDGMENTS

The photograph of the limb flare was made by H. Smith at Sacramento Peak. All the far ultraviolet spectroscopy and photography results are the work of W. E. Austin, C. P. Detwiler, D. L. Garrett, Jr. D. Purcell and R. Tousey. The near ultraviolet spectrophotometric data is based on scientific work of F. S. Johnson, J. D. Purcell, and R. Tousey. The remainder of the data is the result of scientific work by R. Blake, C. Bowyer, E. T. Byram, T. A. Chubb, H. Friedman, R. W. Kreplin, J. F. Meekins, and A. E. Unzicker. Technological support for the rocket and satellite experiments has been furnished by many employees of the U. S. Naval Research Laboratory, including in particular work of D. Bashore, D. Brousseau, W. Griffith, W. A. Nicols, J. Nemecek, and M. Votaw.

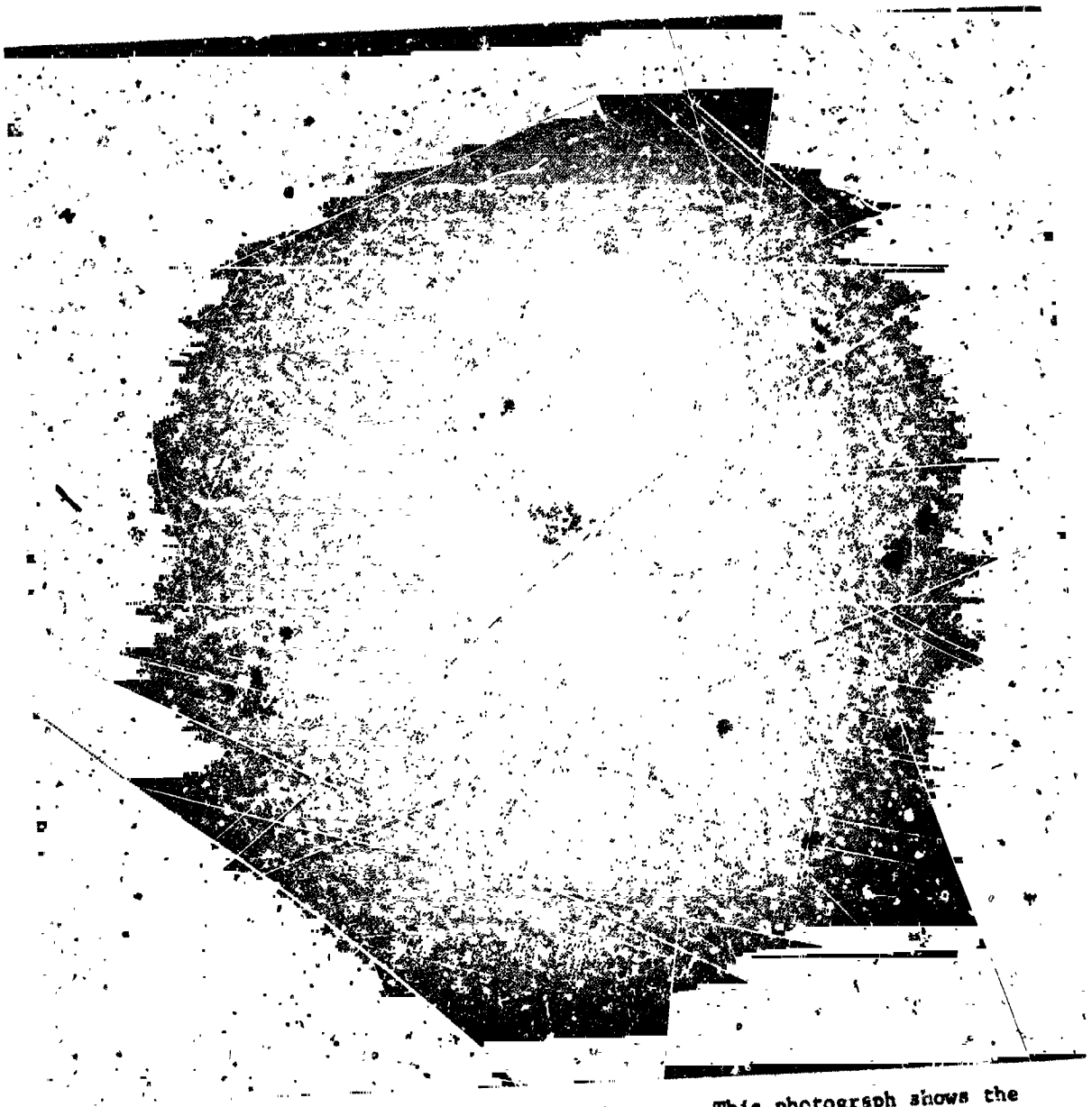

Figure 1: White light photograph of the sun. This photograph shows the incandescent disk of the sun, called the solar photosphere, which emits all but about one part in 100,000 of the energy received by earth. Part of the darkening of the disk near its edge is real. At the edge of the solar disk we see light from a higher, cooler layer than is seen at the disk center.

Figure 2:

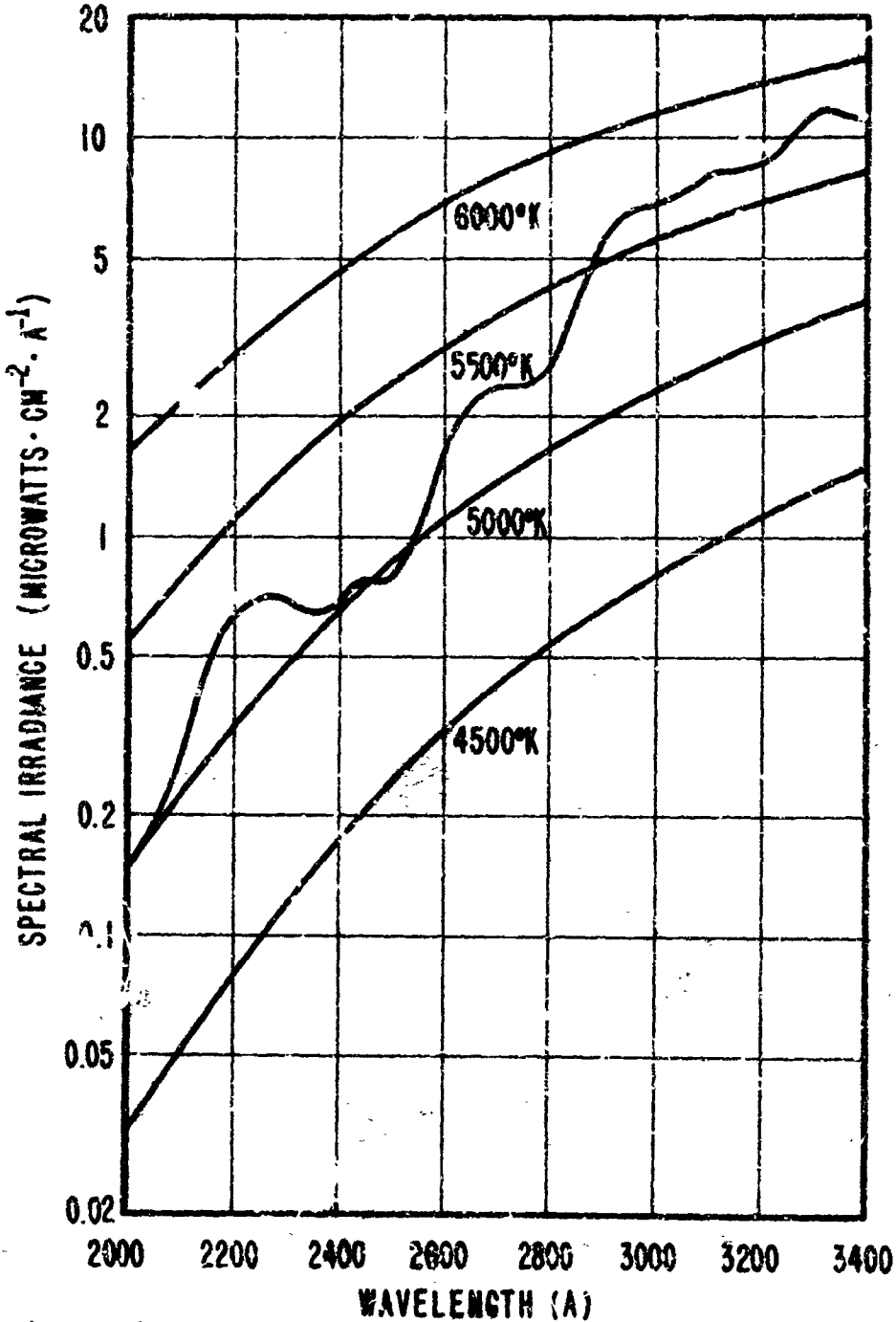

Comparison between ultraviolet emission of the sun and the emission of an incandescent solid at various temperatures. The hypothetical incandescent solid is assumed to be the same size and at the same distance as the sun. The decreasing apparent temperature of the sun as the observing wavelength is shifted to the ultraviolet is caused by the fact that at shorter wavelengths one observes a higher, cooler layer of emitting gas.

Figure 3:

Spectrum of the sun in the far ultraviolet. Below 1400 A the emission of the sun is dominated by strong emission lines arising from a shell of hot gas overlying the solar photosphere. This hot shell is called the solar chromosphere. The intense emission at the right of Figure 3 is the greatly overexposed Lyman α line at 1216 A, with wing emission extending to below 1100 A. The black bands overlaying the wing emission are due to water vapor absorption in the spectrograph. Higher members (β,γ,δ etc.) of the atomic hydrogen Lyman series are marked on the spectrum. Also clearly seen is Lyman continuum radiation below 912 A. The other dominant emission lines shown are due to multiply ionized atoms of C, N, O, Ne, Si, and S.

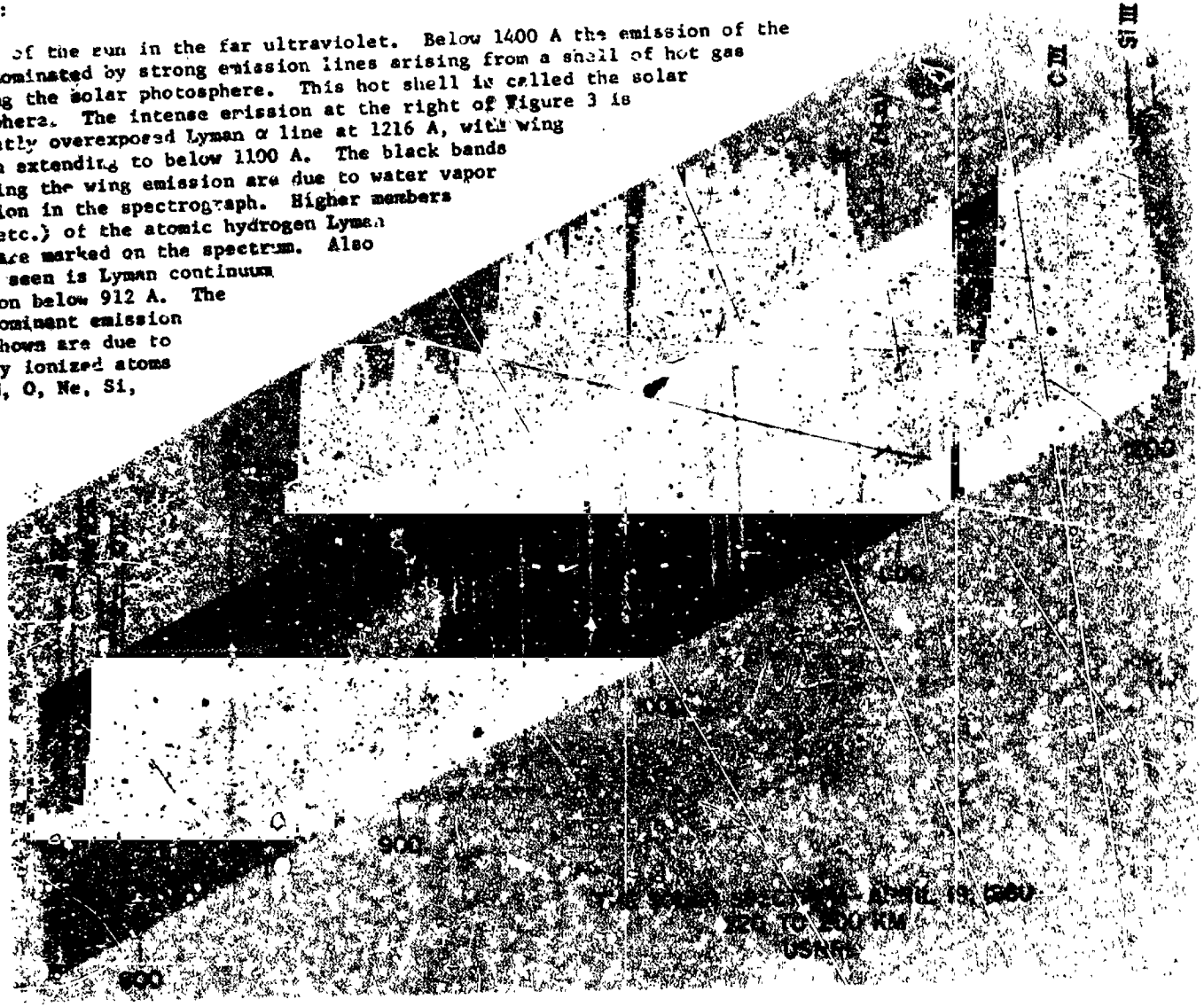

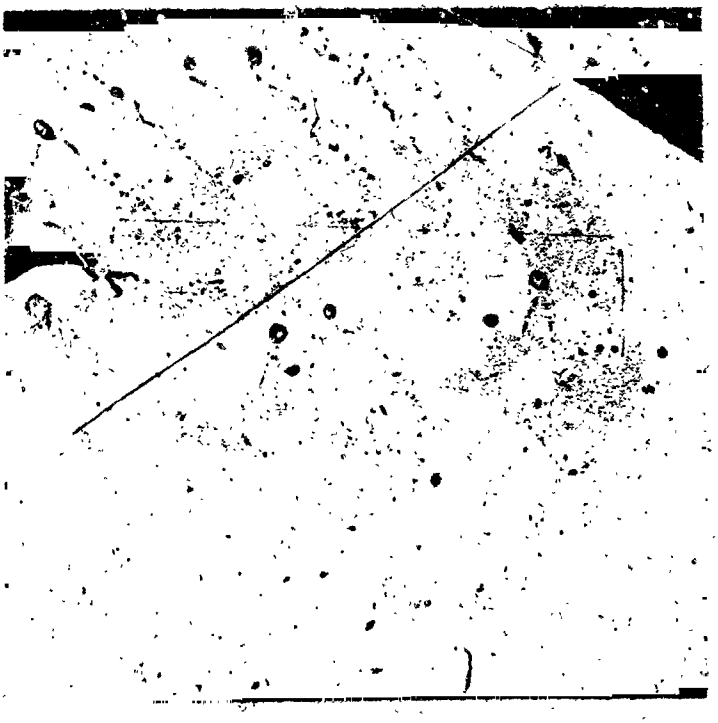

Figure 4: Photograph of sun made using Lyman α radiation at 1216 A. This photograph shows solar emission layers that lie above the solar photosphere. This emission shell is called the chromosphere, and was first seen briefly at the start and end of total solar eclipses. The bright patches of emission are called plages. Plages are regions of high chromospheric density. Plage are a sensitive indicator of solar activity. Intense plages generally overlie sunspot groups.

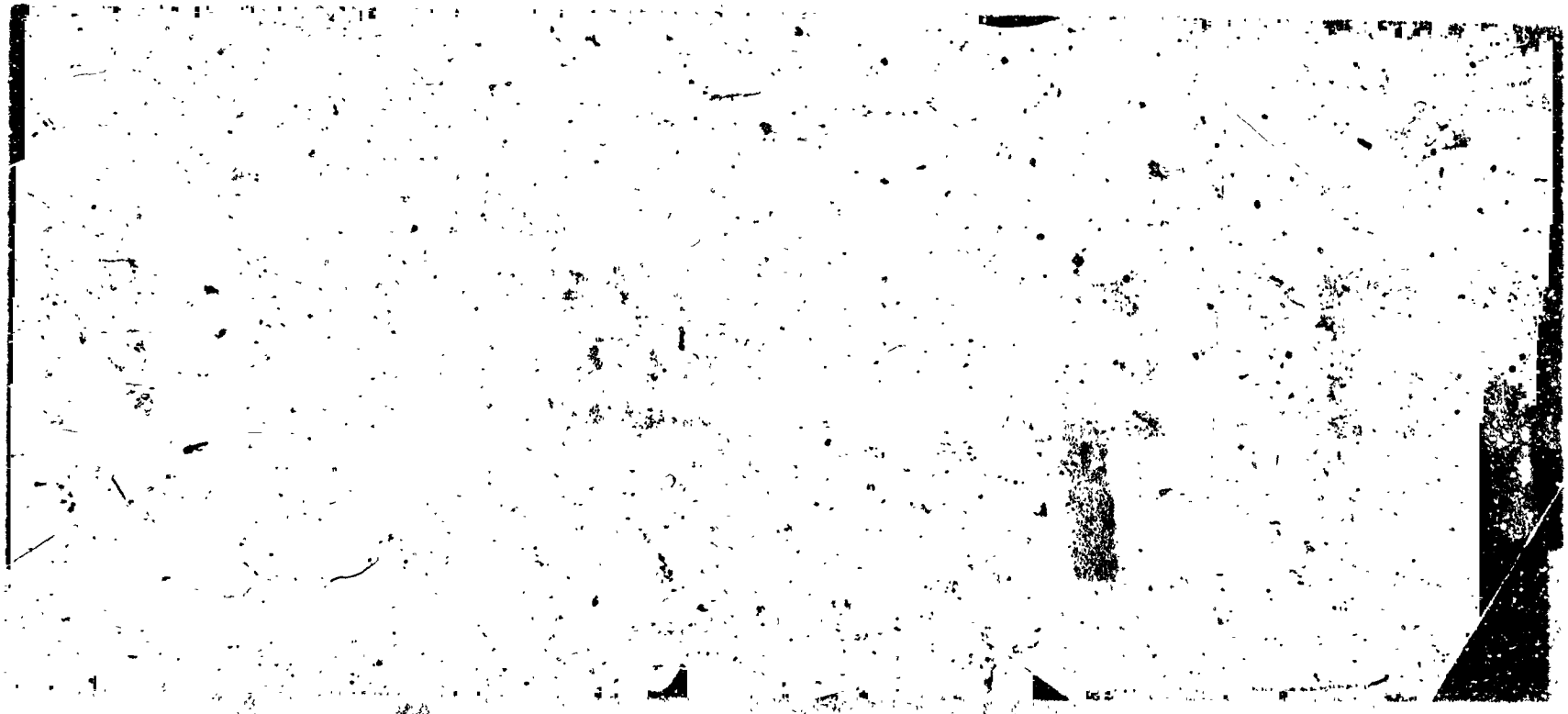

Figure 5: Slice images of the sun made with chromospheric light. The parallelogram images are monochromatic photographs of a slice across the center of the sun, each image being made in light of a different wavelength. Attention is directed to the set of three images occurring near the center of the figure. The left image is an image made in atomic hydrogen Lyman α light from oxygen ions that are missing five electrons. The oxygen images show increased brightness at the edge of the sun. All the images shown are brighter in plage regions than elsewhere on the disk.

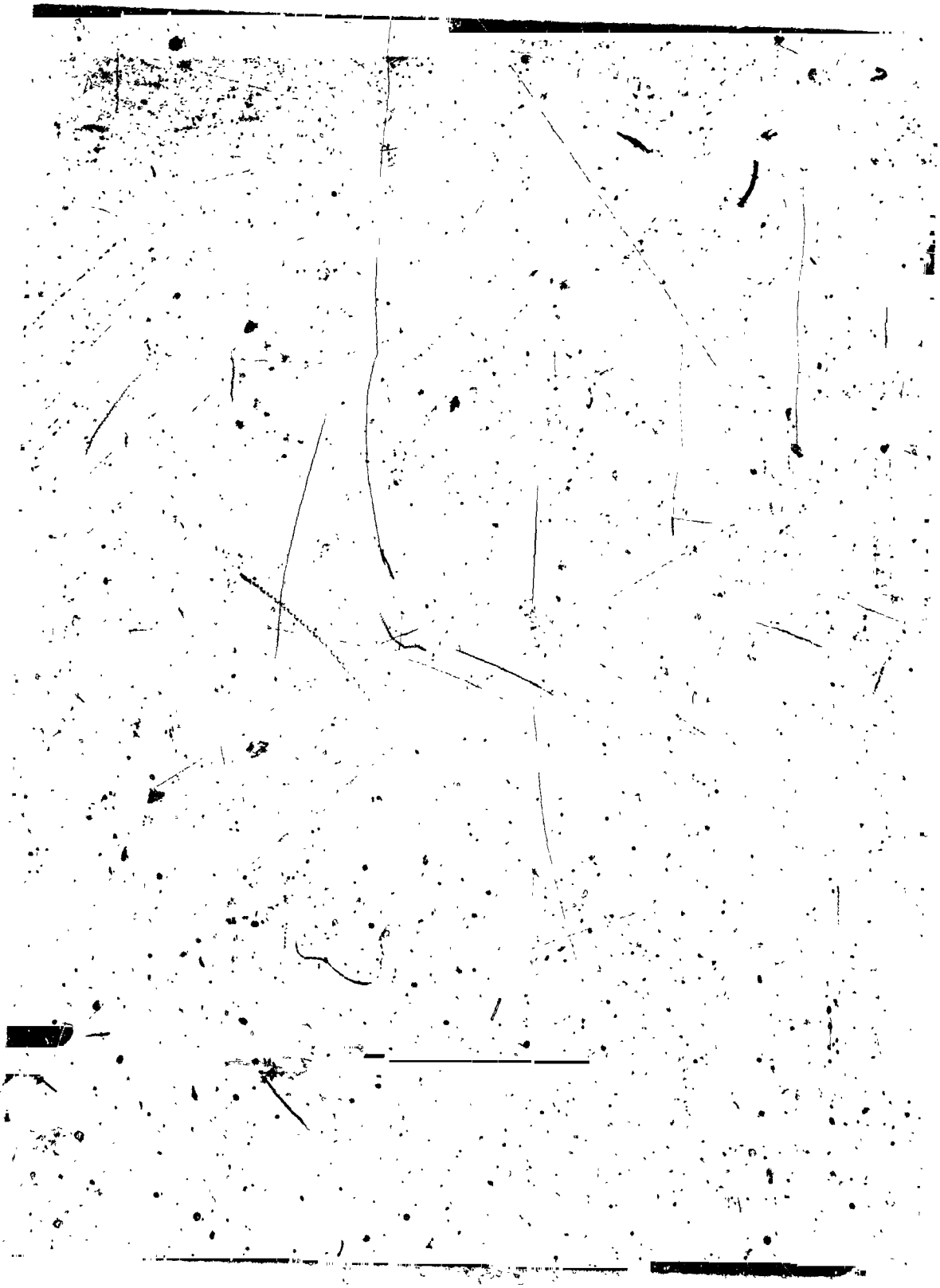

Figure 6:

Disk images of the sun in the 300 Å spectral region. The figure shows overlapping images in the light of ionized helium and in the light of heavier solar ions. The bright image showing a well-developed disk image of the sun with superimposed plage emission is the helium image. Less discernable images of the sun in light of multiply ionized iron atoms occur on both sides of the helium image and partially overlap it. The iron images show no disk pattern, but consist only of bright spots corresponding to the solar plages. The iron atoms responsible for the two sets of plage emissions are atoms that have lost 14 or 15 electrons.

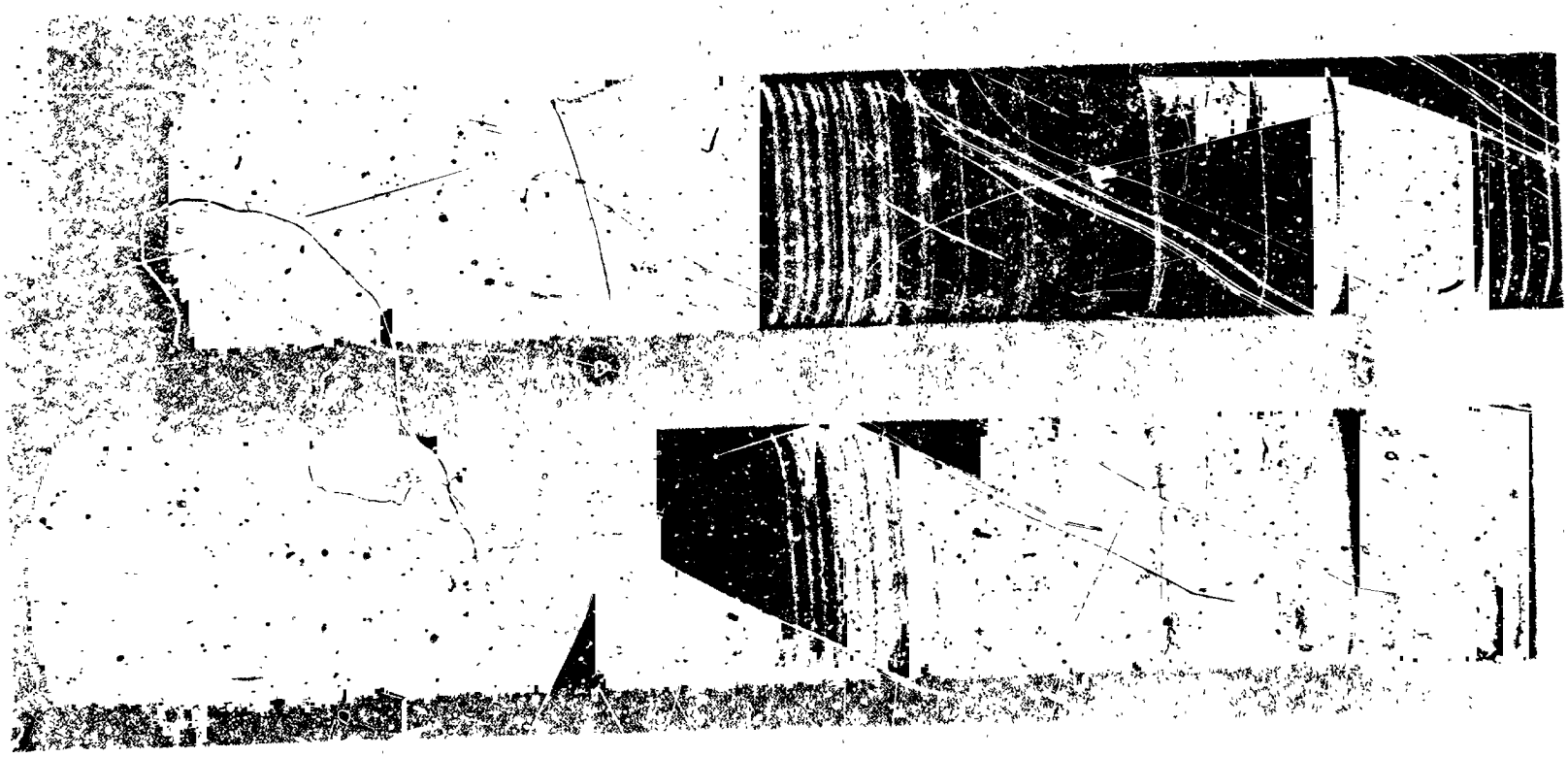

Figure 7: Spectrum of the sun in the 50-300 A region. In the figure the faint lines at the left of the spectrum are x-ray emissions originating in the solar corona. The bright emissions in the center of the figure are a group of largely unidentified lines around 180 A. The brightest line near the right side of the spectrum is the ionized helium emission at 304 A. Many of the intermediate lines are second and third order repetitions of shorter wavelength lines. This photographic spectrum was the first to show the dominant line structure of coronal x-ray emission.

Figure 8

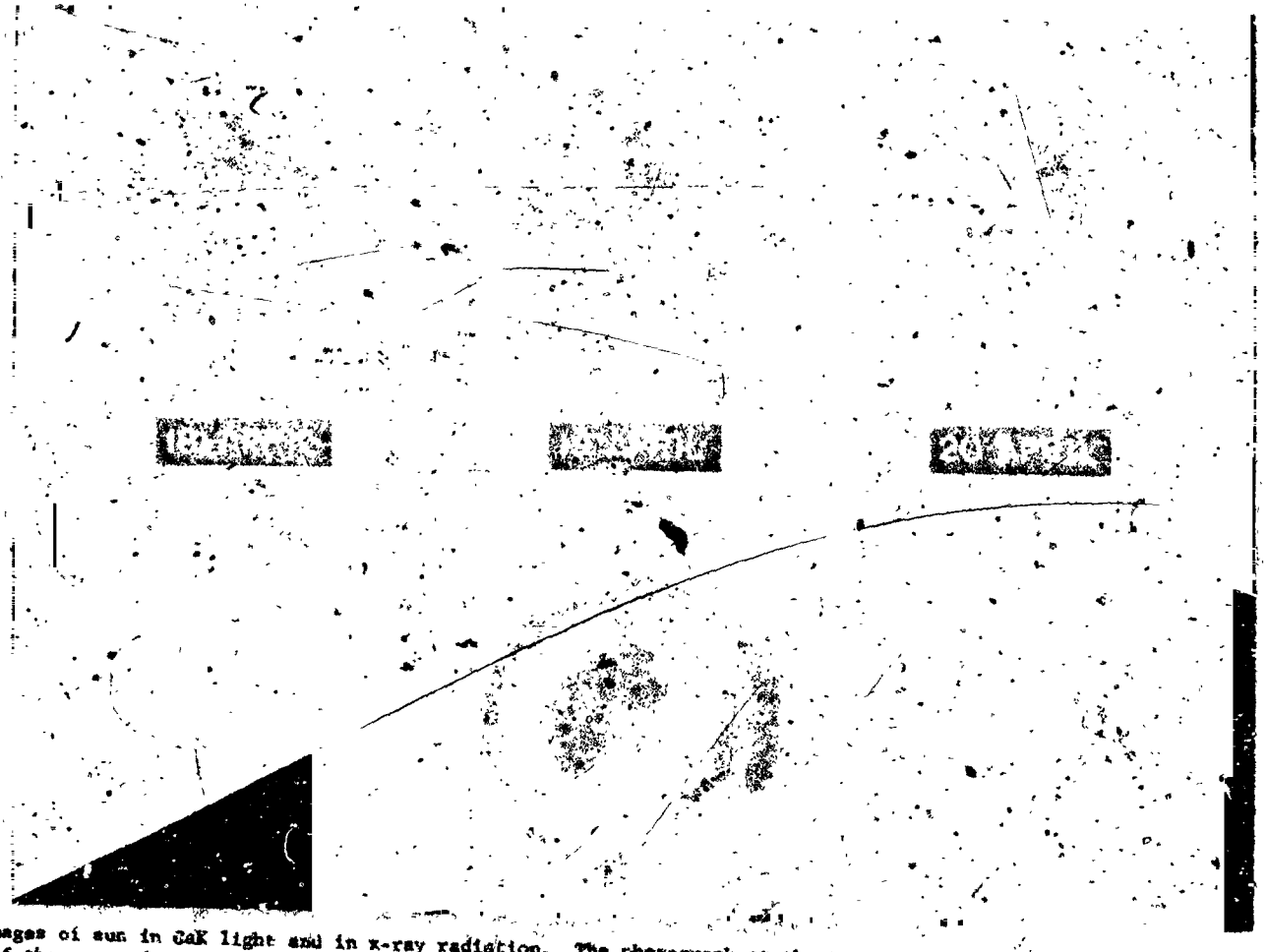

Disk images of sun in CaK light and in x-ray radiation. The photograph at the bottom of the figure is the first photograph of the sun made in x-ray radiation. The photograph was obtained by mounting a "pin-hole" camera on a solar pointing control. The local areas of solar x-ray emission, which originated mainly in the plages shown in the top K-line photographs, produced arc-shaped exposure patterns due to a back-and-forth rotation of the x-ray camera during flight. Camera sensitivity was limited to the x-ray portion of the spectrum by covering the entrance aperture of the "pin-hole" camera with a thin aluminum coated nitrocellulose filter, which transmitted x-rays but reflected or absorbed visible and ultraviolet lights.

Figure 9

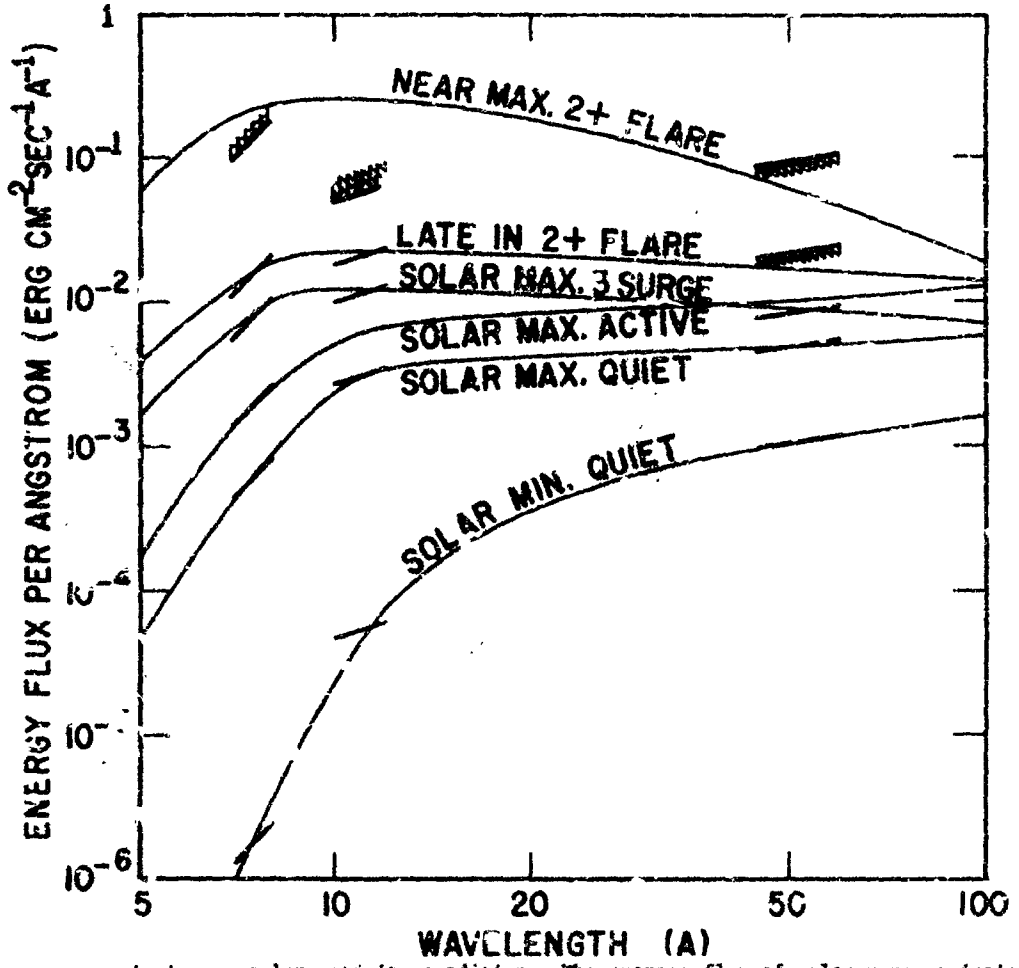

Dependence of solar x-ray emission on solar activity condition. The average flux of solar x-ray emission is strongly dependent on solar activity condition. Rocket measurements with band sensitive photometers show a five-fold solar cycle variation in x-ray flux in the 50 A region. This variability increases as one examines shorter wavelengths, amounting to about a 300-fold variation at 7A. Flare activity causes a further major increase in shortwave x-ray emission, but affects longer wavelength emission less dramatically.

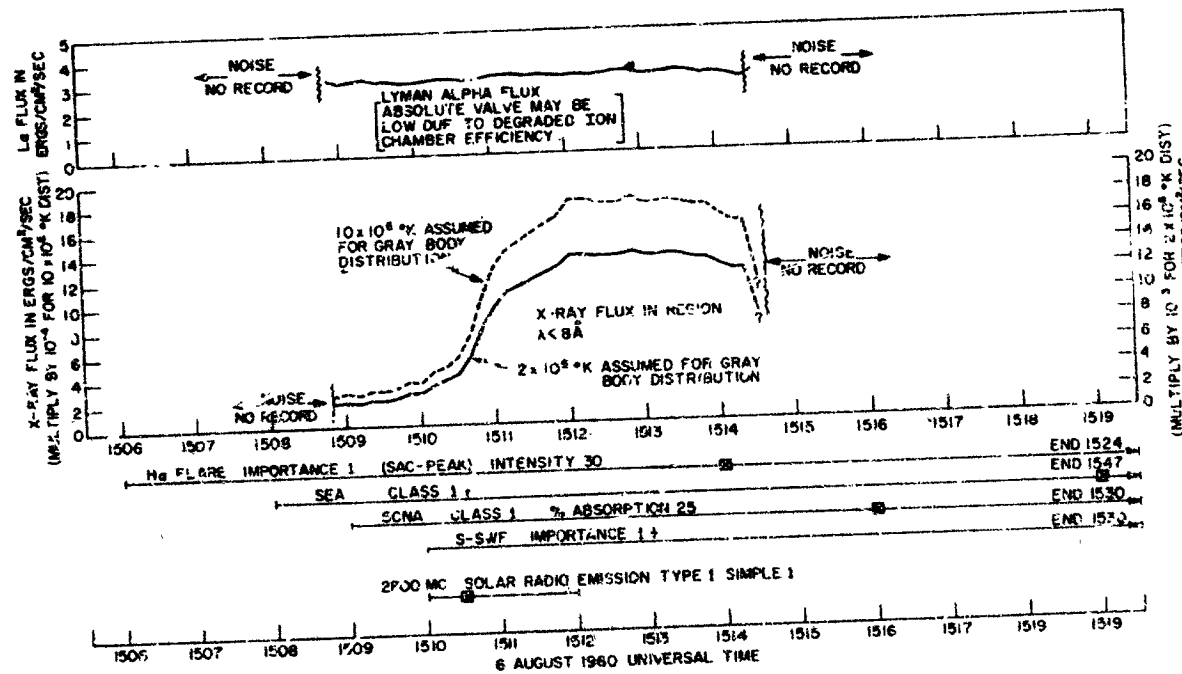

Figure 10: Rapid growth in solar x-ray emission during a solar flare. Solar x-ray and Lyman α ultraviolet fluxes were measured from a satellite during the development of a small flare on the solar limb. During a radio noise burst, which accompanied the most rapid period of flare growth, the 2-8 A x-ray flux from the whole sun increased by a factor of 5, whereas the Lyman α ultraviolet radiation increased by at most 5%. These data provide clear evidence that solar x-ray emission rather than Lyman α ultraviolet emission were the cause of the short wave radio fadeout accompanying the flare.

Figure 11:

Development of a small limb flare as recorded in hydrogen Balmer light. Red light H photographs document the the development of the small limb flare responsible for the solar x-ray burst shown in Figure 10. The flare developed as a series of bright loops on the limb. Although the small size of the flare caused it to be classified only as a Class 1 flare, the strength of the associated x-ray burst suggests that we are really seeing the high altitude portion of a major disk flare.

Summary of Major Events Seen by SR-1 Satellite

Disc Flares Class > 1				Disc Flares Class 1		Limb Flare Class 1		Non-Flare Limb Events			
X-ray > 2 × 10⁻³ erg/cm²/sec No BSL or APR		X-ray < 2 × 10⁻³ erg/cm²/sec No BSL or APR		X-ray > 2 × 10⁻⁴ erg/cm²/sec No BSL or APR		X-ray > 2 × 10⁻⁴ erg/cm²/sec No BSL or APR		X-ray > 2 × 10⁻⁴ erg/cm²/sec No Flare > 1		X-ray < 2 × 10⁻³ No Flare > 1	
Time, Event, X-ray Flux	Ionospheric Effect	Time, Event, X-ray Flux	Ionospheric Effect	Time, Event, X-ray Flux	Ionospheric Effect	Time, Event, X-ray Flux	Ionospheric Effect	Time, Event, X-ray Flux	Ionospheric Effect	Time, Event, X-ray Flux	Ionospheric Effect
07 - 30 - 1047, 1101 2 Flare X = 4.7	2 + SSWF	07 - 22 - 0056 1 + Flare X = 1.6	No SID	10 - 19 - 0048 1 Flare X = 3.4° - Short burst	Small SCNA	08 - 08 - 1509 1 Flare 90° X = 12.7°	1 + SSWF 1 SCNA	07 - 23 - 1824 1 + APR, 2 BSL X = 3.7	1 SSWF 1 SCNA	09 - 04 - 0233, 0327 1 DB - Could be part of 09 - 04 - 0041 event X = 1.6	No SID
09 - 02 - 0542 Early in 2 + Flare X = 3.6°	1 SSWF (slow)	08 - 06 - 1322 3 Flare X = 1.0	Near end of 1 + SSWF			08 - 07 - 0749 1 Flare 34° X = 13°	2 + SSWF	09 - 04 - 0041 3 APR 1+ DB X = 7.25+	2 SSWF 2 SCNA		
09 - 19 - 0711 2 Flare X = 15.7°	2 - SSWF	08 - 07 - 0611 1 + Flare X = 1.5	No SID					09 - 07 - 1308, 1321, 1327 3 + BSL X = 2.6°	1 - SSWF 1 SCNA		
10 - 29 - 1056, 1139 3 Flare X = 5	3 SSWF	08 - 14 - 1221 Start 2 + Flare X = 0.95	2 SSWF Radio after recked					07 - 24 - 0940, 0958, 1049, 1138, 1220, 1506, 1511 3 DB X = 5.2	SID		
11 - 10 - 1129 3 Flare X = 10.3°	2 SSWF	08 - 21 - 0440 1 + Flare X = 1.15	No SID								
		09 - 10 - 2325, 2334 2 Flare X = 1.9	No SSWF 1 SEA								
		08 - 13 - 1145 1 + Flare X = 1.3	No SSWF 1 SEA								

*Means changing X-ray flux during telemetering record.

Figure 12: Summary of major events seen by SR-1 Satellite. The first satellite monitor of solar x-ray radiation recorded x-ray bursts from 13 disk flares, 2 limb flares and 5 non-flare limb events. When the flux of 2-8 A x-rays exceeded 2 x 10^{-3} erg cm^{-2} sec^{-1} $ster^{-1}$, short wave radio fadeout was present on earth. The similarity in the behavior of x-ray bursts from small limb flares, bright surge events on the limb and active prominence regions on the limb to the behavior of x-ray bursts from flares suggests that major limb events are edge views of important disk flares.

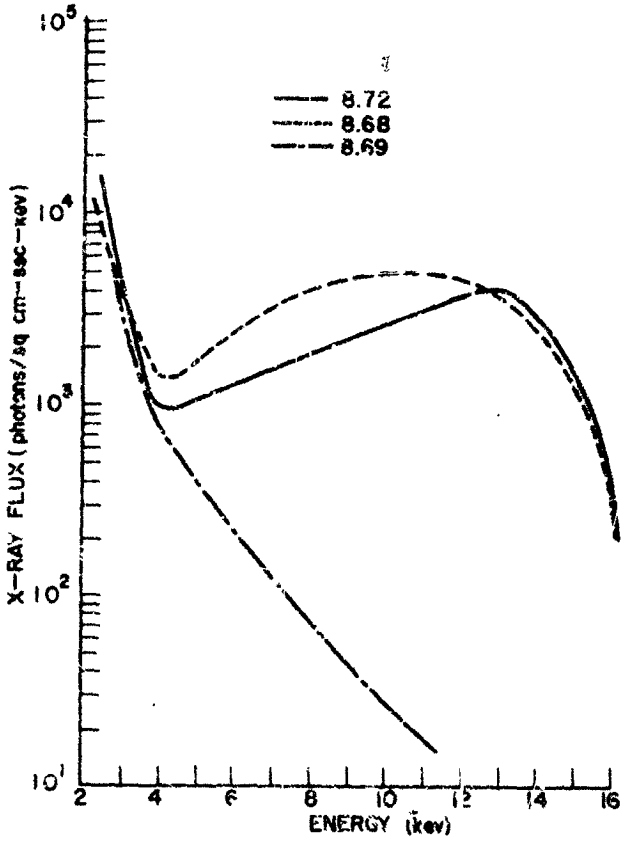

COMPARISON OF SPECTRA OBTAINED FROM PROPORTIONAL COUNTERS ON THREE DIFFERENT FLIGHTS

Figure 13: Short wave x-ray spectrum deduced from proportional counter pulse amplitude distribution. During the last sunspot maximum in 1959 three rocket measurements of the short wave length end of the solar x-ray spectrum were made during non-flare solar conditions. The form of the solar emission spectrum was deduced from the distribution of pulse amplitudes produced in a gas proportional counter. The spectra deduced from two of the rocket flights show an emission maximum of an indicated quantum energy of about 11 kev. It is believed that the indicated peaking in the x-ray spectrum is due to Fe line emission at about 7 kev. This explanation of the data assumes that the proportional counter energy scale calibrations were in error. An alternate explanation is that the peaking is due to iron recombination continuum emission in the indicated 9-12 kev region. The differences in spectrum behavior between flight 8.69 and flights 8.68 and 8.72 reflects differences in solar conditions.

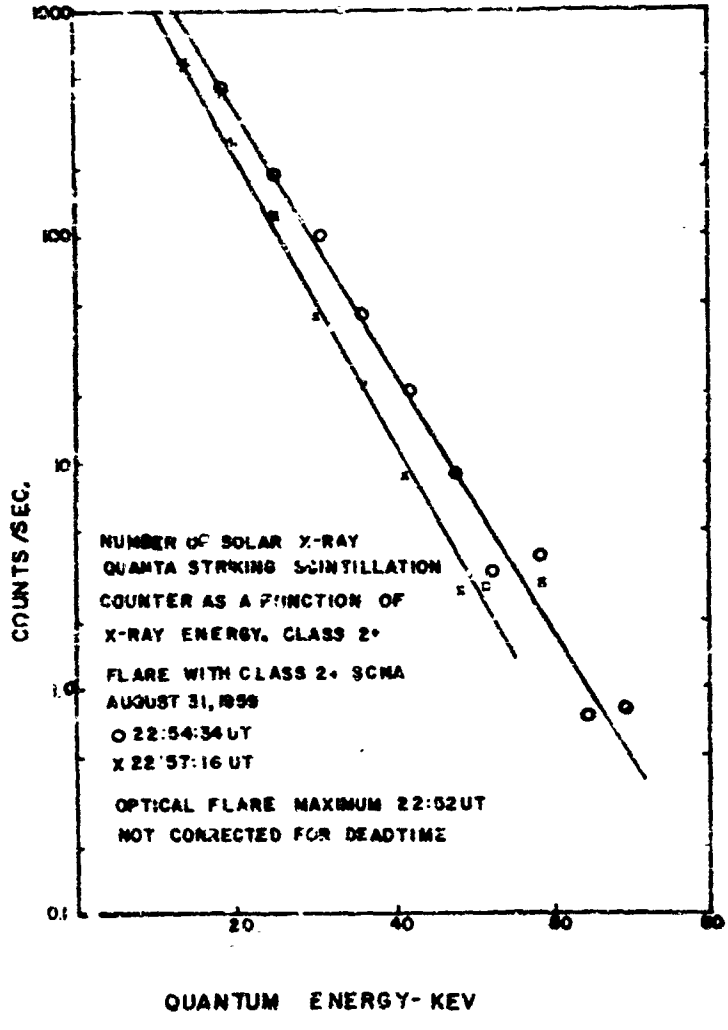

Figure 14: High energy x-ray emission observed during a bright solar flare. During a bright Class 2+solar flare x-ray emission was observed with quantum energies as high as 60 kev. The spectral region 20-60 kev (o.2 - 0.6 A) is a region where solar line emission should be negligible. The observed spectrum is interpretable as being Bremsstrahlung from a hot plasma produced by the flare. The temperature of the electrons in the plasma is calculated to to about 120,000,000°K. The steepening in spectral slope during the flight indicates that cooling of the plasma occurred in the three minute interval between measurements.

Figure 15

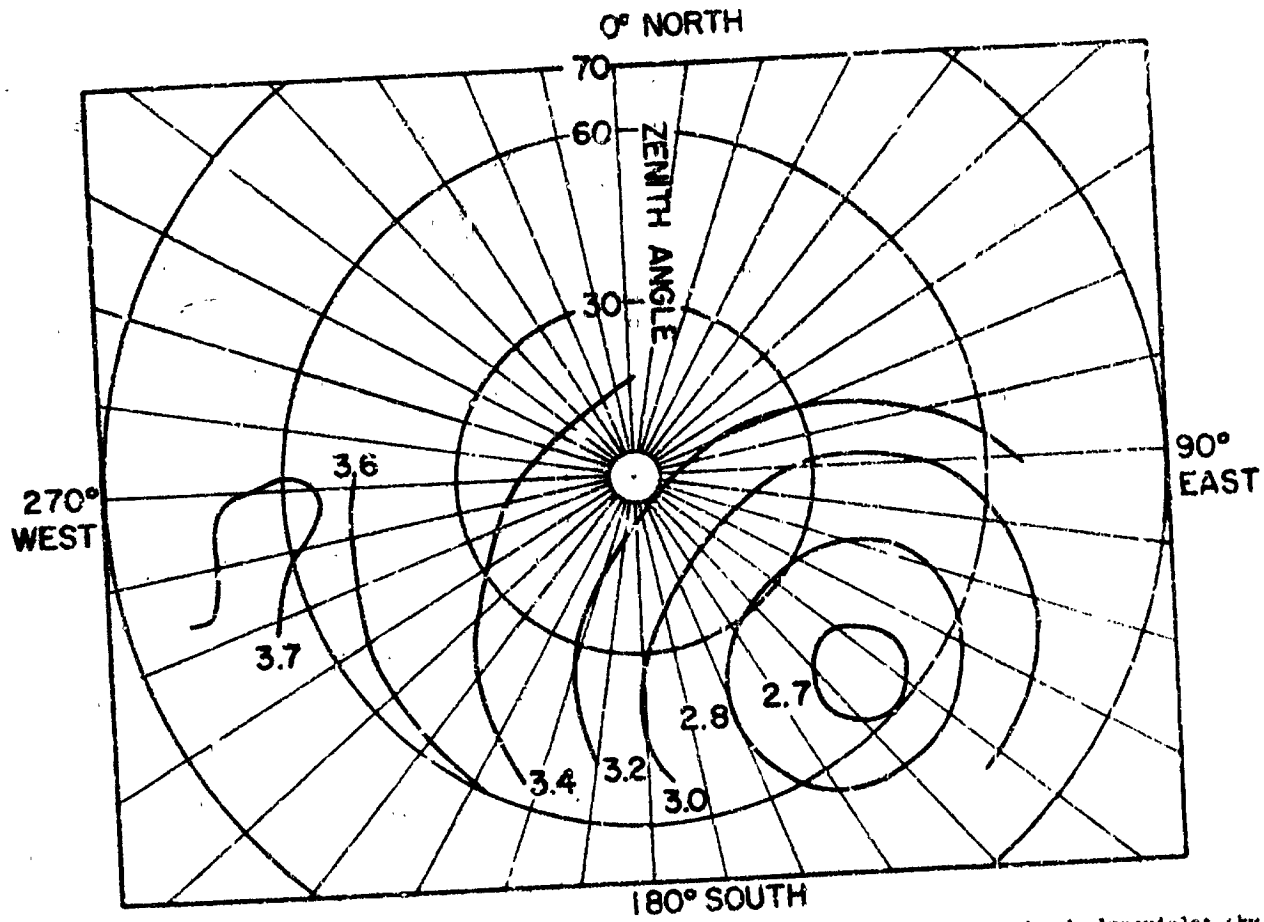

Intensity map of overhead Lyman Alpha radiation in the night sky. At 130 km altitude the overhead ultraviolet sky is bright with a diffuse glow of Lyman Alpha radiation. This night Lyman Alpha glow has an energy content equal to about five times visible starlight. The figure is a map of overhead Lyman Alpha intensity in units of 10^{-3} erg cm^{-2} sec^{-1} $ster^{-1}$. The shallow brightness minimum occurred in approximately the antisolar direction. The night Lyman Alpha glow is largely produced by atomic hydrogen in the upper fringes of the earth's atmosphere, and is believed to be in important measure solar Lyman Alpha rescattered to the dark side of the earth.

Figure 16:

Part of optical section of an Aerobee rocket used in ultraviolet studies of the star. The rocket instrumentation consists of reflecting 4-inch and 6-inch telescopes combined with specialized far ultraviolet photometers. The roll and free precession of the unguided Aerobee rocket enables the telescopes to sweep across the sky. When one of the telescopes scans across the star, the ultraviolet starlight is focussed on the detector and the response signal is telemetered to ground.

Figure 17:

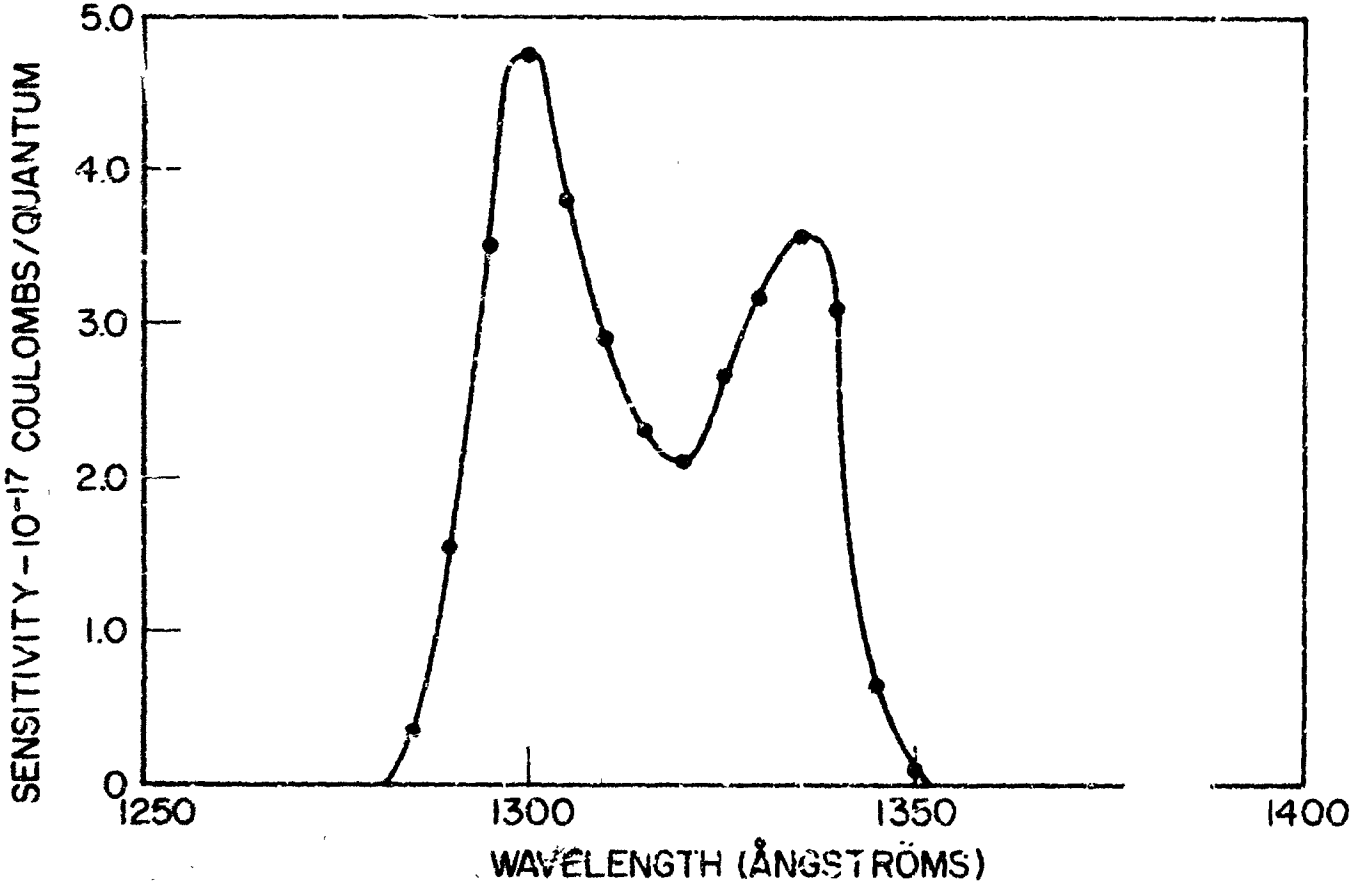

Sensitivity curve of far ultraviolet stellar photometer. The small far ultraviolet photometers shown in Figure 16 are called gas gain ion chambers. They derive their response from the photo-ionization of a filling gas. This Figure shows the response curve of a chamber filled with a nitric oxide-carbon dioxide mix and fitted with a strontium fluoride crystal window. When operated at flight high voltage, the detector delivers about 4×10^{-17} coulombs of charge to the anode for every quantum of 1300 A radiation striking the photometer window.

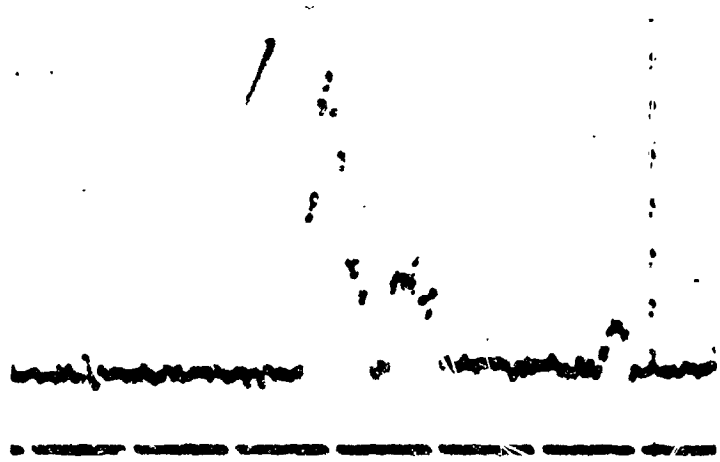

Figure 18: Portion of telemetry record showing telescope-photometer scan of Milky Way. The rocket telescopes are flown with a typical 2 to 3 degree field of view. As the roll of the rocket causes the telescope view vector to sweep across an early type star, signals are generated with the sensing photometers and are transmitted to ground. This figure shows star responses recorded during a scan across the Centaurus and Lupus constellations in the Southern Milky Way. The height of the individual star responses combined with an identification of the stars responsible for each observed signal provides the basis for determining the far ultraviolet emission intensity of bright early (blue) type stars.

Figure 19:

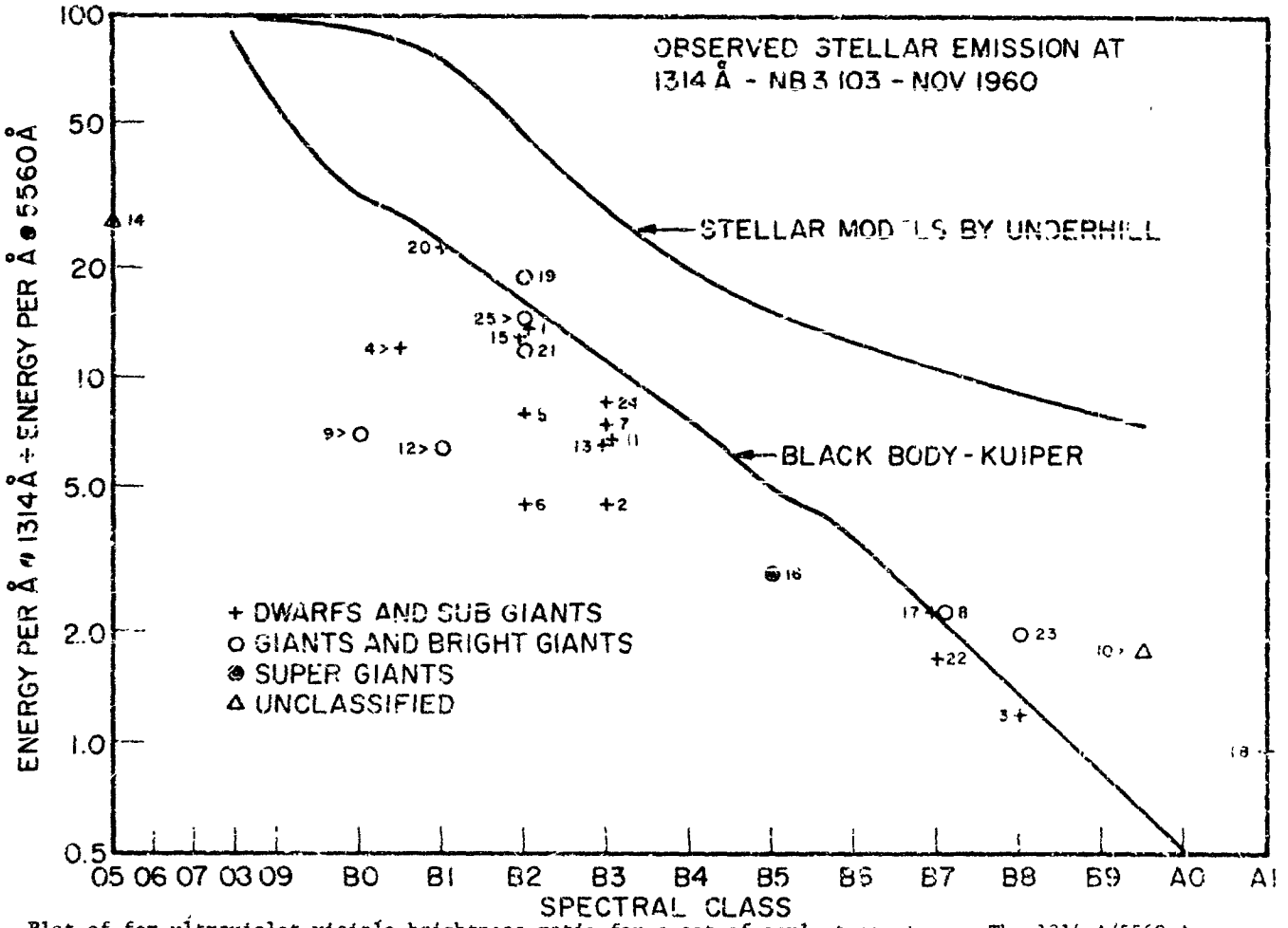

Plot of far ultraviolet visible brightness ratio for a set of early type stars. The 1314 Å/5560 Å brightness ratio for a set of stars measured in 1960 is plotted against spectral type. As expected the earliest type stars in general have the highest relative ultraviolet emission. The half-magnitude scatter in relative ultraviolet brightness for a given spectral type appears to be real. The absolute photometry achieved in the experiment is such that the existence of a significant discrepancy between measured ultraviolet fluxes and those produced in Underhill's indicated models is probably real.

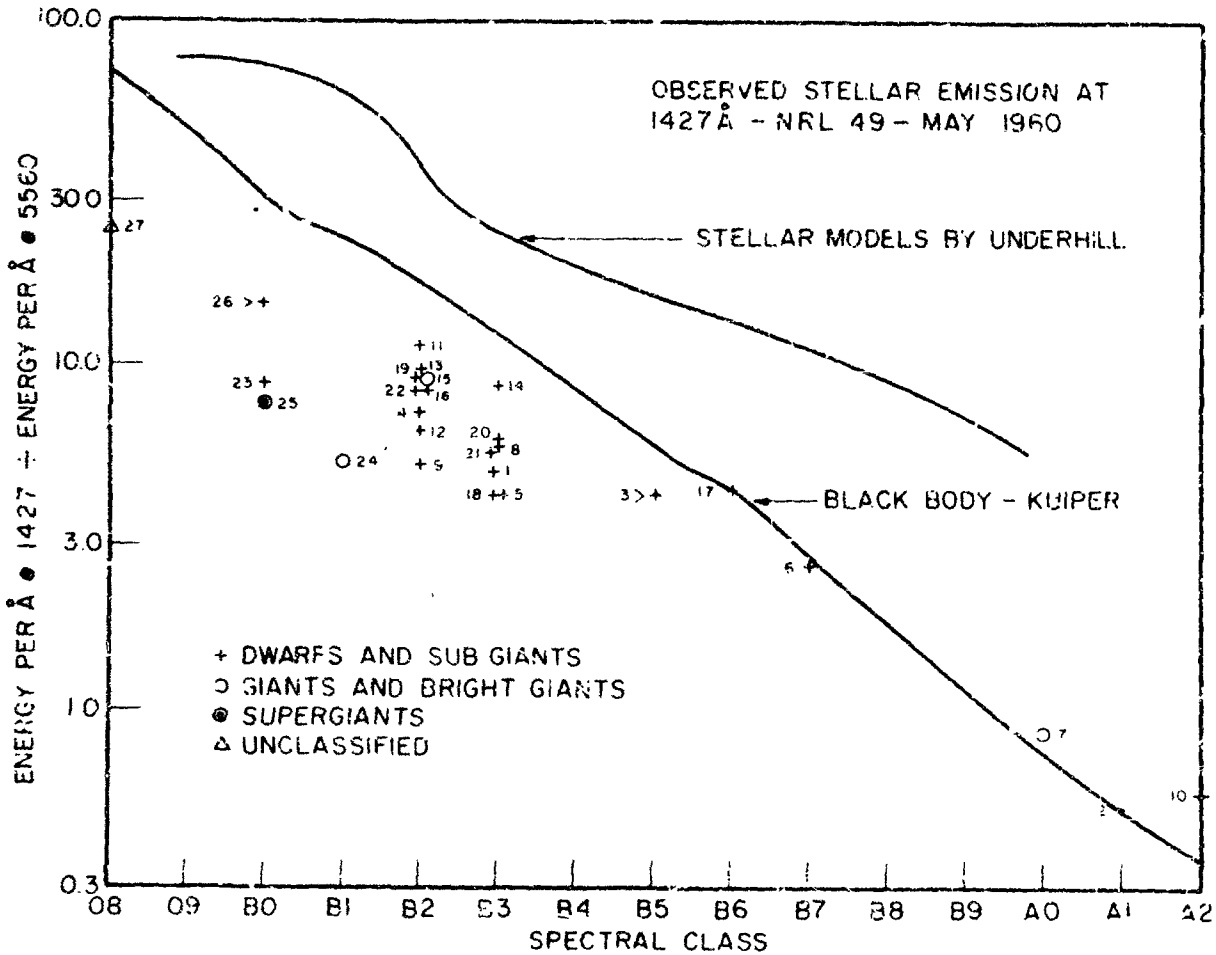

Figure 20:

Plot of the relative brightness of stars at 1427 A as compared to the brightness at 5560 A for a set of early type stars. The 1427 A/5560 A brightness ratio for a set of stars measured in 1960 is plotted against spectral type. Comparison between data shown in Figure 19 and the present Figure indicate that stellar brightness behavior at 1427 A does not greatly differ from the behavior at 1314 A. The absolute photometric accuracy of the data may only be a factor or two.

Figure 21:

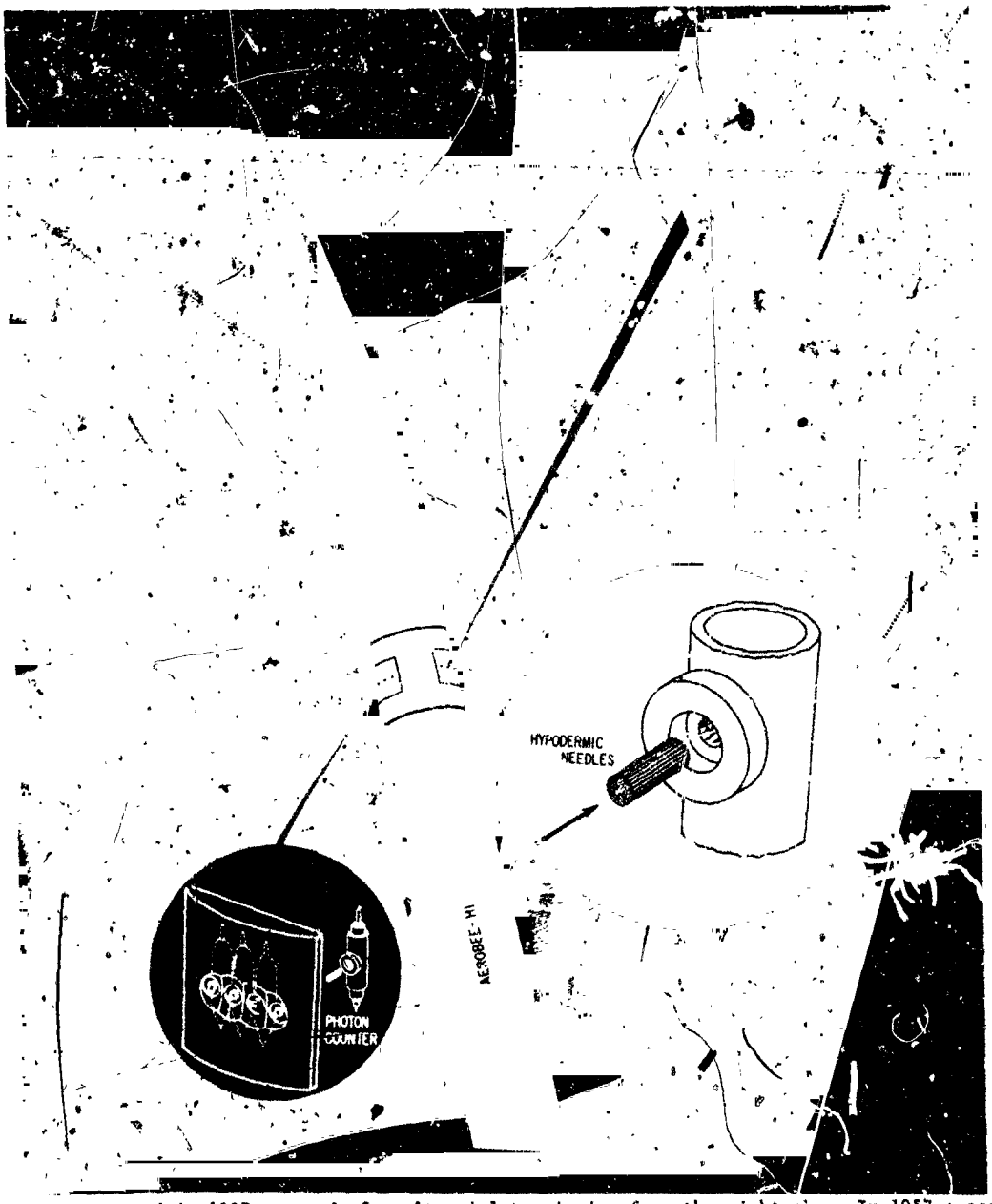

Instrumentation used in 1957 to study far ultraviolet emission from the night sky. In 1957 a scanning survey of the night sky was made with a set of collimated ultraviolet - sensitive Geiger counters. The counters were sensitive to a radiation in a band 1230-1350 A. The counter responses, in contrast to more recent data, were suggestive of the existence of diffuse rather than point sources in the night sky. The data were interpreted as indicating the presence of a far ultraviolet nebulosity surrounding early type stars.

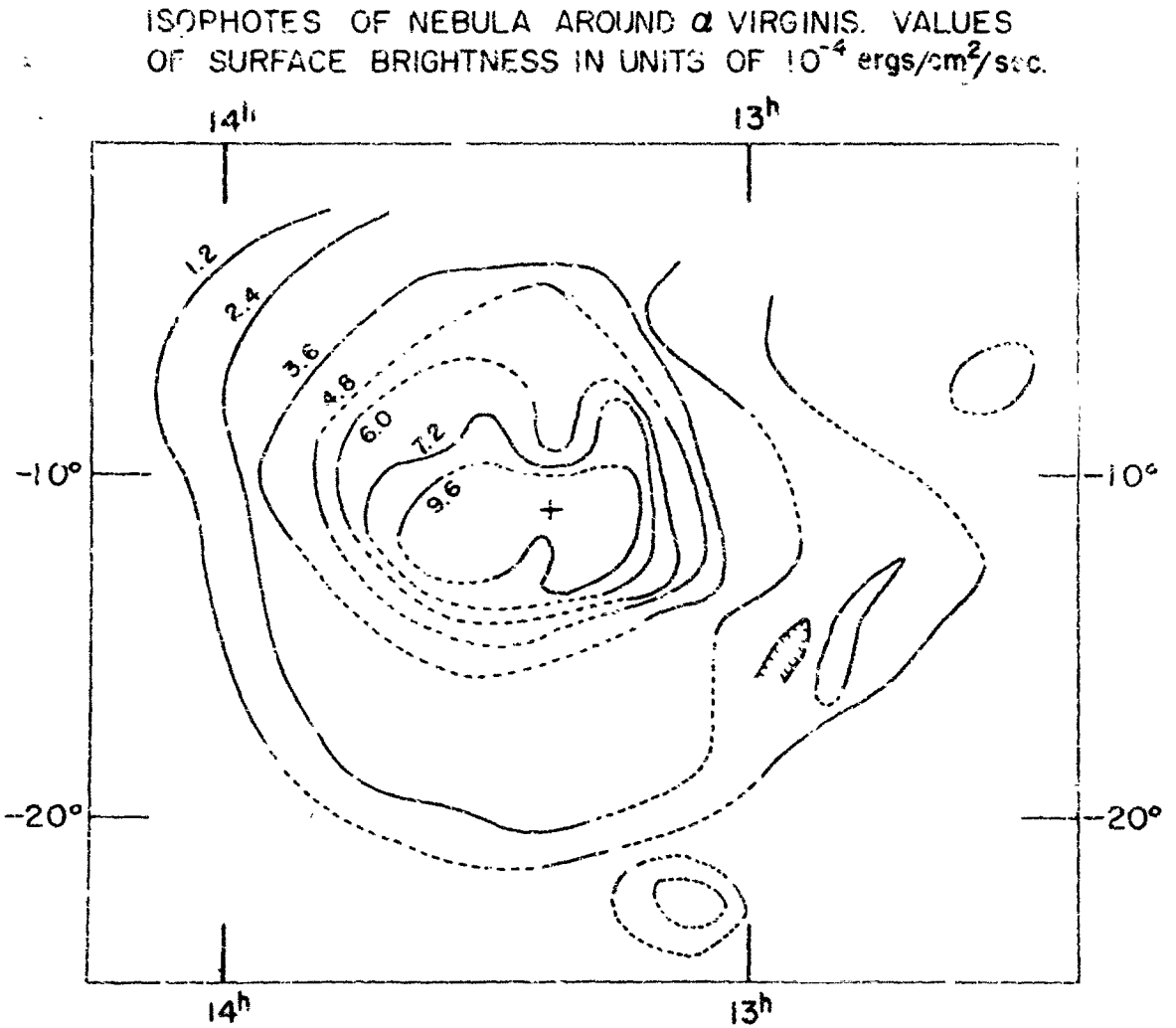

Figure 22:

Brightness contours of the hypothetical "nebular glow" in the neighborhood of Spica. This plot of brightness contours surrounding the star Spica was based on the amplitude of the responses of the Geiger counters shown in Figure 20. The question as to whether the extensive diffuse glow indicated in this plot is real has provided a cricual test of the nebular glow hypothesis, since Spica is an isolated bright early-type star. In the Spica region of the sky there exist no multiplicity of weak hot stars which would be mistaken for a diffuse source.

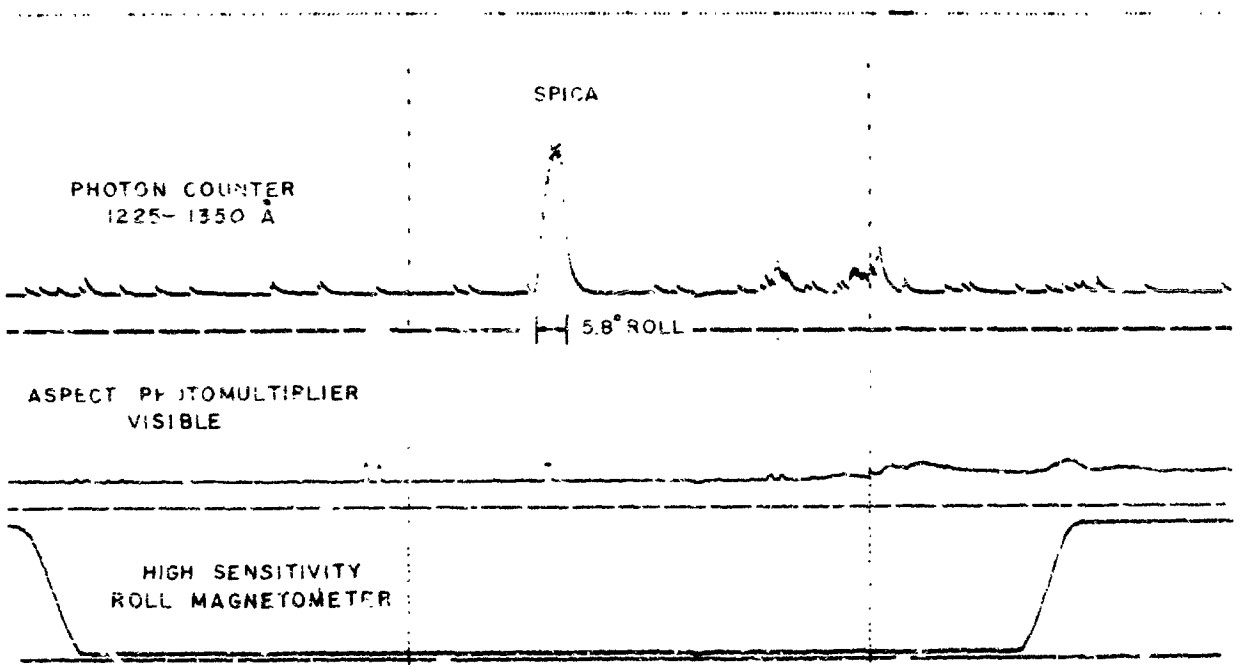

Figure 23:

Telemetry record showing the results of a 1963 photon counter experiment. In 1963 there was flown a collimated ultraviolet-sensitive Geiger counter, of the same type used in the 1957 experiment shown in Figure 21. This collimated counter scanned directly across the star Spica. The telemeter record of this figure shows that Spica appeared as a point source with no surrounding nebulosity. These results indicate that the diffuse character of the 1957 signals were not of celestial origin.

Figure 24

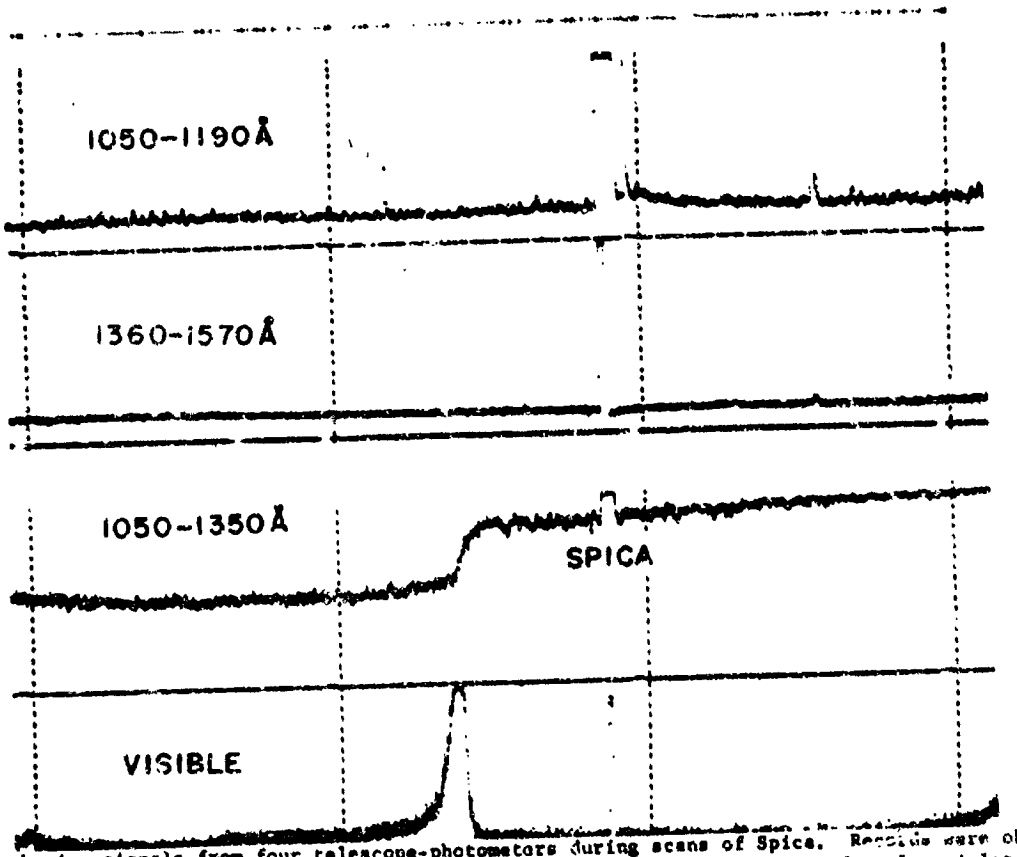

Telemetry record showing signals from four telescope-photometers during scans of Spica. Records were obtained of scans across the star Spica by three telescope-photometer combinations sensitive to different far ultraviolet wavelength bands. The figure shows that in each wavelength band Spica appeared as an intense point source producing more than full scale photometer response. The response of a telescope-photomultiplier combination sensitive to visible is also shown. Of particular interest is the 1050-1350 A photometer signal which shows the Spica signal riding on top of the signal produced by the night Lyman Alpha glow. The point source character of the Spica response means that no bright far ultraviolet nebular glow surrounds Spica even at the Lyman Alpha line. Also of interest is the different character of the horizon responses of the 1050-1350 A Lyman Alpha photometer and of the visible light detector. The bright horizon glow seen in the visible means that air is transparent to its emitted visible light, and the lack of horizon brightening in Lyman Alpha means that the radiation is strongly multiply scattered by atomic hydrogen in the upper air.

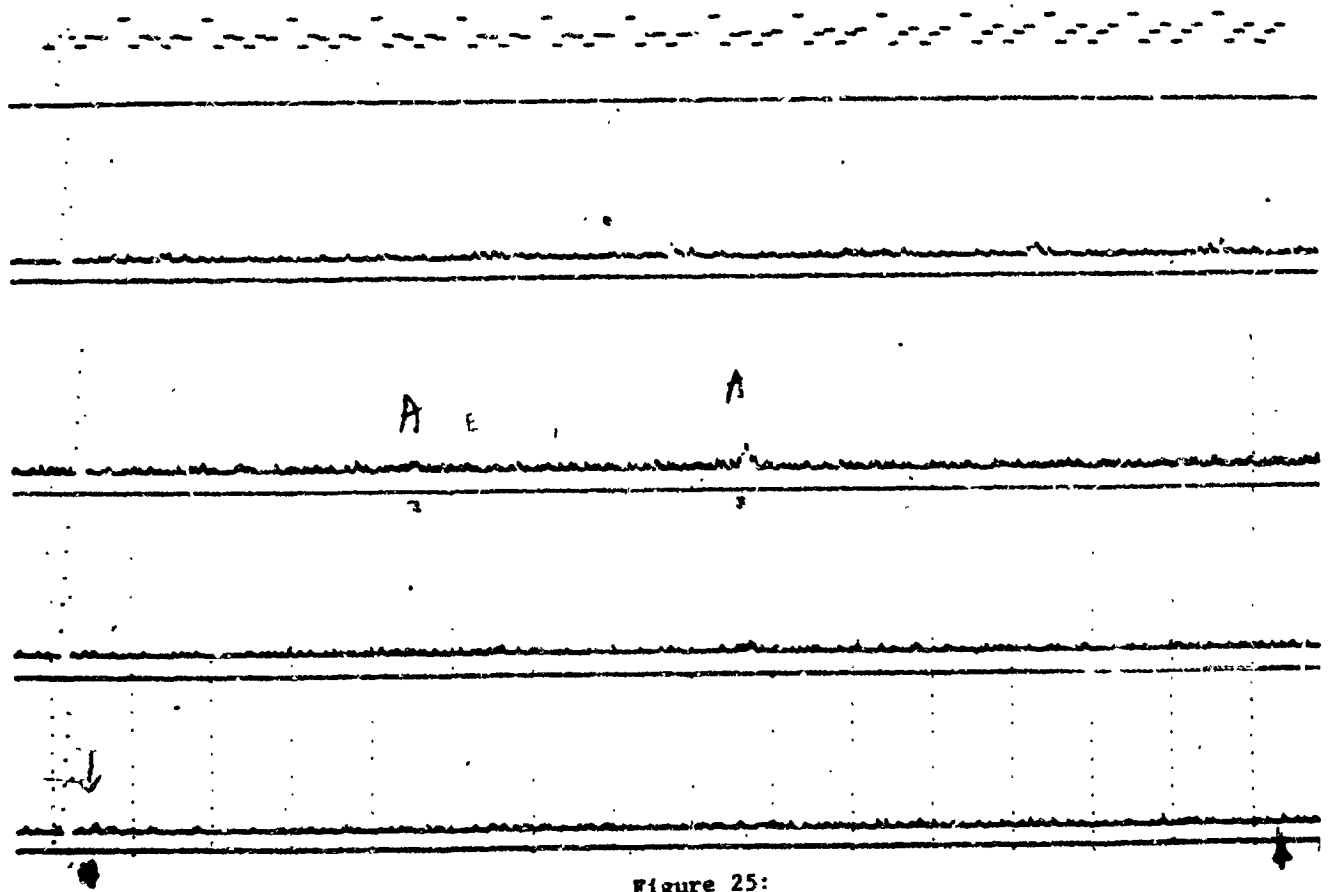

Figure 25:

Telemetry record of scans across the Scorpio x-ray source. A collimated soft x-ray detector of moderately large window area was flown in a celestial scan experiment in 1963. The detector was a combined set of 31 proportional counters. The output pulses were sorted into three amplitude groups corresponding to 0-1.5 A, 1.5-2.5 A and 2.5-8 B bands. The counting rates of each of the three wavelength bands are recorded as the lowest three traces of the figure. The 2.5-8 A twice shows the presence of an easily recognizable source, marked A, which is seen in two consecutive rolls. Solution of the rocket attitude problem has located the source center at 16 hours 15 minutes RA and -15.2 degrees latitude. A second much weaker source was located in the neighborhood of the Crab Nebula.

ATMOSPHERE OF VENUS

BY

CARL SAGAN

ASTROPHYSICAL OBSERVATORY

HARVARD UNIVERSITY

CAMBRIDGE, MASSACHUSETTS

ATMOSPHERE OF VENUS

by

Carl Sagan

The content of the talk presented at the Conference on Artificial Satellites is available from the following sources:

Sagan, C., "The Planet Venus," Science 133:849 (1961)

Kellogg, W. W., and C. Sagan, "The Atmospheres of Mars and Venus," National Academy of Sciences-National Research Council Publication 944 (1961)

Sagan, C., "Structure of the Lower Atmosphere of Venus," Icarus 1:151 (1962)

Sagan, C., and W. W. Kellogg, "The Terrestrial Planets," Ann. Rev. Astron. Astrophys., L. Goldberg, ed., 1:235 (1963)

Sagan, C., and L. Giver, "Microwave Radiative Transfer in the Atmosphere and Clouds of Venus," privately circulated paper (1961)

THE ATMOSPHERE AND SURFACE FEATURES OF MARS

BY

HYRON SPINRAD

JET PROPULSION LABORATORY

PASADENA, CALIFORNIA

THE ATMOSPHERE AND SURFACE FEATURES OF MARS

by

Hyron Spinrad

Jet Propulsion Laboratory

Although most of the papers presented here deal with results from satellite-based observations, or hopes for such results in the future, this review will deal with earth-bound observations of the planet Mars. The writer does not pose as an expert on the nature of the little red planet - only as a skeptical observer. Unfortunately, we really do not understand conditions on Mars well!

To preface this text, the writer feels willing to speculate that in the next few years new and provocative information on the Martian atmosphere and surface will come mainly from the old shopworn techniques of ground-based astronomy. Eventually space probe experimentation will reach the necessary level of sophistication to allow accurate in situ measurements of the various planetary parameters of interest. But the time is now ripe for major advances with existing equipment at almost negligible cost!

Much of this paper will follow closely the excellent review on Mars by Seymour L. Hess (1961). This work is recommended to the reader.

I. The Few Well-Known Data for Mars

The orbit of Mars lies outside that of the Earth and thus the times of closest approach occur at full Martian phase - these events are the Martian oppositions. The orbit of Mars is a fairly eccentric ellipse, so that some opposition occur when the planet is comparatively nearby and others at greater distances. Data on the next few oppositions of Mars are listed in Table I; unfortunately, the favorable oppositions occur when the planet is far south in the sky. This circumstance makes for difficult observing - most telescopes being located in the northern hemisphere.

TABLE I

Future Martian Oppositions

Date	Minimum Distance from Earth (miles)	Maximum Angular Diameter (secs. of arc)
March 8, 1965	61.7×10^6	14.0
April 13, 1967	56.2	15.4
May 29, 1969	45.3	19.1
August 6, 1971	34.6	25.0
October 21, 1973	40 6	21.6

Some of the physical data on Mars which we will employ later are tabulated in Table II - the inclination of the Martian equator to the ecliptic is similar to ours, so that Mars has seasons like the Earth, but almost twice as long since the Martian year is some 687 days.

TABLE II

Physical Data for Mars

Datum	Absolute Units	Relative to Earth
Mean distance from the sun	2.28×10^8 km	1.52
Mean diameter	6739 km	0.53
Length of day	$24^h\ 37^m$	1.001
Length of year	687 days	1.88
Surface gravity	377 cm/sec^2	0.38
Albedo	$\sim$ 0.15	0.4:

II. The Martian Surface

The telescopic appearance of Mars is beautifully illustrated in the new book by E. C. Slipher (1962). The best photographs in the Lowell Observatory collection, plus others like the color composite frontispiece, show much of the detail visible on the Martian disk. In most photographs made in yellow or red light - or the Kodachromes like Leighton's magnificient photograph on page 71 of Silpher's book - the Martian dark areas, called Maria, stand out against the brighter orange background. The most striking features are, of course, the white polar caps which expand to lower latitudes in the Martian winter and then retreat in Spring. The cap in the southern hemisphere never completely disappears.

The polar caps are certainly thin layers of water-ice; I shall call them frost-caps. The empirical evidence for the caps being frost is two-fold. They polarize light in the same way that tiny ice crystals do, and

their near-infrared reflection properties match those of frost (Kuiper 1952). The reflection spectrum of the Martian caps shows a rapid decrease from 1.5 μ to 2.0 μ, as does low temperature ice in the terrestrial laboratory. The reflection spectrum of solid CO_2 is quite different - and the formation of "dry ice" on Mars would require much lower temperatures than those measured near the polar caps. Calculations of the thickness of the frost-caps from their observed melting rate, and the estimated rate of solar heating at the surface, indicate the caps to be quite thin - perhaps in the order of one centimeter. The recent detection of Martian H_2O in the vapor phase is, naturally, compatible with the accepted frost composition of the Martian polar caps.

The dark areas, or Maria, on Mars have been a source of interest and controversy for some time. They were first thought to be seas, and then areas of thick vegetation. We now believe that both these early opinions are incorrect. Much of our information on the appearance of the Maria has come from drawings by experienced visual observers, or from photographs of small to moderate scale, made at Lowell Observatory, Pic du Midi in France, and other observatories. I believe this situation can be improved.

It is customary to say that photography with large reflecting telescopes doesn't really show much detail on the planets - not nearly as much as a good visual observer can see. This writer's experience suggests new attempts with fast film emulsions. Using telescopes of long focal length and large aperture (D $\geq$ 60 inches, say) fine detail on the surface of Mars probably could be photographed far better than they have been to date. Of course this would require significant amounts of valuable observing time under good seeing conditions. Whether or not the physical nature of the

Martian Maria could be uncovered by direct photograph alone is now unanswerable, but certainly the potentially great resolving power of the large earth-based telescopes should be brought to bear on the problem.

The Martian dark areas undergo a marked seasonal variation in contrast - they become darker and sometimes enlarge in their spring season - and then fade in the summer. In addition, non-periodic changes occur. For example, in 1954 Slipher noticed a reappearing dark Maria of considerable extent. These events are completely mysterious - how could a large dark region form in a short time and how can some dark areas apparently "regenerate" after a dust storm has covered them?

Can such changes be due to vegetation? There is a little, albeit crude, evidence on this question. Both Kuiper and R. S. Richardson have found that the dark areas do not have the characteristic near-infrared reflection properties of chlorophyll - and so the reflection spectrum of the Maria do not resemble those of most terrestrial planets near 1μ.

The most widely accepted evidence for organic matter on Mars - in the Maria, at least - is the detection by Sinton (1959, 1961) of the characteristics C-H vibration absorptions in 3.5 μ in the infrared spectrum of the dark areas. These bands do appear in terrestrial plants. The so-called "Sinton bands" are apparently absent in the spectra of the bright orange "deserts." The revised wave lengths of the absorption bands are 3.45, 3.58 and 3.69 μ. Colthup (1961) has pointed out that the 3.69 μ absorption coincides with a band of acetaldehyde and higher aldehydes. If this organic substance is in the gaseous phase, it is surprising that it only be observed over the Martian dark areas. Unfortunately, this region of the Martian infrared spectrum is close to the cross-over region of reflected solar and

emitted planetary radiation. The change of cross-over point and the slope of the emitted energy curve near 3.5 μ depends critically on the ambient surface temperature and this temperature will vary from the dark to the bright areas on Mars. Kea has pointed out that this complication makes the normalization of the Maria spectrum very difficult. It is hoped that there will be more observations of the Sinton bands on Mars and an attempt to find them on the Earth should seem obviously worth trying.

The bright orange areas of Mars gives the planet its red color. Kuiper's studies of the reflection properties of telluric rocks like iron oxides over the wave length region λλ 4000 - 25,000, do not match the Martian "deserts" well. The best spectral agreement was with pulverized brown felsite. From polarization curves of the Martian bright regions, Dollfus matches best with limonite - pure hydrated ferric oxides! These conclusions are in direct contradiction to each other! Apparently neither technique can provide a unique identification for a solid reflecting surface.

Recently, Kiess, Karrer and Kiess (1960) have advanced the hypothesis that NO_2 and N_2O_4 - the oxides of nitrogen in the solid and gaseous states, could account for the white Martian polar caps, the ruddy deserts and the darkening wave which progresses seasonally from pole to pole. However, neither Sinton nor Spinrad have been able to detect the presence of the infrared and red absorption bands of NO_2 in the Martian spectrum. Until such a detection is made, this theory should be considered quite speculative.

Several other Martian surface features, or the lack of them, deserve comment.

There appear to be no very high isolated mountains on Mars. Any high features could be detected by shadowing or by appearing as bright projections

on the terminator at quadratures. However, the presence of the thin Martian atmosphere tends to blur surface detail somewhat and estimates of maximum allowable heights of 5 - 10 thousand feet are probably too severe. There are no Alps or Himalayan ranges on Mars, we are sure. However, there are preferred locations for lingering frost near the south polar cap of Mars. They may be mountainous regions or an elevated plateau.

The famous Martian "canals" were originally discovered and called channels by Schiaparelli in 1877. Many astronomers have visually observed them as long, dark, rectilinear streaks extending for sizeable distances over the surface of Mars. They can occasionally be seen on the best photographs, too. Dollfus has observed canals under the best of Pic du Midi seeing conditions when they apparently break down into di connected fine detail - little spots and streaks which no longer have the continuity of a canal. We do not know what this fine structure is, but the broken canals are a characteristic surface feature of Mars, no matter what their geometry. Any comprehensive interpretation of the Martian surface must explain them - along with the polar caps, Maria and deserts. Lowell's canal hypothesis of a continuous system of artificial waterways has been abandoned by modern astronomers; there is not enough water to wet them anyway! The polar caps must sublime during the spring - they probably do not melt to any large degree.

The so-called Martian "wave of darkening" is the seasonal change of contrast of the Maria. Focas (1962) has shown that the dark areas in middle and high latitudes darken markedly in the spring as their polar cap begins to recede. The wave gradually extends to lower latitudes - down to the

equatorial regions. The average propagation velocity is about 35 km per day. Is this an exchange of atmospheric water vapor from one polar frost cap to the other? Slipher has argued for such an interpretation; he states instances of a cloud obscuring a dark area prior to its contrast increase (greater darkening - lower albedo). The amount of Martian atmospheric H_2O is very low, but even small amounts might be sufficient.

The surface temperatures of Mars have been measured by infrared radiometry; the first observations were made at Lowell Observatory and Mt. Wilson long ago and more recent measurements were made by Sinton and Strong in the 1950's (Sinton and Strong 1960). The emission in the 8-12μ window of the Earth's atmosphere originates mainly from the Martian surface; it is only slightly modified by the thin atmosphere of Mars.

With the 200-inch reflector at Palomar, Sinton and Strong measured Martian temperatures by allowing the planet to drift over a small diaphram which defined the entrance to their radiometer. The so-called drift curves were made parallel to the Martian equator and thus show the diurnal temperature variation on the ground at different latitudes.

Sinton and Strong found the <u>equatorial</u> temperatures to be near -60°C (213°K) at 0700 hours, a maximum of +22°C (295°K) at 1230 and then a decrease to about +10°C at 1400 hours. The minimum temperature expected - near 0500 - should be about -70°C (203°K), and thus the diurnal range is at least 90°C! This range is very extreme by terrestrial standards, and is due to the fact that the Mars atmosphere is thinner and much more arid than ours. The Martian Maria were found to be somewhat warmer than the bright deserts, the difference being about 8°C. This is in the sense to be expected, for the dark areas do not reflect much sunlight back to space.

III. The Molecular Atmosphere of Mars

The thin atmosphere of Mars makes the detection of its constituents by earth-based spectroscopic means a difficult task. Yet, this method does yield positive results. The polyatomic molecular constituents of the Mars atmosphere absorb radiation best in the infrared where our detectors are least sensitive and the Earth's own atmosphere is an effective screen. Luckily, these molecules do absorb sunlight weakly in the near-infrared and red when detectors are better and suitable stellar spectrographic equipment is available.

There are only two positively identified gases in the Martian atmosphere. In 1948 Kuiper detected small absorptions at 1.6μ and 2.0μ which are due to CO_2 on Mars. These Martian absorption bands are superimposed upon the weaker telluric bands of carbon dioxide. The second gas detected was water vapor; in April, 1963, Spinrad, Münch and Kaplan found some eleven weak Doppler-shifted Martian H_2O lines near λ8200 on a high dispersion spectrogram, taken with the Mount Wilson 100-inch reflector.

Figure 1 shows a composite tracing of four of the H_2O lines; the weak Martian component is indicated by an arrow. A. Dollfus in France also probably detected Martian H_2O from a high altitude site in 1963; his method was broad-band filter photometry around the 1.4μ infrared H_2O band. After comparison to the Moon, Dollfus suggested a small amount of H_2O for Mars. The Stratoscope II balloon flight of March, 1963 gave an upper limit to the Martian H_2O abundance which is compatible to the Mount Wilson detection result. Most of the determinations of the absolute amounts of both CO_2 and H_2O in the Martian atmosphere are dependent upon the total gas pressure at

the surface of Mars. Previous estimates for the CO_2 abundance, for example, vary from two to thirty times the amount above a unit area on earth - depending on how the pressure correction was made and what surface pressure was assumed. The reason for the pressure term in the Martian abundances is as follows: The shape of an individual planetary absorption line in a molecular band depends on the prevailing temperature which governs the Doppler width of the line, and the number and kinds of molecular collisions per unit time which determine the so-called Lorentz width. The Lorentz width is mainly dependent on pressure - and the dependence upon pressure is linear. Now the relationship between the strength of an absorption line and the number of absorbing molecules necessary to produce it is a somewhat complex function called the curve of growth. For very weak absorptions, the number of absorbing molecules is directly proportional to the measured amount of absorption - hence this part of the curve of growth is called the linear region. When the absorption is stronger, so that the line becomes very deep at its center, it becomes "saturated." That is, as more molecules are poured into the absorbing column, the absorption line grows at a slower rate than the increase in the number of absorbers would suggest. The rate of increase of absorption depends mostly on the line width - and thus on the pressure.

Now if we are fortunate enough to have observations of several weak and strong bands of CO_2 in the Martian atmosphere, then we can use the curve of growth to establish both the amount of carbon dioxide (from the linear part of the curve) and the total surface pressure from the observations on the strength of CO_2 bands lying on the saturated part of the curve of growth. It is amusing to consider that the principle of this technique, a relatively

common tool of the stellar astrophysicist, is being applied to planetary atmospheres for the first time. I will review the chronology of this work, now.

On April 12/13, 1963 Drs. Münch and Kaplan and the writer obtained a high dispersion spectrogram of Mars with the 114-inch Coudé camera of the Hooker reflector. The linear dispersion was 5.6Å/mm, over the wave length region λλ 7000 - 8000 on ammoniated IV-N (very fine grain and high contrast) emulsion. Our motivation was to use the relative velocities of the two planets (Mars was moving away at this quadrature - the velocity of recession was 15 km/sec on that date) to separate the telluric and Martian H_2O lines. We did find very weak Mars H_2O lines at the correct positions of 0.42Å to the red of their telluric counterparts in eleven cases - the best unblended or nearly unblended - lines in the λ8200 H_2O band. This was the first resolution of individual rotational lines of a molecule in the atmosphere of Mars - and also the first successful application of the Doppler shift technique necessary to move the very weak Mars H_2O lines off their strong telluric counterparts. We compute the abundance of H_2O on Mars to be about 10 μ precipitable H_2O; Dollfus estimates some 100 μ and the stratoscope upper limit was 40 μ. These amounts are not in good accord, but all are far less than the average amount of H_2O above the surface of the earth on a clear day - some 1 - 2 cm.! I should not forget to acknowledge the efforts of Dr. D. Rank and his associates at Pennsylvania State University for their laboratory calibration of the line strengths of the individual H_2O lines in the λ8200 band.

Just for amusement one afternoon we decided to look at the Mars spectrum near λ 8700 - the 5 ν_3 band of CO_2 is visible on Venus there. We

expected nothing, for the accepted amount of CO_2 on Mars was so small compared to that estimated for Venus that no CO_2 lines in this band should have been noticed, even with our high spectral resolution. Well, of course, the unexpected often happens in Astronomy - we could easily see the R-branch and some of the P-branch lines in this CO_2 band on Mars in the microscope.

We have since measured the CO_2 line strengths in this resolved band; unfortunately, the rotational lines are really very weak, ($\sim$4mÅ at maximum) and the resulting measurements are probably not very accurate. These lines are on the simple linear part of the curve of growth, and thus with another valuable laboratory calibration by Dr. Rank, we decided that the atmosphere of Mars contains about 70 meter-atmospheres of CO_2. That is about 27 times as much as over a unit area on Earth. Thus the curve of growth is anchored at the linear section. Now the determination of the surface pressure employs the published observations of Kuiper (1952) and Sinton (1963) for the CO_2 bands between 1 and 2 μ in the saturated regime. There is no place for all the details here, but we may approximate the surface pressure determination in the following way: for a band on the linear part of the curve of growth, the band strength W_1 is proportional to the amount of CO_2, m_1.

$$(1)\quad W_1 \sim m_1$$

and for a stronger band which is partly saturated, the band strength W_2 will depend upon the product of the amount m_2 and the pressure, P.

$$(2)\quad W_2 \sim \left(m_2\, P\right)^{\frac{1}{2}}$$

and since $m_1 = m_2$ because the actual amount of CO_2 is the same in either equation, we can solve for P if W_1 and W_2 are accurately measured, and the constants of proportionality known. This technique gives a resulting surface pressure of some 30 mb, and detailed work including self-broadening and temperature corrections move the pressure down to some 20 mb. The details of the computation are currently in progress, most of the work being done by Dr. L. D. Kaplan. We consider the estimate of 20 mb good to a factor two. The older polarimetric determination of the Martian surface pressure ($\sim$ 85 mb) may be suspect due to particulate scattering added to the assumed Rayleigh scattering by molecules.

If the Martian surface pressure is really this low, then CO_2 becomes a major constituent. The partial pressure of 70 meter-atm. CO_2 on Mars is about 4 mb, and the CO_2 content by mass is then some 4/20 = 20%. What is the remainder? Not H_2O or O_2 - the amounts of these gases are very low (<1%). The bulk of the rest is probably N_2 and A. Argon in the Earth's atmosphere has been radioactively generated in the crust from potassium - 40. If Mars received the same percentage of K^{40} as had the Earth's crust, it should have enough argon to exert a partial pressure of 5 mb - or some 25% of the atmosphere by mass. By default and analogy to the Earth, the remaining 55% should be N_2. But the reader should be warned that this mixture rests on uncertain foundations. The method used to determine the amount of CO_2 and the surface pressure is probably excellent, but the observations need improvement by repetition. And this requires a large reflector with a modern Coudé spectrograph. The cost of the raw material necessary for each observation is reasonable; $3.00 for the plates and $0.05 for the ammonia to sensitize them!

IV. Clouds and Blue Haze

In yellow and red light, the atmosphere of Mars usually is free of large scale cloudiness, at least in the center of the disk. There are often patches of cloud and haze near the evening and morning limbs and over the polar caps of the planet.

From time to time, clouds of varying sizes and color appear over significantly large areas of Mars. The most obvious ones are the yellowish clouds which are interpreted to be composed of dust stirred up by winds. In 1956, large yellow clouds and veils covered a large portion of the planet near the time of opposition.

There are also clouds which appear white; they are most prevalent over the cool regions of Mars where condensation of the small amount of atmospheric water vapor is most likely. Dollfus has found the polarization curves of these white clouds identical to those of terrestrial ice crystal clouds. The hypothesis that the white clouds of Mars resemble our ice-cirrus seems plausible.

The rather general Martian obscuration noticeable at shorter wave lengths in the blue and near ultraviolet, is called the "blue haze." It is usually optically thick enough to prevent the visibility of surface details on blue photographs. The amount of obscuration is variable and often patchy in extent.

Sometimes the blue haze clears away on a planet-wide basis. The time scale of the change is short, perhaps a day or two. The return to the usual blue opacity can also be sudden.

The cause of the blue haze is not understood. In conjunction with the large opacity in the violet, the planet's albedo drops off at short wave lengths, too. Mars reflects only a few per cent of the incident blue and near-ultraviolet sunlight.

Kuiper has shown that a high H_2O ice layer, with particle radii of about 0,2 μ could produce the measured polarization properties demonstrated by the blue haze. The ice-crystal hypothesis cannot explain the low ultraviolet albedo of Mars and Öpik objects to the theory on these grounds. He suggests an effect of pure absorption by a dark substance (like soot?) in some layer of the atmosphere. The photometric evidence for such an absorption in the blue comes from limb darkening curves by Barabashev and Chekardc (1952) made with a small instrument. On large scale blue photographs, the images of Mars seem to show some limb brightening - this would rule against pure absorption in favor of scattering. How either process, absorption by a dark constituent like carbon particles or scattering from ice crystals, can change rapidly on a large geographical scale is very mysterious.

V. Observations For The Future

Besides the conventional optical and radio observations from the ground, which will continue to add to our knowledge of Mars for the next few years, space experiments will eventually also contribute.

The NASA-JPL Mariner series includes a fly-by Mars probe schedule for 1964. The scientific instruments on board to observe Mars itself include a magnetometer, a television (vidicon) system and possibly a two-channel ultraviolet photometer.

In the future, as the allowable payloads become heavier and the equipment more sophisticated, there will undoubtedly be flights of infrared spectrometers and eventually, landing capsules for direct measurements.

What will the experiments tell us? The television will present a picture of the Martian surface with an order of magnitude better resolution than achieved so far from Earth.

The ultraviolet photometry experiment will look for the Lyman α emission from a Martian atomic hydrogen Corona, and possibly may also study the distribution of atomic oxygen around the planet.

An eventual infrared spectrometer, if capable of high resolution at long wave lengths, near the 4.8 μ CO_2 band could provide useful information on the atmospheric composition and structure and perhaps some data on the presence of surface hydrocarbons - the important bands are near 6 μ. The Martian surface will probably be visible in emission at this wave length if our estimate of the H_2O abundance is correct. But are there C-H bond emissions?

The landing capsule pertains a whole new era in planetary observations - and the potential of <u>in situ</u> observations is so great that it seems unwise to speculate now on their nature or results. They are still for the future. This is an exciting age for the planetary observer. In his lifetime he will <u>know</u> whether his earth-bound conclusions were correct or not!

Figure Legend

Figure 1.

The average profile of four H_2O lines in the Mars spectrum. The calculated position of the Martian component ($\Delta\lambda = +0.42\mathring{A}$) is indicated by the arrow below the Mars symbol; the faint Mars water-vapor line is visible there.

References

1. Barabashev, N. P., and Chekirda, A. T. (1952), Ast. Tsirk, Khurkov Obs. 9, 3.

2. Colthup, N. B., (1961), Science 132, 529.

3. Focas, J. H., (1962), Planet. Space Sci., 9, 371.

4. Hess, S. I. (1961), "Mars as an Astronautical Object," in "Advances in Space Science and Technology," F. I. Ordway, ed.

5. Kiess, C. C., Karrer, S., and Kiess, H. K. (1960), Publ. A.S.P., 72, 256.

6. Kuiper, G. P. (1952), "Atmospheres of the Earth and Planets," (Chicago: Univ. of Chicago Press), Chapter 12.

7. Sinton, W. M. (1959), Science 130, 1234.

8. Sinton, W. M. (1961), Science 132, 529.

9. Sinton, W. M. (1963) - to be published.

10. Sinton, W. M., and Strong, J. (1960), ApJ 131, 470.

11. Slipher, E. C. (1962), "A Photographic History of Mars, 1905 - 1961," Lowell Observatory, Flagstaff, Arizona.

AVERAGE MARS H_2O LINES

λ_o=8176.97, 8189.27, 8226.96, 8282.02

SOLAR FLARES AND THE ASSOCIATED EJECTION OF PARTICLES

BY

EINER TANDBERG-HANSSEN

HIGH ALTITUDE OBSERVATORY

BOULDER, COLORADO

SOLAR FLARES AND THE ASSOCIATED EJECTION OF PARTICLES

by

Einar Tandberg-Hanssen

High Altitude Observatory

154 92

Abstract.

Of the main sources of extra-terrestrial hazards to manned satellites the solar flare phenomenon is perhaps the least understood. Great flares may emit both hard X-rays and relativistic particles that can be potential dangers to space travellers as well as to sensitive equipment.

We have some forecasting ability in the case of flares, but much more is desired, both from a practical point of view as well as for purely theoretical reasons. Further progress is not likely before a better understanding of the physics of the flare phenomenon is obtained. Even though there can be little doubt that the physics of flares is intimately linked with the presence of strong magnetic fields in neighboring sunspots, an acceptable theoretical explanation for the formation of flares is at present not available.

Author

I. Introduction.

There are several extra-terrestrial phenomena that are potential hazards to future space travelers. We mention:

1. Collisions with meteorites
2. Radiations from the van Allen belts
3. Effects due to flares.

Flares may emit both hard X-rays and relativistic and nonrelativistic particles. Since the problem of solar X-rays emission has already been treated at this conference, as have the problems of meteorites and van Allen belts, I shall restrict myself to a study of the particle emission.

II. Historical Remarks.

In recent years solar protons have been observed many times at ground level as well as by airborne equipment. However, it was probably in 1933 that solar protons were first recorded. In March of that year a balloon was flown over Stuttgart, Germany and an ionization chamber registered a pronounced increase in cosmic rays simultaneously with the passage over the central part of the solar disk of an active sunspot region. There is no record of a flare occurring but this may be due to lack of observations in those days.

The first instance where a flare was seen simultaneously with the observation of increased cosmic ray counts occurred on June 20, 1941. A coincidence counter in Friedrichshafen, Germany registered this event which apparently was due to an importance 2 flare.

With the great sunspot group of February 1942 came the now famous flare that was responsible for protons with energies as high as 10,000 MeV. This case is also noteworthy since it led to the discovery of solar radio bursts, generated by the flare activity.

Since World War II solar protons have been observed many times. Of special interest is the great flare of February 23, 1956. This case was extensively studied and was to a large extent responsible for the rapid growth of the new solar-interplanetary space research. Then came the Sputnik era. On November 7, 1957 the first observation of solar protons was recorded by Spucnik II. On April 12, 1959 Lunik II observed the heavy particle component of solar cosmic rays, and Pioneer V observed both protons and electrons and/or γ-rays on April 1, 1960.

All of these events seem to have been caused by great or very great flares, but - as already pointed out by Firor nearly a decade ago - small flares may also have a noticeable effect.

III. Flares - A Description.

On rare occasions flares may be observed in white light, i.e., they emit a sufficiently strong continuous spectrum to be noticed as a brightening against the darker - but still quite bright - photosphere. The customary way of observing flares are, however, by recording the emission of some spectral line - the Balmer lines of hydrogen for example, or the H or K line of ionized calcium. This may be accomplished by a narrow filter, centered on the line, or by a spectrograph, selecting the proper line. When viewed by these techniques the flare looks bright against the disk of the sun or, if observed at the limb, against the dark sky background.

The flares always occur in pre-existing bright plage areas in the vicinity of sunspots. The area of flares varies from about 10^{17} cm^2 for smaller flares to as much as 10^{20} cm^2 for big flares. Customarily, the importance of a flare is a measure of its area. When the area is measured in millionths of the sun's hemisphere (for conversion the sun's radius is approximately 700,000 km) we give the importance of the flare according to Table 1.

Table 1

Area of flare in millionths of the sun's hemisphere	Importance
<100	1-
100 to 250	1
250 to 600	2
600 to 1200	3
>1200	3+

The energy output in the line emission is about 10^{30} ergs for an importance 2 flare and may be as much as 10^{32} ergs for the biggest 3+ flares.

The temperature of the radiating gas in flares is about 10,000°K or slightly more, and the density 10^{11} to 10^{12} particles per cm^3. If the 10^{32} ergs come from a flare of area 5×10^{19} cm^2 this would correspond to a flux of 2×10^9 ergs/cm^2/sec. For comparison the radiant energy flux from the quiet photosphere is 6×10^{10} ergs/cm^2/sec.

IV. Flare-associated Phenomena.

There are a number of phenomena in the solar atmosphere that seem to be more or less intimately linked to the occurrence of flares. We mention:

a. Surges - dark or bright prominences shooting away from the flare and apparently triggered by the flare.

b. Radio bursts of Type II and IV seem to be caused by flares.

c. Coronal emission. This is emission from highly ionized metal atoms and occurs often in the corona surrounding flares.

d Sudden disappearance of quiescent prominences seems to be initiated by some kind of disturbance originating in flares.

e. Cosmic rays, high energy particles, are - as we have seen - often expelled from flare regions. The physics of this process is not understood, but is one of our main concerns.

f. Particles responsible for the van Allen belts, aurorae, and geomagnetic storms are likewise expelled from flare regions. They have much lower energy than cosmic ray particles, and take of the order of a day to travel from the sun to the earth while cosmic ray particles traverse this distance in approximately one-half hour.

All these different phenomena should be taken into consideration when we want to derive a flare model and to find a theory to explain the flare itself.

V. Physics of Flares and the Ejection Mechanism for Cosmic Ray Particles.

Since some flares, but far from all, emit energetic cosmic rays there must be some characteristics that determine a cosmic ray flare. Several criteria have been investigated but no one will uniquely determine a cosmic ray flare. We may say that when several of the following characteristics are present there is a good chance of observing increased cosmic ray activity:

1. The flare is accompanied by a Type IV radio burst
2. Part of the flare covers the umbra of the sunspot
3. The flare produces a polar cap absorption, i.e., increased D-layer ionization by 10 - 100 MeV protons.
4. The flare occurs on the western half of the sun's disk - thereby facilitating the arrival at the earth of the particles following curved paths (effect of sun's rotation).

It is still a matter of controversy whether the ejection of particles is to be traced to more or less intrinsic properties of the flare itself (criteria 1, 2 and 3 above) or whether the geometry of the sun-earth configuration (criterium 4) is of prime importance.

The nature of the flare itself is still also a matter of great uncertainty. One often reads or hears the statement that flares are caused by the annihilation of pre-existing magnetic fields. It is true that the fields that exist around sunspots have enough energy to account for the approximately 10^{32} ergs required for a good-sized flare. This amount of energy could for instance be made available by the conversion of all the magnetic energy in a 500 gauss field occupying a cube whose side is 2×10^4 km.

But the difficulty is that no process is known that allows a rapid enough conversion of the magnetic energy. Probably the only hope of a solution along these lines is the possibility of applying to the solar plasma the instabilities recently discovered in some plasma machines. These instabilities due to density gradients seems to be able to destroy magnetic fields very efficiently. The physics is, however, still not well enough understood to allow a meaningful application to flares.

Charged particles can be accelerated to high velocities in a changing magnetic field and it has been suggested that such acceleration is responsible for the ejection of cosmic ray particles from flares. There may be observations to support this point of view. Some authors claim that the magnetic field changes rapidly with the onset of a flare, but others do not seem to find this.

Thus, not only our understanding of the physics of flares themselves but also the theory for the ejection mechanism for cosmic ray particles are still quite rudimentary.

VI. The Possibility of Flare Prediction.

We have heard Dr. Roman's exciting report that some forecasting ability may soon be developed in the case of micro-flares. When it comes to the great cosmic ray flares we can, however, still do very little. It is true that we can give the general rule that such flares are not infrequent at times of sunspot maximum (roughly every 11 years) whereas they are next to non-existing near times of minimum. But this is hardly to be labeled forecasting.

Also, we can say that great flares occur near complex sunspot groups, and for the time being it is along these lines that the forecasting may develop. So the best we can do is to watch the growth of sunspots and if a group develops a complex pattern, chances for flares to occur increase greatly. This may be of some help for short-term missions in space (maybe up to a week), but on a longer time-scale our forecasting ability is extremely poor. As we have seen, this is mainly due to lack of understanding of the flare itself and of the necessary conditions for flares to occur in a given region on the sun.

Consequently, additional theoretical work is of the greatest importance for the future of flare forecasting, and hence for space travel.

METEOROLOGICAL AND COMMUNICATION SATELLITES

TIROS - THE FIRST METEOROLOGICAL SATELLITE

BY

ROBERT M. RADOS

TIROS PROJECT MANAGER

GODDARD SPACE FLIGHT CENTER

GREENBELT, MARYLAND

TIROS - THE FIRST METEOROLOGICAL SATELLITE

by

Robert M. Rados
Goddard Space Flight Center

INTRODUCTION

In the comparatively short time available, I would like to

Describe the TIROS system

Show some of the results

Outline the future programs

Before discussing the TIROS system we must first ask why there is a need for a meteorological satellite. The atmosphere is a global phenomenon that is constantly in motion - motion produced and influenced by complex interaction of many events, such as unequal heating by the sun, the effect of terrain irregularities, and the rotation of the earth. These events take place in the lowest 10 to 15 miles of the atmosphere.

Weather knows no political boundaries. The meteorologist must observe, describe, and understand the behavior of the atmosphere over a large portion of the globe if he is to explain and predict weather in any locality for any purpose. Some types of weather phenomena are short lived; they last only several hours. Therefore, accurate analysis and prediction of weather phenomena require both a rapid means of real-time observation and rapid transmission of these observations.

The observations available to the meteorologist before TIROS were those made in the inhabited areas of the world, or from balloons or aircraft. Atmospheric events in deserts, the polar areas, and oceans were undetected. Only when events moved out of these uninhabited areas did their presence become known, often too late to do anything for the protection of life and property. For example, hurricanes form over ocean areas near the equator and the first warning to a ground observation system occurs when the hurricane strikes a ship, an island, or a coast line.

The meteorological satellite can provide fuller coverage of atmospheric events. With adequate sensors, it also can detect phenomena such as tornadoes and thunderstorms which exist in the inhabited areas but between the normal observational network.

The type of data which satellites provide is different from other observations and therefore contributes not only to operational meteorology but to a more complete understanding of atmospheric events. A satellite can view an entire storm as opposed to only partial observation by other means. It can measure the balance between the solar absorbed and reflected radiation.

The meteorological satellite is not going to solve all weather problems, but it is a major tool in the solution of many problems.

THE TIROS SYSTEMS

TIROS is an acronym for television and infrared observation satellite. The TIROS program was developed for two basic purposes: to demonstrate the technical feasibility of obtaining meteorological data, and to demonstrate the practical utility of the data obtained. To date, seven TIROS satellites

have been launched, at a rate of two per year from 1960 to 1963. TIROS VI and VII are now in routine operation.

The TIROS program can be divided into four systems:

The TIROS spacecraft, which observes the earth and its cloud cover and transmits data to the earth

The three-stage Delta launch vehicle used to place the spacecraft in orbit

The ground stations used to command and control the satellite and to acquire data

The data utilization system, which distributes meteorological information to the scientific community

TIROS SPACECRAFT

The spacecraft includes:

Television subsystems to view the earth's cloud cover and surface

Infrared subsystem to detect the earth's emitted and reflected radiation characteristics

Associated transmitters and receivers for command and data handling

Control and telemetry circuitry for spacecraft stabilization, housekeeping, etc.

The spacecraft has considerable flexibility and the subsystems vary somewhat from one TIROS to another, depending on specific mission requirements.

The spacecraft measures 22½ inches in height and 42 inches across (Figure 1). It consists of a reinforced baseplate and a cover assembly composed of a top frame and 18 side panels (Figure 2). The four elements of the transmitting antenna project from the baseplate and the receiving whip antenna projects from the cover assembly.

The cover assembly provides an unobstructed exposed mounting platform for the solar cells, attitude sensors, and horizon scanners. The attitude control, precession dampers, and despin mechanism are also mounted on the cover.

The majority of the spacecraft components are mounted on the baseplate (Figure 3). The TV camera and two of the IR radiometers observe through openings in the baseplate and cover assembly. Two sets of omnidirectional infrared sensors project from the baseplate on radially opposed booms.

Television Subsystems

The TIROS television subsystems provide both direct and remote picture-taking capabilities. Two types of camera systems are currently available: the recording television subsystems, flown on all TIROS launches to date, and the recently developed automatic picture transmission (APT) system, scheduled to be flown on certain future launches.

Recording Television Subsystems - The recording television subsystem consists primarily of a TV camera and circuitry for magnetic tape recording and TV transmission. Two complete units, capable of concurrent or independent operations, can be flown. The cameras operate in either of two modes: direct picture taking and transmission without storage, within range of the data acquisition stations, or recorded-picture taking and magnetic tape storage over remote areas. In the record mode, one or both cameras may be programmed by ground command to take and store a series of 32 pictures at 30-second intervals over prescribed remote areas. Stored data readout and subsystem programming are accomplished during the next pass over a data acquisition station.

The cameras are mounted on the baseplate of the spacecraft with their optical axes parallel to the spin axis of the spacecraft. The field-of-view and resolution of each camera vary with lens selection (wide angle, narrow angle, etc.) and spacecraft orbital parameters (altitude and nadir angle). One and one half milliseconds exposure time is required to eliminate picture distortion due to spacecraft orbit and spin motion. This function is provided by an electromagnetic focal-plane shutter and suitable timing circuitry.

The TV tubes are 500-scan line 1/2-inch vidicons with a persistence that permits a 2-second scan with less than 20 percent degradation in picture quality.

Sufficient tape is provided for recording 32 frames at a speed of 50 inches per second. During recording, the mechanism operates only during individual frame recording; during play-back, the mechanism runs continuously (at 50 inches per second in the reverse direction) until all the tape has been transferred and the end-of-tape switch actuated. The tape is erased immediately after playback, and again just before recording.

APT Subsystem - The APT subsystem is designed to provide wide-angle cloud cover pictures in real time. The equipment employs the same basic principles as the TV camera - a camera-vidicon arrangement designed to operate from a spin-stabilized spacecraft. The APT subsystem takes and transmits pictures continuously on command during sunlit portions of the orbit.

The APT vidicon is similar to the TV vidicon except for the addition of a polystyrene layer to provide extended image storage capability. The tube is operated through the prepare, expose, and readout phases by varying the mesh potential with respect to the target potential. The image is projected on a prepared photoconductive layer, then transferred by potential change to the

storage layer for readout. The prepare, expose, and transfer operations are accomplished during the first 8 seconds of each 208-second picture cycle, the remaining 200 seconds are required for readout at a scan rate of 4 lines per second.

The vidicon output is transmitted to local APT ground stations, where the TV picture is reproduced by facsimile for immediate local use.

Radiometer Subsystems

The radiometer subsystems are designed to perform infrared and visible radiation measurements in selected spectral regions. These data provide the basis for analysis of radiation distribution for various regions for measuring the earth's heat budget, and for measuring the attenuating effects of water vapor in the atmosphere (Figure 4).

Three types of sensors have been flown: the scanning radiometer, the nonscanning radiometer, and the omnidirectional radiometer. The functions and objectives of the radiometers are:

> The scanning radiometer measures the emitted and reflected radiation of the earth and atmosphere over five channels ranging from 0.2 to 30 microns.
>
> The nonscanning radiometer, last flown on TIROS IV, measured the total radiation from the vicinity of the earth in the 0.2 - to 50-micron region and, separately, the radiation emitted by the earth in the 5 - to 50-micron region.
>
> The omnidirectional radiometer provided measurements for determination of the earth's thermal radiation characteristics.

The IR recorder records continuously except during playback, erasing immediately before recording. A 200-foot endless-loop mylar tape provides full

orbit coverage at a recording speed of 0.4 inches per second. Upon interrogation, the tape is played back at 12 inches per second through the 237-Mc IR subsystem transmitter.

Command and Control Subsystem

The command and control subsystem receives, stores, and executes command and data acquisition (CDA) station commands that control the various spacecraft and subsystem operations. The subsystem consists primarily of a 148-Mc receiver, decoder, and bandpass network. The unit receives and demodulates the tone-modulated CDA station transmissions and channels the various commands (represented by a series of audio-frequency tones) into the proper control and programming circuits. Operating in conjunction with subsystem switching circuitry for immediate action, and with subsystem clocks for remote operation, the system controls the following functions:

Direct TV picture transmission

Recorded TV and IR data transmission

TV subsystem programming for remote operation

Telemetry transmission

Spinup rocket selection and firing

Beacon transmitter switching

Operation of the magnetic attitude control

Command Functions - All command functions are performed when the spacecraft is within communications range of a CDA station. The CDA stations are so located that at least one will be within communications range for a minimum of 6 minutes for an average of eight of the 14 orbital passes each day. During a pass

over a station the recorded TV and IR data are transmitted The TV subsystem is programmed for remote operation, and stored or direct TV is transmitted.

Direct Picture Transmission Commands - Direct TV pictures are taken and transmitted directly to ground while the spacecraft is within radio range of a CDA station. Either camera may be used or both may be employed alternately. Two sequences of pictures (one before and one after recorded data transmission) are possible depending upon the selected duration of each picture sequence and spacecraft pass time.

Recorded TV Data Transmission and Programming Commands - Recorded TV data playback follows direct camera sequence. TV tape-recorder readout sequence is selected to eliminate transmitter warm-up time by employing the camera subsystem transmitter in operation at the time of switchover from direct to playback mode of operation. Start of a playback sequence causes the direct picture-taking sequence to end immediately regardless of direct sequence programming. Four playback selections are available: camera 1 only, camera 2 only, camera 1 then 2, and camera 2 then 1.

Programming the TV subsystem for a remote picture-taking sequence takes place during readout and transmission of the previously recorded picture data. Either, neither, or both camera subsystems may be programmed. However, each subsystem clock is set independently; that is, subsystem 1 clock is set during playback of subsystem 1, and subsystem 2 clock during subsystem 2 playback. A pulse from the CDA station master clock starts the spacecraft clocks. If only one camera subsystem is programmed for remote operation, the pulse must occur either at the end of that camera playback sequence, or at least 40 seconds after the

start of direct camera sequence II. When both subsystems are programmed the pulse must occur after 40 seconds of direct camera sequence II.

Recorded IR Data Transmission Commands - The IR equipment operates continuously, recording at all times except during playback. Two seconds after playback of the TV data begins, a time-reference pulse from the CDA station master clock is recorded on the IR tape, indicating the end of the IR recording cycle. Actual playback of the IR data begins 20 to 25 seconds later upon completion of TV data playback.

Stabilization and Control Subsystem

The primary requirements of the stabilization and control subsystem are to orient and spin-stabilize the spacecraft. Proper selection of the ratio of principal moments of inertia, together with an internal energy absorber, permit the spacecraft to be spin-stabilized without wobble or precession about the desired spin axis.

Precession Damping - Precession damping is accomplished by two turned energy-absorption mass (TEAM) mechanisms installed vertically, 180 degrees apart, on the spacecraft inside wall. The TEAM mechanisms convert the kinetic energy, tending to cause the spacecraft to precess.

Spin Rate Reduction - The spin-stabilized third stage of the launch vehicle imparts a spin rate of approximately 120 rpm to the spacecraft at separation; however, optical considerations require that the spacecraft spin rate be reduced to approximately 12 rpm before TV subsystem operation. Effective spin-rate reduction is provided by a despin device, known as a yo-yo mechanism, consisting of a pair of cable-attached masses affixed at points 180 degrees apart on the

periphery of the spacecraft. During launch and injection, the cables are wrapped around the spacecraft and the masses are secured by squib-actuated release mechanisms. After spacecraft separation the despin release circuitry (or, if required, a ground station back-up command) frees the masses, permitting centrifugal force to unwind the cables. As the cables unwind, kinetic energy is transferred from the vehicle to the despin masses. When the cables extend radially from the spacecraft, sufficient energy has been transferred to accomplish the required reduction in spin rate. The cable-attached masses then slip from open hooks and separate from the spacecraft.

Spin-Up Rockets - Because of the "drag" effect of the interaction between the earth's magnetic field and the magnetic material in the spacecraft, the spin rate would eventually drop below the desired 9-rpm minimum. To maintain the spin rate within acceptable limits, 9 to 12 rpm, five diametrically opposed pairs of solid-propellant rocket motors are mounted around the periphery of the spacecraft baseplate. When fired in pairs, by ground command, the motors provide a 3-rpm increase in spin rate to compensate for the "drag" effect.

Attitude Control Device - The attitude control device consists primarily of a 250-turn coil of aluminum wire wound around the periphery of the spacecraft and a pulse-controlled, solenoid-operated stepping switch. The stepping switch, operating in response to ground station commands, permits the coil to be energized in either direction (current flow) at six voltage values from zero to 6.3 volts. Each change in current effects a corresponding change in the induced magnetic field of the spacecraft, providing, through the interaction of the magnetic fields of the spacecraft and the earth, the mechanical force necessary for attitude control.

Position Indicators

Attitude Indicator Subsystem - The attitude indicator consists of a narrow-field (1-degree by 1-degree) infrared bolometer, complete with differentiating and amplifying circuitry. The sensor, mounted with its optical axis perpendicular to the spin axis of the spacecraft, scans space below as the vehicle rotates. The sensor spectral response (flat between 7 and 30 microns) and time constant (2.0 milliseconds) are selected to provide an accurate response to the earth's heat output during the horizon-to-horizon portion of each scan. The occurrence and duration of the earth's heat pulse constitute the indicator output.

In operation, the output of the sensor is differentiated to avoid de-amplifier and temperature stability problems, and is amplified prior to transmission from the spacecraft. The leading and trailing edges of the "earth pulse" are amplified to provide a nominal 5-volt peak-to-peak analog signal. The analog signal frequency modulates the 1300-cps beacon oscillators, which in turn amplitude modulate the beacon transmitters. The attitude-indicator output is transmitted continuously except during telemetry transmission.

Simply, this subsystem allows us to locate the spacecraft relative to the earth.

North Indicator - The north indicator consists of a series of nine light-sensitive sensors mounted behind vertical slits spaced evenly around the periphery of the spacecraft. Rotation of the spacecraft causes the sensors to view the sun sequentially. Each sensor is connected to a one-shot multivibrator that produces a coded pulse (short, medium, or long pulse duration) when triggered. Sensor-mounting sequence provides pulse width combinations that permit determination of sensor position (with respect to a zero reference line) from the output of two

sensors. The sun-angle pulses are shaped and amplified by the north indicator electronics for transmission with the TV data. Actual north indication is computed from this sun-angle information and spacecraft spin rate at the ground station.

Again, simply, this indicator allows us to orientate the spacecraft with respect to the sun.

Spacecraft Telemetry Subsystem

Two telemetry switches are provided in the satellite, one associated with each beacon transmitter. The output of these switches amplitude modulates each beacon transmitter upon receipt of a command from the CDA stations.

All telemetered information is in the form of a dc voltage lying within the limits of ± 2.5 volts. Various spacecraft temperatures and functional parameters of each subsystem are monitored, the telemetry switch dwell time being approximately 1 second for each of its 39 contacts, stepping automatically until it reaches step 40, the last position.

Communications and Data Handling

The TIROS communications system provides the radio links for receiving ground-command signals and for transmitting tracking, telemetry, and experiment intelligence from the spacecraft. Spacecraft transmitting capabilities are provided by radio links consisting of:

Beacon transmitters (136.23 and 136.92 Mc)

TV transmitter (200-Mc band)

IR transmitter (237 Mc)

APT transmitter (136.95 Mc)

Antenna Subsystem

The antenna subsystem consists of a transmitting antenna and a whip or dipole receiving antenna

The transmitting antenna is made up of a pair of crossed dipoles fed in quadrature to produce circular polarization. Each of four radiating elements (mounted radially on the lower surface of the spacecraft) consists of a 32.5-inch rod (0.36 wavelengths at 135 Mc), which also serves as the center conductor of a coaxial sleeve extending 12 inches (¼ wavelength at 235 Mc) from the base end of the rod. The rod and sleeve are connected at the base and to form a short-circuited transmission line within the sleeve. Suitable matching and coupling networks permit the system to transmit each of three frequency bands with sufficient isolation between transmitters to prevent interaction.

The receiving antenna is a separate ¼-wave monopole positioned vertically at the top-center of the spacecraft (the neutral plane of the crossed dipoles). By virtue of this positioning, approximately 45-db attenuation is achieved between the transmitting and receiving antennas preventing transmitted energy from blocking the receiver.

Thermal Control

A combination of passive thermal-control techniques are employed to provide acceptable average temperatures throughout the spacecraft. The techniques employed include:

Proper absorptivity/emissivity ratio surfaces and surface coatings

Construction techniques and material selection that provide a suitable heat flow pattern

Solar cell filters

The top and side surfaces of the spacecraft are subjected to the greatest incident energy flux and are therefore provided with surface coatings that reject the maximum amount of energy. Owing to the large area-to-mass ratio of these surfaces, however, the temperature would tend to exceed desired limits if only radiation cooling were used. To prevent overheating and to increase the temperature of the lower surfaces, the structural design permits maximum radiant energy exchange. All possible interior surfaces are blackened and thermal resistance is minimized by providing adequate heat flow paths.

Power Supply

Power is obtained from the conversion of solar energy by silicon cells located on the top and side surfaces of the spacecraft. The cell requirement (9,200 1-cm by 2-cm cells) is based on the variation in load due to spacecraft and experiment demands during light and dark periods; the period of coincidence of illumination time versus interrogation time; and an analysis of cell mortality on previous satellites. The cells are connected in series-parallel arrangements based on the voltage current requirements of the spacecraft in conjunction with the fluctation in illuminated cell area due to spacecraft rotation and orbital day duration. Power is stored in 21 series-connected nickel-cadmium cells.

LAUNCH VEHICLE

The launch vehicle for TIROS I was a Thor-Able; however, all subsequent TIROS spacecraft were launched by the three-stage Delta consisting of a Thor first stage, Aerojet General second stage, and an Allegheny Ballistic Missile third stage (Figure 5). Stages one and two are liquid; the third stage is solid. The rocket is 92 feet high, 8 feet in diameter, and weighs about 112,000 pounds

at liftoff (Figure 6). During liftoff, the Delta consumes oxygen enough for 6 million people.

The delta, successful on all but its first attempt, has had 19 straight successes.

The satellite is put into a nearly circular 400-mile orbit (Figure 7) and takes approximately 100 minutes to circle the earth. The angle of inclination was 48 degrees for TIROS I through IV and 58 degrees for TIROS V, VI, and VII. The angle of inclination is limited because the first and second stages must be disposed of over uninhabited areas. All launches have been from the Atlantic Missile Range in a northeast direction.

Tracking of the TIROS spacecraft for purposes of orbit determination is performed by the NASA satellite tracking and data acquisition network (STADAN). The orbit is determined after launch and is continually updated. From this information the time of acquisition of the spacecraft is determined for each of the data readout stations.

COMMAND AND DATA ACQUISITION

Two primary CDA stations have been established to acquire and process TIROS data: Wallops Island, Virginia, and San Nicolas Island, California, at the Pacific Missile Range (PMR). An auxiliary command station, used to start spacecraft clocks, is located at Santiago, Chile. A secondary CDA station in Princeton, New Jersey, is used for local analysis of system operation. A third primary CDA station is being established at Fairbanks, Alaska. The Alaskan station is expected to be operational in 1964.

The satellite orbits the earth approximately 14 times per day. Because of the location of the CDA stations, an average of 8 orbits can be interrogated. The

other 6 orbits cannot be utilized except by a special technique which allows one additional orbit to obtain pictures. This special technique is to program the cameras after the last pass over PMR and then trip the clock to start on a future orbit which over-flies Santiago, Chile. In this way, a specific area may be viewed during one of the orbits which does not pass over either Wallops or PMR.

Of the eight orbits usually obtained daily, two are available at Wallops only, two are available at PMR only, and four are common to both.

The CDA stations perform the following tasks:

Transmit signals to the spacecraft for programming its operation and data transmission

Receive signals carrying TV, IR, attitude, and telemetry data from the spacecraft

Extract the TV, IR, attitude, and telemetry data from the carrier signals

Record and identify the data

Relay recorded data to the TIROS Technical Control Center at Goddard Space Flight Center and to the U. S. Weather Bureau in Suitland, Maryland

Antennas

The receiving antenna for the PMR CDA station is a 60-foot-diameter parabolic reflector type (Figure 8). The antenna has a gain of 30 db at 235 - 237 Mc, and a gain of 24 db at 136 c. Both the 136-Mc and 235 - 237-Mc elements permit polarization diversity reception.

The two antenna systems at the Wallops CDA station are a General Bronze high-gain (235- and 237.8-Mc) multielement array used for TV and IR tracking (Figure 9), and a Kennedy multielement array for beacon and other telemetry tracking (136 Mc) (Figure 10). The General Bronze Antenna has a gain of 28 db and the

Kennedy antenna a gain of 23 db. Both of the antennas provide for polarization diversity reception.

The antenna at the Fiarbanks data-acquisition facility is an 85-foot parabolic reflector having approximately 33-db gain at 235 Mc and 28-db gain at 136 Mc (Figure 11). The system has provision for polarization diversity reception.

Command and Readout Equipment

Each CDA station is equipped with a complete complement of equipment for the command, reception, recording, and display of TIROS television, infrared, and other telemetry data.

DATA UTILIZATION

The data from the satellite are recorded in several formats. All data are recorded on magnetic tape which can be played back at a later time. The telemetry, recorded on strip charts, includes housekeeping information such as location of the satellite, battery power, temperature of sensors, etc. The IR data are processed and placed on separate magnetic tapes which are then mailed with orbital information, calibrations, and altitude. Finally, the data are plotted on maps or used in computations of radiation balance, etc. The TV picture is played through a kinescope. Pictures are taken of the scope, processed, and prints are made.

Attitude Determination

Attitude-determination teams are located at each CDA station. Assisted by a digital computer, the teams determine the operational attitude of the spacecraft

spin-axis. They use all available sources of attitude for their determination. Upon determination of attitude values, the on-site teams prepare longitude and latitude overlay perspective grids to be used in the TV data analyses.

The final definitive attitude is accomplished on a GSFC 7094 computer by the GSFC Theory and Analysis Office.

IR Data Reduction and Analysis

The IR data are recorded on magnetic tape at the CDA station. The tape is forwarded to GSFC where the data are demodulated and converted from analog to IBM 7094 digital format. The IR digital data, together with satellite definitive orbital and attitude information and calibration data, are processed on the IBM 7094 computer to produce a Final Meteorological Radiation Tape (FMRT) (binary).

Meteorological Analyses

Each CDA station has meteorologists on site as an integral part of the station team who are responsible for making real-time analyses of the TIROS TV picture tube. These analyses are transferred to a map chart in the form of graphical identification of the cloud elements observed. The charts, called nephanalyses, are transmitted by line facsimile to the National Weather Satellite Center (NWSC) by GSFC. At NWSC, the nephanalyses undergo a quality control check, are redrawn, and scheduled for transmission to some 600 recipients over the high-altitude and national facsimile circuits. The nephanalyses are retransmitted from these circuits on the west, east, and southeast coasts to the Far East, Europe, and South America.

In addition to the graphic nephanalyses, coded teletype nephanalyses are produced at the NWSC for transmission over national and international weather teletype circuits.

In addition to the graphic nephanalyses transmissions, selected gridded photographs are transmitted by GSFC to the NWSC using photofacsimile equipment. These photofacsimile pictures are selected to provide samples of original data from which the analyses are made and to provide complementary or additional data to the nephanalyses. NWSC retransmits these photofacsimile pictures to regional and other weather centers throughout the United States over the national and high-altitude facsimile circuits. The recipients of the photofacsimile data include Honolulu, Hawaii; San Juan, Puerto Rico; Anchorage, Alaska; San Francisco, California; Miami, Florida; Kansas City, Missouri; New Orleans, Louisiana; Point Mugu, California; Idlewild Airport, New York City; Charleston Air Force Base, South Carolina; Patrick Air Force Base, Florida; and Cape Canaveral, Florida.

Archival Activities

Archiving of the TIROS TV and IR data is the responsibility of GSFC. The photographic facilities of the CDA stations, a special film control office at Wallops Station, and NWSC are utilized for film preparation and production for archival storage. The final repository of TIROS archival film is the National Weather Records Center (NWRC) at Asheville, N. C. The final Meteorological Radiation Tape is the archival record for IR data, and it, too, is available at the NWRC, Asheville, N. C.

TIROS Technical Control Center

A technical control center is located at GSFC to coordinate and direct the operational activities of the project, as well as to monitor in real-time the spacecraft and CDA station functions. Requests for data are received and evaluated in terms of the current or real-time capabilities. The magnetic attitude-control program is directed from this heart of the system. Using

all available information, the technical control center establishes the daily program of the satellite and schedules the CDA station activities. It is here that any emergency procedures are established and here exist the focal point of all operational analyses for future benefit to the project.

PROJECT RESULTS

Table I summarizes the results obtained by the seven TIROS satellites launched to date.

Some additional results of the satellites are:

TIROS I

Demonstrated the feasibility of providing and using TV pictures for meteorological analysis and forecasting

Proved utility of certain types of satellite dynamics and thermal control

Proved versatility of electronic and mechanical components

Power failure caused by a "stuck" relay

Analyses of spin-axes motion

TIROS II

Demonstrated feasibility of the IR experiment

Demonstrated feasibility of magnetic attitude control

TIROS III

First satellite to be quasi-operational

First satellite hurricane observation

Observed hurricane Esther 2 days before other methods

Developed analyses techniques

International cooperation

Failure caused by 1 recorder and 1 vidicon degradation

TIROS IV

Initiated continuous coverage

Provided ice reconnaissance

Supported the Glenn Orbital Flight Ranges - Antarctic supply

Improved techniques of attitude steering

Shutter circuit and tape recorder failures

TIROS V

Increased coverage - 60°

Failure due to vidicon-shutter electronics

TIROS VI

Still functioning - 335 days as of August 15 - 60,000 pictures

Loss of one camera - vidicon failure

TIROS VII

Northern and southern hemisphere coverage with phase opposition to TIROS VI orbit

Useful life of 60 days as of August 15, 1963

Figure 12 shows a typical TIROS picture after the grids have been computed and superimposed on the picture.

Figure 13 is a TIROS picture of the Red Sea and the Nile, showing the clouds associated with the jet stream and some clouds associated with mountain wave phenomena.

Figure 14 is a comparison between a geographical presentation of the Great Lakes Area and photographs produced by TIROS. The TIROS photographs show clouds over Southern Canada caused by moisture picked up over the Great Lakes.

Figure 15, another comparison of a geographical presentation with an actual photograph, shows clouds over Sicily, Italy, and the Alps.

Figure 16 shows the southeastern section of the United States, primarily Florida, which is covered by cumulus or thunderstorm activity. The squall line extending east to west over the Gulf of New Mexico would not have been detected by normal means of observation.

Figure 17, the swirling vortex of Hurricane Daisy (fourth tropical storm during 1962) was photographed by TIROS off the east coast of the United States. TIROS detected all tropical storms in the Atlantic and Pacific Oceans during the first half of the 1962 hurricane season.

Figure 18 is a series of pictures of Typhoon Karen in the Pacific, taken on different days during its course from northeast of New Guinea to Japan.

In Figure 19, the lower photographs are a mosaic of pictures taken by TIROS over the eastern Pacific, the United States, and southern Canada; the upper chart shows the corresponding cloud depiction after rectification and synoptic analysis. The cloud structure as seen by TIROS follows the classic description of clouds associated with a polar front.

Figure 20 is a mosaic of cloud pictures taken by TIROS on a single day in the southern hemisphere, illustrating the quantity of normally unobserved area that can be put under the surveillance of the TIROS weather satellite.

Figure 21 is a composite of all nephanalyses made on one day from TIROS passes. On this particular day, five major tropical storms and vortices were observed by TIROS: hurricanes Carla, Debbie, and Esther, and typhoons Nancy and Pamela.

In Figure 22, the upper map shows thermal isolines plotted from infrared data obtained by TIROS; a nephanalysis of cloud cover photography is superimposed on the lower map. Since the colder temperatures indicate that the cloud structures are at higher altitudes and the maximum cloud-top heights represent the most intense development, the infrared analysis proves to be consistent with the cloud pictures obtained by TIROS.

Figure 23 is a photograph taken by TIROS just before John Glenn's reentry from his earth orbit. The arrow indicates the point where Glenn landed. This photograph is one of many taken by TIROS in support of Project Mercury.

Figure 24 shows the Mediterranean, the Riviera, and snow cover in the Alps. TIROS photographs are being studied to determine whether these observations can be useful in evaluation of water resources.

Figure 25 is a photograph of ice cover in the Gulf of St. Lawrence. The large mass of white is ice, not cloud. TIROS photographs have been used in ice reconnaissance and in support of the Navy's Artic Resupply Task.

Figure 26 was photographed near the Canary Islands. The cloud patterns observed demonstrate the feasibility of streamline analysis in the equatorial area. The numerous patterns in the cloud formations show the eddies in the wind field.

Figure 27 is a TIROS photograph taken over Ontario, Canada.

FUTURE TIROS PROGRAM

The current TIROS has several limitations. It is limited by power, by the orbit, altitude, sunlight, and ground stations. These limitations in turn affect the coverage, the timeliness of data, the accuracy and frequency of observations, as well as the type of observations. The future program - seven

additional TIROS satellites to be launched in the next 2 years - is designed to decrease these limitations and to contribute to technologies of future satellite systems. At the same time as these missions aim toward these goals, daily observations will be provided. All of this will contribute to a better understanding of the atmosphere and its motion. Advantage is being taken of the developments in the field of space and associated sciences, e. g., the increased capability of the Delta rocket will allow optimum orbits.

Specifically, the future program is designed to:

(1) Develop a local readout capability and thereby provide immediate operational use of satellite data

(2) Increase the area of observation of the earth's cloud cover and radiation budget

(3) Increase the frequency of observations

(4) Increase the accuracy of observations

(5) Develop sensors and techniques for a synchronous meteorological satellite

(6) Develop techniques for more effective acquisition of data

(7) Develop techniques for more effective processing and use of data

The next TIROS, TIROS H, will be similar to TIROS VI except that one of the TV cameras will be the automatic picture transmission (APT) type. This APT system consists of a wide-angle camera and a transmitter which transmits a picture continuously as it is taken. With comparatively inexpensive ground-station equipment, the picture can be received and used immediately for local analysis and forecast. It eliminates the need to transmit the picture to a central point and then retransmit to the users. The accuracy of weather forecasts varies inversely with the time of observation on which the forecast is

based. With the APT system, cloud observations will be provided to the local users in minimum time.

TIROS I (eye) is designed to increase the area of meteorological observations and to improve the accuracy and resolution of the picture. The spacecraft will be configured in a wheel mode, with cameras pointing radially from the spacecraft (Figure 28). After launch, the spacecraft will be positioned normal to the plane of the orbit. The wheel configuration will result in pictures taken with a minimum nadir angle, thereby effecting greater accuracy.

With the increased capability of the Delta vehicle, the orbit will be approximately 82 degrees retrograde, or sun-synchronous. This will afford maximum coverage of the earth each day within the limitations of camera angles.

About a third to a fourth of the earth will be observed each day with the total earth being viewed every 3 days, as compared to the one-fifth now being viewed each day.

The data-acquisition facility at Gilmore Creek, Alaska, will be used, allowing acquisition of a greater percentage of data. Ten of the 14 orbits will be acquired daily.

The TIROS J and K missions will be aimed toward developing a capability for continuous single-picture observations of the earth. The continuous observation capability will allow us to observe mesoscale and other phenomena which have lifetimes that can be complete between two successive observations of the area. These missions will be eccentric orbits in the order of 300 to 3000 miles and 300 to 22,000 miles. At the apogee of each mission, the cameras will view the entire disc of the earth; in 22,000-mile apogee orbit, they will view a particular portion of the earth continuously for 6 hours. The specifics of the camera and lens required, the transmitter, etc., are being investigated.

The remaining missions are intended to further develop the techuologies associated with the current or planned missions.

In closing, I would like to note that the results of TIROS have been of direct benefit to each and every one of us. I do not know of anyone who is not benefiting from weather forecasts based on TIROS data.

One other note. The success of TIROS is due to many people with a will to succeed - a combination of people from many government agencies and industry, and scientists working together with a common aim.

Table I

Summary of TIROS I Through VII

TIROS	LAUNCH DATE	USEFUL TV LIFE	USEFUL IR LIFE	TOTAL PICTURES	SENSORS	SPECIAL ACCOMPLISHMENTS
I	Apr. 1, 1960	77 days	--	22,952	Wide- and narrow-angle TV	Proved feasibility of meteorological satellites
II	Nov. 23, 1960	231 days	141 days	76,156	Wide; narrow-angle TV; two IR systems	IR subsystem successful; magnetic attitude control successful; ice reconnaissance feasible
III	July 12, 1961	145 days	81 days	35,033	Two wide-angle TV; three IR systems	Hurricanes, typhoons observed; photofacsimile pictures obtained routinely
IV	Feb. 8, 1962	131 days	146 days	32,593	Wide-, medium-angle TV; three IR systems	Ice reconnaissance project established; supported Mercury, Ranger, Antarctic Resupply, Joint Task Force 8
V	June 19, 1962	330 days	--	58,226	Wide-, medium-angle TV	Hurricane coverage
VI	Sept. 18, 1962	321 days as of Aug 3 63	--	58,413	Same as TIROS V	Hurricane coverage
VII	June 19, 1963	45 days as of Aug 3 63	45 days as of Aug 3 63	9,211 as of Aug 3 63	Wide-Angle TV, two IR systems, one ETP	Hurricane coverage, special IR study for horizon sensors

REMARKS: TIROS II last TV pictures 301 days after launch - last IR data 525 days after launch.
TIROS III last TV pictures 237 days after launch - last IR data 203 days after launch.
TIROS IV las TV pictures 266 days after launch - last IR data 169 days after launch.

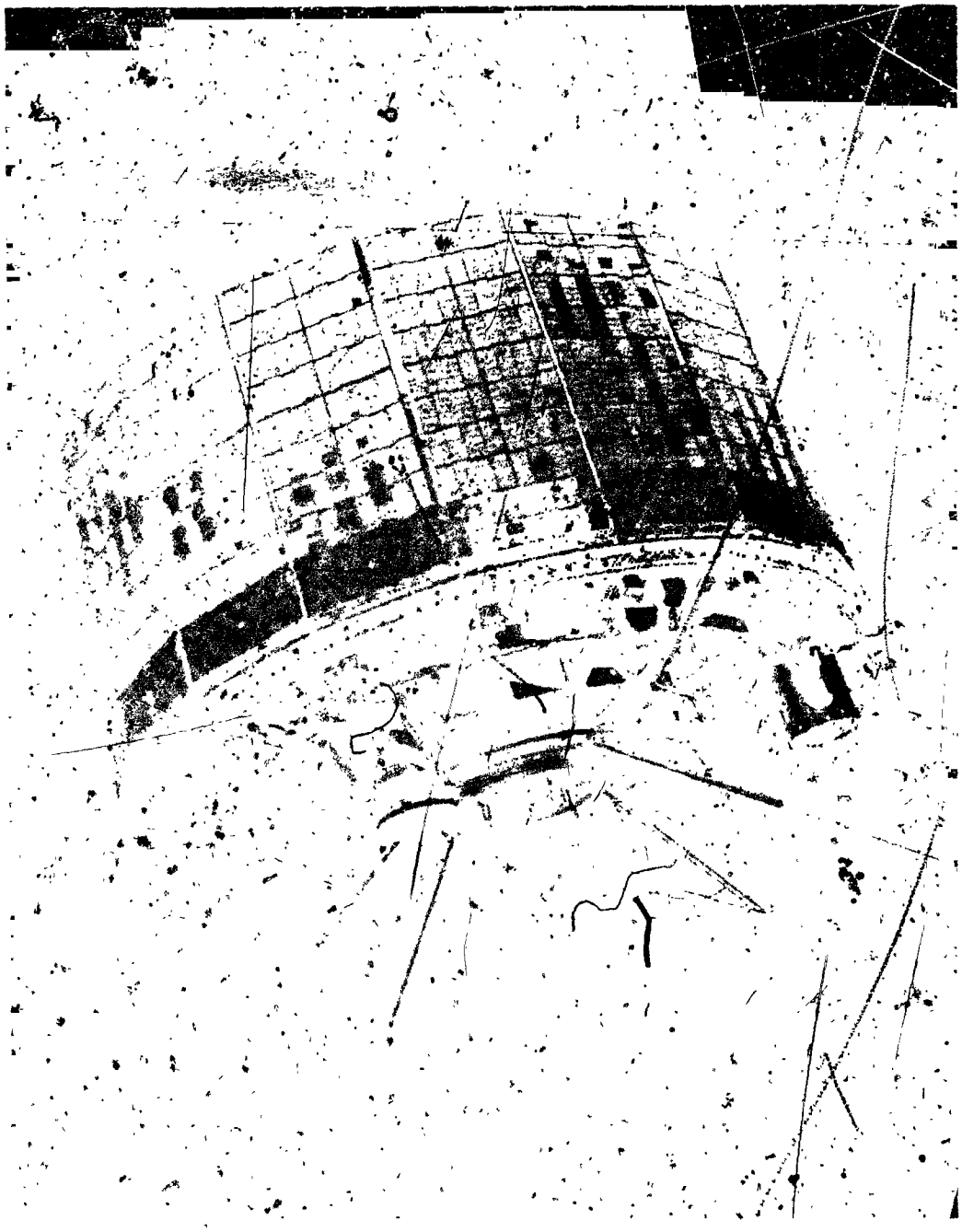

Figure 1 – TIROS Spacecraft

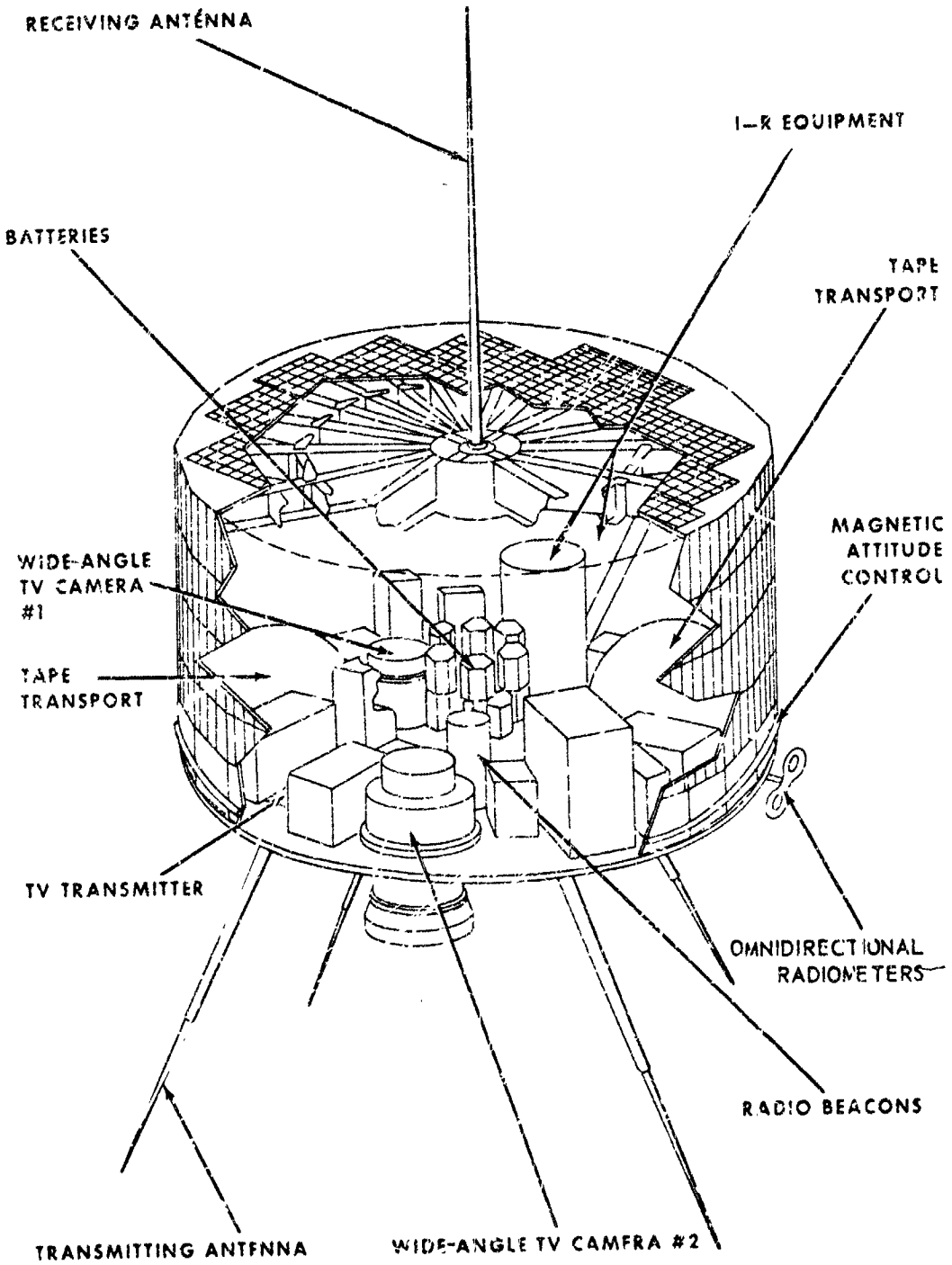

Figure 2 – Standard TIROS Satellite Configuration

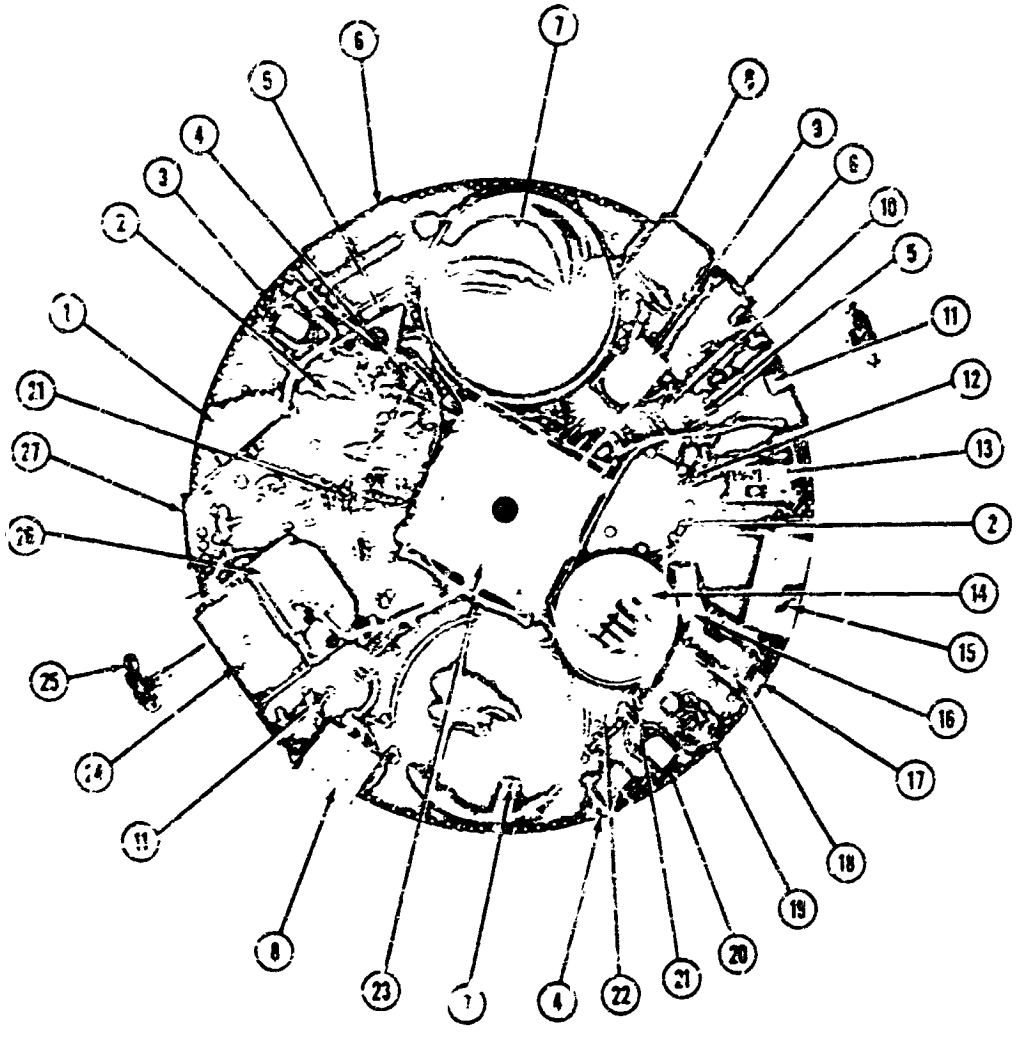

1 TV Camera No. 1
2 Electronic Clock
3 TV Transmitter No. 1
4 TV Transmitter Power Converter
5 TV Camera Control Unit
6 TV Camera Electronics
7 TV Tape Recorder
8 TV Tape Recorder Electronics
9 TV Camera No. 2
10 IR Control Unit
11 TV Tape Recorder Power Converter
12 Command Address Unit
13 Beacon Transmitter and (Hidden) Commana Receiver
14 IR Electronics Unit
15 Scanning IR Radiometer
16 Electron Temperature Probe Electronics
17 Attitude Indicator
18 Beacon Transmitter
19 Attitude Control Switch
20 Despin Tower and (Hidden) TV Transmitter No. 2
21 Power Supply Protection Unit
22 Omni-directional IR Electronics
23 RF Matching and Coupling Network and (Hidden) Storage Batteries
24 FM Tone Turn-On Unit
Omnidirectional IR Sensor
26 IR Tape Recorder
27 Auxiliary Control Unit

Figure 3 – TIROS VII, Top of Baseplate

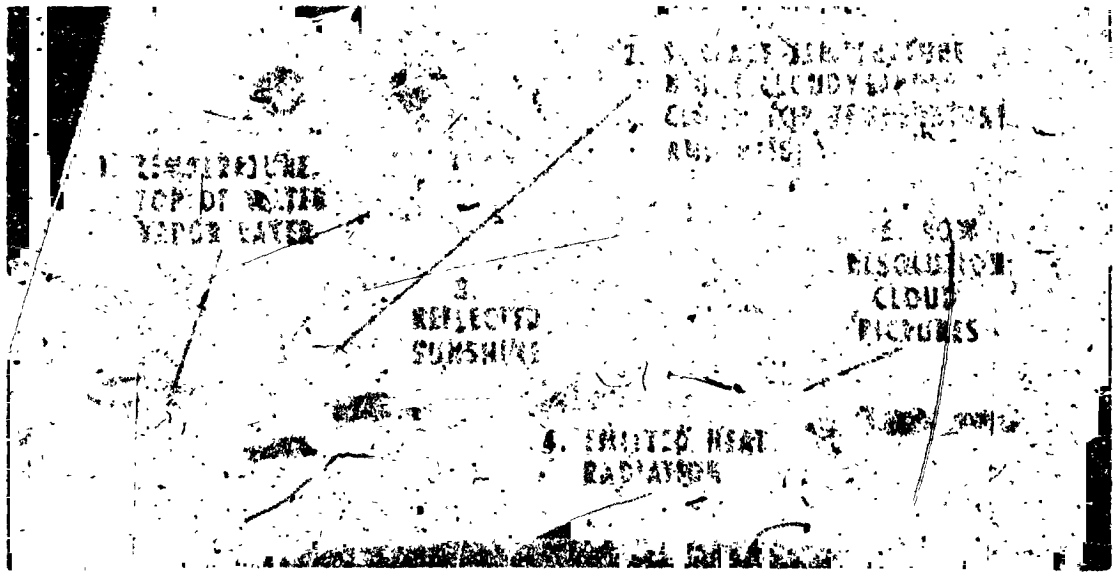

Figure 4 – TIROS II Infrared Measurements

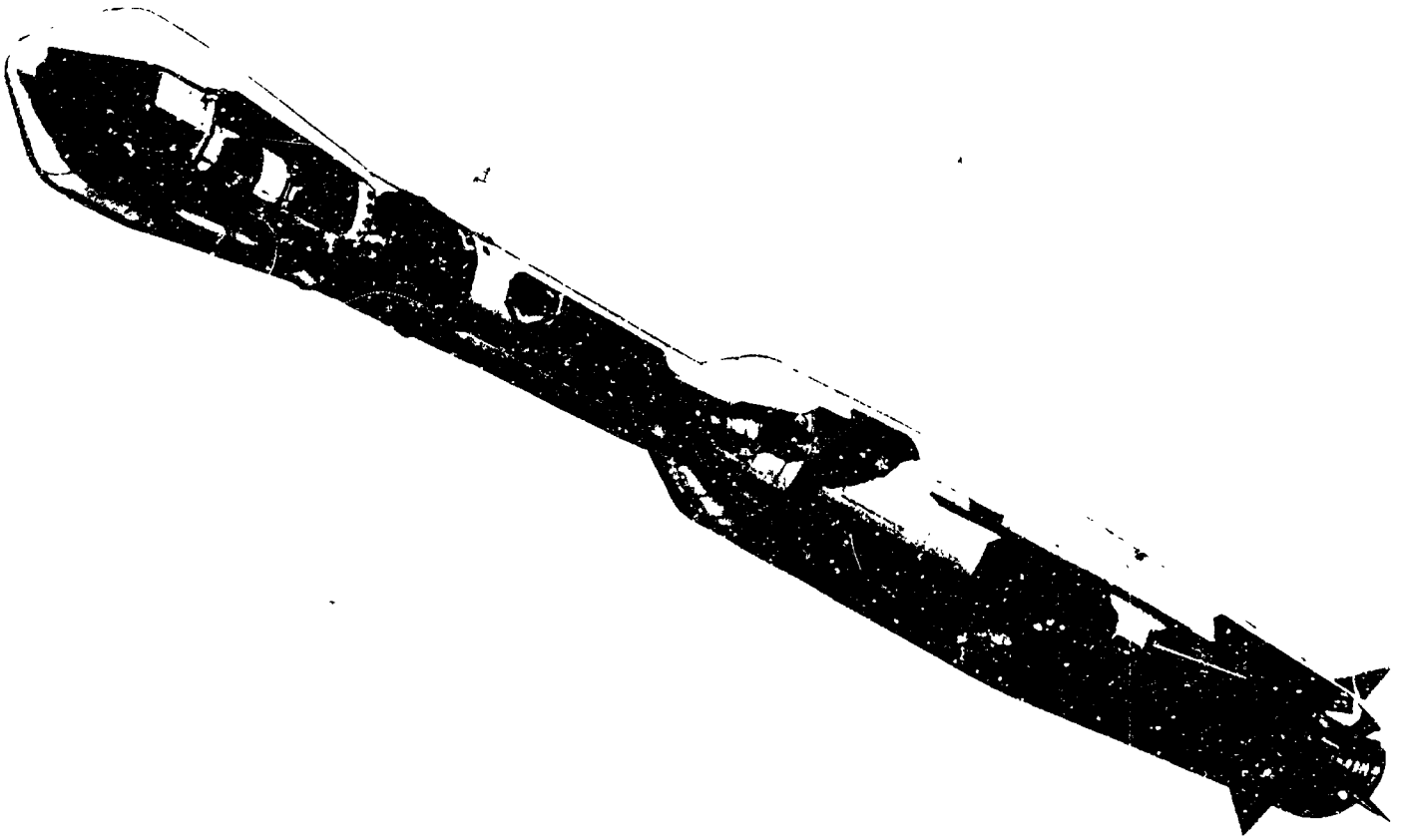

Figure 5 – Three-Stage NASA Delta Launch Vehicle and the TIROS Spacecraft

Figure 6 - Delta Launch Vehicle with a TIROS Spacecraft Lifting Off from Cape Canaveral, Fla.

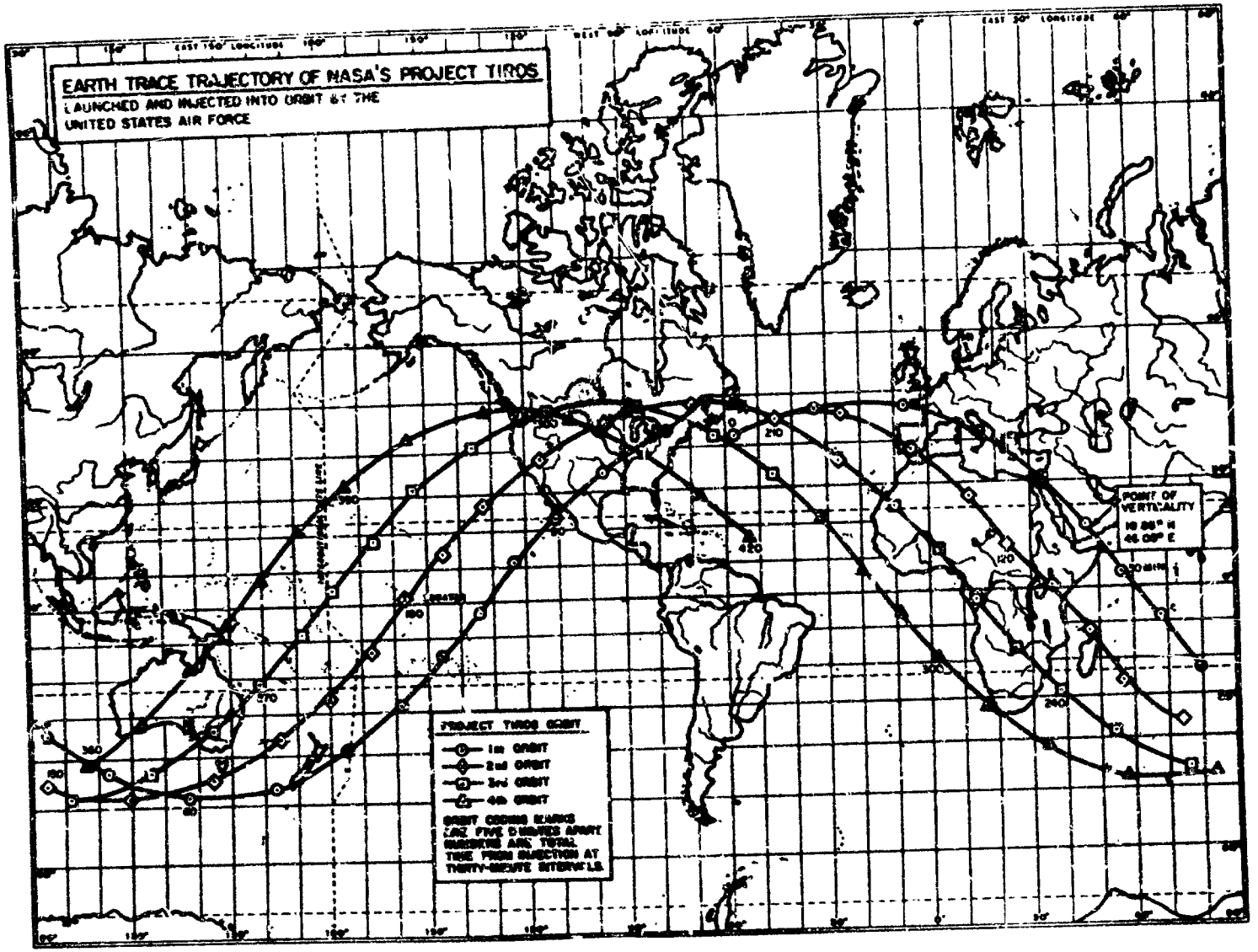

Figure 7 – TIROS I Orbital Map

Figure 8 – Sixty-Foot-Diameter Parabolic Antenna, PMR

Figure 9 – General Bronze Multielement Array, Wallops Island

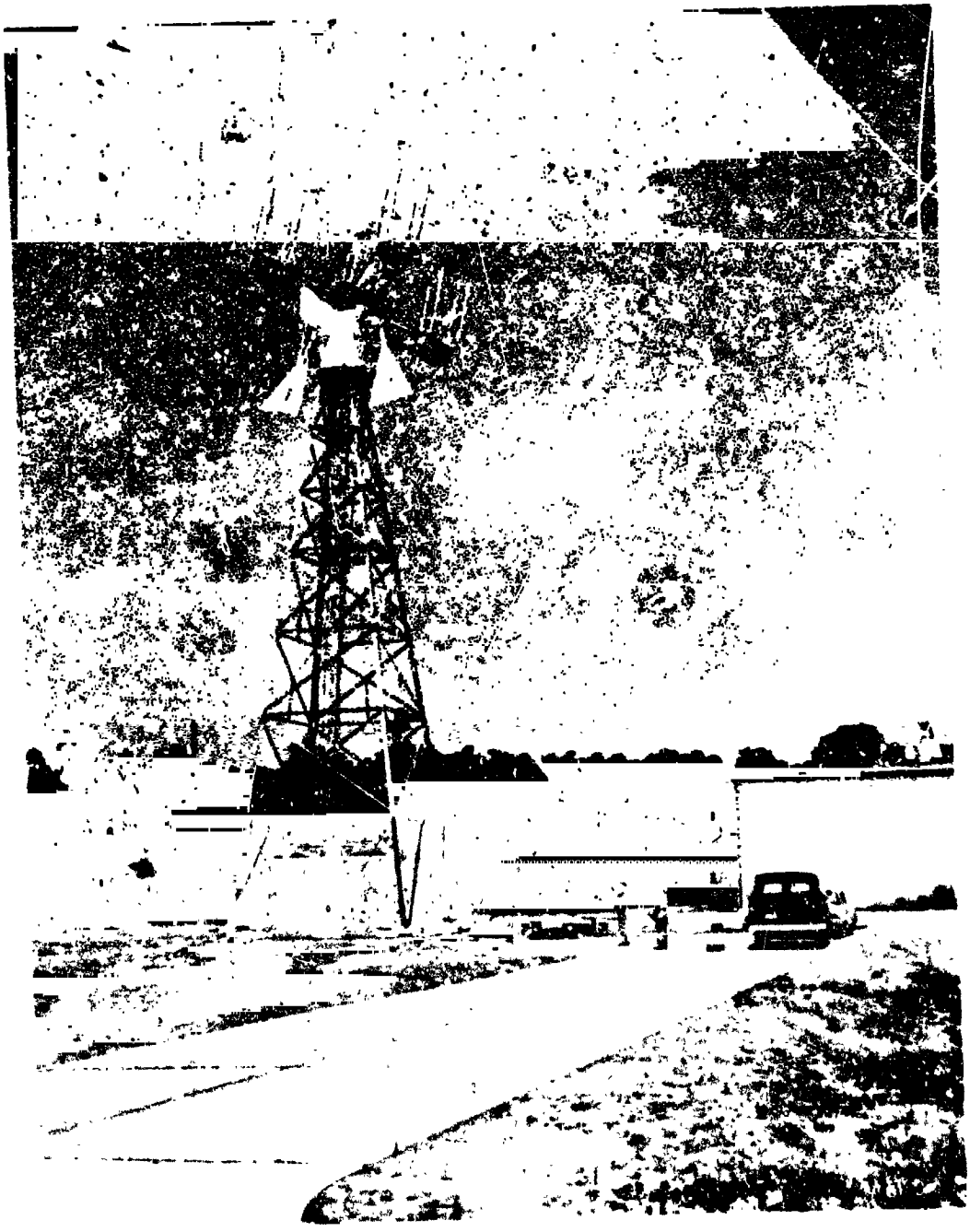

Figure 10 – Kennedy Multielement Array, Wallops Island

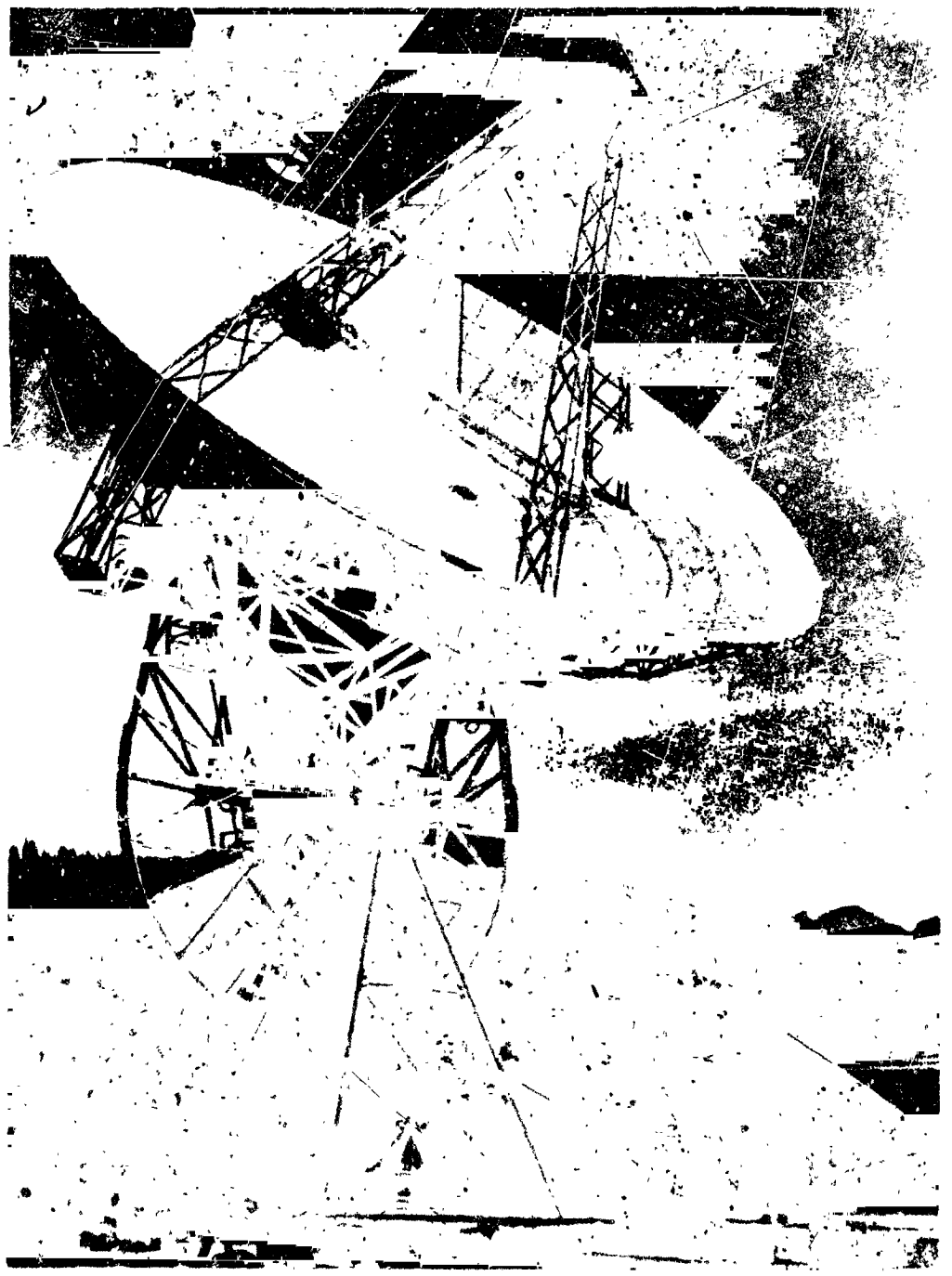

Figure 11 - Eighty-Five Foot Parabolic Antenna, Fairbanks

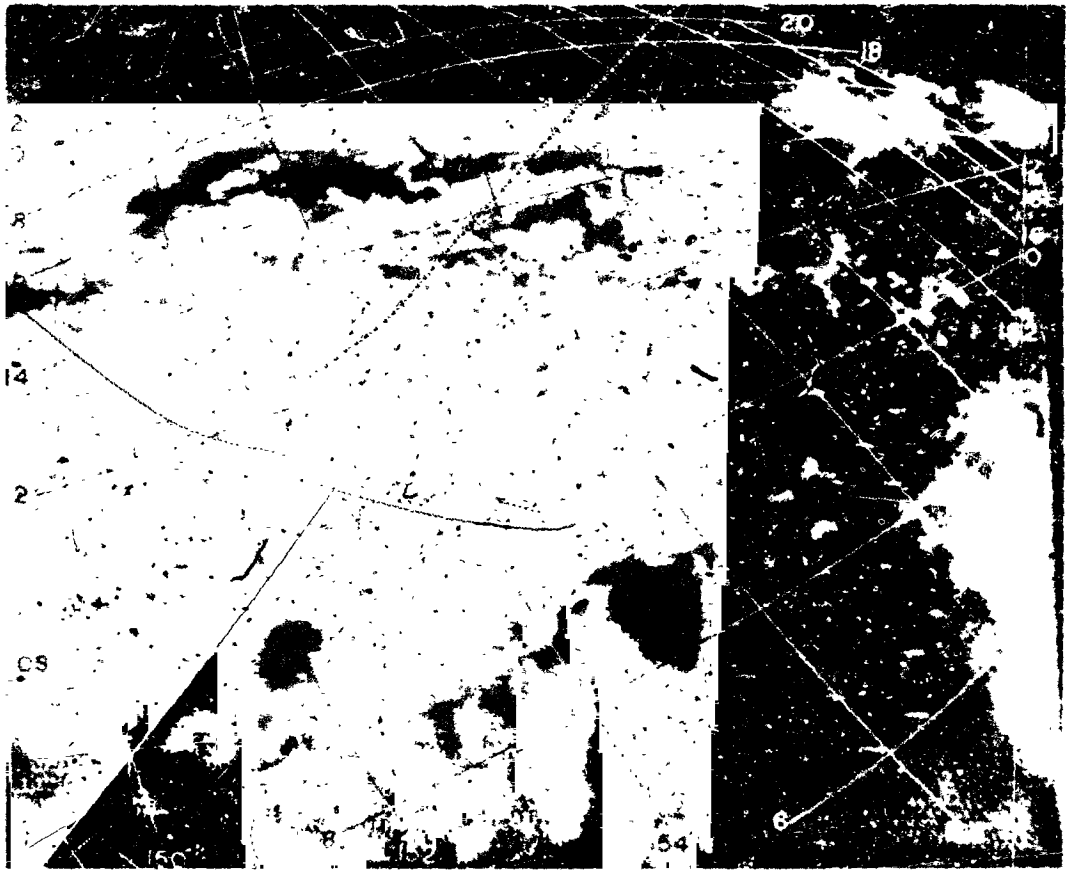

Figure 12 – Typical TIROS Photograph with Grids

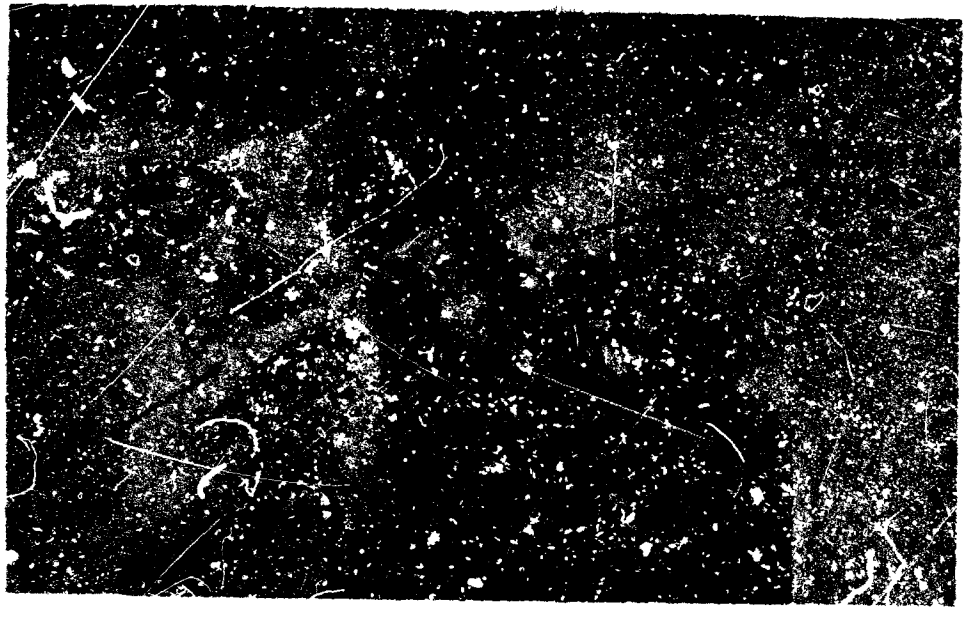

Figure 13 - ATS Photograph Showing Jet Stream and Mountain Clouds

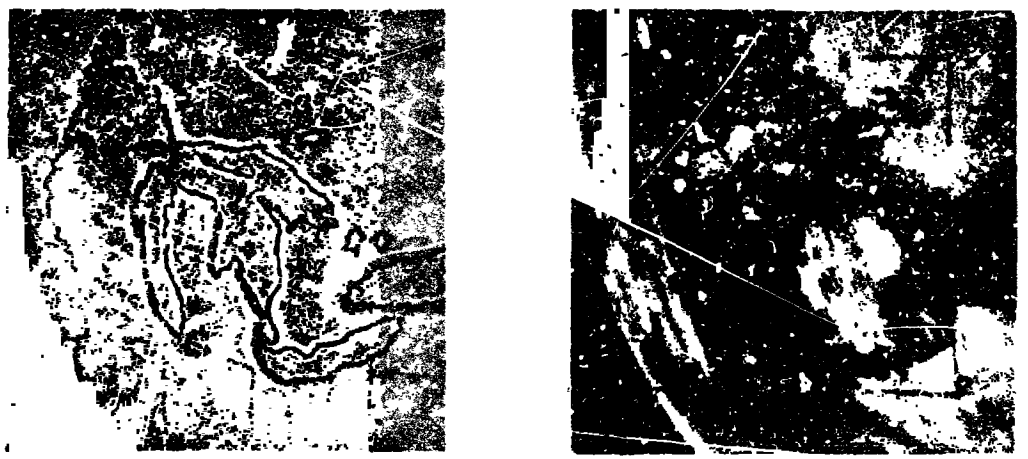

Figure 14 – TIROS Looks at the Great Lakes

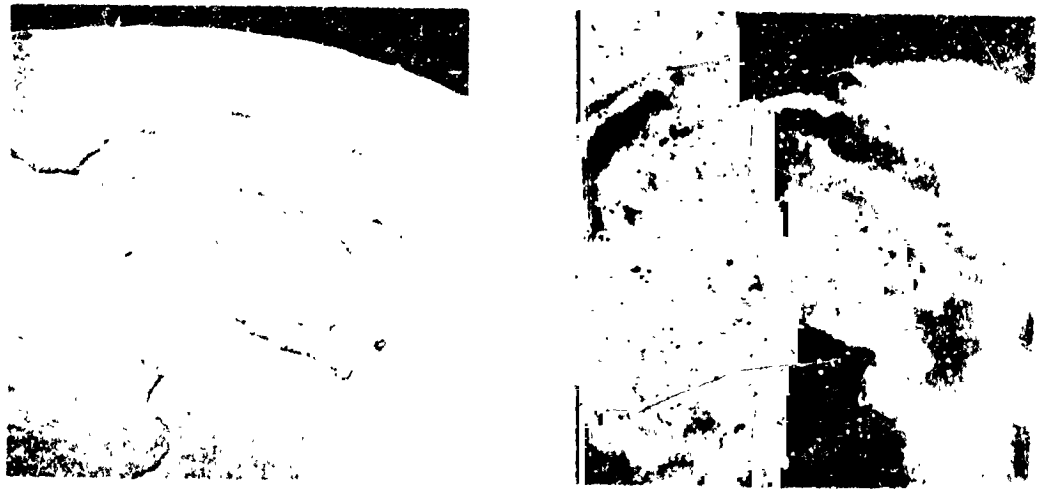

Figure 15 – TIROS Looks at Italy

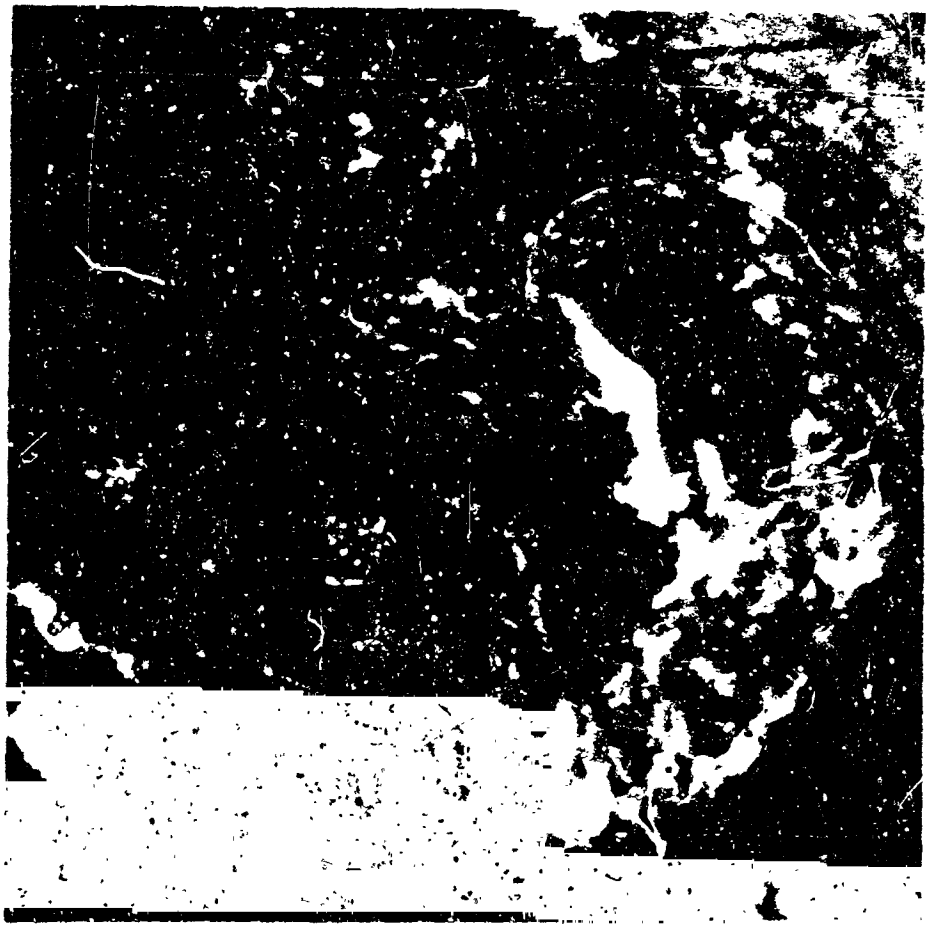

Figure 16 – TIROS Photograph Showing Southeastern United States

Figure 17 – TIROS Photograph of Hurricane Daisy

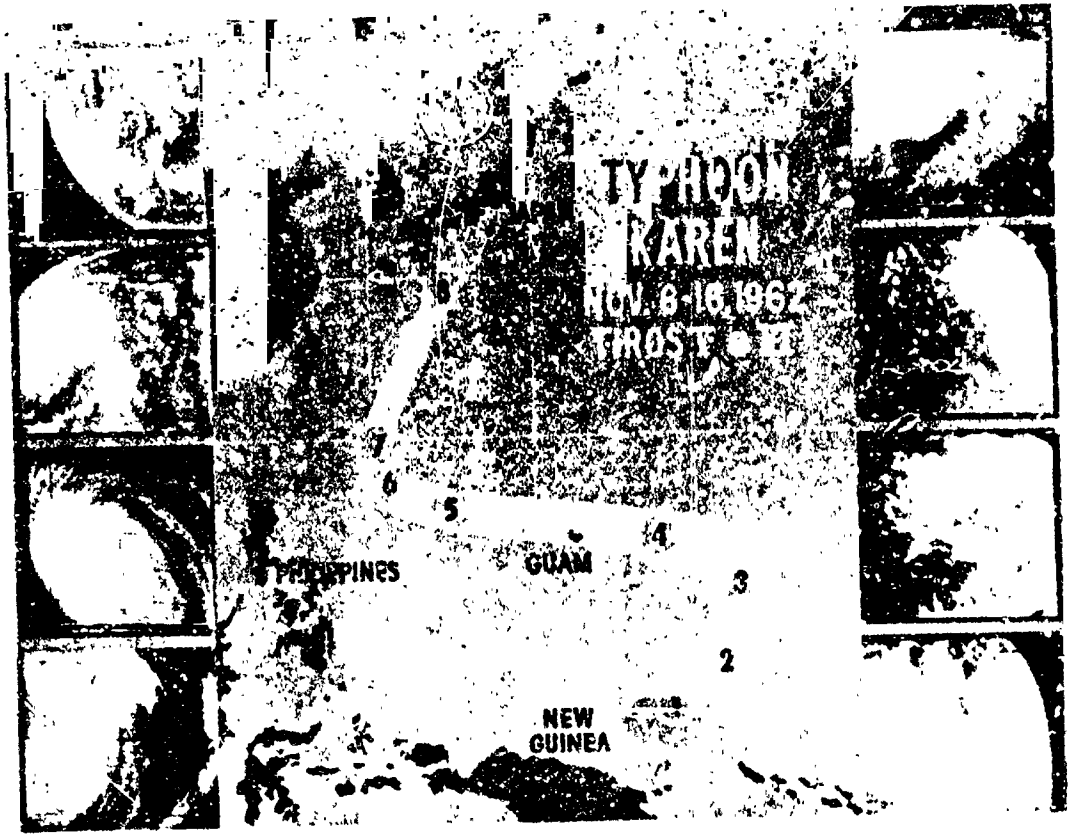

Figure 18 -- TIROS Photograph of Typhoon Karen

EXPERIMENTAL CLOUD DEPICTION CHART PREPARED BY THE UNITED STATES WEATHER BUREAU FROM TIROS PICTURES

MOSAIC OF PHOTOGRAPHS TAKEN ON MAY 20, 1960 BY THE NASA-GODDARD SPACE FLIGHT CENTER TIROS SATELLITE

Figure 19 – Cloud Analysis Made from TIROS Photographs

Figure 20 – TIROS Cloud Photographs of Southern Hemisphe

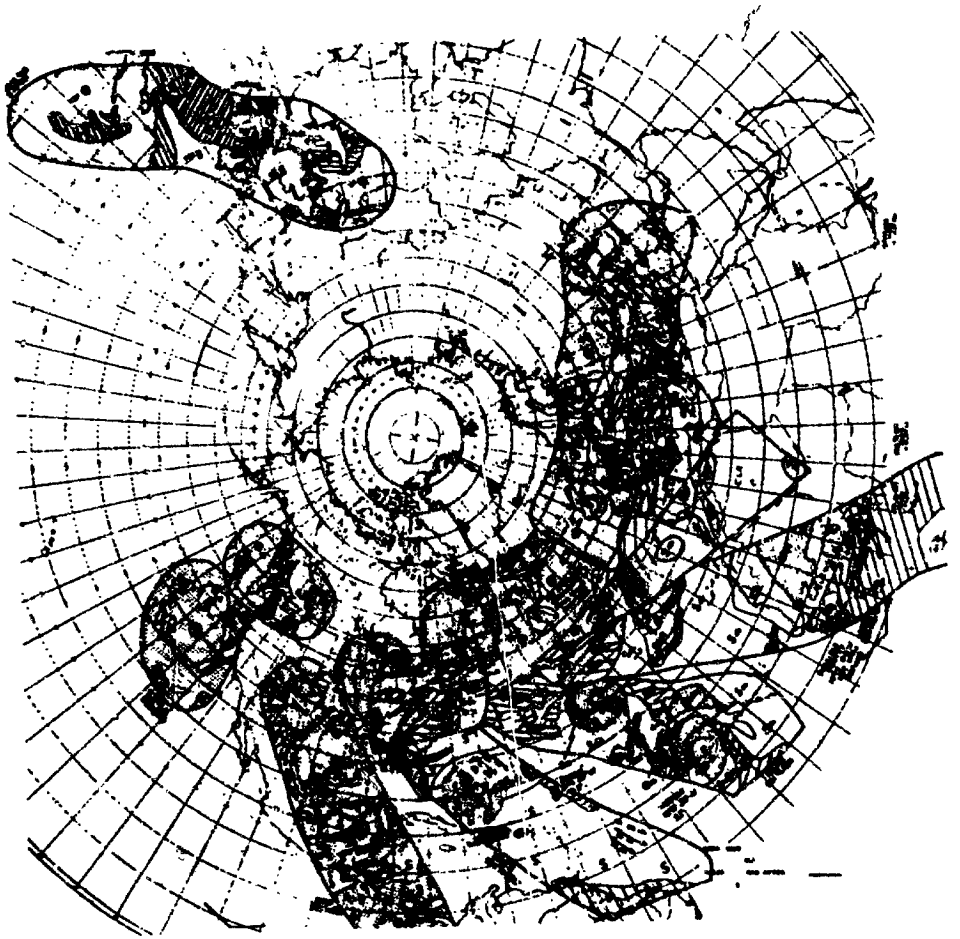

Figure 21 – Composite of Nephanalyses of One Orbital Day by TIROS

Figure 22 – TIROS II – Infrared Data and Cloud Analysis

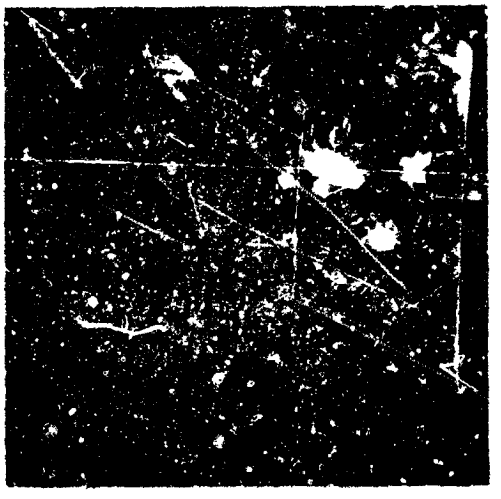

Figure 23 – TIROS Photograph Showing Freedom VII Impact Area

Figure 24 – TIROS Photographs Showing the Mediterranean, the Riviera, and Alps

Figure 25 – TIROS Photograph of Ice Cover in the Gulf of St. Lawrence

Figure 26 – TIROS Photograph of Cloud Patterns near the Canary Islands

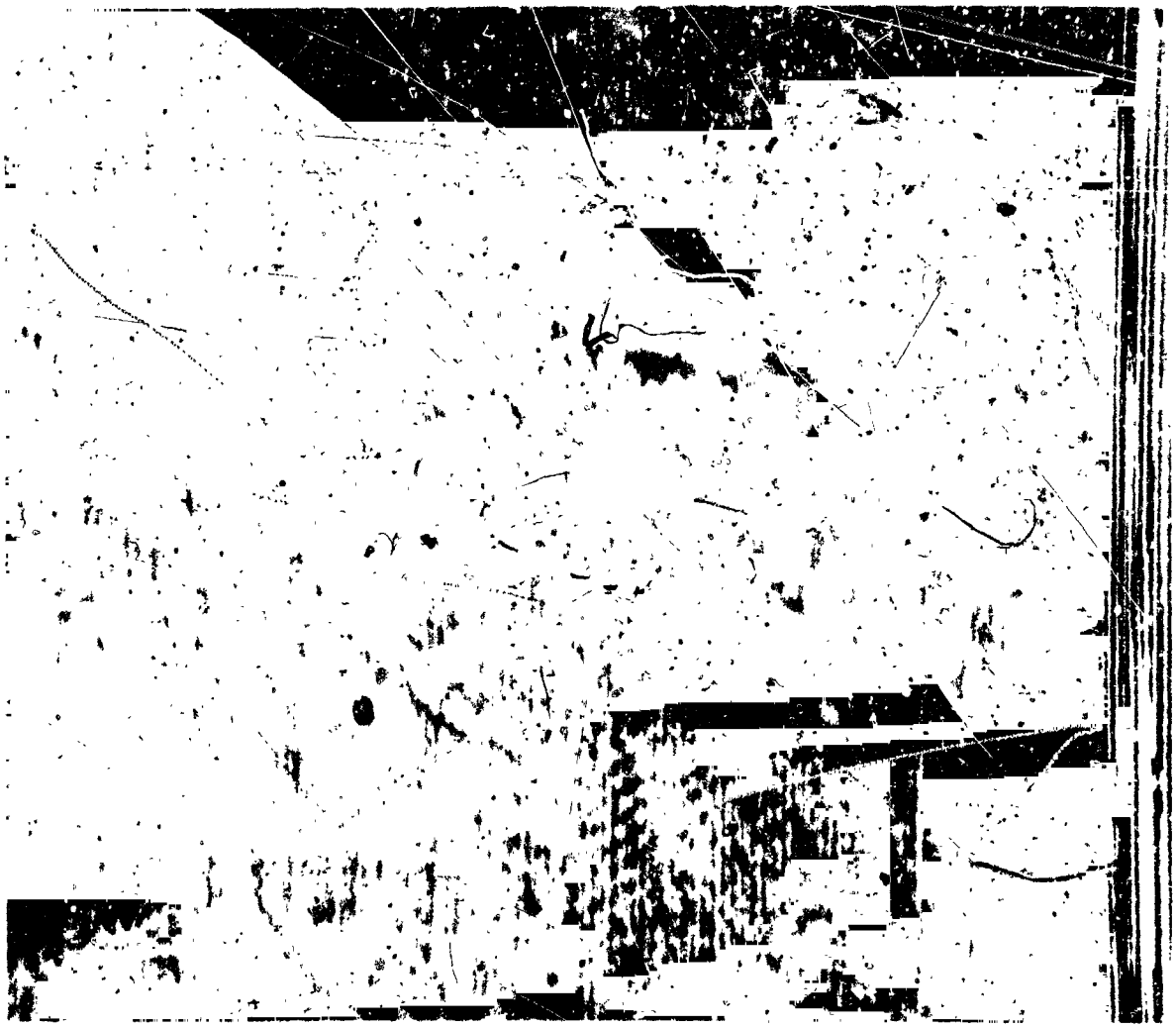

Picture taken by Tiros II on 4 April 1961 with narrow-angle camera. Location of picture center is 49°N latitude, 81°W longitude. Photograph covers town of Cochrane and adjacent areas, Ontario, Canada.

Figure 27 – TIROS Photograph Taken Over Ontario, Canada

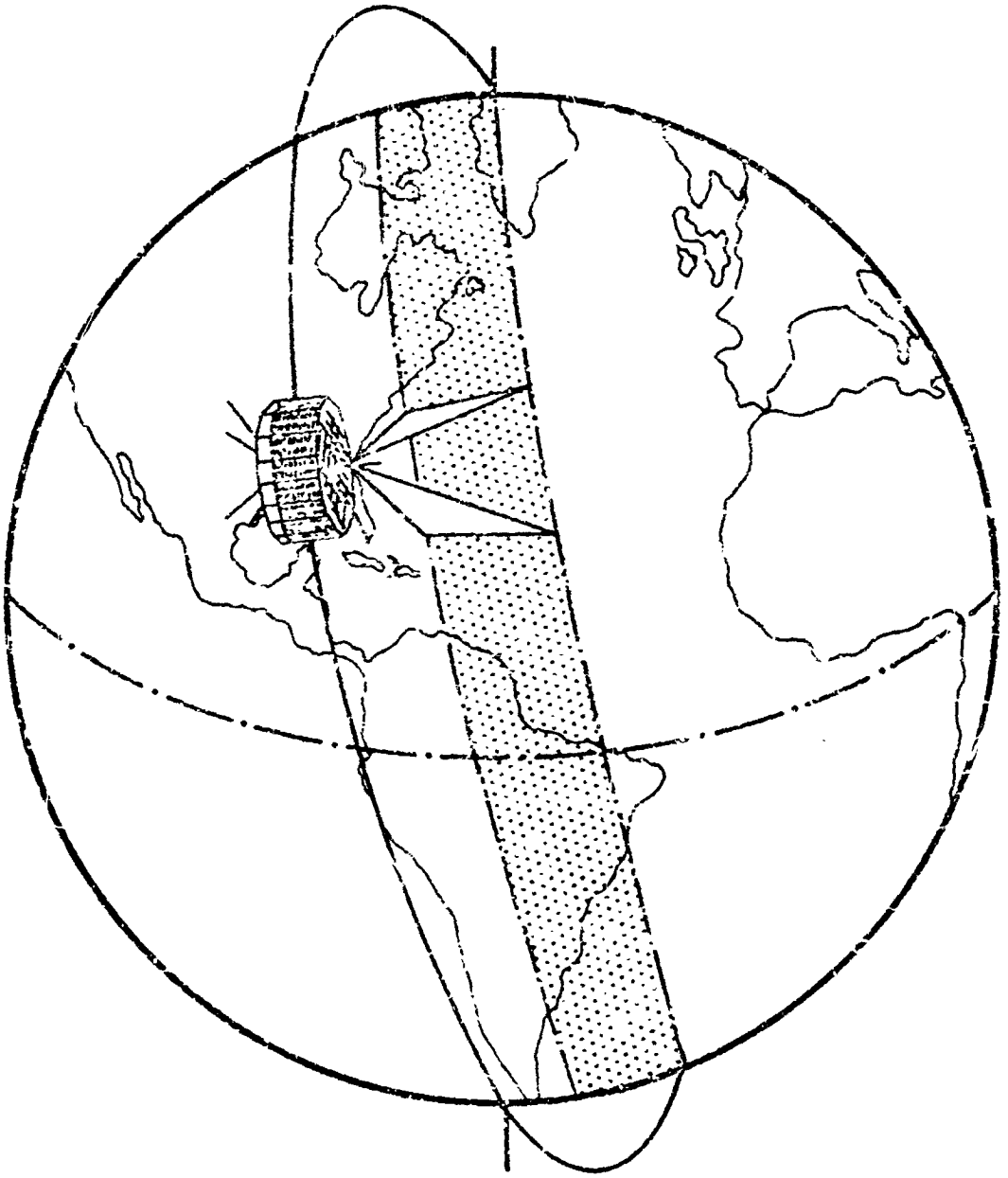

Figure 28 – Cartwheel TV Coverage

THE NIMBUS SPACECRAFT SYSTEM

BY

HARRY PRESS

GODDARD SPACE FLIGHT CENTER

NATIONAL AERONAUTICS AND SPACE ADMINISTRATION

GREENBELT, MARYLAND

THE NIMBUS SPACECRAFT SYSTEM

by

Harry Press

National Aeronautics and Space Administration

INTRODUCTION

The Nimbus project is the follow-on to TIROS in the NASA meteorological satellite program. In Nimbus, a major effort is being made to achieve a global operational meteorological satellite system of great versatility; meteorological in the sense of earth atmosphere viewing, operational in the sense of providing global data in real time, and versatile in the sense of a large and expanding capability.

The Nimbus project was initiated early in 1960 as a NASA research and development project. A team at NASA's Goddard Space Flight Center evolved a basic preliminary design. Procurement of components and spacecraft subsystems for prototype and flight hardware construction and qualification began in 1960 and 1961; a separate procurement for construction of the spacecraft structure and for integration and testing of the complete spacecraft began in early 1961.

At present, the design phase is essentially complete and all the individual systems have completed prototype construction and qualification. Full prototype spacecraft integration and testing is now under way, while the first flight spacecraft is concurrently being assembled. A series of flights has been scheduled with the initial one scheduled for this winter.

The purpose of this paper is to discuss:

The fundamental criteria and conditions that formed the basis for the Nimbus spacecraft design

The characteristics of the Nimbus spacecraft and its major subsystems

Some of the problems encountered in the spacecraft development

The current status of the program

COMPARISON OF OVERALL FEATURES OF TIROS AND NIMBUS

To indicate the technological advance desired in the Nimbus program, it will be helpful to compare the overall features of the Nimbus spacecraft with those of its predecessor, the TIROS spacecraft. Table 1 shows a general comparison of some of their significant features. In all respects, it can be seen that Nimbus represents a more sophisticated and complex spacecraft. Perhaps the most significant features are the choice of an earth-stabilized platform and the polar orbit. This combination yields the significant result of providing full-earth coverage on a daily basis in contrast to the limited TIROS coverage. Other significant improvements include the use of three multiple cameras with higher resolution capabilities, an appreciably larger power supply, and the addition of a high-resolution infrared radiation system (HRIR) to provide nighttime cloud coverage.

BASIC NIMBUS DESIGN CRITERIA AND APPROACH

Basic design criteria governing the Nimbus spacecraft design are summarized as follows:

A system design tailored to support the basic sensors required to measure atmospheric phenomena, these sensors initially to

provide television pictures of the earth's cloud over and infrared radiation measurements

Inherent flexibility in the design to facilitate system and sensor modifications and evolution

A geometry and mass distribution that supports the control system action

Complete global coverage on a daily basis

System dimensions and weight compatible with a medium-sized booster system (Thor-Agena)

Long satellite life with a design objective of 6 months

Application of current state-of-the-art to ensure system reliability and early flight capability

Rapid data acquisition and transmission to permit application to weather forecasting

Minimum overall system costs per data point

These design criteria and conditions resulted in a concept of the Nimbus spacecraft that included the following characteristics:

A polar ("high-noon") orbit to permit complete earth coverage by utilizing the rotational motion of the earth; an 80-degree inclination, retrograde orbit to maintain the high-noon sun aspect for long periods

A three-axis earth-stabilized vehicle, with pointing accuracy of ± 1 degree in all axes and slow (0.05 degrees per second) rotational rates

A 600-nautical-mile flight altitude, chosen as a design compromise- (The TV camera resolution requirements favor a lower altitude, while the higher altitude reduce the number of ground data-acquisition stations required.)

A 650-pound spacecraft (design goal), with a primary weight allocation as follows:

Control system	150 lbs.
Power supply system	200 lbs.
TV and IR sensors	200 lbs.
Telemetry and command system	90 lbs.
Structure (torus and truss)	60 lbs.

A modular approach in spacecraft layout to permit exchange and evolution of subsystems and sensors with minimum difficulty – (For example, the control system is a separate package.)

An S-band data transmission system, as well as a VHF system, to permit rapid transmission of the voluminous data

The wide use of redundancy to achieve long satellite life

The basic spacecraft design consists of three major elements:

A 57-inch diameter toroidal-like ring to house the basic sensors and electronics

A hexagonal upper package to house the complete control system

Large (8 by 3 feet) solar paddles attached to the controls package by a drive shaft and free to rotate in order to permit direct sun viewing

Figure 1 shows a detailed schematic view of the spacecraft layout and indicates the location of all the principal systems. Because of booster performance limitations, all the systems shown and the redundancies will not be flown on the early flights.

It is appropriate at this point to discuss some of the conditions that governed choice of this basic design, particularly those relating to the orbital and stabilization system selection. Details of the other major systems will be described later.

ORBITAL SELECTION AND VEHICLE STABILIZATION

Full sensor coverage of the earth on a daily basis can be obtained by an earth-stabilized vehicle in a polar orbit. This approach permits full utilization of the rotational movement of the earth to provide the primary mechanism for longitudinal coverage, while latitude coverage is obtained by the spacecraft orbital motion. In addition, a small amount of inclination of the orbital plane to the earth's polar axis introduces a slight rotation of the orbital plane due to the earth's oblateness. By choosing an inclination of 80.1 degrees to the equator for a 600-nautical-mile orbit, the rate of regression of the orbital plane will be roughly 1 degree per day, equivalent to that of the sun's mean rotational movement around the earth in terms of celestial coordinates.

The best conditions for earth viewing are obtained by choosing an orbit-injection time near midnight or noon; this launch time yields an orbital plane that contains the earth-sun line. Consequently, the satellite will always view the earth at near local noon on the daylight side and near midnight on the dark side. An error analysis for the system, based on launch-vehicle performance scatter, indicates that errors of 1 degree in inclination angle are possible, but will cause only an 18-degree deviation from the mean sun position after a half-year.

The choice of this particular or "high-noon" orbit has the additional advantage of simplifying the sun-pointing requirement for the solar paddles. Inasmuch as the orbital plane contains the earth-sun line, only 1 degree of freedom is required to provide direct sun pointing for the paddle. A sun sensor on the paddle shaft provides the sun attitude which is then used to turn the paddle shaft.

In order to achieve the full benefit of this orbit, a three-axis earth-stabilized spacecraft is considered both necessary and desirable. A long-duration

earth-stabilized spacecraft system had not yet been demonstrated but was considered a feasible objective in the timescale available. It will suffice here to note that error signals are generated by horizon sensors for the pitch and roll axes. For the yaw axis, a sun sensor is used for initial stabilization and a rate gyro is used thereafter. Inertia wheels are used in conjunction with a pneumatic gas jet system to achieve the 1-degree accuracy in stabilization. Angular rates are controlled to plus or minus 0.05 degrees per second in all three axes, a value which enters directly as a design parameter into the optical scanning systems.

The combination of the near-polar orbit and the earth stabilization provide an ideal set of conditions for the TV camera system. The camera system consists of three cameras; one faces straight down, and the other two are cocked at 35 degrees to the vertical in the plane normal to the velocity vector. This combination provides a three-array picture covering 1450 nautical miles (latitude) by 450 nautical miles (longitude). The coverage is illustrated by Figure 2. Successive frames overlap by roughly 10 percent and are spaced at time intervals of 108 seconds; 32 picture frames will provide complete daylight orbital coverage. The next orbit, displaced about 25 degrees in longitude westward at the equator, provides an adjacent picture of the first orbit, the overlap increasing with the distance from the equator.

Using a polar orbit also simplifies considerably the problem of ground data acquisition. Ideally, a single ground station near the north or south pole could acquire the satellite data from every orbit, but the logistic problems that would arise at a polar station preclude this solution. Instead, the first station is planned for Fairbanks, Alaska. Figure 3 illustrates the orbital paths and the range of acquisition for the Fairbanks site. The two circles shown cover a radius of 1400 nautical miles and 1200 nautical miles. The circles are the intercepts of a

conical view 5 and 10 degrees, respectively, above the horizon from Fairbanks with an orbital altitude of 600 nautical miles. If a minimum view time of either 5 or 10 minutes is required for data readout, 10 of the 14 orbits will be covered from the 600-nautical-mile altitude. Complete coverage of all orbits will require either higher orbital altitudes or additional stations, or both. Current plans include a ground station located close to the northeastern coast of the North America continent. In addition, a higher orbital altitude is being considered for later flights. This combination could readily provide adequate coverage for all orbits.

Figure 4, a picture of the Fairbanks CDA station, shows the 85-foot tracking antenna and the buildings housing the ground-station equipment.

LAUNCH SEQUENCE

Figure 5 illustrates the major events in the Thor-Agena Nimbus launch. The space vehicle is launched at PMR at approximately midnight in order to achieve the desired high-noon orbit. Following first-stage burnout, the Agena is separated and enters a coast phase. First burn is then initiated and the shroud covering the payload is separated. First burn provides the impulse to place the Agena and Nimbus into the desired transfer ellipse; once this is achieved, propulsion is cut off and the Agena B-Nimbus enters a coast phase. When the Agena-B-Nimbus reaches the orbital altitude, second burn is initiated to achieve the desired orbital velocity and inclination.

The Agena will then be pitched up to 10 degrees off vertical in order to place the spacecraft in a favorable attitude for earth acquisition and stabilization, and to preclude Agena-spacecraft collisions after separation. The spacecraft is then separated by releasing the Marman clamp and using carefully calibrated springs

to achieve a separation velocity of about 5 feet per second. The Agena is then programmed through a yaw maneuver to avoid the possibility of a collision with the spacecraft. The spacecraft stabilizes in roll and pitch to the desired orbital attitude, and the solar paddles are unfolded shortly after the spacecraft separation. Once these maneuvers are achieved, yaw control is initiated and the spacecraft is turned to the desired yaw attitude. Complete attitude stabilization is achieved before the first pass over the Fairbanks station, and should be verified at that point.

BASIC SPACECRAFT

The spacecraft consists of two distinct elements, the basic spacecraft systems and the sensory subsystems. The basic spacecraft provides the services needed by the sensory subsystems to perform their tasks: structure, stabilization, power, telemetry, timing, and command capability. These systems will be discussed first; then the sensory systems will be described.

Structure

Figure 6 shows the Nimbus structure separated into its major elements: The sensory ring, the control box, the connecting truss, and the solar paddles. The dumbbell-like mass distribution is achieved by a 48-inch separation between the control system, which weighs about 150 pounds, and the sensory ring, which weighs about 300 pounds. Forces are transmitted between the sensory ring and control box through three hardpoints on each body and the connecting truss. A gridlike skirt over part of the truss extends the command antenna ground cone. During launch, the two solar paddles are kept folded lengthwise, along the spacecraft structure.

Figure 7 gives a view of the sensory ring structure, which is a 57-inch toroid (40-inch inside), 13 inches tall and 8 inches deep. The ring contains eighteen 13 x 8 x 6-inch cavities to house electronic modules. The eighteen V-shaped ring separators house insulation and thermal controllers. Magnesium was chosen as the basic structure material, because of its high strength-to-weight ratio, and because of favorable stiffness and damping characteristics.

A number of advantages accrue from this design approach:

The control system is a separate entity, both mechanically and thermally, relying only on power from the spacecraft.

The many compartments in the sensory ring make it easier to adjust the balance, thereby maintaining the principal axis close to the symmetry axis.

A large base area is available for interference-free installation of optical sensors and scanners.

The cylindrical volume within the sensory ring offers flexibility in packaging bulky equipment such as cameras and tape recorders.

The accessibility of the spacecraft center-of-gravity permits dynamic testing of the spacecraft by placing it on a gas lubricated bearing.

The control system is easily aligned because only three points are effected; alignment of cameras within the sensory cylinder and on the base plate is also facilitated.

The design does not depend on rigidity offered by structural members within the sensory cylinder, and flexibility for future changes is thus preserved.

The relatively high packing density in the ring promotes the design objective of an approximately isothermal ring.

The design promotes execution of the testing philosophy as discussed in a later paragraph.

The control system and sensory system, as well as the solar paddles, are virtually thermally independent and with the exception of the solar paddles are thermostatically controlled. Radiation from the spacecraft is controlled by application of radiation barriers, and by use of venetian-blind-type shutters to change the absorptivity-to-emissivity ratio. Shutters are located on the control system and at the outer area of all 18 sensory compartments. The system has been designed to provide a mean temperature of 25° C ±10° C with much smaller fluctuation for many of the compartments.

Power Supply

The solar-conversion power supply is one of the major service subsystems of the Nimbus spacecraft. It consists of a solar array, used to convert the sun's energy into electrical power, and the electronics equipment required to store and convert the power into the form needed by the other Nimbus subsystems. The power supply, although closely associated with the design of the spacecraft structure and control subsystem, was designed as a separate unit to allow for flexibility and interchangeability.

Some of the major system characteristics are:

Regulated bus voltage of -24.5v, regulated within ±2 percent of nominal voltage

Transient response of 25 microseconds to a 4-amp changing load

Total system weight of 173 pounds

The solar array consists of two honeycomb platforms and transition sections clamped to the shaft of the spacecraft control system (Figure 8). The platforms and transition sections are designed with a high strength-to-weight ratio, using a 1-mil (.001-inch) aluminum honeycomb core material covered with a 3-mil (.003-inch) aluminum foil skin. The platform has one flat face for mounting solar cells; the reverse side tapers from a 1-inch thickness in the center to 1/4-inch thickness at the tip. Total weight of the solar array is 78 pounds.

Each platform measures approximately 3 by 8 feet, giving about 45 square feet of mounting space; this space is covered with 10,500 2 x 2-cm silicon solar cells to gather the sun's energy and convert it into electrical power. The cells are wired in parallel and series combinations to form an array with an average power output of 400w during the sunlit portion of the orbit.

The basic building block is a module, consisting of ten cells connected in parallel with an output of about 1 amp. at .46v. Eighty-two of these modules are wired in series to increase the voltage to about 30. This is called a solar board, and there are seven solar boards on each platform. The boards are connected in parallel to yield a total current of about 12 amperes.

Figure 9 shows the solar module, ten cells connected in parallel by means of beryllium-copper interconnecting strips. A 6-mil (.006-inch) microsheet glass cover coated with suitable filters is mounted on each cell to reduce the heating effects of those wavelengths of solar radiation outside the response region of the solar cell.

Temperature extremes of the Nimbus orbit are -80° to 60°C and constituted a serious design problem. During thermal cycles testing, serious solar cell degradation was observed.

The solar cells initially used for the power supply were made by standard industry techniques; the contacts were formed by a nickel film deposited by an electrolysis nickel-plating process. It was concluded that the degradation could not be appreciably reduced without using solar cells whose contacts are made by the more reliable sintering techniques. It was therefore decided to switch to solar cells made with the more reliable sintered contacts.

The solar-cell problem was further complicated by the creation of the artificial radiation belt in July 1962, because of considerable degradation resulting when solar cells are exposed to radiation. To alleviate this problem, the more radiation-resistant n-on-p solar cells had to be used instead of the p-on-n type earlier employed.

The storage and regulating assembly previously mentioned consists of seven identical battery modules (Figure 10) and an electronic control module. The battery module consists of hermetically sealed nickel-cadmium storage cells, supporting electronic protection circuitry, and an output-voltage regulator (Figure 11). Two serious problems were encountered during vibration-testing of the module: internal mechanical failure caused by core movement, and leakage of electrolyte through the ceramic-to-metal seals. The core movement is restrained by use of a crimping technique, and the electrolyte is contained by applying a potting compound over the seal area.

Twenty-three of these cells connected in series form the battery, whose capacity is 3.2 ampere-hours at a nominal output voltage of -28v. A protective charge-current

regulator is provided to limit the maximum amount of current supplied to the battery.

A number of protective circuits are provided in the regulation system. These include a charge-current limiter to protect the batteries from being exposed to currents in excess of 1.5 amps, battery-temperature and pressure sensors to control charging rates, and over-voltage protection circuitry.

Figure 12 shows the spacecraft power demands over a typical orbit. About 100 watts are required to support the basic spacecraft systems including clock, controls, and telemetry; 40 watts are required for the camera systems, and an additional 150 watts are required for interrogation.

Controls

Perhaps the most significant feature of the Nimbus meteorological satellite is the provision of a three-axis closed-loop attitude-control subsystem for stabilization and control. Figure 13 shows the arrangement of the main components of the control subsystem in the Nimbus configuration, and indicates the arrangement of the scanners, flywheels, slipring and shaft, and gas nozzles.

The control loops appear in simple block diagram in Figure 14. The pitch and roll control loops have common elements, and the block diagram therefore represents them as partially combined. Error-sensing for the pitch and roll loops is performed by two horizon scanners. One scans forward in the direction of the velocity vector, and one scans rearward. Each horizon scanner generates a voltage pulse as it scans across the interface of cold sky and warm earth. The scanner viewing cone and the Nimbus/earth space geometry for stabilized pitch-roll axes are shown in Figure 15.

As indicated in Figure 15, the field-of-view of the horizon scanners is approximately 3 x 10 degrees; this scanning aperture is rotated at 16.2 cps about an apex angle of 90 degrees. Scanning is accomplished by a rotating prism; energy transmitted through the prism and associated scanner optics is focused on a bolometer. The passband for the optics is 12 to 18 microns, with peak response at 14 microns, corresponding to the CO_2 absorption band of the earth's atmosphere. The scanning action generates a voltage pulse once per scan; this pulse, processed through the computer, serves to establish the pitch and roll position error. Pitch error is measured by the difference in pulse-width of the front and rear scanners. Roll error is determined by measuring the position of the pulse with respect to a body-aligned reference; a magnetic pickup positioned in the scanner housing generates a reference pulse which will in effect bisect the scan pulse when the roll-position error is zero. A pulse from either the front or the rear scanner is thus sufficient to establish roll error.

Operation of the pitch and roll loops is similar in that portion of the loop used for processing the error signal. The error signal is passed through a lead network which generates rate information for use in stabilization. A combination of position and rate error signal is fed to the pneumatic and flywheel control loops. For large error signals, the control torques are provided by firing the pneumatic jets; for small error signals, fine-control torques are provided by the flywheels. These flywheels, of which there are three (one each for pitch, roll, and yaw), are motors whose speed is a function of the input voltage and generated torque. Torques which accelerate the flywheel also accelerate the vehicle. In summary, the pneumatic system serves for coarse control and the flywheels for fine control; the pneumatics also serves to unload the flywheel momentum which is used for momentum removal when flywheel speeds approach saturation.

As indicated in Figure 14, the yaw loop has two modes of control. The first is the coarse sun-sensor mode, normally used only during initial stabilization. Briefly, in this mode, the yaw position error is determined by the yaw coarse sun sensor with a 360-degree field-of-view in yaw and a +70-to-40-degree field-of-view in pitch. The response-characteristic of the coarse sun sensors is such that by means of the control loop it will attempt to drive the negative roll axis to point toward the sun; this is the orientation desired for yaw. As shown in the yaw-control loop, the erros sensed by the coarse sun sensor is processed as an error signal through electronics, pneumatics, and flywheel similar to those used in the pitch and roll loops.

The second mode of control for the yaw loop is an integrating gyroscope used in the rate mode to sense yaw error. An error signal is generated when the gyro's input axis is rotated. The input axis of the gyro is aligned in the roll-yaw plane so that is senses the component of orbital pitch rate due to a yaw error. Although the gyro senses any roll rate, these rates are nearly zero after initial stabilization. The actual alignment of the gyro input axis also results in a signal proportional to negative yaw rate which serves to stabilize the closed yaw loop.

The three control loops (the pitch, roll, and yaw loops) serve to control the attitude of the body axes of the satellite. The fourth control loop, also shown in Figure 14, maintains the position of the solar array perpendicular to the sun for maximum interception of solar energy. When the vehicle is in a high-noon orbit, with the earth-sun axis in the orbital plane, only one axis control is necessary to drive the solar array about its axis. (In case of poor orbit conditions, ground commands yaw the vehicle for optimum solar-energy collection.) Two solar-array sun sensors, similar to the yaw coarse sun sensors, generate an error signal proportional to the paddle misalignment with the sun; the amplified error signal

energizes a two-phase motor, which through a gear reduction drives the solar drive shaft. The rotational rate for the solar array corresponds to the orbital pitch rate, and only low shaft speeds are involved. Included in the solar-array position loop are provisions for driving the array while the satellite is in the earth's umbra.

The development of the control system, perhaps the most difficult in Nimbus, has been plagued by a number of serious problems which now appear to have been resolved. The most serious problem was the development of the IR sensors for attitude measurement. The high precision required could not in fact be achieved for all sky conditions.

Clock

Present-day tracking systems such as the Minitrack interferometers can furnish information about the satellite's position in space with sufficient accuracy for the task. A time reference for satellite events is required to relate the events to orbital position. Quartz crystals now being produced for crystal-stabilized oscillators will perform with an accuracy of 10^{-7} at frequencies about 1 mcps in a thermostatically controlled environment. If set at launch, 6 months later the clock will be 1.6 seconds off; a clock reset capability is therefore included.

A 800-kc aged quartz crystal is a sealed glass container was chosen and is heated by a coil to 60°C. A regulator maintains this temperature at very close range. This frequency is then divided by a chain of multivibrations to the series of frequencies required for the spacecraft: 400 kc, 50 kc, 10 kc, 500 cps, 400 cps, and 100 cps.

Both 50- and 10-kc signals are amplitude-modulated with the standard NASA time code. The code has a frame rate of one per second, and uses a binary coded decimal

system. Nine 4-bit groups are employed (for seconds, tens of seconds, minutes, tens of minutes, hours, tens of hours, days, tens of days, and hundreds of days). A 2-millisecond pulse is used for "zero" and a 6-millisecond pulse for "one". Zeros are interlaced between groups so that an average 100-pulse-per-second pulse rate results. The code is generated by a small computer which uses a magnetostrictive delay line as the temporary storage element. The timing code then modulates the two coherent carriers, 50 kc and 10 kc. The lower frequency of the two is radiated continuously through the beacon.

The availability of a minimum computer in the clock suggested the use of certain logic components for the secure command system which naturally cannot be described here. Two receivers connected in parallel, with fail-safe isolation circuitry to implement redundancy, receive binary-coded signals and feed the command logic. The timing is arranged so that approximately 30 commands can be given on an average pass and up to 128 different commands can be transmitted in total. In case of clock failure, unencoded commands are available for telemetry interrogation for purposes of analysis.

Telemetry

A spacecraft as complex as Nimbus must transmit a multiplicity of engineering-type data to permit evaluation of its proper functioning in space. For example, it is necessary to know the performance of the horizon scanner in the control system, the gyros, inertia wheels, the status of the power supply, and many others. These data are required to establish the validity of the scientific measurements and to determine improvements for future designs.

For this purpose two systems are provided: one records information over the entire orbit and plays back upon command, the other provides only instantaneous data

upon command. Both systems use pulse-code modulation because of the generally recognized advantages of digital systems. A 7 bit code and a maximum frame rate of 1 per second were chosen. In the recorded telemeter, which shall be referred to as the "A" telemeter, a frame consists of 64 words and each word of 7 bits plus a word sync bit. A total of 544 channels are available with facility for some extension. Two of the channels are required for frame sync and subcommuntation sync.

A 500-pulse-per-second rate was chosen and is supplied by the master clock. In case the clock fails, it is replaced by a tuning-fork oscillator on unencoded ground command. A coherent 500-cps subcarrier is modulated by the coder output and recorded on an endless loop recorder. The 240-foot tape passes the single record/playback head at 0.4 inches per second. Upon command to play back, power is applied to the playback motor which drives the tape through an appropriate drive mechanism at 12 ips, thirty times faster than the record speed. The 500-cps subcarrier is now converted to 15 kc, covering a spectral bandwidth from very low-frequency components up to 30 kc. Any one of three signals, time, telemeter A, or (as to be explained shortly) telemeter B, modulates the 300-milliwatt beacon-transmitter to 80 percent of amplitude. Telemetry must be provided especially when the spacecraft malfunctions, and this requirement makes it mandatory that the antenna design does not rely on spacecraft stabilization. In spite of the unfavorable configuration (the body is in the order of one wavelength), a pattern was achieved with only one null dependent on the position of the solar paddles.

Many data points are required only once per orbit and at an arbitrary time. These data are transmitted through the B telemeter which transmits three sync words and 125 channels in sequence. Again a 7-bit code is used with a word-sync bit.

The clock rate derived from the master clock is 10 cps, so that the entire pulse-train is transmitted in 104.8 seconds. It modulates a 5000-cps coherent carrier in its phase 180 degrees (phase-shift-keying), which in turn is transmitted through the beacon by 80-percent amplitude modulation.

SENSORY SYSTEMS

Television

The choice of television-system parameters is influenced by many considerations such as linear resolution, maximum transmission time per pass, bandwidth, or orbit characteristic. Careful study of the inter-relations and trade-offs lead to the present set of choices.

The three cameras, as previously mentioned, use 1-inch vidicons with 800-line resolution. The size of the resolution element is ½ mile for the zenith to approximately 1.5 miles at the corners for a 600-nautical-mile altitude. The three cameras are driven by a common timer which provides the picture sequence. The advanced vidicon camera subsystem (AVCS) prototype is shown in Figure 16.

A 40-millisecond exposure time is used and the signal is scanned by the electron beam of the vidicons for 6.5 seconds for the entire frame. Separate local oscillators are frequency-modulated and recorded on separate tracks of a double-reel tape recorder. A fourth track records a continuous timing signal so that picture-exposure time can be identified. Sufficient tape is provided for recording 64 pictures (or two orbits) which can be played back in 10 minutes. Fewer frames require less time, allowing the control center to use passes with less receiving time.

Compensation for the reduced light level for sun angles less than 90 degrees is accomplished by a variable iris, the setting of which is derived from the solar-paddle shaft.

Major characteristics of the AVCS design and the measured characteristics of the prototype AVCS system are summarized as follows:

Characteristics of AVCS design:

Lens-focal length - 17mm

Field of view - 37°

Trimetrogon field of view - 107°

Shutter - double bladed focal plain

Shutter speed - 40 ms

Continuously variable iris f/4 to f/16

Dynamic range - minimum brightness 14-foot lambert at f/4

- maximum 11,400-foot lambert at f/16

Measured characteristics of AVCS prototype:

Brightness ratio of 32:1 (10 gray scales)

60-kc video bandwidth

6.5 sec readout

9½ sec between frames

Limiting resolution 725 TV lines

Linearity 0.5 percent

Stores 32 pictures per orbit

Ground resolution ½-mile per TV line

A directional antenna was chosen to cover approximately the terrestrial view angle underneath the satellite (122 degrees) and the largest possible transmission time.

Upon ground-station command, the tape recorder plays back, and local oscillators convert the four subcarrier-modulated signals to other bands, thus forming a frequency-multiplexing spectrum. The composite signal modulates the frequency of a 1707-MC 5-watt transmitter ±1.5 Mc, the center frequency of which is held stable to 10^{-5} by using a crystal discriminator in a feedback loop. The transmitted signal will be received and processed by the ground station at Fairbanks and transmitted back to Washington, D. C. by microwave link in real time for application to weather forecasting.

Automatic Picture Transmission System

The second TV camera system to be carried by Nimbus is the automatic picture transmission system, perhaps the most useful meteorological system providing direct pictures to local users. The automatic picture transmission system (APTS) is composed of a satellite camera and transmission subsystem, and a ground-station receiving and recording subsystem.

The satellite camera and transmission subsystem* is a storage vidicon system capable of long-duration storage and a very slow readout rate. It takes wide-angle pictures from a satellite and transmits them in real time on a very narrow information bandwidth to the ground station for recording on facsimile equipment.

The ground-station receiving and recording subsystem** consists of an antenna, receiver, and facsimile equipment which is relatively simple, inexpensive ($30,000 per station), and appropriate for wide distribution. Thus, the flight-ground system

---

* Designed and fabricated by Radio Corporation of America/Astro-Electronics Division

** Designed and fabricated by Fairchild-Stratos/Electronics Systems Division

is well suited for application to local weather observation and forecasting applications. All major weather stations can be expected to have these stations in due time.

The spaceborne system (Figure 17) consists of optics, including the shutter; a 1-inch electrostatic-storage vidicon camera; and a telemetry-type FM transmitter for relaying video signals to ground stations equipped with an FM receiver and facsimile-recording equipment.

The camera is programmed for continuous cycles of prepare, expose, and readout. The image is projected on the storage vidicon through a 108-degree lens; the exposed picture, stored electrically in the insulating layer of storage vidicon target, is then available for very slow readout. During readout, the transmitted narrowband video signal is picked up by the ground-station antenna and fed to the receiver, which in turn feeds it to an automatically phased facsimile recorder.

The lens is a Tegea Kinoptic 108-degree f/1.8 lens with a focal length of 5.7 millimeters. Optical exposure is through a double-bladed shutter operated by two solenoids; exposure time is 40 milliseconds.

Once this subsystem is turned on, it operates continuously throughout the daylight portion of each orbit, reading out one picture every 208 seconds. Signals from the day-night switch turn it off each orbital "night," and turn it on again at the beginning of each orbital "day."

When the shutter is triggered, the image is projected on the photoconductive layer, after which it is electronically "developed"; that is, it is transferred to a polystyrene storage layer. This occurs during the first 8 seconds of every picture sequence. During the remaining 200 seconds, the picture information is read out at a scanning rate of 4 lines per second.

The output of the transmitter is fed to the Nimbus APT antenna mounted on the surface of the spacecraft which faces the earth at all times. The antenna produces a linearily polarized radiation pattern, so that the satellite-antenna ground-antenna relationship remains constant.

On the ground, the signal is received by a relatively simple antenna and is processed by the FM receiver and the facsimile recording equipment, producing a real-time cloudcover picture for the locale of the particular ground station.

The sequence just described assumes automatic receipt of a picture sequence from the beginning of the 208-second frame. It is more likely that the satellite will come into view of the ground station at some time after the first 8 seconds; however, as soon as the satellite signal is detected, the faxsimile machine can be started and phased manually so that the maximum amount of information may be obtained. This should result in at least three pictures during a pass over the ground station. At an orbital altitude of 500 nautical miles, each picture will cover a ground area of approximately 1050 by 1050 nautical miles, with a north-south overlap of 300 nautical miles between adjacent pictures.

The system has a linearity of 0.5 percent and a resolution of approximately 700 lines, based on the picture printed out on the facsimile recorder. Sensitivity is 0.7 foot-candle-seconds for highlight brightness (whitest white). The cutoff point where noise is the influencing factor is 0.03 foot-candle-seconds. The signal-to-noise ratio is 26 db, and approximately seven shades of gray are observed with a change in density of 0.12 per step.

Nimbus Radiometry

Two scanning radiometers have been designed for Nimbus, the medium-resolution

infrared radiometer (MRIR) and the high-resolution infrared radiometer (HRIR).

The MRIR is shown in Figure 16. The scan-mirror drive motor, the scan-mirror, the reflection of three of the five telescopes, the preamplifiers, and the chopper motor are visible; the electronics module is not shown.

This radiometer measures emitted infrared and reflected solar radiation in five spectral regions, using thermistor bolometer detectors. The spectral regions, and the reasons for selecting them, are listed in Table II. The spectral regions are similar to those measured by the TIROS five-channel radiometer. The 6.6-7.0-micron channel, covering an intense water-vapor or temperature distribution above the cloud tops. The 10-11-micron region lies within an atmospheric window and is well suited for determining surface and cloud-top temperatures, or cloud-top heights. The 7.5-30-micron channel will be used to determine the total radiant emission of the earth. Two visible-light channels are also included. The 0.6-0.75-micron region is the most transparent portion of the visible spectrum; this red end of the visible spectrum is less scattered by the atmosphere than the blue portion. This channel can be used to measure cloudcover during daylight, and can serve as a comparison to the television measurements. The 0.2-4.0-micron channel spectrally encompasses about 99 percent of solar radiation and is intended to measure the earth's albedo (reflected solar radiation).

Scanning is accomplished similarly in both radiometers; they scan the surface of the earth in strips perpendicular to the orbital track. The optical axis is in the direction of the subsatellite point, and the scanning rates and fields of view are chosen so that subsequent scan paths overlap reasonably well at the subsatellite point. The width of an individual scan path, as well as the amount of overlap, increases considerably toward the horizon.

The MRIR scanner consists essentially of a scanning plane mirror oriented at 45 degrees to the axis of rotation, a Cassegrainian telescope for each channel, a chopper to modulate the incoming radiation, and one detector per channel. The detector "sees" the difference between the radiation from the target and that from the chopper disc, whose temperature must be measured and telemetered. Four of the channels have light pipes between the chopper and detectors to converge the beam onto the tiny bolometers. There is no light pipe for the 6.6-7.0-micron channel which, for greater optical gain, uses an immersed bolometer.

Both the MRIR and HRIR will have a calibration check in orbit, which is a significant improvement over the TIROS system. For both radiometers, the space scan will serve as the zero reference, and during each scan a housing target of known temperature is seen which will serve as a second calibration point for the infrared channels. The temperature of this target must be telemetered. The sun will be the target of the second calibration point for the two solar-radiation channels. This point will be measured once during each orbit when the lower portion of the spacecraft is exposed to direct sunlight.

The MRIR instantaneous field-of-view is about 2.8 degrees which, at 600 miles, corresponds to a 30-mile linear resolution directly below the vertical. It scans at 1.9 rpm and has an information bandwidth of 8 cps. Total power consumption is 7.2 watts and the total weight, including the electronics module, is 11 pounds.

Figure 19, a block diagram of the MRIR subsystem, shows that the radiometer output is fed into a voltage-controlled oscillator (VCO), the output of which is put on tape along with a 500-cps time-reference signal from the master clock; the figure gives the frequency range of each of the five VCO channels. On playback (at a speedup ratio of 1:30) the stored information is transmitted via an FM

transmitter to the ground station, where it is stored on tape. Real-time application of the window-channel data may be possible in plotting cloud maps with associated cloud-top heights. Full data processing will be performed in Washington, D. C., using equipment similar to that used for TIROS.

The single-channel HRIR is shown in Figure 20. This equipment will be used to map nighttime cloudcover and cloud-top temperatures or heights. The cylindrical projection shown at the right holds the motor which drives both the scan mirror and the chopper. The white collars are sunshields; the scan mirror is visible between them. At the bottom left is the rectangular pyramid used to cool the detector by radiation. Cooling by liquid nitrogen or cryogenics is not feasible on Nimbus. The radiometer electronic items are located around this pyramid. This radiometer uses a photoconductive lead selenide (PbSe) detector operating in the 3.4-4.2-micron region, which is considered reasonably free of atmospheric absorption. The HRIR has an instantaneous field-of-view of 8.6 milliradians, which at 600 miles corresponds to a linear resolution of 5 miles below the vertical. The field-of-view, originally 2.8 mr, was changed when tests showed that the radiometer was not sufficiently sensitive.

TIROS measurements indicate that the equivalent blackbody temperature of a cloud can frequently be as low as 200°K, and the field-of-view was opened up to permit detection of these cold clouds. The scanning rate of 44.7 rpm was chosen so that the radiometer would make one complete scan during the time required for the satellite to advance the width of one line on the ground directly below the vertical, at a 600-mile altitude.

The total weight of the HRIR is 11.3 pounds, and it draws approximately 4 watts of power. The radiometer motor, which consumes about 1 watt of power, will be on

continuously; however, the electronics equipment will be turned off during the daylight hours by means of a day/night switch.

A tape recorder, almost identical in design to the television recorder, records the signal at 3.75 inches per second. A four-track head, similar to the TV camera recorder, is used. One track receives the radiometer signal; another records the 10-kc timing signal from the master clock. When one tape reel is fully unwound, the movement is reversed and the signals are switched to the remaining two tracks. The recorder continues to record until the reel is empty again and then stopped by a limit switch. For transmission, the tape speed is increased eightfold and all tracks are also applied to four heads simultaneously. Local oscillators and mixers generate a frequency-multiplexing spectrum.

Both television and HRIR tape recorders carry momentum compensation motors to reduce spacecraft disturbances.

The composite frequency-multiplexed signal is added as part of the composite TV signal and transmitted through the same transmitter. Design principles of FM/FM telemetry system have been treated exhaustively in the literature. It may suffice to state here that all channels have adequate post detection signal-to-noise ratio so that the limitation is the detector itself; e.g., the vidicon or the lead selenide transducer.

Full earth coverage of the earth's IR transmission should provide a new and fundamental atmospheric parameter for detailed study and should lead to new understandings.

Weight considerations necessitated the removal of one of the radiometers from the first Nimbus. The choice was made to fly the HRIR, because it will photographically display nighttime cloud cover with comparatively high resolution, which was

felt to be of great immediate need. This radiometer also contains some unique features, such as a radiation-cooled detector, which it was desired to test in orbit.

OPERATIONAL GROUND STATIONS

Operational ground stations consist basically of a receiving antenna, preamplifier, FM receiver, and facsimile recording equipment. Auxiliary equipment for each station consists of a test signal source and a facsimile test set.

The ground antenna (Figure 21) is an 8-turn helix, 14 feet long and 27 inches in diameter, with a ground plane 72 inches in diameter. It has a beamwidth of 34 degrees at the half-power points and a gain of 13 db.

The pedestal contains the position motor drives, gearing, position synchro transmitter, and limit switches. It is capable of 720-degree rotation from stop to stop in azimuth, and 180-degree rotation (horizon to horizon) from stop to stop in elevation. Total weight including antenna counterbalances is approximately 850 pounds.

The position control and indicator units located in the ground station console (Figure 22) provide independent rate control of both azimuth and elevation and continuous display of the antenna position.

The preamplifier, mounted on the antenna pedestal, and the receiver, located in the console, are standard "off the shelf" equipment. The preamp is a two-stage RF amplifier with a 5-Mc passband and a gain of 22 db, the latter required to compensate for losses in the RF cable when the antenna and the receiver must be located some distance apart. Maximum separation can be 1000 feet with the present cable.

The FM receiver is crystal-controlled from 130 to 140 Mc, with a second oscillator vernier control which allows tuning across 150 kc on either side of the operating frequency. The receiver has a selectable bandwidth of 50 or 100 kc.

The presence and condition of the input signal can be determined both aurally and visually, as the unit has a speaker and four indicators: signal strength, tuning, video output, and deviation.

The facsimile recorder, a modified version of the Fairchild Camera and Instrument Co. Scan-a-Fax, is a helix and writing-blade-type machine, using electrosensitive (wet) paper and forming the picture by depositing ions on the paper. The machine operates at 240 rpm with a resolution of 100 lines per inch, has an aspect ratio of 1 on an 8-by 8-inch format, and will produce ten shades of gray varying from black to white. The unit will start and phase automatically upon receipt of the 300-cps start tone and the 5 seconds of phasing pulses from the satellite equipment, or it can be started and phased manually.

The characteristic of direct real-time picture transmission makes this system particularly attractive to local users for short-range forecasts and aeronautical operations. It should find wide application.

PROGRAM STATUS

Now that we have described the Nimbus spacecraft and its subsystems in considerable detail, it is appropriate to review the status of the system development and note some of the major developmental problems encountered. As noted earlier, following preliminary design, development and hardware construction contracts were entered into late in 1960 and early in 1961 for all major subsystems. A separate integration and test contract was also entered into early in 1961. In the 2-½

years since that time, tremendous effort has been exerted to bring the Nimbus spacecraft into reality, and, although a number of delays have been encountered, significant progress has been achieved. Achievements to data include these significant milestones:

Breadboard construction and testing of all subsystems

Construction of preprototypes of all subsystems, for electrical and mechanical system testing and proof

Construction of prototypes of all subsystems, and demonstration of satisfactory subsystem performance

Environmental qualification of all subsystems in a rigorous test program which included acceleration, humidity, and vibration and vacuum thermal tests

Development and construction of adapter and spacecraft separation system

Construction, testing, and integration of all ground-station subsystems

Construction and operational readiness of Fairbanks command and data-acquisition sites

Integration of the prototype spacecraft, which is now in full swing

Construction of initial flight hardware for all subsystems, already completed on most subsystems, with only a few subsystems in final stages of construction and qualification

With these milestones accomplished, the tasks remaining before the first flight are confined to completion of the prototype environmental qualification and the

assembly and qualification of the first spacecraft. These tasks include full spacecraft system tests on an air bearing in a large vacuum-thermal chamber (Figure 23) when full flight simulation will be demonstrated for sustained operating periods. Hopefully, these remaining tasks can be completed before next winter and the first flight can be undertaken.

Table III summarizes some of the major design objectives, showing what has been possible to achieve in the actual flight hardware. In most respects, design objectives in regard to performance have been closely approximated. Spacecraft weight however has increased considerably over the original design objective of 650 pounds, and the full initial configuration would now weigh in excess of 900 pounds. Because of launch vehicle limitations, early flights will carry a reduced spacecraft configuration lacking the redundant sensors which are desirable for long life. Use of the Thrust-Augmented Thor on later flights will permit a fuller payload.

The remaining design objectives were largely achieved, with two significant exceptions: Detailed studies indicate that the desired 1-degree pointing accuracy cannot be achieved under all weather conditions, because high altitude and cold clouds may introduce errors of as much as a few degrees in the altitude sensing. This limitation, however, is not considered serious. Also, the full design objective for the resolution of the HRIR could not be achieved in the initial prototype, and a compromise to 5 miles resolution was found necessary. Later designs should permit some improvement, however. In total, the initial design objectives for the subsystem appear to have been met quite well; the remaining task involve only the successful integration and qualification of the full spacecraft.

DATA FLOW

Before closing, I should like to describe the data flow from the Nimbus satellite. Figure 24 illustrates the flow of data from the satellite in flight. Once per orbit the satellite will be interrogated from the CDA site and the data transmitted to the ground. On the ground, the data will be processed and transmitted by microwave link to the Technical Control Center located at the Goddard Space Flight Center. Engineering and research data will be transmitted to Goddard for real-time spacecraft evaluation and for scientific analysis. The cloud-picture data and, if feasible, the infrared radiation data will be transmitted to the National Weather Satellite Center of the U. S. Weather Bureau for incorporation into the daily weather forecasts. The complete coverage and the regularity of service promised by the Nimbus system should, in the long run, constitute a real boon to weather forecasting.

CONCLUDING REMARKS

The foregoing remarks have described the Nimbus spacecraft system and its development status. The initial development of the Nimbus system is now drawing to an early conclusion with the first flight hopefully only months away. A large and versatile spacecraft has been developed with some attractive initial meteorological sensors, AVCS, APT, MRIR, and HRIR. Basic spacecraft systems of considerable refinement have also been developed. Flight test will demonstrate the extent of our achievements. The meteorological mission in space is clear and attractive as one of the focal efforts in the space program.

Many of us feel that this mission will find its most glorious fulfillment as the Nimbus system evolves with new sensory developments and with improved

basic spacecraft systems. To this end, we hope we can rally a larger share of the national astronautical talent. We welcome your comments and contributions.

Table I

Comparison of Nimbus and TIROS

	TIROS	NIMBUS
Geometry	Pillbox	Dumbbell
Weight (lbs)	300	650
Orbital altitude Nautical miles	380	600
Orbital inclination	48° equatorial	80° polar, retrograde
Stabilization	Spin-stabilized	3-axes earth oriented
Earth Coverage	10 to 25	100
Camera Raster	500 lines / frame	800 lines / frame
TV resolution (miles)	1	½
Maximum power available (watts)	20	400
IR sensors (resolution, miles)	MRIR (30)	MRIR (30) HRIR (5)

Table II

Spectral Regions Measured by MRIR

WAVELENGTH (MICRONS)	FUNCTION
6.6 - 7.0	Water vapor absorption
10.0 - 11.0	Surface and Cloud radiation
0.6 - 0.75	Cloud cover
7.5 - 30.0	Total earth emission
0.2 - 4.0	Albedo (reflected solar radiation)

Table III

Nimbus Performance Achievements

	Design Objective	Achievement
Weight	650 pounds	775 pounds
Stab. accuracy	± 1 degree	± 2 degrees
Power (maximum)	450 watts	400 watts
AVCS (resolution)	½ mile	½ mile
PCM telemetry	128 (real time)	128 (real time)
	544 (recorded)	544 (recorded)
HRIR (resolution)	2 miles	5 miles
MRIR (resolution)	30 miles	30 miles
Commands	128	128

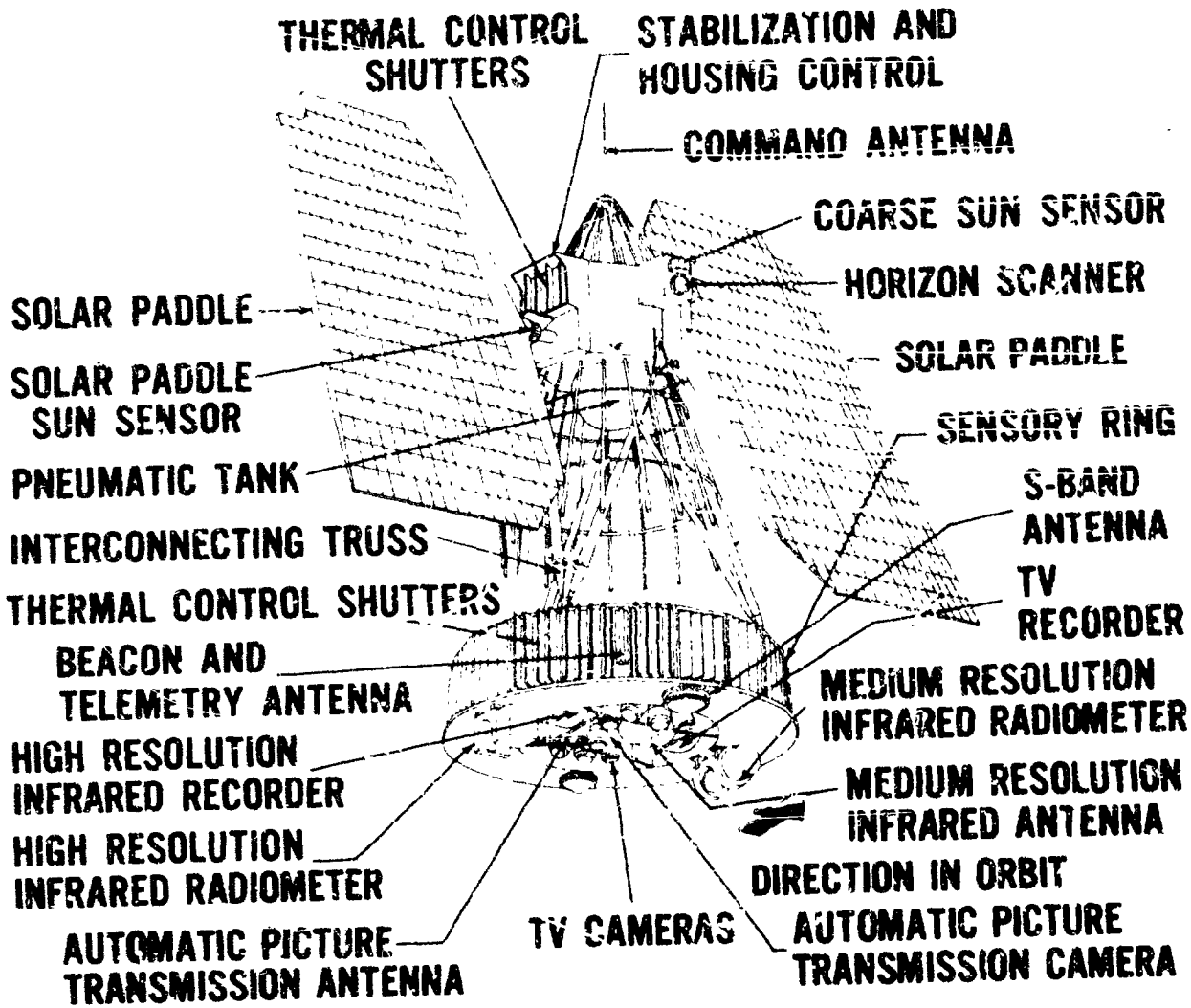

Figure 1 – Nimbus Spacecraft

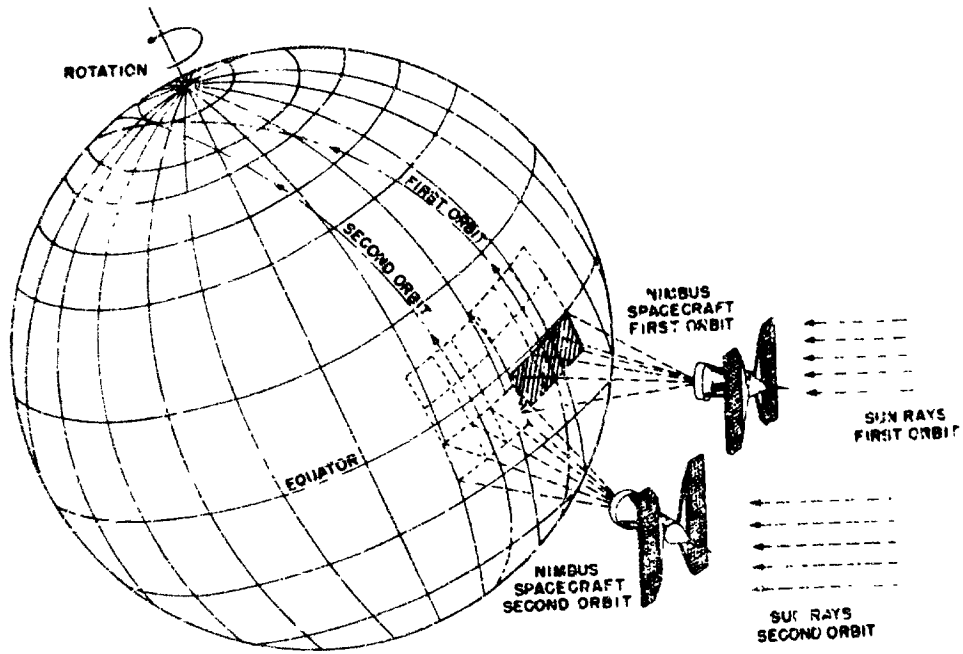

Figure 2 – Nimbus Television Coverage

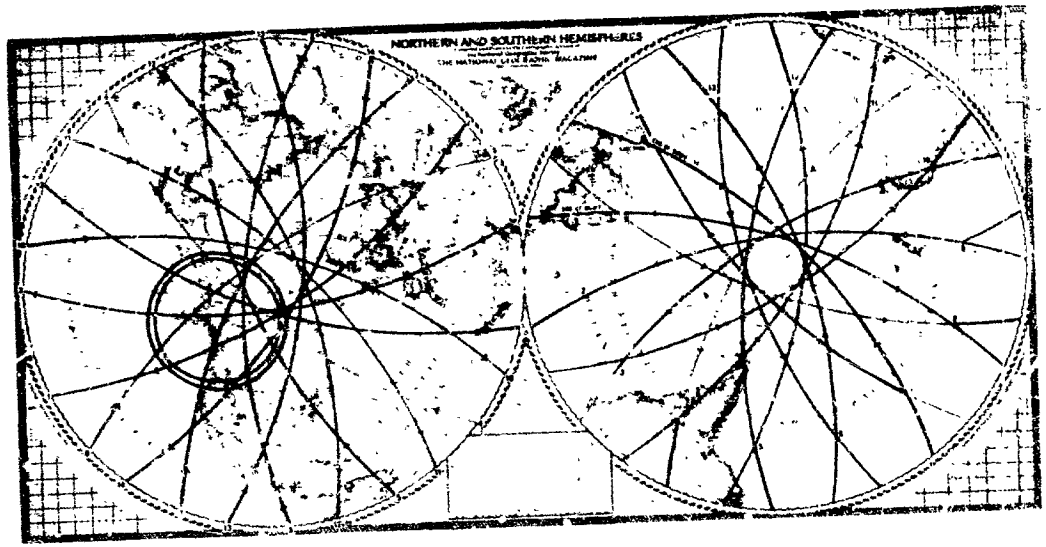

Figure 3 – Orbital Coverage from Fairbanks, Alaska

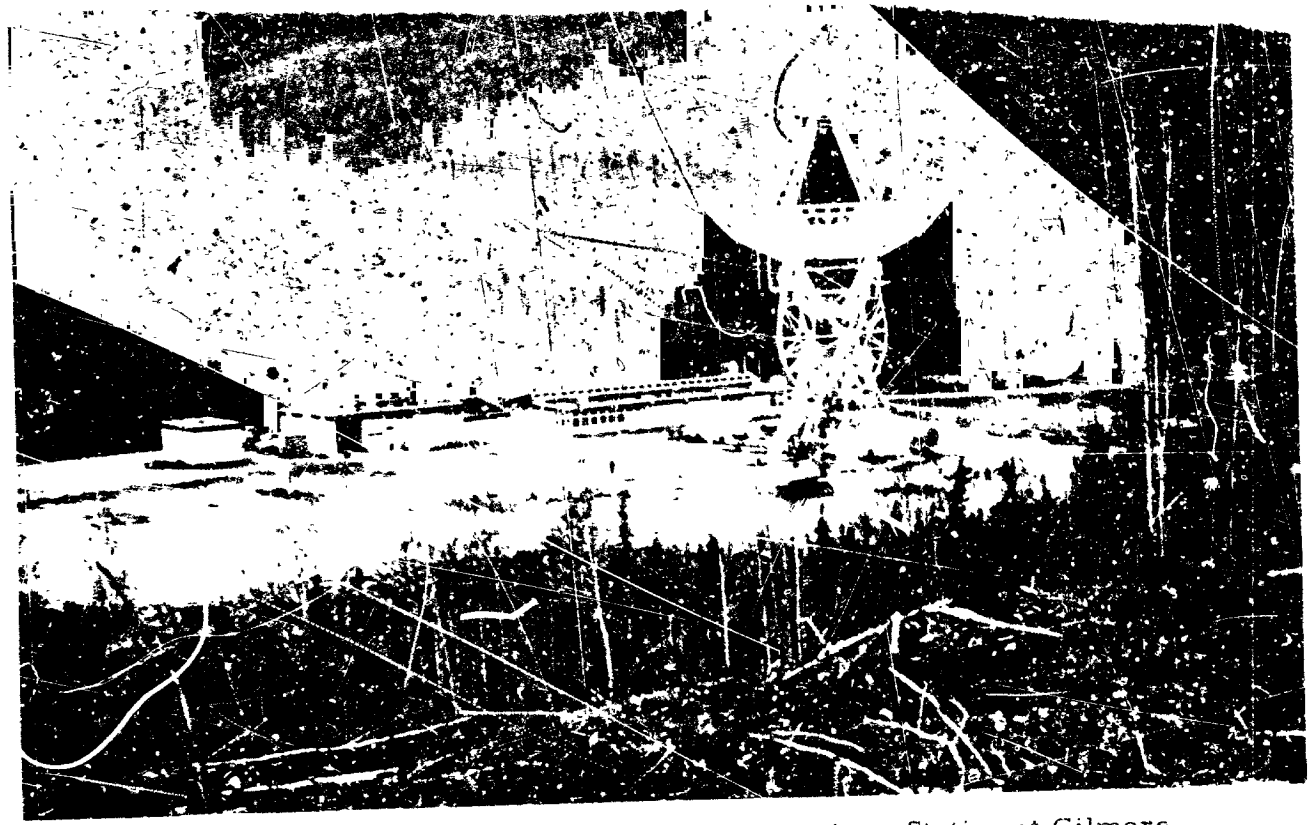

Figure 4 – Command and Data-Acquisition Station at Gilmore Creek near Fairbanks, Alaska

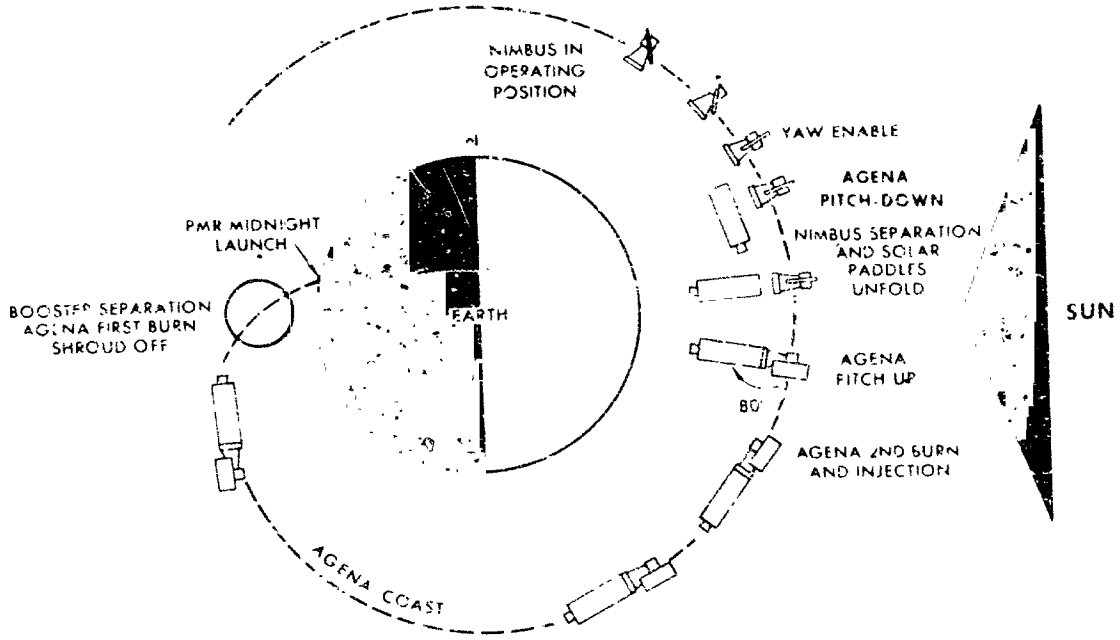

Figure 5 - Nimbus Launch Sequence

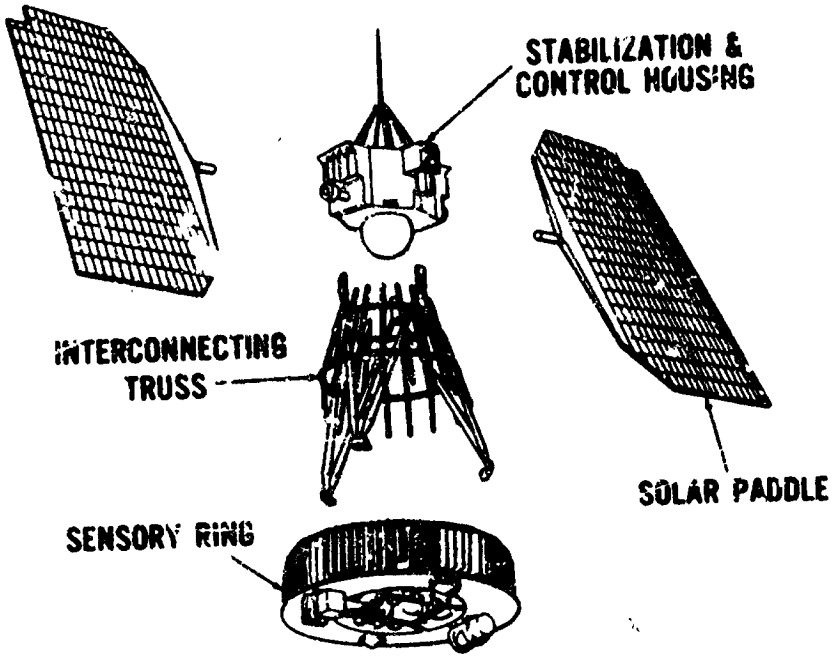

Figure 6 - Nimbus Breakaway

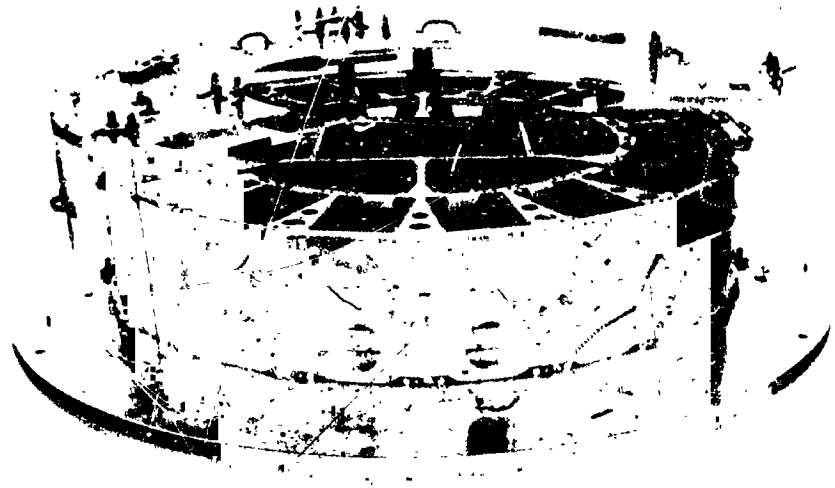

Figure 7 – Empty Prototype Sensory Ring

Figure 8 – Flight Solar Platforms

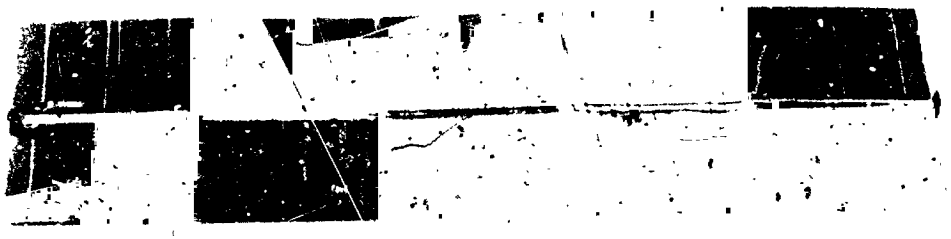

Figure 9 – Solar-Cell Module

Figure 10 – Battery Modules

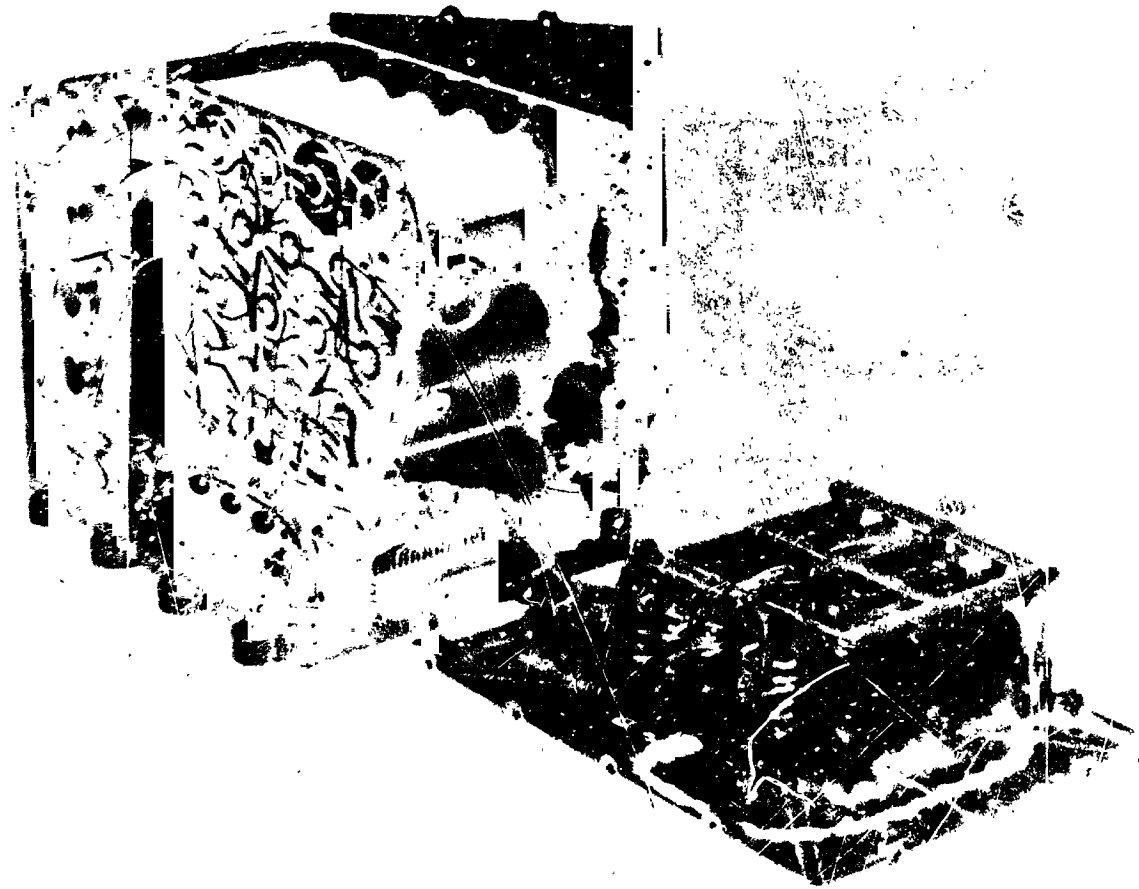

Figure 11 – Battery Module, Showing the Two Major Subassemblies

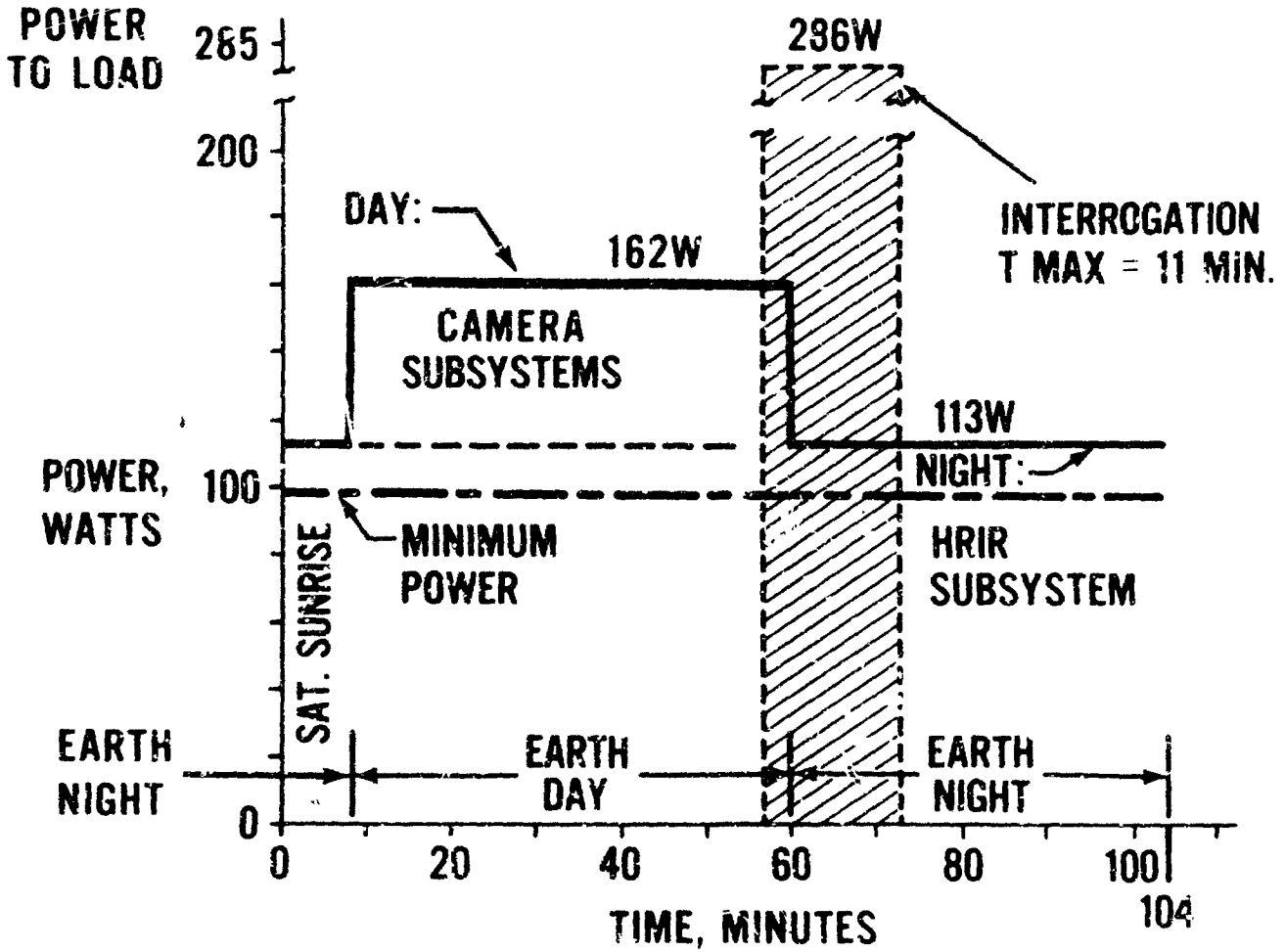

Figure 12 – Nimbus Space Orbital Power Demand

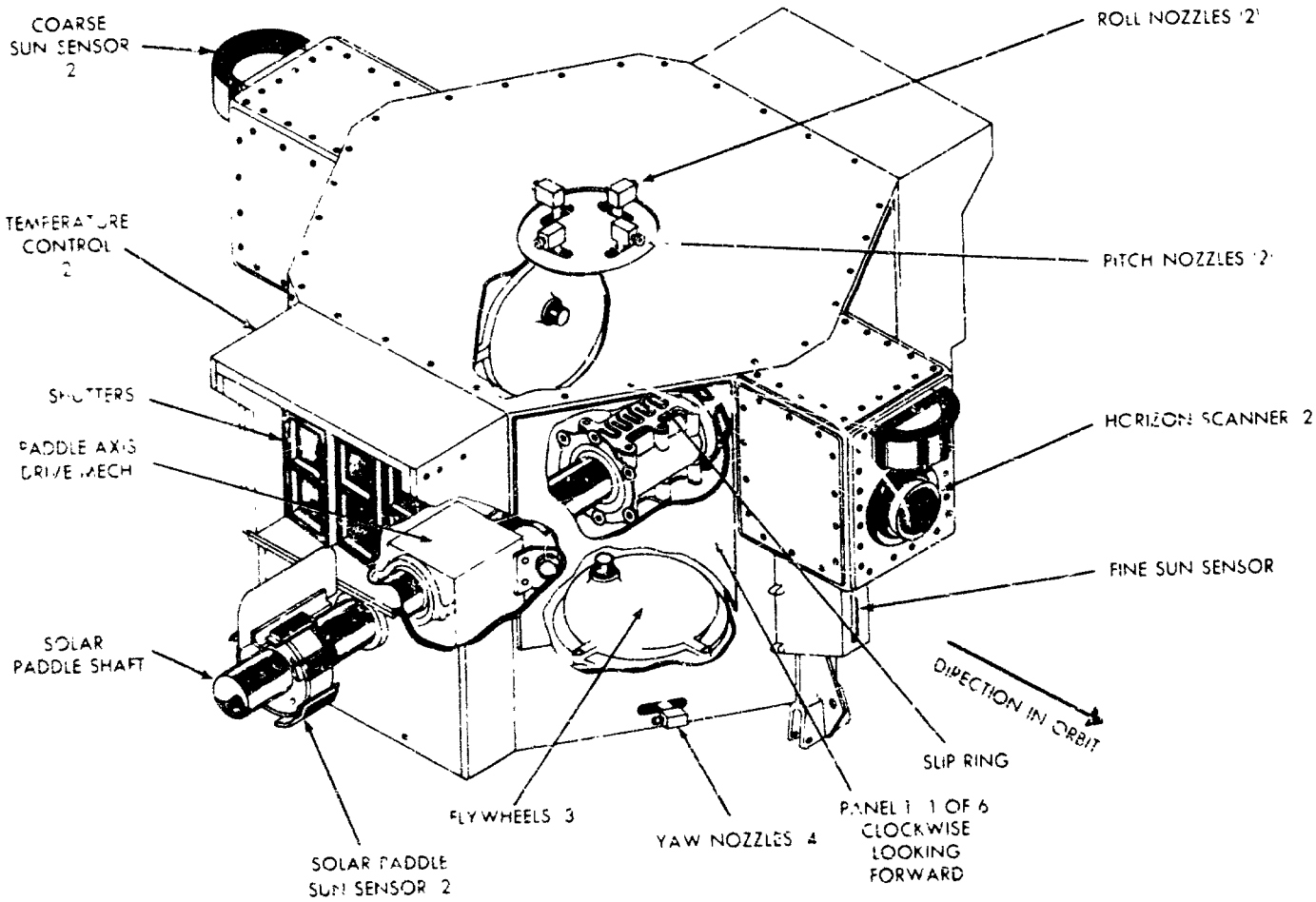

Figure 13 – Nimbus Control Subsystem Prototype

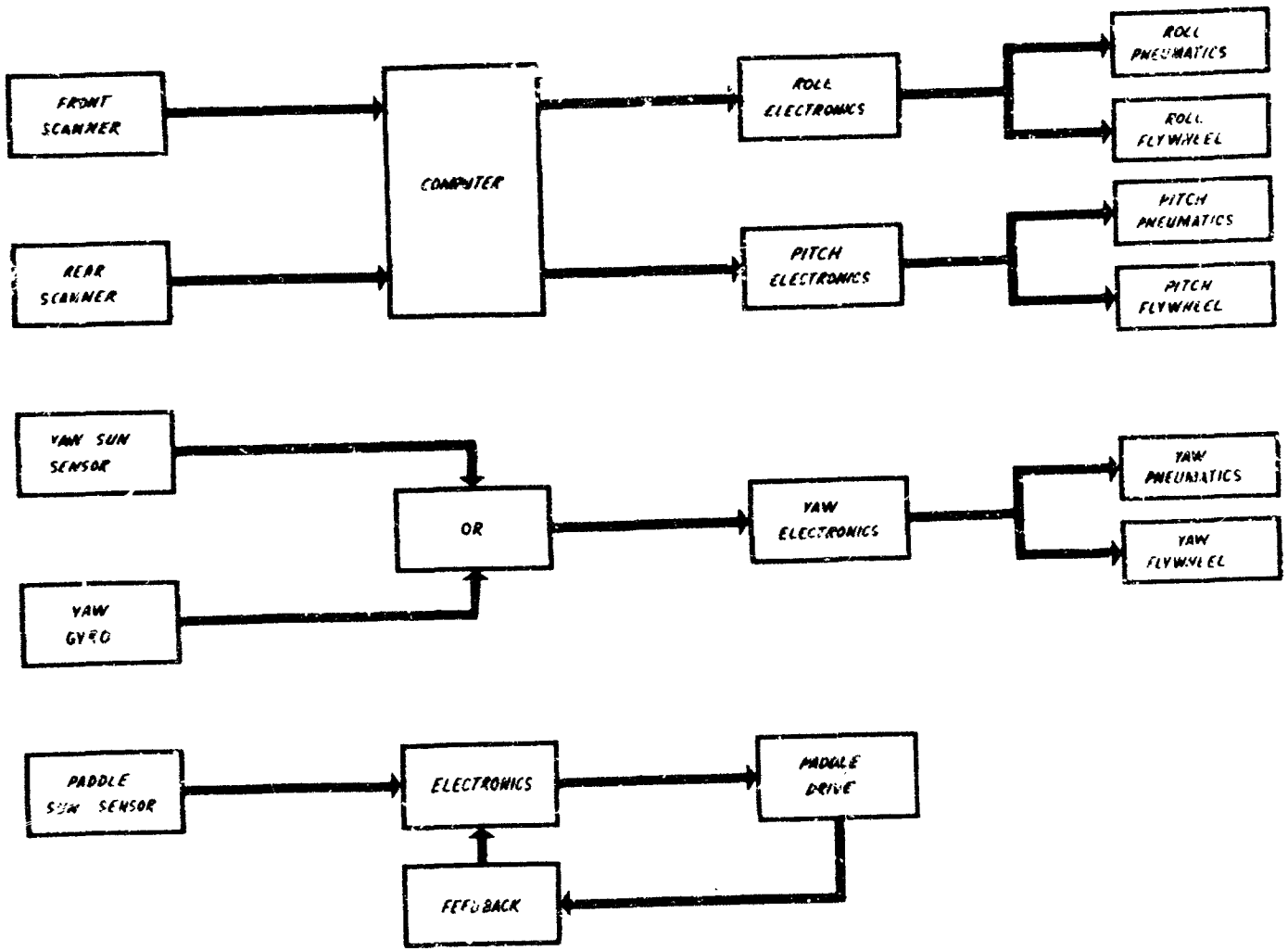

Figure 14 - Nimbus Control Subsystem, Block Diagram

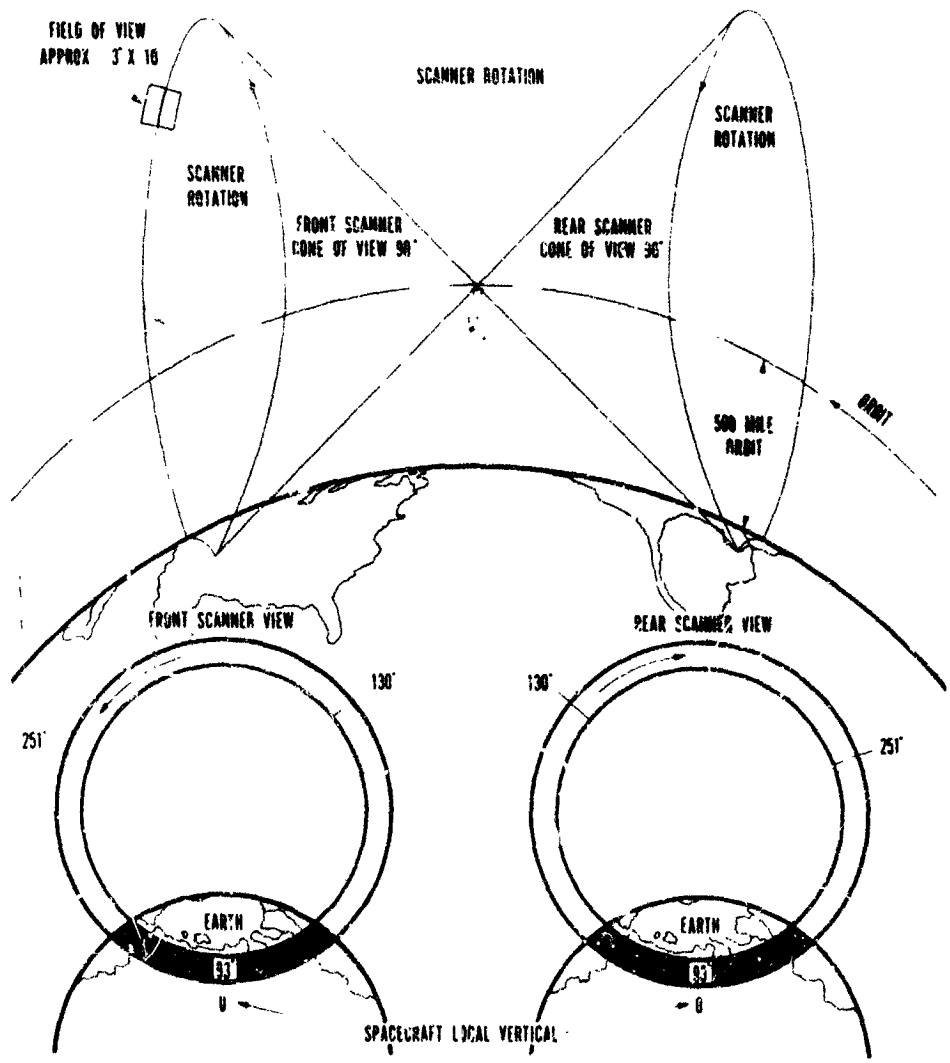

Figure 15 - Earth as Seen by Scanners in Stabilized Nimbus

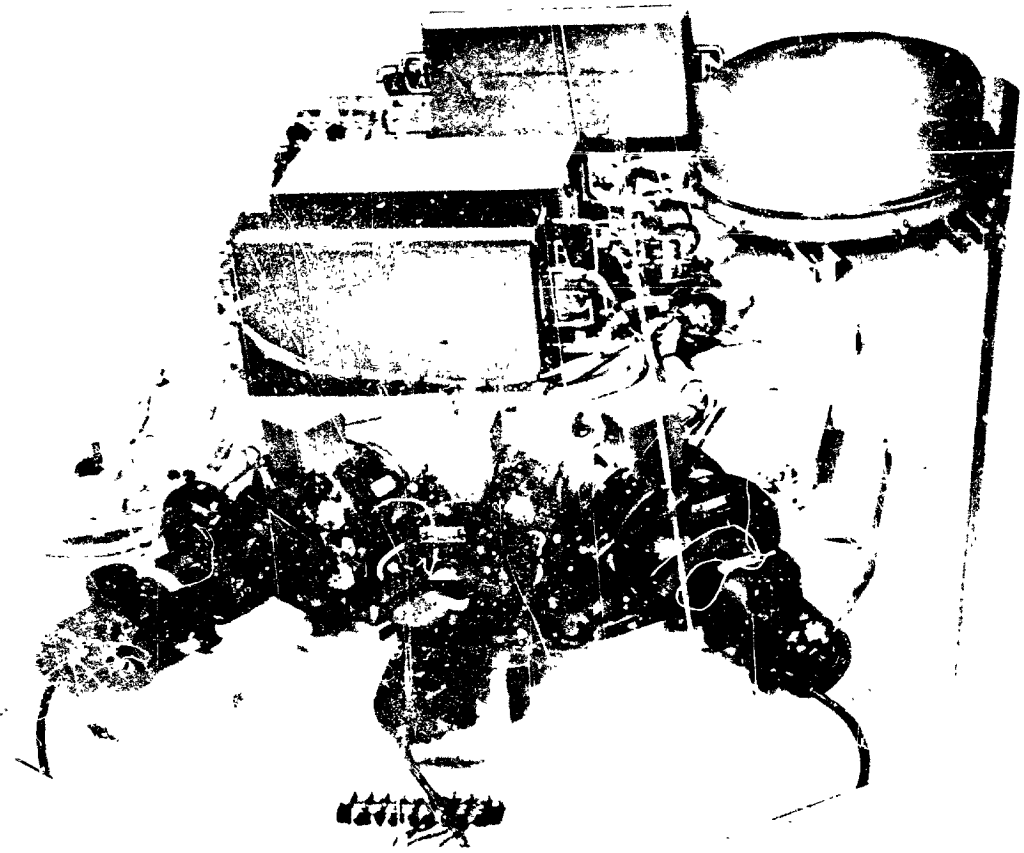

Figure 16 – Nimbus Advanced Vidicon Camera Subsystem Prototype No. 2

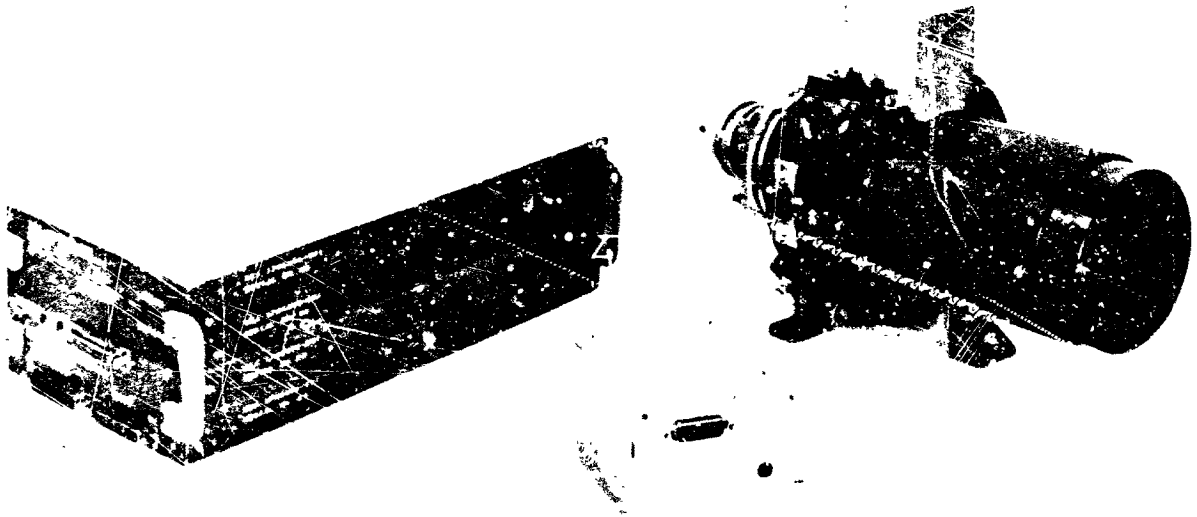

Figure 17 – Automatic Picture Transmission Camera and Electronics

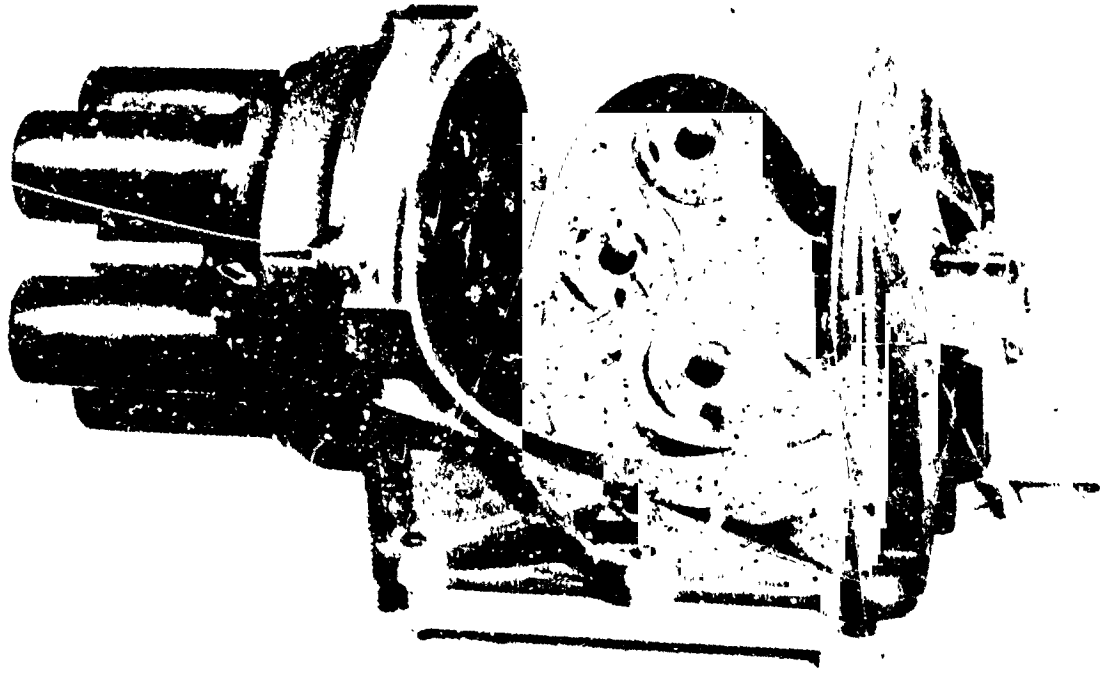

Figure 18 - Nimbus 5-Channel Medium-Resolution Infrared Radiometer

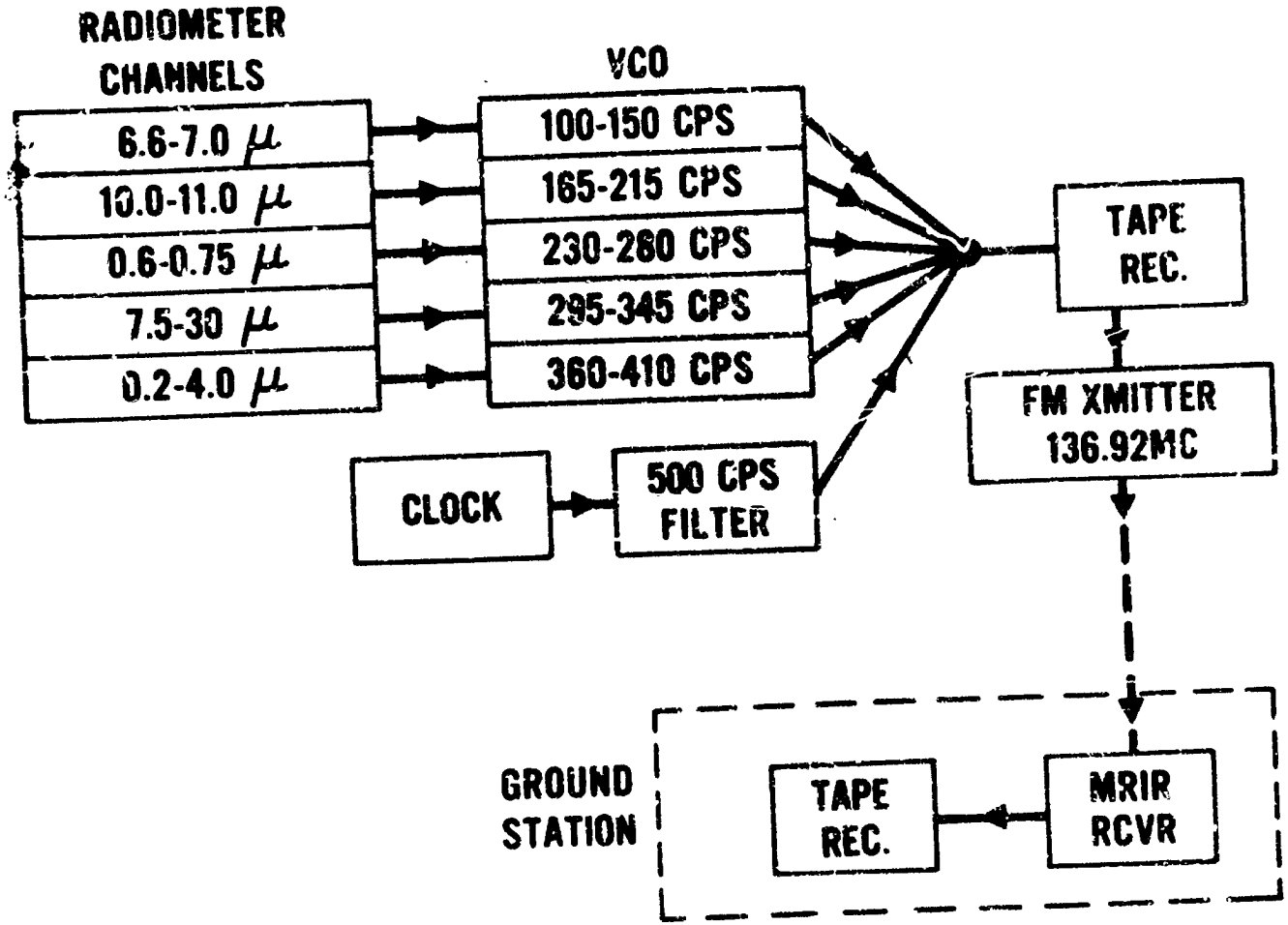

Figure 19 – Nimbus MRIR Subsystem, Block Diagram

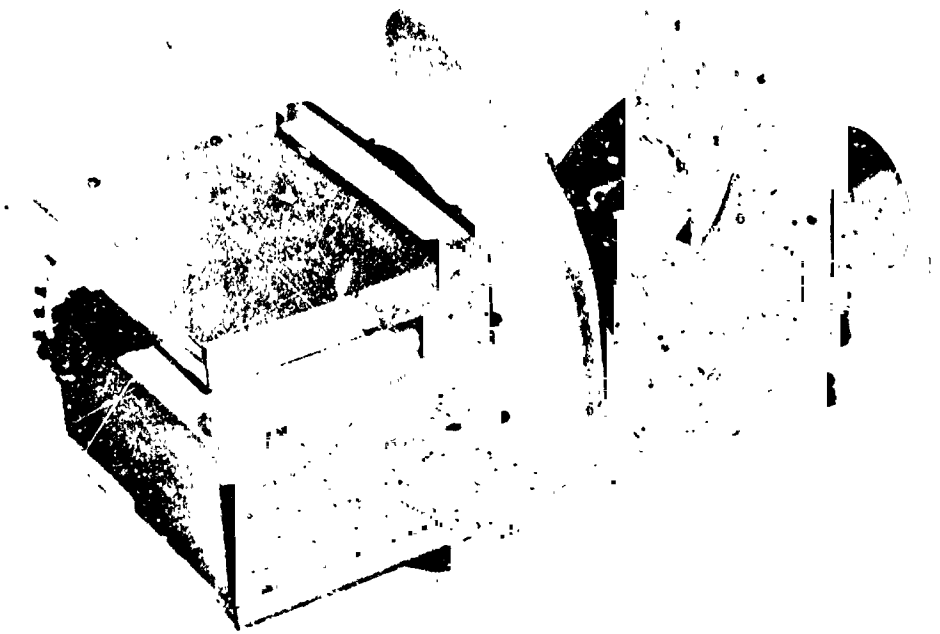

Figure 20 – Nimbus High-Resolution Infrared Radiometer

APT ANTENNA AND PEDESTAL

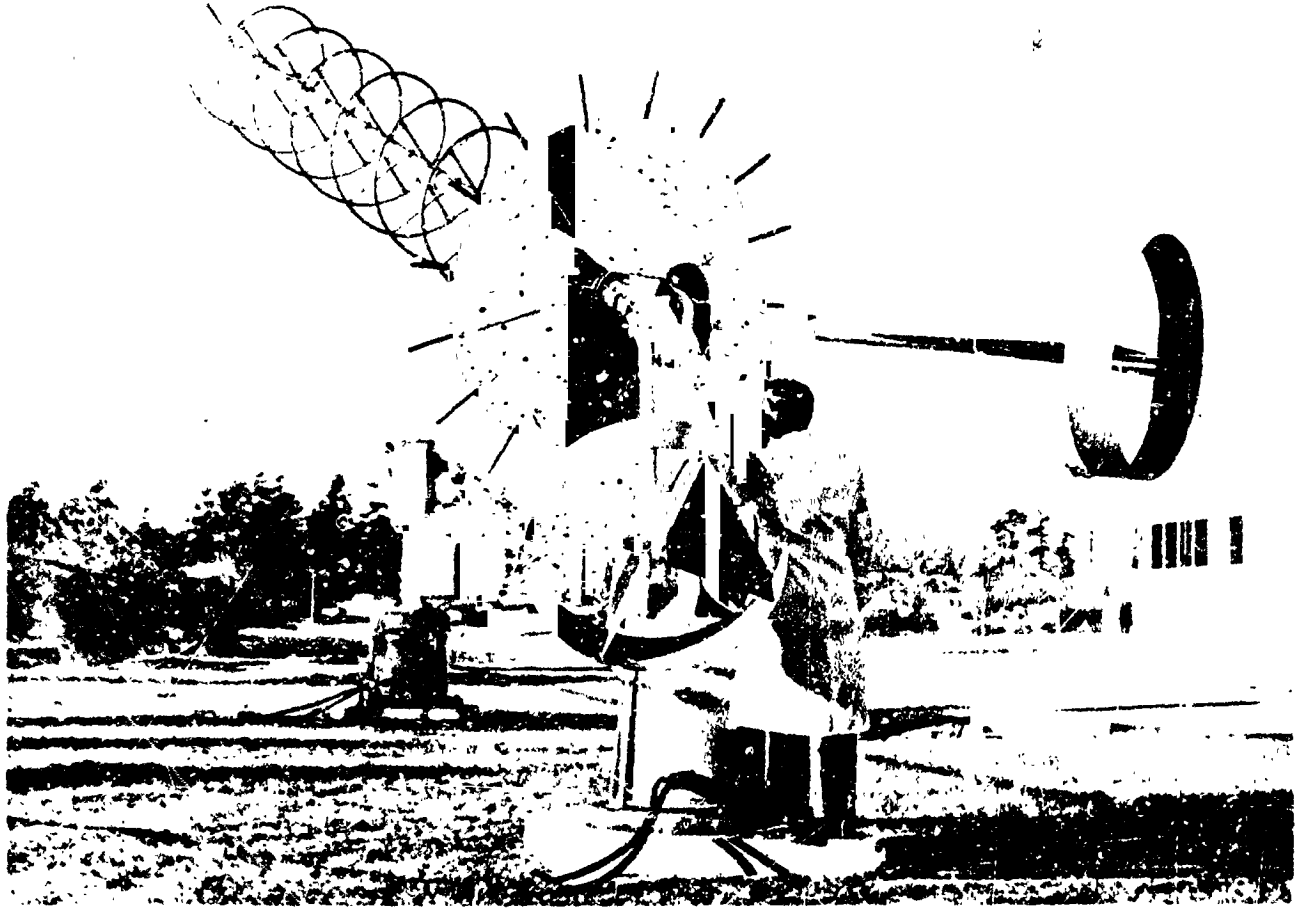

Figure 21 – Automatic Picture Transmission Antenna and Pedestal

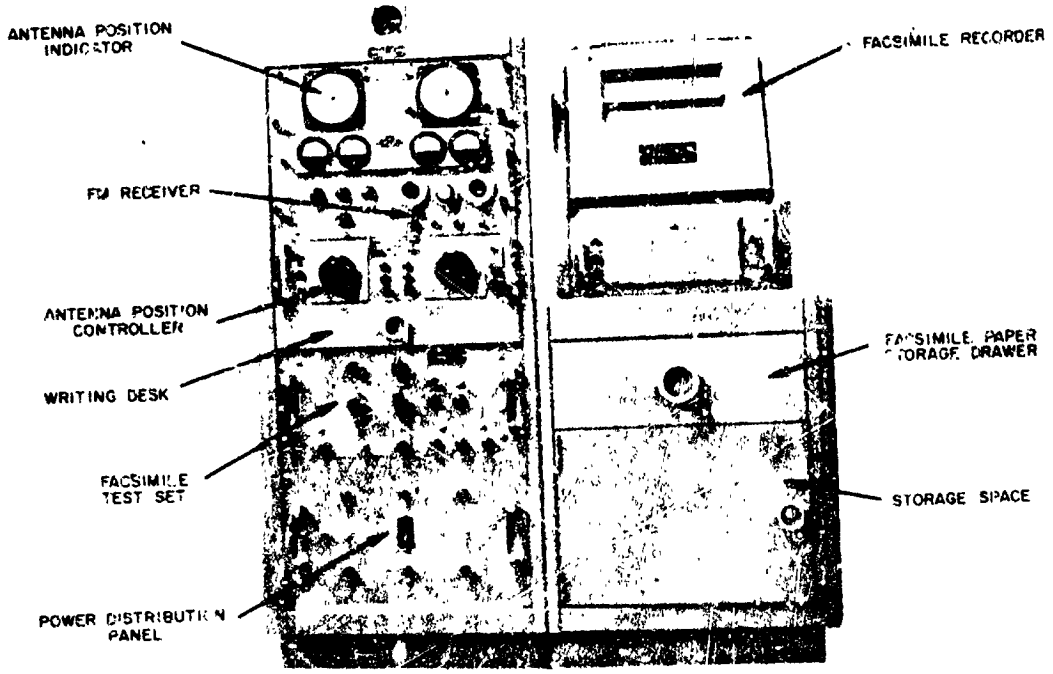

Figure 22 – Automatic Picture Transmission Ground-Station Console

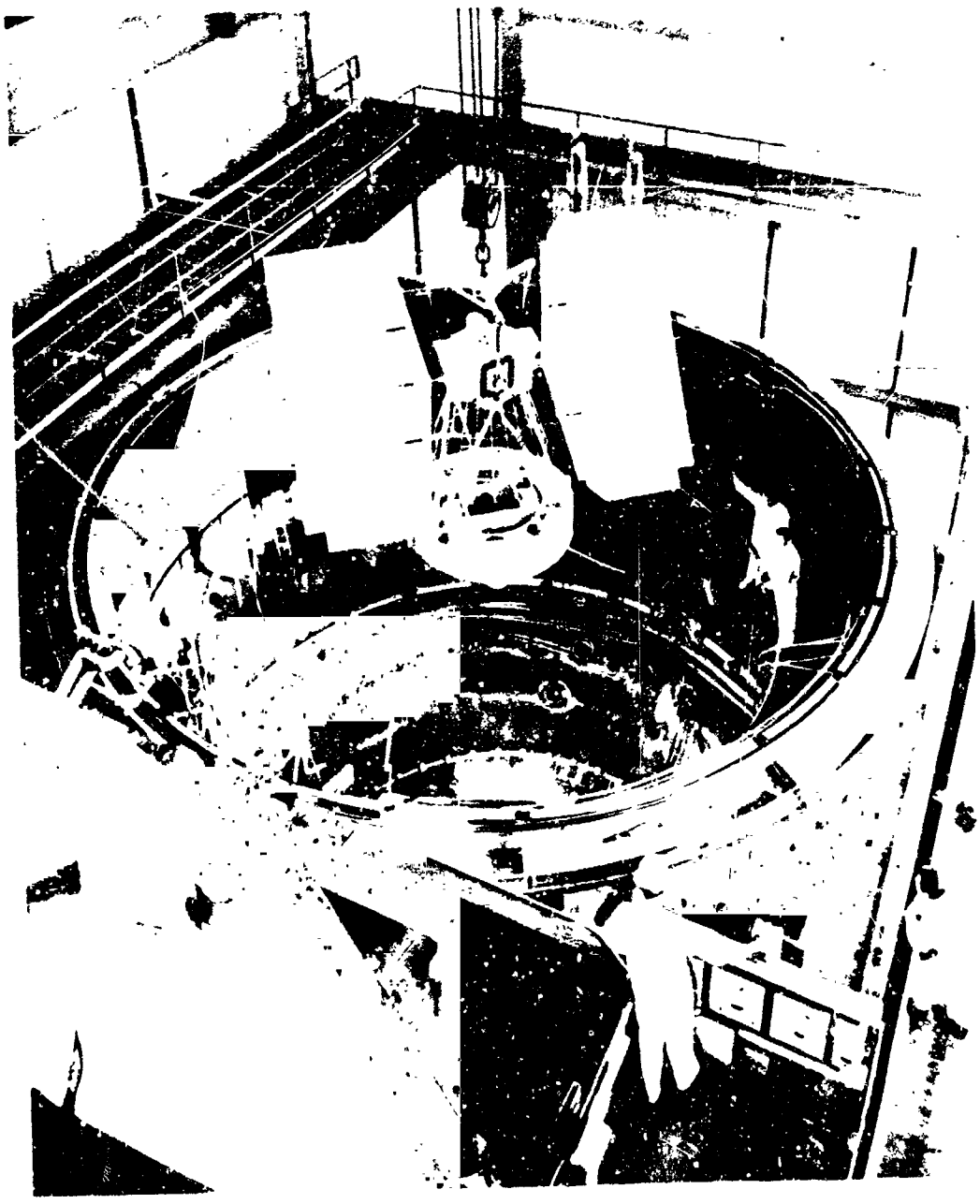

Figure 23 – Thermal-Vacuum Test Chamber

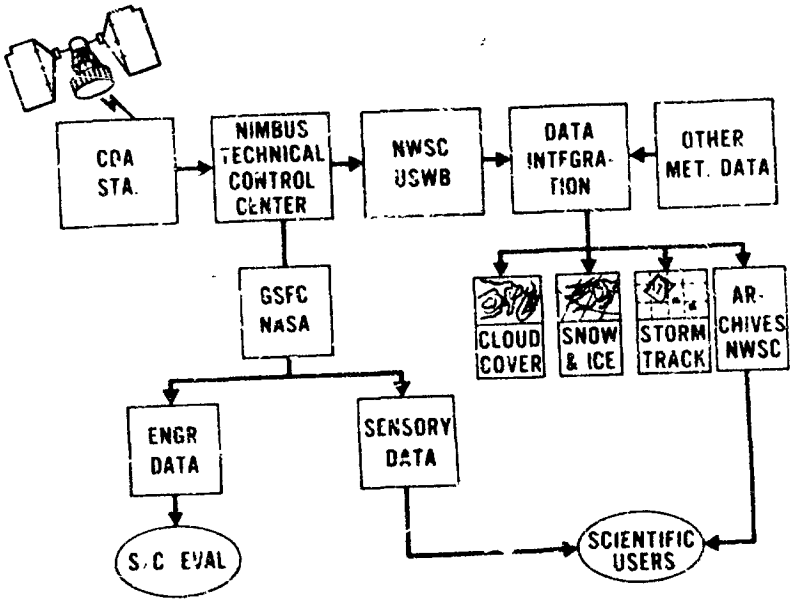

Figure 24 – Data-Utilization System

ANNA

BY

RICHARD B. KERSHNER

APPLIED PHYSICS LABORATORY

(Paper not available for publication)

PASSIVE COMMUNICATIONS SATELLITES

BY

WILLIAM J. O'SULLIVAN, JR.

NASA, LANGLEY RESEARCH CENTER

HAMPTON, VIRGINIA

PASSIVE COMMUNICATIONS SATELLITES

by

William J. O'Sullivan, Jr.

National Aeronautics and Space Administration

INTRODUCTION

Of the many uses that have been proposed for space, few, if any, give such great promise of being of commercial importance and general benefit to mankind as communication satellites. History and reason attest that all new scientific and engineering achievements of man that are of commercial value must, by virtue of their commercial significance, be subject to evaluation from an economic viewpoin . The present status of communications satellites in general is that there is now being gathered and evaluated the scientific and engineering information necessary for determining the most economically feasible satellite communications system. By "system" is meant not only the satellites, but also the ground transmitting and receiving stations that connect the earth and the satellites, as well as the links between the ground transmitting and receiving stations and the consumer or customer who originates or receives the communication. These are the things with which this discourse must deal in order to accomplish its objective of acquainting you with the current problems, findings, and most recent accomplishments. It will not be all inclusive in that it will be confined to the so-called "passive" communications satellite, as distinct from the "active" satellite that is discussed in a companion paper of this conference.

Much of the earth-based portion of either "active" or "passive" communications satellite systems makes use of already existing local ground distribution networks, such as telephones and local radio and television stations, with which you are already familiar. Accordingly, this discussion deals primarily with that which is new and less familiar, namely, the satellites themselves and the transmitting and receiving stations that link them with earth. These new components of the entire system present interesting and challenging new problems that demand for their best solution the drawing upon knowledge from many different scientific and engineering disciplines that prior to the Space Age have had little or no common ground of mutual contact and stimulation. In the firm belief that the deliberate cultivation of interdisciplinary activity will lead to better solutions of the problems of communications satellites in particular, and the most rapid advancement of science and engineering in general, a deliberate attempt is made in this discussion of the passive communications satellite to develop the several aspects of the topic from first principles in order to build a common ground of understanding between a number of different scientific and engineering disciplines. This, it is hoped, will provide an introduction to the subject to many who are not now actively participating in it, as well as assisting others who are working on highly specialized aspects of the problem and desire a better understanding of the orientation of their efforts relative to the over-all problem.

PART I THE PHYSICAL CHARACTERISTICS OF PASSIVE COMMUNICATIONS SATELLITES

On August 17, 1960, the National Aeronautics and Space Administration initiated its program of research on communications satellites by placing into orbit the Echo I Passive Communications Research Satellite. Currently, it is developing a larger and rigidized version, now identified as A-12, and when placed into orbit will be named Echo II. These two satellites, designed by the NASA Langley Research Center,

are shown in figure 1 as they were undergoing structural static inflation tests in a balloon hangar at Weeksville, N. C. Both of them are spheres. Echo I is 100 feet in diameter and weighs 130 pounds. Echo II is 135 feet in diameter and weighs 512 pounds.

In figure 2 is shown how such large spacecraft are transported into orbit. They are compactly folded in a special manner, and snugly packed inside a container that is mounted on the nose of the launching rocket. The Echo I container is spherical and has an inside diameter of 26 inches. The Echo II container, shown in figure 2, is ellipsoidal with a major internal diameter of 39.5 inches and minor internal diameter of 29.5 inches. Otherwise, the containers are essentially similar and their principles of operation are identical. When so packed within their containers, the satellites can withstand the heavy accelerations and vibrations imposed on them by the launching rocket. A nose cone that is jettisoned above the earth's atmosphere is placed over the container to protect the container and satellite from aerodynamic forces and heating during the ascent through the earth's atmosphere. When the rocket has carried its payload into orbit, the container is then released from the nose of the rocket by a separation mechanism that includes some springs that propel the container away from the rocket with a velocity of several feet per second. When the container has reached a distance of several hundred feet from the rocket, so that there is no danger of the inflating satellite enveloping the rocket, the container is opened. The container is constructed of two halves that accurately fit together, and have flanges at the joint. An explosive placed between the flanges opens the container and imparts to the two container halves, a separation velocity of about 50 feet per second.

In figure 3 is shown an opening test of the Echo II container in a 60-foot diameter vacuum chamber at the NASA Langley Research Center. The container and

the satellite are evacuated to a pressure of the order of a few millimeters of mercury so that upon opening of the container in the hard vacuum of space, the satellite is not explosively inflated. The minute amount of air remaining in the satellite is sufficient to initiate unfolding of the satellite. Inside the satellite is placed in the form of a powder, an inflating material that will sublime, that is, change directly from the solid state into the gaseous state. To do so, the inflation material must acquire heat since sublimation is an endothermic reaction. The mass of the inflation material itself, and the mass of the satellite, provide the initial supply of heat to the inflation material as heat stored in them by virtue of their specific heats. Thereafter, the heat is obtained from the sunlight falling upon the satellite. The process is readily regulated by limiting the amount of subliming material; for after conversion of all of the subliming material into gas, the pressure is thereafter proportional to the absolute temperature of the satellite, which temperature is fixed by the optical properties of the satellite's exterior, namely, the ratio of its absorbtivity to solar radiation to its emissivity to thermal radiation. Among the subliming materials that have been used are benzoic acid, anthraquinone, and acetamide.

In figure 4 is shown, approximately to scale, cross sections of the material of which the Echo 1, Echo II, and the Explorer IX are constructed. The Explorer IX is a 12-foot diameter inflatable sphere that was placed into orbit by the NASA Langley Research Center to measure the density of the earth's upper atmosphere, and has proven so successful that another is now scheduled for launching. All three satellites employ a very strong plastic film called Mylar which gives them the requisite toughness to withstand folding into their containers followed by pneumatic erection in orbit. Also, plastics, technically called polymers, are composed of very long chain molecules containing hundreds of thousands of atoms,

so that their vapor pressures are so very low as to be far beyond reliable measurement. For this reason, their rate of evaporation in the hard vacuum of space is so slow that they will last almost indefinitely.

The Echo I is constructed of Mylar film 0.5 mil in thickness, that is, one half of a thousandth of an inch. The exterior surface of the satellite is coated with vapor deposited aluminum to a thickness of about 2000 Angstrom units, which is so thin that the entire amount of aluminum on the 100-foot diameter Echo I satellite is only about 4 pounds. This aluminum coating serves several purposes. It gives the satellite a reflectivity to radio waves of more than 99 percent. It protects the Mylar film from the deleterious effects of the unattenuated solar ultraviolet radiation in space. It provides the proper ratio of absorbtivity to solar radiation to emissivity to thermal radiation for proper operation of the satellite's inflation system. And finally, it makes the satellite highly reflective of sunlight so that it may readily be tracked optically. This satellite has now been in orbit three years. The fact that it has not evaporated attests to the very low vapor pressure of the plastic film of which it is constructed. The fact that it is still a fairly good reflector of radio signals, and that its optical brightness has not undergone any large change is proof that its thin coating of vapor deposited aluminum has not been eroded away by sputtering, cosmic dust, or other phenomena at its orbiting altitude of about 1000 miles.

The Echo I satellite was not designed to be a rigid structure. It was designed to maintain its spherical shape by virtue of an internal gas pressure. As the inflating gas slowly leaked out, due to porosity of the satellite's skin and punctures produced by micrometeoroids, it became limp; and as a reflector of radio waves it has undergone a moderate deterioration. Because it is under a weightless condition in orbit, and is at an altitude such that it experiences almost no aerodynamic forces, the most severe loading upon it is the very small force produced

by solar radiation pressure. The very slight stiffness of its 0.5 mil thick plastic film is almost, but not quite, enough to maintain it spherical.

The Echo II material, shown in cross section in figure 4, is composed of 0.35 mil thick Mylar film to each side of which is bonded 0.18 mil thick aluminum foil, giving a total thickness of about 0.71 mil. Because Young's modulus of elasticity is about 500,000 for Mylar, and about 10,000,000 for aluminum, it is immediately seen that the Echo II laminate is the structural equivalent of a homogeneous I-beam whose flange width is about 20 times the thickness of its web section. It is therefore very stiff for its thickness and weight. In fact, it is much stiffer and heavier than it need be, and this is only because at the time its design was frozen, which was two years ago, thinner aluminum foil in the requisite width of about 50 inches could not be manufactured. Today, aluminum foil thinner than 0.1 mil can be produced. In addition, plastic film equaling Mylar in tensile properties, but of only three-fourths the density of Mylar, has been developed. The Echo II material provides not only the flexibility needed for compactly folding the satellite into its container for transport into orbit, but also, after the satellite has been pneumatically erected to spherical shape, it provides more than the necessary stiffness for the satellite to accurately retain its spherical shape after complete loss of the inflating gas. Thus, it can last in orbit almost indefinitely. Aluminum foil, however, does not possess the proper ratio of absorbtivity to solar radiation to emissivity to thermal radiation to provide a radiative thermal balance temperature of the satellite when in sunlight that is conveniently usable, especially if electronic equipment, such as a radio tracking beacon, is to be carried on the satellite. Accordingly, a chemical treatment of the aluminum was developed to provide the desired optical properties at almost negligible change in weight. This gives the Echo II material a greenish cast.

The comparatively heavy weight Explorer IX satellite material, also shown in figure 4, serves to illustrate the tremendous increase in stiffness, even for a 12-foot diameter sphere, that is required for it to withstand aerodynamics force in the altitude range from 100 to 700 kilometers.

Research in the field of polymer chemistry has recently resulted in the development of plastic film that approximately equals the strength of Mylar, but which exhibits almost no deterioration in its mechanical properties under the influence of ionizing radiation such as found in space. This and other research suggests that it might be possible to develop a plastic film which is flexible here on earth, yet in the hard vacuum of space, there will evaporate out of it a volatile constituent so that it becomes very stiff. If this can be done, then it may be possible to construct very much lighter weight passive communications satellites coated only with vapor deposited aluminum like Echo I.

PART VI THE BASIC TRANSMISSION THEORY OF COMMUNICATION SATELLITES

Probably the greatest barrier to the comprehension of the scientific and engineering aspects of communications satellites, irrespective of whether they be active or passive, is understanding of the basic transmission theory that governs them. This theory is in reality quite simple and readily understood by all with a scientific or engineering background. The difficulty lies in that it is commonly known only to specialists in the subject, and is found usually in rather advanced works that presuppose familiarity with a large body of related information. This situation tends to discourage scientists and engineers of other disciplines from contributing their special skills and knowledge to the solution of communications satellite problems. To remedy this situation and provide an opportunity for all to participate, there is first discussed the essentials of

the basic transmission theory of communications satellites, starting from first principles, and emphasizing the physical significance of the several equations rather than their mathematical derivation, yet retaining technical correctness.

At the top of figure 5 is shown schematically the essentials of a radio transmission link. It consists of a transmitter, a transmitting antenna, a receiving antenna, and a receiver. Let the transmitting and receiving antennas be separated by the distance D. If P_T is the radio frequency electric power supplied by the transmitter to the input terminals of the transmitting antenna; and assuming no dissipation of the power as heat in the transmitting antenna, in the propagation path between the transmitting and receiving antennas, or in the receiving antenna, which assumptions are quite good in a well designed link; then the power P_R received at the output terminals of the receiving antenna is given by equation (1) which is also shown in figure 5.

$$P_R = \frac{P_T G_T A_R}{4\pi D^2} \qquad (1)$$

In the equation G_T is the gain of the transmitting antenna and A_R is the effective area of the receiving antenna.

The physical meaning of equation (1) may be readily understood as follows. If the radio frequency power P_T were emitted from the transmitting antenna uniformly in all directions, then the power that would pass through a unit area at the distance D would be $P_T/4\pi D^2$, where $4\pi D^2$ is the surface area of a sphere of radius D whose center is at the transmitting antenna. If, instead, the transmitting antenna focuses the power into a beam directed at the receiving antenna, the power per unit area at the receiving antenna is increased by the factor G_T which is the gain of the transmitting antenna. Therefore, $P_T G_T/4\pi D^2$ is the power per unit area at the receiving antenna. This, multiplied by the effective area A_R

of the receiving antenna is the power P_R available at the output terminals of the receiving antenna.

The second fundamental equation, also shown in figure 1, is

$$\frac{G}{A} = \frac{4\pi}{\lambda^2} \qquad (2)$$

which relates the gain G of an antenna to its effective area A, and to the wavelength λ of the radio wave. Unfortunately, the derivation of this equation is quite lengthy which precludes giving it here (an excellent derivation is given in reference 1, page 772) but the usual manner of its derivation may be briefly stated, and affords an insight into its physical meaning. First, there is derived the radiation from an elemental length of a conductor carrying a current, from whence is then obtained the ratio of the gain to the effective area of a dipole, and involves the wavelength λ of the radiation. This particular result for the dipole, or the particular result for any other specific antenna, is then extended to the general case of any antenna by invoking the reciprocity law which states that the gain to effective area ratio is a constant for all antennas at a given frequency. Thus, equation (2) is quite general, and in view of the physical meaning of antenna gain already given in connection with equation (1), equation (2) may be thought of as defining the effective area A of radiation of an antenna having a given gain when emitting or receiving radiation of a given wavelength.

Substitution of equation (2) into equation (1) yields the power P_R received at the output terminals of the receiving antenna in terms of antenna effective area A, or in terms of antenna gain G, as equation (3) shown in figure 5, which is

$$P_R = \frac{P_T A_T A_R}{\lambda^2 D^2} = \frac{P_T G_T G_R \lambda^2}{(4\pi)^2 D^2} \qquad (3)$$

and wherein the subscripts T and R refer respectively to the transmitter and receiver ends of the communications link. This equation is sometimes called the fundamental communications link equation, and is the building block from which the general communications satellite equation is constructed.

At the top of figure 6 is shown schematically a satellite communications link consisting of a ground transmitting station, a satellite, and a ground receiving station. For the sake of generality, the satellite shown is an active one wherein the received signal power can undergo amplification before being retransmitted to the ground receiving station. The ground transmitting station consists of a transmitter (x mtr.) of power P_T feeding a transmitting antenna of gain G_T. The distance from the transmitting antenna to the receiving antenna of the satellite is D_1. The gain of the satellite's receiving antenna is $G_{S,R}$. The receiver and transmitter (x mtr.) may increase the power of the signal passing through the satellite in the ratio G_S, which is the gain of the satellite. The gain of the satellite's transmitting antenna is $G_{S,T}$. The distance from the transmitting antenna of the satellite to the receiving antenna of the ground receiving station is D_2. The gain of the ground receiving station's antenna is G_R. The power delivered to the ground receiving station's receiver is P_R.

By successive application of the fundamental communications link equation (3), which is repeated in figure 6 for convenience, the general communications satellite equation (4), shown in figure 6, is immediately obtained. Applying equation (3) to obtain the power at the output terminals of the satellite's receiving antenna gives the quantity contained within the large parentheses in equation (4). Multiplying this power by the gain G_S of the satellite's receiver and transmitter gives the power delivered to the input terminals of the satellite's transmitting antenna as the quantity contained within the brackets in equation (4). Again applying

equation (3) to obtain the power P_R at the output terminals of the ground receiving station then yields equation (4) in its complete form as the general communications satellite equation.

$$P_R = \frac{P_T G_T G_{S,R} C_S G_{S,T} G_R \lambda^4}{(4\pi)^4 D_1^2 D_2^2} \qquad (4)$$

that is applicable to all communications satellites irrespective of whether they be active or passive.

Although the application of the general communications satellite equation (4) to active satellites is evident from its derivation, its application to passive satellites requires a clear recognition and understanding of their essential differences from active satellites. To clearly identify and illustrate these essential differences, the general equation (4) will now be reduced to the special form that applies to a passive spherical communications satellite like Echo.

This is illustrated in figure 7, where for convenience the general equation (4) is repeated. In applying the general equation to passive satellites, three quantities must be examined: the gain $G_{S,R}$ of the passive satellite as a receiving antenna, the gain G_S within the satellite, and the gain $G_{S,T}$ of the satellite as a transmitting antenna.

As a receiving antenna, a passive satellite in general possesses a gain $G_{S,R}$ that is related to its effective area A by equation (2) already discussed and again shown in figure 7. For a sphere that is large relative to the wavelength λ its effective area A is simply its frontal area, since this is the area that intercepts the oncoming waves, so that $A = \pi d^2/4$, where d is the diameter of the sphere. The spheres gain as a receiving antenna relative to an isotropic radiator is then by equation (2)

$$G_{S,R} = \frac{\pi^2 d^2}{\lambda^2} \qquad (5\text{-a})$$

The very essence of the definition of a passive communications satellite is that by virtue of it having no power within itself it cannot amplify a signal. Therefore, if it reflects the signal with neither amplification nor attenuation, the gain within the satellite is unity, so that

$$G_S = 1 \qquad (5\text{-b})$$

It is to be noted that if the surface of a passive satellite like Echo does not possess a reflectivity to radio waves of unity, then it will attenuate the signal so that G_S will be less than unity. The physical significance of G_S in a passive satellite like Echo is that it is the reflectivity of the satellite's surface to radio waves. Reflectivities in excess of 99 percent are readily attained with metal surfaces only a few thousand angstrom units in thickness.

The gain $G_{S,T}$ of the passive spherical satellite as a transmitting antenna relative to an isotropic antenna is unity, because a sphere whose diameter d is large compared to the wavelength λ reflects the signal incident upon it equally in all directions, and thus behaves like an isotropic radiator. Consequently, for the sphere

$$G_{S,T} = 1 \qquad (5\text{-c})$$

Substituting equations (5-a), (5-b), and (5-c) into the general communications satellite equation (4) gives the passive spherical communications satellite equation as

$$P_{R_{sphere}} = \frac{P_T G_T d^2 C_R \lambda^2}{256 \pi^2 D_1^2 D_2^2} \quad (6)$$

shown at the bottom of figure 7.

The derivation first of a general equation applicable to both passive and active communications satellites of all types, and then the derivation therefrom of the spherical passive communications satellite equation is unconventional and has been done to clearly bring out the essential differences between passive and active satellites. For the assistance of those accustomed to radar practice there is given in the appendix to this paper a direct derivation of the passive spherical communications satellite equation along conventional lines.

One further step is required to bring the equations to their final usable form. The ability to unmistakably read a radio message sent in code against a background of noise which is commonly called static, or to clearly understand a voice communication against a background of noise, or to obtain a sufficiently clear television picture against a background of interfering noise, is dependent upon the signal-to-noise ratio, S/N, which is the ratio of the power of the signal that constitutes the intelligence to the power of the interfering noise. It is unnecessary to here give a derivation of the equation expressing noise as power, since this is available in many textbooks on radio communications. However, the general concepts involved are here briefly given for the benefit of those not familiar with them.

Noise power may be thought of as generated by virtue of molecular agitation resulting from temperature, and hence is a function of absolute temperature, and increases in intensity the higher the temperature. Temperature may be thought as generating noise of all frequencies, and thus producing a spectrum that is a

continuum, analogous to the continuum spectrum emitted by a hot solid. Hence, the amount of noise power contained within any given range of frequencies, called the bandwidth, is proportional to the bandwidth B, to the temperature T, and to a constant of proportionality k known as Boltzman's constant, and equal to 1.38×10^{-23} watt second/degrees Kelvin. Consequently, if P_R represents the signal power, the equation for the signal-to-noise ratio S/N is

$$\frac{S}{N} = \frac{P_R}{k\,T\,B} \tag{7}$$

which is shown in figure 8.

Substituting the S/N ratio equation (7) into the previous equations (4) and (6) gives equations (8) and (9) which are respectively the final general communications satellite equation applicable also to active satellites, and the final passive spherical communications satellite equation.

$$\left(\frac{S}{N}\right) k\,T\,B = \frac{P_T\,G_T\,\sigma_{S,R}\,G_S\,G_{S,T}\,G_R\,\lambda^4}{256\,\pi^4\,D_1^2\,D_2^2} \tag{8}$$

(General and active)

$$\left(\frac{S}{N}\right) k\,T\,B = \frac{P_T\,G_T\,d^2\,G_R\,\lambda^2}{256\,\pi^2\,D_1^2\,D_2^2} \tag{9}$$

(Passive sphere)

Equations (8) and (9) are in reality simplified equations in that they contain only the main variables to the exclusion of several factors of secondary significance that the communications specialist would include in accurate design calculations. For example, attenuation of the signal in passing through the earth's atmosphere has been ignored on the grounds that practical interest exists only in frequencies within the so called "transmission window" of the atmosphere, which extends from about 1,000 to 10,000 Mc/s, and in which the atmospheric attenuation

is of secondary significance. In the general or active satellite equation (8), it is assumed that no degradation in the signal, such as bandwidth B or signal-to-noise ratio S/N, is suffered in passing through the active satellite; that is, high quality electronics is assumed in the satellite so that any degradation is of secondary significance. No such degradation occurs in a passive satellite since it is simply a reflector. Thus, equations (8) and (9) are to be recognized as simplified equations which ignore several factors that can be considered secondary in well designed systems, and are thus satisfactory equations for the purpose at hand.

PART III COMPARISON OF THE CHARACTERISTICS AND ECONOMICS OF PASSIVE AND ACTIVE COMMUNICATIONS SATELLITE SYSTEMS

The active and passive communications satellite equations (8) and (9) provide the foundation upon which may be made a comparison of the characteristics and the economics of passive and active communications satellite systems.

The essential physical differences between the two type of satellites can be brought out by imagining an active and a passive satellite communications link of identical length, identical capacity, and carrying identical kinds of signals of equal quality. Under these assumptions, many quantities in equations (8) and (9) become the same and can be transferred to one side of the equations, and the equations then equated, whereupon there is obtained equation (10), shown in figure 9.

$$\left(\frac{P_T G_T G_S G_R \lambda^2}{\pi^2} \right)_{\text{active}} = (P_T G_T d^2 G_R)_{\text{passive}} \qquad (10)$$

Inspection of equation (10) shows that for any given wavelength of transmission, if other things are equal, the power gain G_S achievable in the active satellite is

paired against the diameter d of the passive spherical satellite. Since large power gains are achievable in active satellites which permit the use of low power of the transmitter, and low gain of transmitting and receiving antennas; it follows that the competing passive spherical satellite system is characterized by high power of the transmitter, large transmitting and receiving antennas of high gain, and large-diameter satellites. Although equation (10) discloses the relative physical characteristics of the active and passive systems, it does not disclose their relative costs and reliability, which are the economic grounds upon which they must compete in any commercial application.

As soon as one begins to compare the active and passive communications satellite systems on economic grounds, one immediately encounters quantities that are unlike the physical quantities thus far discussed in that these new cost quantities change with time. For example, the cost of a satellite launching vehicle per pound of satellite placed into orbit is currently decreasing very rapidly from year to year as larger payload-carrying vehicles are being developed, and as vehicle reliability is being substantially increased. With vehicles currently under development it will soon be possible to launch into orbit much larger and heavier passive communications satellites, and also to carry several of them into orbit by the same launching vehicle, thus effecting substantial reduction in launching costs. As another example, the rapid development of large size steerable transmitting and receiving antennas, transmitters operating in the hundreds of kilowatts power range, and sensitive receivers having very low noise temperatures, are likewise passive communications satellite system components whose costs are decreasing each year. It is characteristic of these developments that they benefit the passive satellite communications system rather than the active satellite system that does not employ them. Thus, any economic comparison of active and passive communications satellite systems that does not project these cost changes to that time in the future when a system would be placed into operation is misleading.

From another viewpoint, an economic comparison of passive and active commercial communications satellite systems must consider from whence their earnings are to come; for out of these earnings must be paid the initial cost of the system, the cost of operation including maintenance and repair, and finally the profits earned upon the capital invested. At present there is much disagreement upon the kind of traffic a commercial satellite communications system should carry in order to be most profitable. To a first crude approximation, one television channel is the equivalent of 600 voice channels, or 30,000 teletype channels. Can the revenue earned by one television channel equal that of 600 voice channels, or 30,000 teletype channels? Many people think it cannot on the following grounds. Commercial communications are needed to connect centers of population. Most people live in the temperature zones. Across the land masses in these areas, such as North America and Europe, there are already established microwave relay networks that can carry television as well as voice or teletype. Therefore, satellites are needed primarily to bridge oceans, such as between Europe and America, since submarine cables cannot provide the bandwidth needed by television. The maximum television audience is available at about 8 p.m. When it is 8 p.m. in the eastern part of the United States, it is 1 a.m. in western Europe; and when it is 8 p.m. in western Europe it is 3 p.m. in eastern United States. Thus, for showing events as they happen, trans-Atlantic television tends to be good only in one direction, and for but a few hours. Airplanes are now crossing the Atlantic in about 7 hours, and the coming supersonic transport will halve this time. Thus, current events can be recorded on film or magnetic tape, and flown across the Atlantic for television showing at the time of first maximum audience availability. For this reason many think that television communications satellites would not be as profitable as voice communications satellites. Just as telephone communications is preferred to teletype in the conduction of business, since by telephone one can ask questions and

receive answers immediately, so also it is argued that voice communications satellites can show a profit better than teletype satellites. Perhaps the best satellite from the revenue earning viewpoint is one that is primarily intended for voice communications, is usable for teletype when the voice communications load is low, and has the capability of transmitting television in slower than real time for recording and showing in real time a few minutes later or at the time of maximum audience availability.

Having arrived at a general idea of the kind of commercial satellite communications service most likely to succeed from an economic viewpoint, the question now is: can such service be provided by a passive communications satellite system, and if so, what would the system be like? To answer this question, the commercially most important link, namely, that between North America and Europe is examined. The characteristics and performance will be calculated using the passive spherical communications satellite equation (9), which is repeated in figure 10 for convenience, and solved for the parameter of interest involving the bandwidth B, the satellite diameter d, and the transmitter power P_T.

The assumption in now made that the transmitting and receiving antennas are identical for economy, so that their gains G_T and G_R are equal. Antenna gain G is, by the previously discussed equation (2), a function of wavelength λ and antenna effective area A. The effective area A can be expressed as a fraction c of the geometric frontal area a of an antenna; and assuming the use of the familiar paraboloidal dish antenna, the effective area A is then given by equation (13) as

$$A = c\,a = \frac{c\,\pi\,d^2}{4} \qquad (13)$$

where ℓ is the diameter of the paraboloidal antenna. Substituting equation (13) into equation (9) then yields equation (14) of figure 10 as

$$\frac{\Sigma}{d^2 P_T} = \frac{\pi^2 c^2 \ell^4}{256 k D_1^2 D_2^2 T \left(\frac{S}{N}\right) \lambda^2} \qquad (14)$$

Inspection of equation (14) shows that, other things equal, bandwidth B increases the shorter the wavelength λ. Since communications capacity increases with bandwidth, the shortest possible wavelength is desired. But this must be tempered by the consideration that the wavelength must lie within that portion of the radio spectrum in which noise coming to the receiver from space, called galactic noise, and that coming from the earth's atmosphere, due primarily to oxygen and water vapor, is a minimum. This low noise radio window extends from roughly a frequency of 500 to 10,000 megacycles per second, provided the restriction is imposed that the receiving antenna is never lowered to an elevation angle of less than 5° above the horizon. Below 5° elevation angle the mass of atmosphere through which the receiving antenna looks increases so rapidly that the atmospheric noise also increases very rapidly. The transmission frequency is therefore selected as 6,000 megacycles per second, corresponding to a wavelength of 5 centimeters or 0.05 meter, with the additional constraint of 5° minumum antenna elevation angle.

The gains G_T and G_R of the paraboloidal transmitting and receiving antennas are most conveniently determined by considering the efficiency factor c relating the antenna effective area A to its geometric frontal area a. Using the most modern construction techniques, values of c of 0.5 are considered achievable, and 0.6 only hopefully so. Steerable paraboloidal antennas have been developed in discrete diameters: the 60-foot-diameter size being commonplace, the 85-foot-diameter size rapidly becoming the commonplace size, and the larger sizes being not so common.

Antenna cost increases rapidly with diameter. Therefore, for maximum economy the most common size is selected, namely, one of 60-foot-diameter, whose gain, based upon a value of c of 0.5, is found to be 58.2 decibels, or 660,000.

The selection of the wavelength λ and the minimum antenna elevation angle has bearing on the noise temperature T. The temperature corresponding to the galactic and atmospheric noise at the selected wavelength and minimum elevation angle is approximately 30° Kelvin for standard atmospheric conditions. A receiver having this low a noise temperature would be very expensive, probably employing a maser. Under unfavorable atmospheric conditions the atmospheric noise temperature increases. The noise temperature of the entire system is essentially dictated by whether the atmosphere or the receiver has the higher noise temperature. The approximate optimum condition is therefore for the atmospheric and receiver noise temperatures to be equal. But since the atmosphere varies, and in order to keep the receiver cost low, the noise temperature T is selected as being 100° Kelvin, corresponding to a very good, but not extremely expensive receiver.

The distance D_1 from the transmitting antenna to the satellite, and the distance D_2 from the satellite to the receiving antenna, are next considered. The restriction that the minimum antenna elevation angle be 5° above the horizon, restricts each antenna to "seeing" only within a conical volume of space whose apex is at the antenna, whose total apex angle is 170°, and the axis of which cone coincides with the local vertical. Transmission from the transmitter to the receiver by way of the satellite can only occur when the satellite is within that volume of space that is common to both the transmitting and the receiving antenna's conical seeing volumes of space. For a satellite orbiting at a given altitude above the earth, the satellite is mutually visible to the transmitting and receiving antennas when it lies within the boundaries of a spherical surface that is "almond" shaped.

This can readily be seen by drawing on a sphere two circles that overlap, the resulting almond shaped common area of the circles being the area of mutual visibility of the satellite to the transmitting and receiving antennas. The distances D_1 and D_2 are each maximum when the satellite is at one or the other of the two corners of the almond-shaped mutual visibility area, so that this is the design condition on D_1 and D_2. The maximum value of D_1 and D_2 is a function only of satellite altitude, and not of the distance between the transmitting and receiving antennas, provided the transmitting and receiving antennas are not so far apart that there is no area of mutual visibility. The higher the altitude of the satellite, the greater the area of mutual visibility and the fewer satellites required to maintain continuous communications; but also the larger and more costly the ground transmitting and receiving stations. An optimum satellite altitude is about 1,000 nautical miles, for which the maximum value of D_1 and D_2 for 5° antenna elevation angle is 2,523 nautical miles. It is to be observed that the area of mutual visibility decreases to zero when the distance between the transmitting and receiving antennas is equal to the sum of D_1 and D_2, or 5,046 nautical miles. The shortest distance from North America to Europe is from St. Johns, Newfoundland to northeastern Ireland, a distance of 1,658 nautical miles. From Glace Bay, Nova Scotia, to Ireland is 1,920 nautical miles, and from the easternmost part of Maine to Ireland is 2,238 nautical miles. Thus, for any of these distances between the transmitting and receiving antennas, the area of mutual visibility of the satellite will be quite large, as can be seen from the fact that even for the longest link of Maine to Ireland, if the satellite were going in the direction from Maine toward Ireland, communications could begin before the satellite had reached the Maine station by 285 nautical miles.

There is now but one remaining quantity to be decided upon, namely, the signal-to-noise ratio S/N. This may be thought of as dictating the ability to discern the signal against the background of noise, and hence the quality of the reception. It is the S/N ratio at the output terminals of the receiver that counts, rather than that in equations (9) or (14) which is at the output terminals of the receiving antenna. It has already been assumed that a very good quality, but not excessively expensive, receiver is employed; and consistent with this it is now assumed that the receiver does not substantially change the S/N ratio, so that it may be taken as applying at the antenna terminals. The S/N ratio needed for satisfactory reception must, be by its very nature, based upon a large amount of experimental data. Drawing upon these data, the S/N ratio selected is 20 decibels, or 100. This value may be considered slightly high by some, and may therefore be considered slightly conservative.

In figure 11 is shown the performance of the assumed North America to Europe passive spherical satellite communications link in terms of bandwidth, transmitter power, and satellite diameter. Bandwidth is the measure of communications capacity of the link. Ordinary commercial television, as presently practiced in the United States, uses a bandwidth of 5 to 6 Mc/sec for one channel. This accustomed standard came into being a good many years ago. Because of the crowded conditions, and the resulting competition for space, in the radio spectrum, research is in progress on how to squeeze television as well as other transmissions into a narrower bandwidth. Some researchers claim to have accomplished satisfactory television transmission in a bandwidth of about 3 Mc/sec. Thus, exactly how much bandwidth is required for a satisfactory television channel

is a subject of considerable debate, which apparently will only be answered by much more experimental research. At present, for the trans-Atlantic satellite communications link, which is not constrained by established practice or investment in existing equipment, a satisfactory television channel can only be defined as requiring between 3 and 6 Mc/sec bandwidth. If 6 Mc/sec bandwidth is needed, figure 11 shows that this would require a spherical passive satellite of 150 feet diameter and a 450 Kw transmitter, or a 200 foot diameter satellite and a 250 Kw transmitter. In regard to satellite size, the NASA had already designed and tested in space in a sub-orbital flight, a 135 foot diameter satellite, so that one of 150 feet diameter may be considered as almost a straight forward engineering task, but one of 200 feet diameter would require both research and development, but there exists no known fundamental barriers to its accomplishment. In regard to transmitter power, single beam klystron tubes operating at 6000 Mc/sec are available up to 35 Kw, and could conveniently be operated in parallel up to about 8 tubes, giving about 280 Kw. Tube manufacturer claim that tube power can be doubled in a year, giving over 500 Kw if needed, and more than tripled in several years. It is therefore concluded that a 6 Mc/sec bandwidth television channel between North America and Europe can be made feasible with a passive spherical communications satellite with a year or two of research and development on the satellite, the transmitting tubes, or both. If, however, only 3 Mc/sec bandwidth is required for the television channel, figure 11 shows that this can be accomplished now since, at the presently available 280 Kw transmitter power, a satellite of 135 feet diameter is required which has already been developed. It is concluded, therefore, that a North America to Europe television channel using spherical passive communications satellite and giving 3 Mc/sec bandwidth is possible today, and

one of 3 Mc/sec bandwidth can be provided in several years with research and development of the satellite, the transmitter power, or both. If half speed television transmission for later showing at full speed is the most profitable commercially, this is feasible today.

The capacity of the passive satellite communications link for voice and for teletype transmission can most easily be evaluated by scaling from its television capacity using bandwidth. Ordinary multiple voice channel transmission requires, for good quality, a bandwidth of about 5000 cycles per second per voice channel. Therefore, in the 3 Mc/sec bandwidth attainable today, there can be carried about 600 voice channels, or in the achievable 6 Mc/sec bandwidth about 1200 voice channels. Ordinary multi-channel teletype communications requires a bandwidth on only about 100 cycles per second, so that roughly 30,000 teletype channels could be accommodated in the 3 Mc/sec bandwidth attainable today, or roughly 60,000 in the 6 Mc/sec bandwidth that is achievable.

The capability of such a passive communications system for growth to meet future needs is a very important economic consideration. The passive satellite being simply a reflector like a mirror, can work at any frequency, and with any kind of modulation. Therefore, additional ground transmitting and receiving stations can be added to increase the capacity of the trans-Atlantic link without adding more satellites. The inherently long life and reliability of the passive satellite in orbit, as demonstrated by the Echo 1, and the fact that all of the active electronics of the system that require maintenance and repair are located on the ground where they are readily accessible, are very important economic advantages of the passive satellite as compared to the active satellite.

PART IV ADVANCED PASSIVE COMMUNICATIONS SATELLITE CONCEPTS

Numerous ideas have been proposed as to how to improve the passive communications satellite. Only two of the most promising will be discussed as indication of future developments and improvements over the spherical version of the passive satellite thus far considered.

A spherical satellite whose diameter is large compared to the wavelength, will reflect incident parallel radio waves with equal intensity in all directions as seen in the far field. That is, at a distance from the satellite that is large compared to the diameter of the satellite, the reflected radio waves appears to emanate from a point at the center of the satellite. In all cases of practical interest, the diameter to wavelength ratio is very large so that the phenomenon of reflection of the radio wave from the surface of the satellite obeys the law of optics that the angle of incidence equals the angle of reflection. Therefore, one may use optical ray tracking methods to determine from what point on the satellite was reflected the ray that came from the transmitter and arrived at the receiver. When this is done, it is found that only the bottom part of the spherical satellite reflects radio waves back to the receiver. If it is required that the transmitter and the receiver be locatable at any place on the surface of the earth that can be seen at a given instant of time from the satellite, then it can be shown that the only portion of the satellite's surface that can reflect the radio wave back to earth is a segment of the sphere located on the bottom and whose angular diameter is a function only of satellite altitude. For example, at 1000 nautical miles altitude, the angular diameter of the segment is about 78 degrees, and represents about 11 percent of the sphere's surface. The remainder of the sphere can be removed and its weight used for other purposes.

If this segment satellite is to be pneumatically erected, part of the weight saved will have to be spent to close the top side of the segment and part for a toroidal rim around the edge of the segment to make it structurally stable. Finally, since such a segment satellite would have to be kept facing towards the earth, part of the saved weight would have to be spent for a stabilizing system, probably a gravity gradient stabilization system. Hopefully, some saved weight will be left over which could then be used to make the segment satellite bigger, thus getting the equivalent of a larger sphere for the same satellite weight, and, hence, a stronger return signal to the receiving station. One concept of such a gravity gradient stabilized segment passive communications satellite is shown in figure 12. A study of such communications satellites is now progressing.

Almost every study of passive and active communications satellites has assumed that they will be randomly distributed around their orbits rather than equally spaced. Even if the satellites are initially spaced in their orbits with the maximum precision attainable; the minute errors of altitude, velocity, and direction, together with minute perturbations of their orbits, from such things as anomalies in the earth's gravitational field, and lunar and solar attractions, will in time cause them to become randomly spaced. Loss of spacing to the point where interruptions of communications, called outages, will occur because of lack of a satellite within the area of mutual visibility of a transmitting and receiving station of a link will develop in a surprisingly short time that is but a small fraction of the system lifetime of 5 to 10 years that is required for the system to be economically feasible. Because the density of a passive satellite is exceedingly low as compared to an active

communications satellite, the passive satellite can experience comparatively large orbital perturbations caused by solar radiation pressure. The advocates of active communications satellites have frequently pointed out this characteristic of the passive communications satellite, and at the same time shown that the active satellite is comparatively free of this perturbation because its frontal area per unit of mass is so small that the very weak solar radiation pressure can have very little effect upon it. It appears that this reasoning has caused the other perturbing forces that act both upon the passive and the active satellite to be forgotten.

There have been numerous proposals that the passive satellite be made of a wire mesh so as to reduce the force of solar radiation pressure upon it. These proposals all show that if the size of the holes in the wire mesh are properly proportioned compared to the wavelength of the transmission, very little loss of radio reflectivity is experienced at wavelengths down to the design wavelength. For such a wire mesh satellite to be pneumatically erectable in space, it must be made gas tight by being covered with a plastic film which has two effects. First, it increases the weight of the satellite so that any reduction in weight resulting from the holes in the wire mesh is largely consumed. Second, the plastic film is not perfectly transparent to all wavelengths of solar radiation and will usually become less transparent under the influence of the electromagnetic and corpuscular radiation encountered in space, so that some of the reduction of the force of solar radiation pressure upon the satellite is lost. To prevent this loss, it is proposed to employ a special plastic film, called a photolizable film, that under the influence of the radiation encountered in space, usually the ultraviolet radiation, will disintegrate and evaporate,

leaving only the wire mesh. Still another proposal for erecting the wire mesh satellite in space is to spin it so as to generate a centrifugal force, which tends to flatten the satellite out into a dish, which then requires the installation of an erectable strut inside the satellite at the axis of rotation to push the poles of the spinning satellite out. Still another, and most ingenious, proposal is to construct the mesh of plastic fibers coated with vapor deposited metal to make them radio reflective. The special plastic fibers would possess the so-called "memory effect," so that mechanical energy can be stored in them and released by the application of heat. The folded satellite, upon arrival in orbit, would be heated by sunlight, releasing the mechanical energy in the fibers that would cause them to return to their unfolded sheet, thus erecting the satellite. This proposal has the advantages of eliminating both the photolizable firm as well as the subliming material that generates the erecting gas, and thus saves much weight. Research is in progress upon it.

But all of these mesh passive satellite proposals have one defect in common. They seek only to diminish, rather than to completely negate, the perturbation arising from solar radiation pressure. A recent proposal appears to not only offer the avility to completely negate the solar radiation pressure perturbation but also to cancel all the other aforementioned perturbations as well as accomplishing a number of other very beneficial effects. It works as follows.

In figure 13 is shown a spherical passive communications satellite orbiting around the earth in an elliptic orbit. The figure is drawn in the plane of the orbit, upon which imaginary plane falls the shadow of the earth. Since the earth is round, it casts a cylindrical shadow, assuming for simplicity that the sunlight is parallel. The oblique intersection of the cylindrical earth shadow with the imaginary plane of the orbit casts on the orbit plane the elliptic

shadow shown. As the satellite recedes from its point of closest approach to the sun to the point where it enters the earth's shadow, the work done upon the satellite by the solar force F is $F d_1$, where d_1 is the distance of recession. As the satellite approaches the sun from its point of emergence from the earth's shadow to its point of closest approach to the sun, the work that the satellite does in moving against the solar force F is $-Fd_2$, where d_2 is the distance of approach. For the case illustrated in figure 13, the net energy change experienced by the satellite in the course of one orbit about the earth is negative because d_2 is greater than d_1. If the satellite is in circular orbit, d_1 and d_2 are equal, so that the net energy change per orbit is zero.

It is desirable to keep communications satellites in circular orbits so that their altitude remains constant, for as has already been seen by equation (4), the power of the signal at the receiver varies inversely as the product $D_1^2 D_2^2$, which product in turn varies approximately as the fourth power of the altitude. If the passive communications satellite is in circular orbit, how then can an energy change in it be accomplished by use of solar radiation pressure to overcome orbit perturbation?

From the theory of radiation pressure, it is recalled that the pressure is proportional to the amount of electromagnetic energy per unit of volume, that is, the energy density, adjacent to the surface upon which the radiation exerts its pressure. Therefore, the radiation pressure upon a perfect mirror that reflects back the radiation, thereby doubling the energy density, is exactly twice the pressure upon an ideal black surface that absorbs all of the incident radiation. This provides a method of changing the force of solar radiation pressure upon a satellite so that an energy change of the satellite can be gotten in a circular orbit. Let one side of the satellite be made a mirror, and the other side be

made a black absorbing surface. If the mirror side is turned toward the sun as the satellite recedes from the sun, and the black side turned toward the sun as the satellite approaches the sun, then the net energy change experienced by the satellite in one orbit about the earth is a gain of energy. If the reverse process is used, that is, the black side facing the sun as the satellite recedes, and the mirror side facing the sun as the satellite approaches the sun, then the net energy change in one orbit is a loss of energy by the satellite. Thus, solar radiation pressure can be made to add or remove energy from the satellite.

How can the addition or subtraction of energy from the satellite be used to overcome orbit perturbations? If energy is added to the satellite it must respond by moving to a higher altitude orbit. Therefore, its period of rotation around the earth becomes longer, so that relative to other satellites in the same orbital plane that have remained at the original altitude, the satellite will fall back around the orbit, thus changing its angular position around the orbit relative to the other satellites. Conversely, if energy is removed from a satellite, it will change its angular position around the orbit relative to other satellites by moving forward around the orbit. When the satellite has reached the desired angular position around the orbit relative to the other satellites, the energy added to it can be removed, or the energy subtracted from it can be restored, thus putting the satellite back to its original altitude. This moving forward or rearward of a satellite so as to maintain its position around an orbit relative to other satellites is called station keeping.

How can a passive spherical communications satellite be rotated so as to turn its mirror or black side toward the sun to accomplish station keeping? Three mutually perpendicular electric coils can be placed around the satellite and electrical energy to operate them derived from solar cells. When, upon

command, a coil is energized, the coil reacts against the magnetic field of the earth and turn the satellite in such a way that the coil aligns itself perpendicular to the direction of the earth's magnetic field at the satellite. Since the position of a satellite around its orbit will be known from tracking, the direction of the earth's magnetic field at the satellite relative to the earth is known and also relative to the sun. From solar cells on the satellite, perhaps the same ones used to power the coils, the direction to the sun relative to the satellite is known. Thus, the orientation of the satellite relative to the earth's magnetic field and to the sun are always known, as well as the position of the satellite around its orbit. Consequently, it is known which coil or combination of coils to energize by radio command from the earth to orient the satellite in any desired direction.

It is to be observed that this method of station keeping of passive communicacions satellites by use of solar radiation pressure and torques produced by reaction against the earth's magnetic field, has the unique feature of not expending anything carried aboard the satellites, and thus, except for eventual wearing out or failure of some component, can theoretically operate forever. It is thus fundamentally different from all other proposed methods of station keeping which expend something carried aboard the satellite, such as gas for operation of control jets. It is true that in the sense of this system requiring the placing aboard the passive satellite a few electrical and electronic components the satellite is no longer purely passive, but it must be realized that the quantity of such components is several orders of magnitude less than is contained in an active satellite, and that most of the components are of a nature such as to be either uneffected by the space environment or capable of being so overdesigned as to insure very long operating life. A preliminary

study of the application of this control system to the A-12 Echo II 135-foot diameter spherical passive communications satelllite indicates that all of the components aboard the satellite would weigh between 25 and 50 pounds.

As an indication of the economic importance of this novel method of station keeping of passive communications satellites, the following approximate numbers of satellites would be required for the previously discussed Maine to Ireland communications link if the satellites are randomly spaced. For 50 percent probability of communications, 21 satellites would be needed. For 90 percent probability of service, 71 satellites. For 99 percent service, 140 satellites. For 99.9 percent service, 3000 satellites. Thus, to approach continuous service, the number of random satellites grows very large. But, if station keeping is employed, 100 percent probability of service is achieved with only 30 satellites. Although these numbers are only approximate due to the statistical method of computing them, their relative values are correct, and serve to illustrate the large reduction in the number of satellites required by use of station keeping.

Other economic advantages of station keeping exist. For example, on a single large launching vehicle, a number of satellites could be transported into orbit and released at one place around the orbit, from which point they can be distributed around the orbit by the station keeping method. Preliminary calculations indicate that the station keeping method can also be used to slowly change orbit inclination. Thus, it permits changing the orbits to accommodate changing needs of communications system, the making of space between the satellites to accommodate the insertion of additional satellites if needed, and even the removal from orbit of damaged or worn out satellites by flying them back to earth.

Finally, it is to be noted that this method of station keeping of passive communications satellites which turns radiation pressure upon such satellites

from a detrimental into a very beneficial thing, is not possible with the active satellite because of its high density, and, thus, the passive communications satellite possesses some very important advantages over the active satellite.

REFERENCE

Radar System and Components, Bell Telephone Laboratories Staff, D. Van Nostrad Company, 1949

APPENDIX

The passive spherical communications satellite equation can be derived directly using the more familiar methods customarily employed with radars. Comparison of this direct derivation here given with that in the main text of this paper affords a better insight into the physical significance of the equation.

In figure 1A is shown, schematically, a passive spherical satellite communications link. It contains a transmitter of radio frequency power output P_T; a transmitting antenna of gain G_T; a 100 percent reflective passive spherical communication satellite of diameter d, located a distance D_1 from the transmitting antenna; a receiving antenna of gain G_R, located a distance D_2 from the satellite; and a receiver.

If the transmitting antenna were to radiate isotropically, that is, equally in all directions, the power density at a distance D_1 would be $P_T/4\pi D_1^2$, where $4\pi D_1^2$ is the surface area of a sphere of radius D_1 centered at the transmitting

antenna. If the transmitting antenna focuses the radiated power into a beam directed at the satellite so as to increase the power density at distance D_1 by the factor G_T, which is the gain of the transmitting antenna relative to an isotropic radiator; then the transmitted power density at the satellite is given by equation (1A) of figure 1A. This power density multiplied by the frontal area $\pi d^2/4$ of the spherical satellite is then the power intercepted by the satellite, which is given by equation (2A) of figure 1A, and assumes that the diameter of the satellite is large compared to the wavelength λ of the radio signal. Assuming that the reflectivity of the surface of the satellite to radio waves is unity so that all power is reflected; and employing the experimentally and theoretically derived result from both optics and radio that a specularly reflecting sphere reflects an incident parallel beam equally in all directions, that is, isotropically; the reflected power density at the receiving antenna is then the power intercepted by the satellite divided by the surface area $4\pi D_2^2$ of a sphere of radius D_2 centered at the satellite, as given by equation (3A) of figure 1A. This power density multiplied by the effective area A_R of the receiving antenna is then the power P_R at the receiving antenna terminals. By means of equation 2 of the main text of this paper, which relates the effective area A of an antenna to its gain G and the wavelength the effective area A_R of the receiving antenna is expressed in terms of its gain G_R and the wavelength λ, giving the equation for P_R as equation (4A) of figure 1A. This equation is identical to equation (6) of the main text of this paper.

STATIC INFLATION TESTS

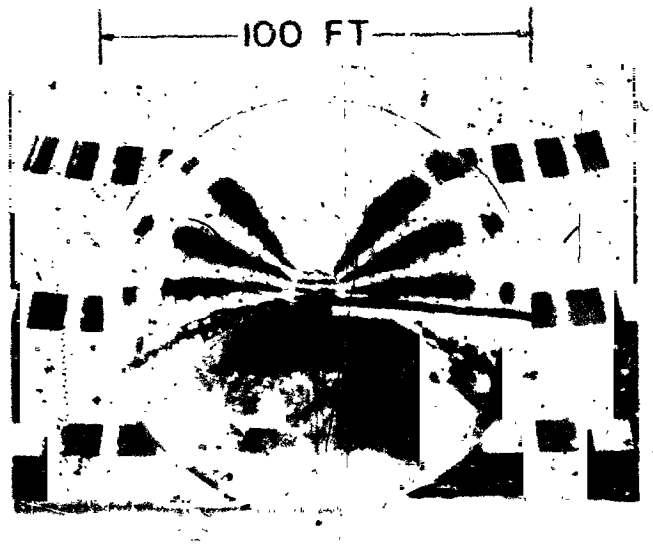

ECHO I

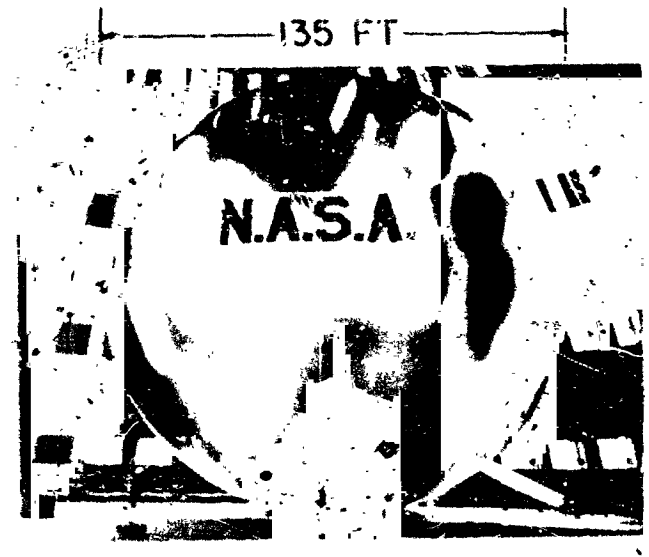

ECHO II

Figure 1

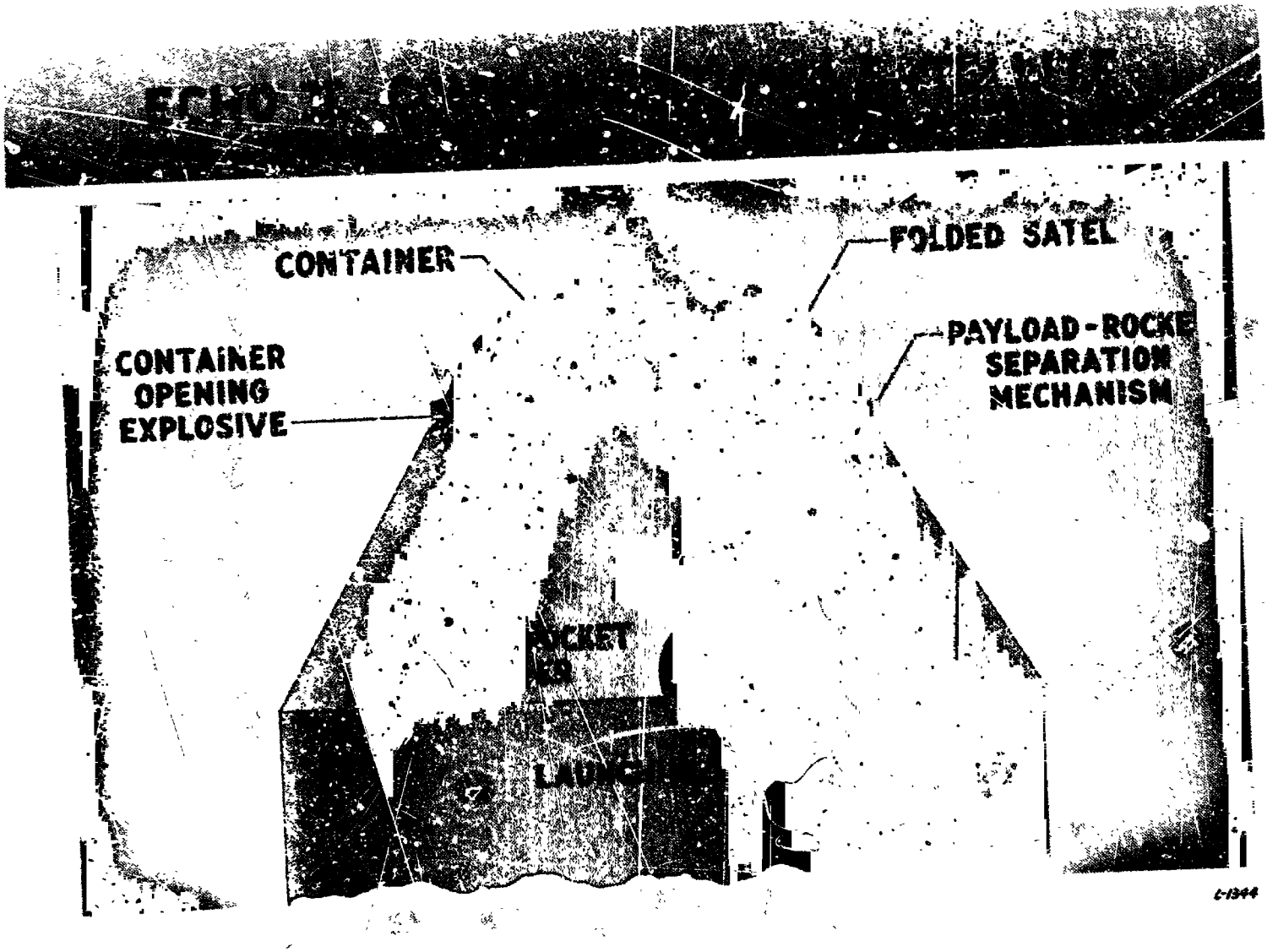
CONTAINER
FOLDED SATEL
CONTAINER OPENING EXPLOSIVE
PAYLOAD - ROCKE SEPARATION MECHANISM
L-1344

Figure 2

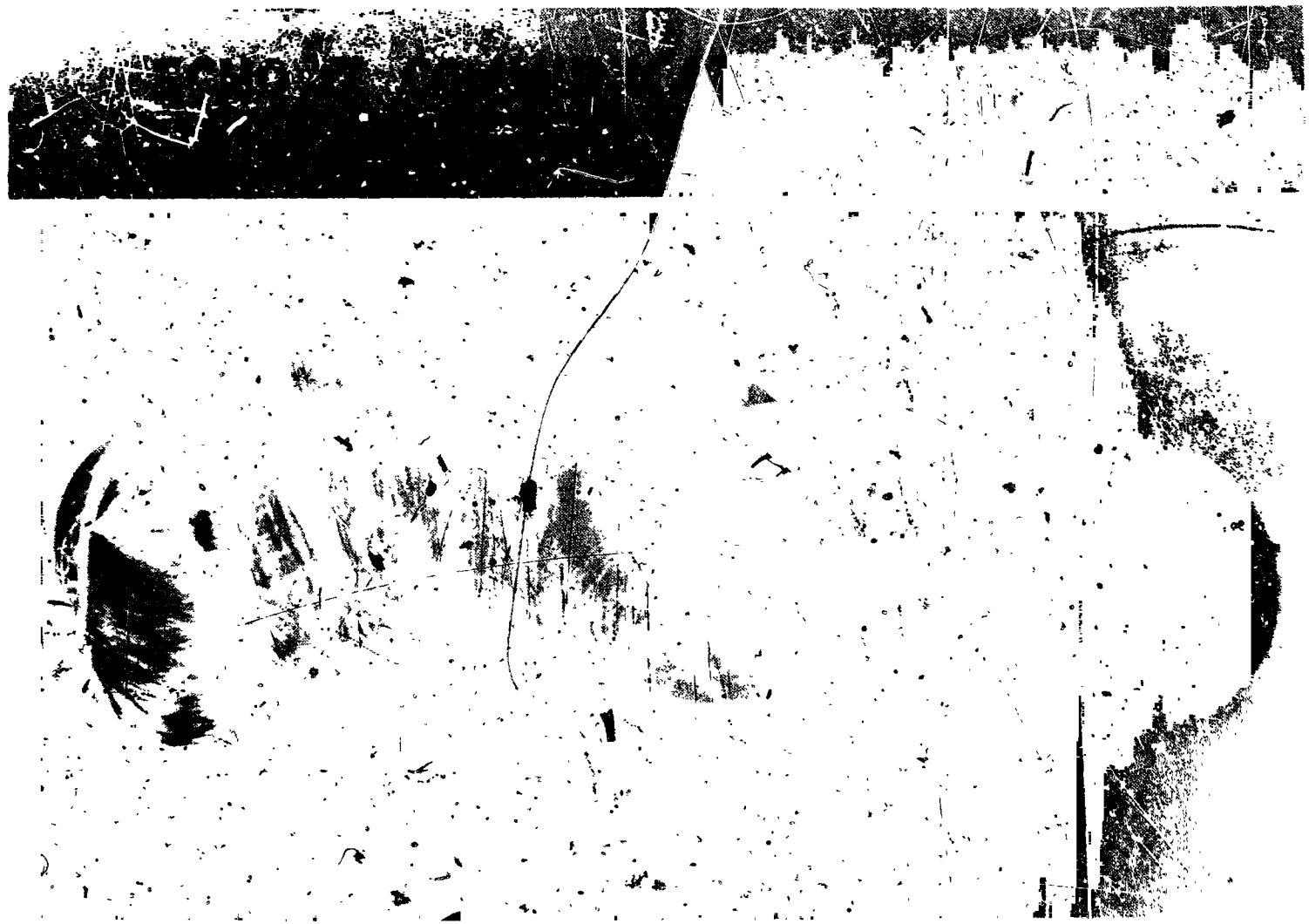

Figure 3

CROSS SECTIONS OF ERECTABLE SPACECRAFT SHELL

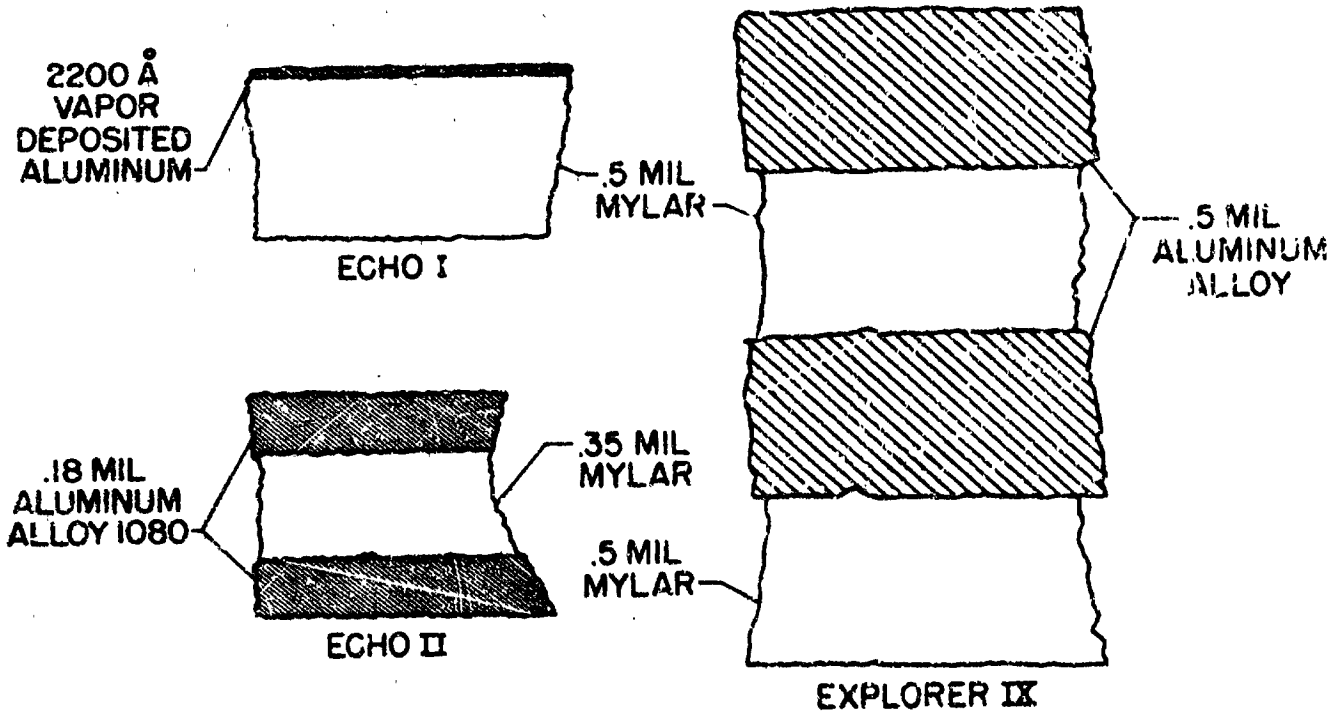

Figure 4

FUNDAMENTAL TRANSMISSION EQUATIONS

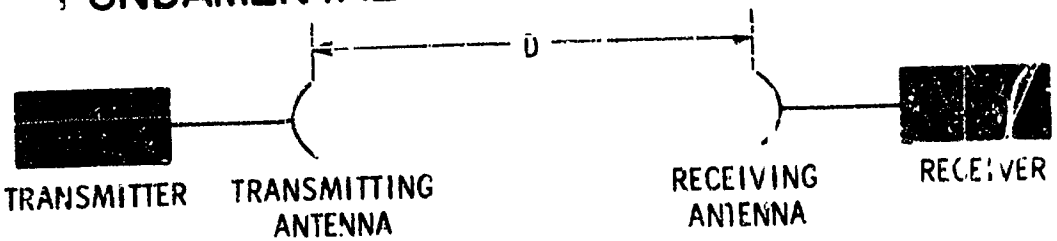

$$P_R = \frac{P_T G_T A_R}{4\pi D^2} \tag{1}$$

P_R = RECEIVED POWER, WATTS

P_T = TRANSMITTED POWER, WATTS

G_T = TRANSMITTING ANTENNA GAIN, DIMENSIONLESS

A_R = RECEIVING ANTENNA EFFECTIVE AREA, METERS^2

D = TRANSMISSION DISTANCE, METERS

$$\frac{G}{A} = \frac{4\pi}{\lambda^2} \tag{2}$$

G = ANTENNA GAIN, DIMENSIONLESS

A = ANTENNA EFFECTIVE AREA, METERS^2

λ = WAVELENGTH, METERS

$$P_R = \frac{P_T A_T A_R}{\lambda^2 D^2} = \frac{P_T G_T G_R \lambda^2}{(4\pi)^2 D^2} \tag{3}$$

A_T = TRANSMITTING ANTENNA EFFECTIVE AREA, METERS^2

G_R = RECEIVING ANTENNA GAIN, DIMENSIONLESS

L-2086-1 O'SULLIVAN

Figure 5

GENERAL COMMUNICATIONS SATELLITE EQUATION

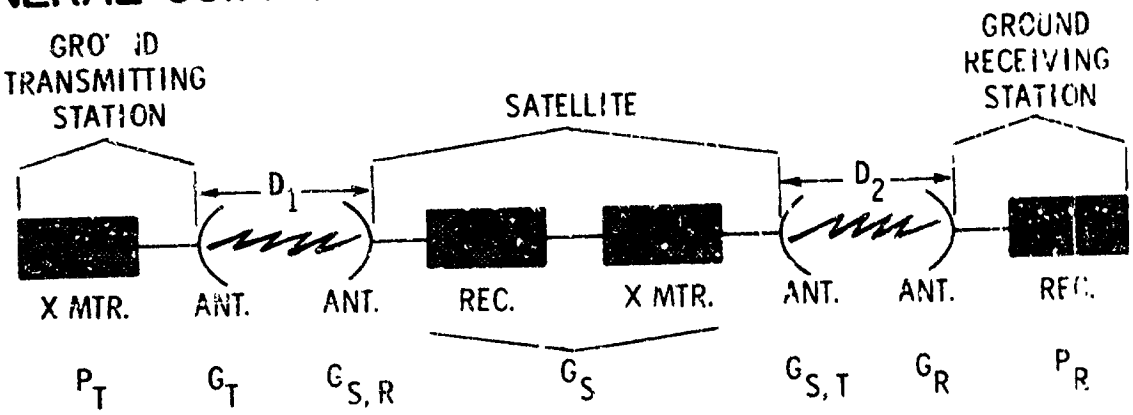

FUNDAMENTAL COMMUNICATIONS LINK EQUATION:

$$P_R = \frac{P_T G_T G_R \lambda^2}{(4\pi)^2 D^2} \tag{3}$$

GENERAL COMMUNICATIONS SATELLITE EQUATION:

$$P_R = \left[\left(\frac{P_T G_T G_{S,R} \lambda^2}{(4\pi)^2 D_1^2}\right) G_S\right] \frac{G_{S,T} G_R \lambda^2}{(4\pi)^2 D_2^2}$$

$$= \frac{P_T G_T G_{S,R} G_S G_{S,T} G_R \lambda^4}{(4\pi)^4 D_1^2 D_2^2} \tag{4}$$

L-2086-2 O'SULLIVAN

Figure 6

DERIVATION OF PASSIVE COMMUNICATIONS SATELLITE EQUATION FROM GENERAL COMMUNICATIONS SATELLITE EQUATION

GENERAL COMMUNICATIONS SATELLITE EQUATION:

$$P_T = \frac{P_T G_T G_{S,R} G_S G_{S,T} G_R \lambda^4}{256 \pi^2 D_1^2 D_2^2}, \text{ WATT} \tag{4}$$

FOR A PASSIVE SPHERICAL SATELLITE:

$$G_{S,R} = \frac{4\pi A}{\lambda^2} \qquad \text{BY EQUATION (2)}$$

$$A = \text{SPHERE FRONTAL AREA} = \frac{\pi d^2}{4}$$

d = DIAMETER OF SPHERE, METERS

$$G_{S,R} = \frac{\pi^2 d^2}{\lambda^2} \tag{5A}$$

$$G_S = 1 \tag{5B}$$

$$G_{S,T} = 1 \tag{5C}$$

PASSIVE SPHERICAL COMMUNICATIONS SATELLITE EQUATION:

$$P_{R_{SPHERE}} = \frac{P_T G_T d^2 G_R \lambda^2}{256 \pi^2 D_1^2 D_2^2} \tag{6}$$

L-2086-3 O'SULLIVAN
Figure 7

GENERAL OR ACTIVE, AND PASSIVE SPHERICAL COMMUNICATIONS SATELLITE EQUATIONS IN S/N RATIO

$$\frac{S}{N} = \frac{P_R}{kT\,B} \tag{7}$$

$\frac{S}{N}$ = SIGNAL-TO-NOISE RATIO, DIMENSIONLESS

k = BOLTZMAN'S CONSTANT, 1.38×10^{-23} w SEC/^{0}K

T = TEMPERATURE, ^{0}K

B = BANDWIDTH, CYCLES/SEC

GENERAL OR ACTIVE COMMUNICATIONS SATELLITE EQUATION:

$$\left(\frac{S}{N}\right) kT\,B = \frac{P_T\,G_T\,G_{S,R}\,G_S\,G_{S,T}\,G_R\,\lambda^4}{256\,\pi^4\,D_1^2\,D_2^2} \tag{8}$$

PASSIVE SPHERICAL COMMUNICATIONS SATELLITE EQUATION:

$$\left(\frac{S}{N}\right) kT\,B = \frac{P_T\,G_T\,d^2\,G_R\,\lambda^2}{256\,\pi^2\,D_1^2\,D_2^2} \tag{9}$$

L-2086-4 O'SULLIVAN

Figure 8

COMPARISON OF EQUAL LENGTH, CAPACITY, AND QUALITY ACTIVE AND PASSIVE SATELLITE COMMUNICATIONS LINKS

$$\left(\frac{P_T G_T G_S G_R \lambda^2}{\pi^2}\right)_{\text{ACTIVE}} = \left(P_T G_T d^2 G_R\right)_{\text{PASSIVE}} \qquad (10)$$

P_T = TRANSMITTER POWER, WATT

G_T = TRANSMITTER ANTENNA GAIN, DIMENSIONLESS

G_S = ACTIVE SATELLITE GAIN, DIMENSIONLESS

G_R = RECEIVING ANTENNA GAIN, DIMENSIONLESS

λ = WAVELENGTH, METER

d = PASSIVE SPHERICAL SATELLITE DIAMETER, METER

L-2086-5 O'SULLIVAN

Figure 9

TRANS-ATLANTIC PASSIVE SATELLITE COMMUNICATIONS LINK

$$\frac{B}{d^2 P_T} = \frac{\lambda^2 G_T G_R}{256 \pi^2 k D_1^2 D_2^2 T \frac{S}{N}} \qquad (9)$$

FOR $G_T = G_R$

$$G = \frac{4\pi A}{\lambda^2} \qquad (2)$$

$$A = ca = \frac{c\pi l^2}{4} \qquad (13)$$

$$\frac{B}{d^2 P_T} = \frac{\pi^2 c^2 l^4}{256 k D_1^2 D_2^2 T \frac{S}{N} \lambda^2} \qquad (14)$$

WAVELENGTH, λ	= 0.05 m
MINIMUM ANTENNA ELEVATION ANGLE	= 5^0
NOISE TEMPERATURE, T	= 100^0 K
PARABOLOIDAL ANTENNA DIAMETER, l	= 60 ft
ANTENNA GAIN AT c = 0.5	= 58.2 db = 660,000
SATELLITE ALTITUDE	= 1000 n. m.
MAXIMUM SATELLITE-TO-ANTENNA DISTANCE	= 2523 n. m.
SIGNAL-TO-NOISE RATIO	= 20 db = 100

L-2086-6 O'SULLIVAN

Figure 10

PASSIVE SATELLITE BANDWIDTH, POWER, AND SIZE RELATIONS FOR 1,000 N. M. ORBIT

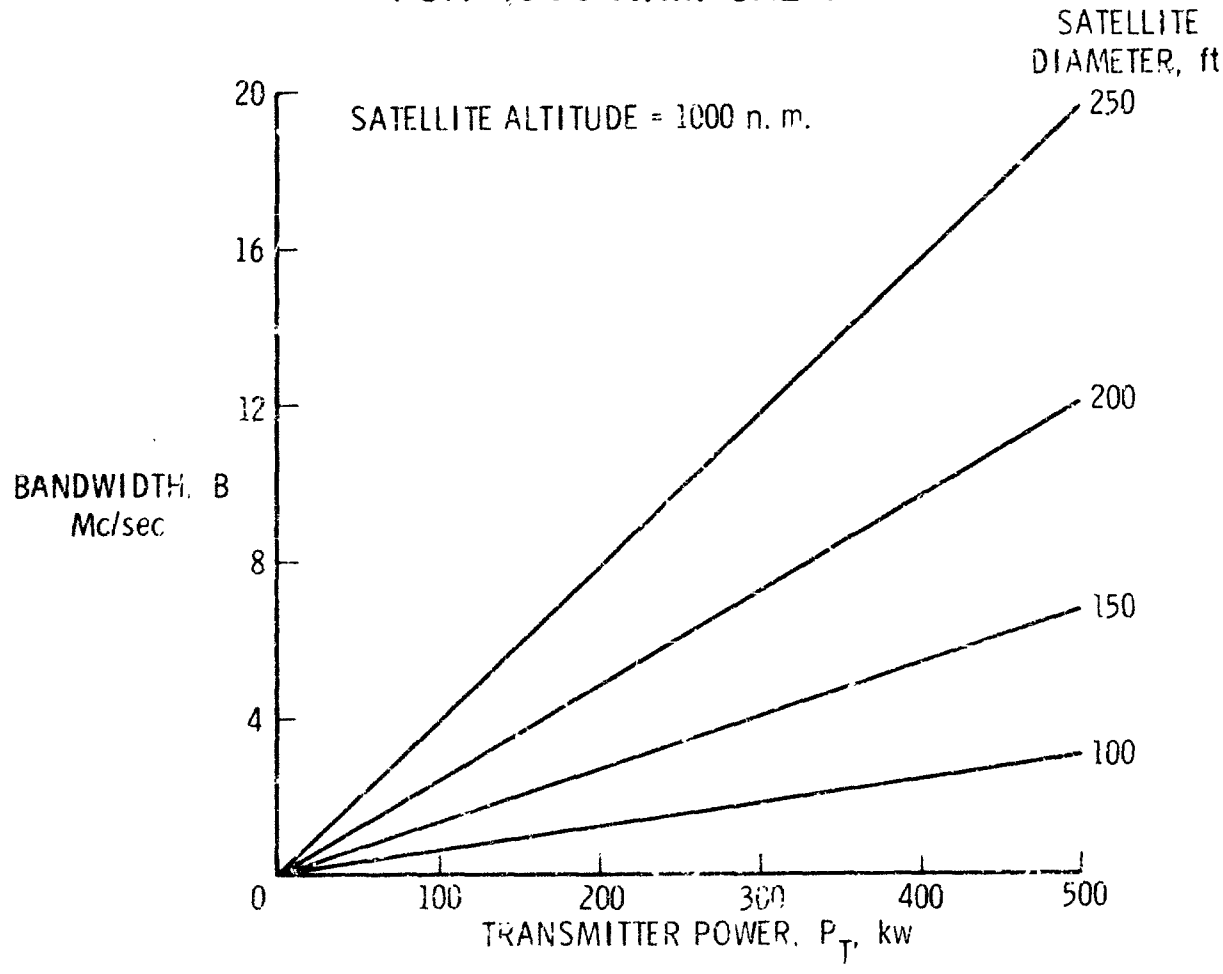

L-2086-7 O'SULLIVAN

Figure 11

A METHOD OF CONSTRUCTION FOR ORIENTED REFLECTOR

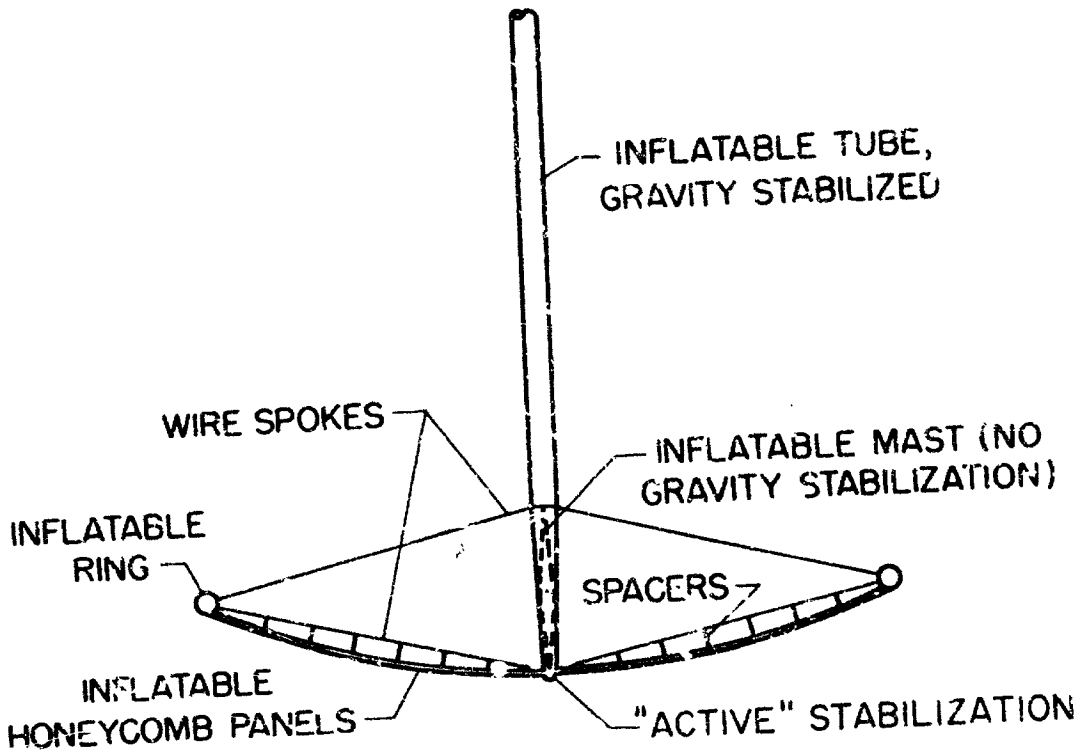

Figure 12

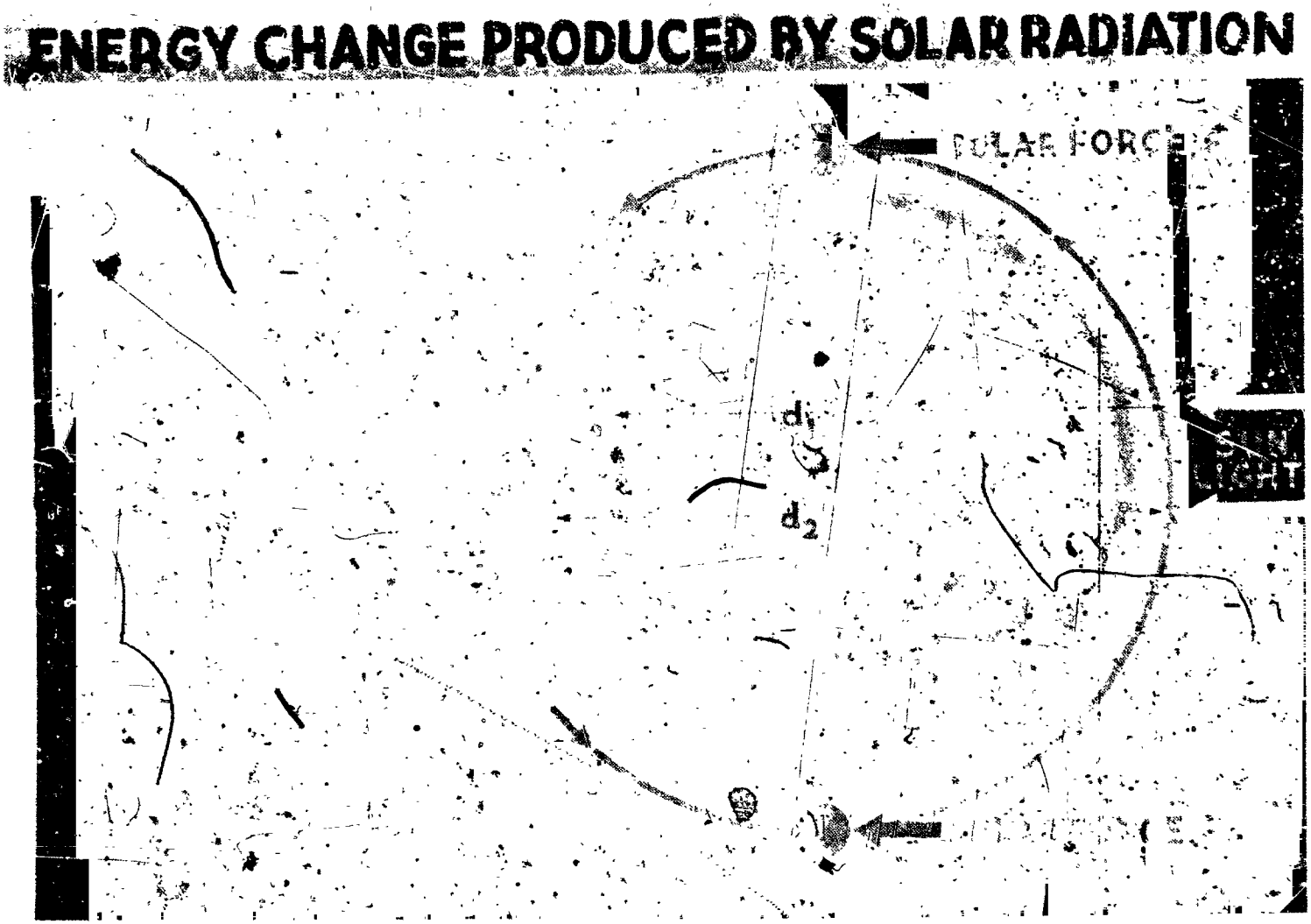
ENERGY CHANGE PRODUCED BY SOLAR RADIATION
SOLAR FORCE
d_1
d_2

Figure 13

ALTERNATE DERIVATION OF PASSIVE SPHERICAL COMMUNICATIONS SATELLITE EQUATION

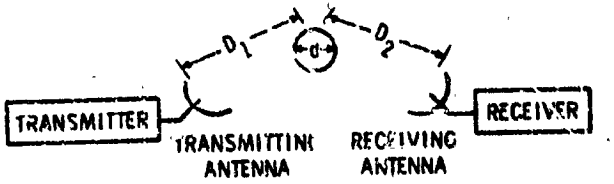

TRANSMITTED POWER DENSITY AT SATELLITE $= \frac{P_T G_T}{4\pi D_1^2} \cdot \frac{w}{m^2}$ (1A)

POWER INTERCEPTED BY SATELLITE $= \frac{P_T G_T}{4\pi D_1^2} \frac{\pi d^2}{4}$

$= \frac{P_T G_T d^2}{16 D_1^2} \cdot w$ (2A)

REFLECTED POWER DENSITY AT RECEIVING ANTENNA $= \frac{P_T G_T d^2}{16 D_1^2} \frac{1}{4\pi D_2^2}$

$= \frac{P_T G_T d^2}{64\pi D_1^2 D_2^2} \cdot \frac{w}{m^2}$ (3A)

POWER AT RECEIVING ANTENNA TERMINALS $= P_R = \frac{P_T G_T d^2}{64\pi D_1^2 D_2^2} \frac{A_R}{1}$

$= \frac{P_T G_T d^2}{64\pi D_1^2 D_2^2} \frac{G_R \lambda^2}{4\pi}$

$= \frac{P_T G_T d^2 G_R \lambda^2}{256\pi^2 D_1^2 D_2^2}$ (4A)

L-2086-1a O'SULLIVAN

Figure 14

ACTIVE COMMUNICATION SATELLITE SYSTEMS

BY

DOREN MITCHELL

BELL TELEPHONE LABORATORIES

MURRAY HILL, NEW JERSEY

ACTIVE COMMUNICATION SATELLITE SYSTEMS

by

Doren Mitchell

Bell Telephone Laboratories

I will give a brief description of our Telstar experiment and then point out some interesting engineering comparisons between medium orbit and high orbit systems.

I might first very quickly review the history of intercontinental communications. The first transatlantic telegraph cable was put in service almost 100 years ago, in 1866. The first telephone circuit was in 1927. I well remember it because I was a young man just starting off and I worked on it. It was long-wave and the quality was sometimes not very good, but it talked. Of course, this was followed in the 1930's by a short-wave (HF) and this extended telephone communications practically all over the world as of today.

In 1956, we laid the first transatlantic telephone cable. It was capable of carrying 36 telephone conversations with much better quality than HF. We have increased this to 72 commercial telephone conversations by the time sharing device "Tasi". There are now three cables systems across the Atlantic. The fourth one is being laid right now, which will have the capacity of 120 voice channels, and in addition, as probably many of you know, a new system is being designed with the capacity of 720 voice channels, or one two way medium quality monochrome TV channel. This raises the question of why do we consider satellite communication for commercial purposes.

There are three very good reasons. First the tremendously increasing demand for telephone communication to all parts of the world, second the need for diversity in types of communications and, third the requirement for high grade communication to remote parts of the world can only be reached now by HF.

Figure 1 illustrates the growth of telephone traffic calls per year, overseas. You will notice that it is practically a straight line on logarithmic paper and it's still rowing at about this same rate of 20 percent per year. Thus it doubles about every four years. It would be possible to provide for future growth to some points of the world by laying more cables, particularly of the higher capacity type, but this would not take care of the demand for communication o remote parts of the world. As was mentioned earlier, we make use of microwave radio very extensively to carry a package of either 600 telephone channels or one TV channel. That's the standard unit and this is very fine, but microwaves travel in straight lines and we therefore need some kind of a relay up in the sky. This led to the Echo balloon experiments which were mentioned just previously.

As compared to the Echo 1 experiment, we need a receiver which will respond to 1000 times the bandwidth of a single voice channel and thus it picks up about 30 db more noise. It is certainly possible to cope with this by larger balloons and higher power transmitters. I do think however that some rather serious questions would be raised as to interferrence with other services if you got up into hundreds of KW of power in land transmitters.

At any rate, we have gone down the road of the active satellite, and Figure 2 shows a Telstar satellite like the ones that were recently launched. It has electronic equipment onboard, which amplifies the signals about 93 db or about ten million times, giving them a fresh start at a level of about two watts.

It's 34 inches in diameter, and weighs about 170 pounds. It receives the signals, amplifies them, and shifts them to a different frequency, and transmits them back to the ground. It also has considerable sensing and control equipment within it. The antenna that receives the 6 thousand megacycle signals is the band of smaller openings around the equator and the antenna that transmits back down at 4 thousand megacycles, is the band of larger openings.

These antennas give a fairly uniform pattern around the satellite except in the directions corresponding to the poles. This satellite is spin stabilized as a good many of you may know, and in this way it is made to point in a favorable direction a large part of the time.

The electronic equipment is operated by power from solar cells. We can see them in these panels around the outer skin. Each one of these squares has about 100 cells. There are 3600 total. In this satellite the power is not great enough to operate the equipment continuously, and for this reason, we use a storage battery which can be turned on by command to operate the transmitting amplifier.

Telstar also contains telemetering equipment which operates at around 130 megacycles, using the helical antenna up there.

Incidentally, this is a picture of an earlier model. Figure 3 shows a cutaway view of Telstar with the antenna there the way it actually is on the two Telstars. Commands can be sent to the satellite and also in effect, it can be asked questions. This has been a very important part of the experiments. It has helped to determine the effects of outerspace environment on all of the components. One of the most important factors is high-energy bombardment and radiation counters.

Typical telemetry quantities are density and energy of electrons and protons in the Van Allen Belt, temperature of the satellite skin and of the interior of the satellite, pressure inside the satellite, and radiation effect on the conductors

and also the conditions of various electronic circuits. All of the components in telstar, except one, are solid state devices, transistors, dials and etc. The one vacuum tube is a traveling wave tube amplifier, shown in Figure 3, which provided the relatively high power of two watts.

Telstar would have been impossible without the solar cell, the transistor and the traveling wave tube, all of which were developed at the Bell Laboratories.

The performance of the solar cells is of great concern. We know they don't maintain their full effeciency when subjected to radiation and heat. These are p on n cells, mounted on a ceramic base in a platinum frame, and protected from bombardment by electrons and protons by coverings of artificial sapphire. These materials were chosen from the point of view of endurance. All the materials expand and contract at about the same rate and up to now, there has been no evidence of any difficult with the solar cells. The sapphire is transparent to the light waves, but attenuates destructive radiation. We believe this type of solar cell should maintain satisfactory performance for several years.

Telstar also has a torquing coil as was mentioned for some of the other satellites and it was used a couple of times on Telstar 1. We did not have to use it on Telstar 2 but it can be used to adjust the spin axis.

We also have mounted mirrors on three of the blank panels, which do not contain cells. The mirrors are not shown, they are merely pieces of very flat alumium. The purposes of these mirrors is to reflect brief flashes of sunlight as the satellite rotates about is spin axis. The time at which these flashes can be seen at a particular observation spot has helped us to determine the direction of the spin axis, and their rate tells us the spin rate. This has been very valuable in interpretation of the data from the radiation counters and the heat measuring devices.

Now a little recent history. Telstar 1 was put in orbit in July of 1962. It failed first due to radiation damage in November of 1962. It was revived in December and kept in operation till February of '63. It's still in orbit and it is rather interesting, that its spin rate and the attitude of its spin axis are still being determined and there have been no unexplained perturbations in either. We are reasonable certain that radiation damage caused the failure in some of the transistors associated with the command receiver in Telstar 1. These were nearer to the outer skin than most of the other transistors and they were incapsulated with inert gas.

In Telstar 2, we changed this and put in transistors which were evacuated. It was put in orbit on May 7, 1963, and performed perfectly up until July 16th of this year. But then, as most of you know, it failed suddenly and mysteriously. On August 12, on orbit 622, it just as mysteriously responded to the regular VHF command and came on again. As nearly as we can tell it is working just the same as it was working when it left Johannesburg about 4 weeks ago and then wouldn't respond when it went over Woomera, Australia.*

We have no indication of what caused the failure but it is obviously some kind of intermittent trouble.

It's of interest that we were able to observe the mirror flashes throughout the whole period that it was out and up to now, they have indicated no appreciable perturbations. This does not rule out a collision with a very small meteorite but makes it unlikely as the cause of trouble.

---

* As of June 8, 1964 it is still working perfectly.

Well, you have seen that we have quite complex electronic equipment to help give the signal strength for large numbers of telephone channels or TV.

We also need a very sensitive receiving station such as we have at Andover, Maine. I always like this (Figure 4) because maybe someday, there will be a similiar sign reading "moon station".

The antenna, the sensitive receiver, and the high powered transmitter are all enclosed in the radome shown in Figure 5. Now, we are looking at the radome from 5 miles away. There it is, it looks like a lost golf ball.

Now, you'll note that the radome is in a sort of shallow dish formation in the surrounding terrain. This site was carefully picked for this reason. It is desirable to have some shielding in all directions from terrestrial microwave systems.

Remember that up to now at least, we are told, that these systems will have to share frequencies with regular terrestrial microwave systems. But it is desirable to have the surrounding mountains low enough that a clear view can be obtained down to about 5 degrees elevation. Andover, Maine is one of the best sites in the U. S. from these considerations.

Now we can see that it is a pretty big golf ball. Figure 6 was taken just shortly after the final radome was inflated and it actually consists of a very thin dacron bag about 300 feet in diameter which is kept inflated at all times by slight air pressure.

The electrical performance of this radome material is very good. It's loss in clear weather, at microwave frequencies, is only about .15 db which results in added system noise of about 9 degrees Kelvin.

Figure 7 shows a cutaway view of the horn antenna and the other equipment in the radome. The antenna is sort of like a giganic air trumpet. The aperature at

the open end of the trumpet, is actually 60 x 60 feet. The whole horn is 170 feet long and with it's equipment weighs about 350 tons.

The antenna has a beam width of only 1/5th of a degree and to get the desired performance it must be pointed with an accuracy of about 1/50th of a degree.

It was the requirement, which led to covering it with a radome. Otherwise, wind would make it very difficult, if not impossible, to point with the necessary accuracy. We very recently have found something quite interesting and that is that the radome itself brings in certain penalties during rain. Although the dry radome materials have very low loss, this is not the case when rain produces a thin layer of water on the outside of the radome. Even moderate rainfall will produce a fairly uniform layer of water about 10 mils thick and we have made measurements rather recently in the laboratories which show that even a layer as thin as this produces considerable reflection at 4 kmc. (4 thousand megacycles).

We have measured loss of about 3½ db with a water layer of 10 mils. This, not only puts in an attenuation but raises the system noise quite substantially and we have measured added system noise of about as much as 150 degrees Kelvin, during moderate rainfall at Andover, Maine. This may mean that uncovered antennas will be more attractive than was originally thought particularly for the smaller stations. It appears that there will be an engineering compromise between the larger antenna which can be successfully pointed, even during wind, with a radome and the smaller antenna with less gain but which does not suffer the excess degredation during rain. We're still studying this subject.

Figure 8 shows the small end of the horn. We are inside the radome, where the radio transmitter and receiver are located. I think you can also see the outer circular track. The inner one there is not so easily seen. The whole antenna with

the cabs for equipment and operating personnel revolve upon this track and the inner one. The outer track is about 150 feet in diameter, the inner one about 40 feet and they were made level to .030 inch, which I think was quite a feat of mechanical engineering. This was done by one of the 500 sub-contractors on this job. The motion allows the horn to be rotated in azimuth and then the horn can also be rotated on its own long axis so that it can be changed in elevation. We can thus point at any spot in the sky.

Figure 9 is just a slightly different view from about the same spot and shows the small cab up above which has the equipment which needs to be right at the end of the horn.

Figure 10 shows the interior of the upper cab at the small end of the horn. This device here, although all you can see is a cabinet, is a very interesting one. It contains the Maser amplifier. It's main operating component is a piece of artificial ruby which is imursed in a bath of liquid helium. Thus it operates at a temperature almost absolute zero, actually about 4 degrees Kelvin. This allows signals to be effectively picked up and amplified which are about 30 db or 1 thousand times weaker than the weakest usable signal for ordinarly amplifiers.

Many of you know that low noise amplifiers like the Maser have turned out to be very valuable in radio astronomy.

A little digression along this line may be of interest. The only two spectrum lines from outer space which are readily observed on earth, in the microwave window, are hydrogen at 1.42 kilo-megacycles and the OH radical at 1.667 kmc. Hydrogen produces a pretty strong signal and it has been seen and measured for quite some time. Up to now, the OH radical has not been detected but some astronomers, I understand, believe it exists in our galaxy. It's energy level is so low that it is

not significant to communications because of the level of general background noise. One of our people though is looking into this as a sort of research project in astronomy using an improved, very sensitative radiometer receiver. We are now reasonably certain that the energy in this region due to OH is less than .1 degrees Kelvin if in fact it exists at all. It may not exist. At least we know it's less than .1 degree K.

The ground transmitter is also located in the upper cab. It's off back there where we can't see it. It uses a 2 KW traveling wave tube. The upper cab contains primarily the radio equipment which needs to be located near the end of the horn.

Figure 11 shows the equipment in the lower end cab which controls the pointing of the horn. Two methods are used to point. One involves using prediction information, and the other automatic tracking. Prediction information is sent over ordinarily telephone facilities to the control equipment and can then be used to point the horn. Once the horn has successfully picked up a satellite, however, a special radio receiver called a vernier autotrack starts observing the signals.

This receiver operates in a manner similar to monopulse radar. It picks up the signals in two different modes as they come in through the circular wave guide and compares these modes in amplitude and phase.

This tells whether the satellite is exactly in the center of the pattern and signals can be produced, which in effect tells what direction it is out. This is used to cause the horn to follow a satellite very precisely during the rest of the pass.

Any new satellite has to be found and tracked to determine its orbit very precisely. Figure 12 shows arrangements at a different location about ½ miles away to do this. They include a precision tracker at the left which is very much like a

Nike-Zeus radar and a coarse tracker at the right which operates down at the lower frequency around 130 kc. It's also used to send the commands and to receive telemetering information. The building in the center contains equipment to control the trackers and digest the information received.

Figure 13 is an overall view of the control room inside the control building. The equipment on the first row is used for observing the operation of the horn antenna and also for sending and receiving celemetering commands. The same equipment, could be used for quite a large number of satellites if they were in orbit.

You will notice that there are several television monitors in the second row and they are capable of monitoring either a standard picture or a picture of a different standard such as is used in Europe. However, we in the Bell System are not supplying the conversion devices. This would be the responsibility of the broadcasting companies if they are needed. Up to now the Europeans have been very kind and have been converting at their end.

A computer at the far end of the room digests the tracking information and gets it ready for actual use by the big horn.

Figure 14 shows how Telstar is put into the nosecone of a Thor-Delta rocket similiar to the one actually used for launching. As you know, we have had two of them launched and in each case, we had very fine cooperation from NASA and the other organizations but we paid 3 million dollars for each launch.

Figure 15 shows the Telstar 1 orbit. It is inclined about 45 degrees to the equator and is elliptical. At its lowest point it's about 593 miles and it's highest point 3500 miles above the earth.

Telstar 2 has a very similiar orbit but it ranges from 575 to about 6600 miles. Telstar 1 has a period of 2.6 hours and Telstar 2 has a period of 3.7 hours.

As mentioned in one of the earlier talks, such an orbit would not be desirable for commercial systems. It actually was desirable though for these experiments because this made the two satellites move in and out of some of the most intense portions of the Van Allen Belt and we were in this way able to get a lot of valuable data on radiation.

It's quite apparent that a usable commercial system would require a good many low level satellites and they ought to have higher orbits which should be circular, ideally.

As of right now, we believe that the best engineering compromise for a system that might be activated in the next few years is a height of around 6000 miles and it appears that about 25 satellites in such an orbit would give reasonably good service for Europe and the Orient.

Figure 16 illustrates a multiple satellite system using polar orbits. This type of system brings in another problem which has also been mentioned. It is necessary to switch from one satellite to the other, as the first one goes out of view and the next one becomes available. Incidentally, a commercial system we believe, should have some polar orbits and some inclined, about half and half.

Figure 17 illustrates this important operational problem. We would have to have several radomes and several antennas for a medium orbit system. Probably three as a minimum, to allow for maintance and occasional trouble. It would be necessary to be able to switch from one to the other very quickly so as not to disrupt service.

There is also another very important operational problem. Any one satellite will often be visible to many ground stations so it is necessary to somehow adequately assign their use to the different stations. This problem is both technical and administrative. It appears that one or more assignment centers would

be needed in the world to obtain and digest orbit information on a large number of satellites. A large computer would then work out the most efficient assignment taking into account traffic and all other problems. Of course, there also is a very big administrative and business problem in working out all the arrangements with the different nations and so on. This is one of the jobs the Satellite Corporation will be tackling.

Another unusual feature of a satellite is that after it's launched, it really becomes a part of nature, and to all practical purposes, is beyond the direct control of human beings. It can be used or misused by anyone on earth who has a technical capability of building ground equipment. Submarine cables are subject to physical damage but a satellite is subject to other types of difficulty. These questions, are broadly similiar to questions that we have had with us for many years, involving interferrance and allocation of frequencies and so on. They are being considered very seriously by the FCC and international bodies such as CCIR and CCITT.

Figure 18 is a simplified illustration of the 24-hour satellite system. It shows three satellites at just the right altitude of 22000 miles so that their period of rotation is the same as the rotation of the earth. If they are launched in an easterly direction and in an equitorial orbit, they seem to be fixed above a given spot on the equator.

Now, this system has some important advantages. It would allow us to get by with simplier ground antennas, since the tracking problem would be so much simplier. Fewer satellites would be needed because they would be visible over greater areas.

Theoretically, three would be enough to cover the whole earth but I would imagine that for practical systems you would almost certain need about six as insurance against failure. So it is apparent that this system has many attractive features.

We are actively studying it in comparisons to other systems. There are two disadvantages though that are rather important. One is the round trip delay which over one link of such a circuit is about 6/10th of a second. This is three times that of a lower orbit system and nearly five times that of a present day Hawaii - London connection, which is the longest that we ever get as of now.

The other problem is the technical problem of putting a satellite into such a high and precise orbit. Syncom has been put into orbit quite successfully and I think it is a very fine accomplishment and this makes it look as though this problem will be solved someday.

The delay has no effect on television relays but it does have important effects on telephone conversations.

Probably many of you know that this subject has been under intense study by a good many organizations in the last few years.

I would like to read a few excerpts from a draft recommendation which was put out July 3 of this year by the CCITT. "In June, 1962, Study Group 12 proposed to recommend as a maximum, allowable limit, a round trip propagation time between subscribers of 700 miliseconds in the absence of Echo or Echo supressors. Data submitted on the effects of propagation time alone shows some user dissatisfaction with delays of 600 miliseconds but study group 12 proposes to retain the 700 miliseconds limit for the Echo condition."

"Further experiments with Echo and several commercial and experimental Echo surpressors show a strong user reaction as delay is increased toward 700 miliseconds. Rejection rates by test subscribers as a function of delay are of serious concern in commercial telephany, and provide a strong incentive to minimize the delay in international connections."

"On the basis of these recommendations of study group 12 proposes to recommend the following limitations on round trip delay when Echo exists and present day types of Echo surpressors are used."

"Recommended delay limit 300 miliseconds. This limit should be met by substantially all telephone circuits on the major communications routes."

"Maximum delay limit 650 miliseconds. There will be some communications routes in the range of 4000 to 15000 miles where there are strong technical and economical reasons for exceeding the shorter limit."

"This maximum of 650 should be approached only in those cases where the only practical alternative to a longer delay is a circuit which cannot meet the CCITT standards of transmission. For example, HF radio."

We agree with these recommendations and in fact some of the data used in arriving at them came from tests made in our laboratories. We expect to publish the results of these tests before the end of this year.

It might be of interest at this point to consider the use of the medium orbit and 24-hour orbit system for data transmission. We have sent data of every speed from 75 bits per second up to 875 kilobits per second over Telstar. The tests indicated that a satellite in effect provides a very high grade broad band communication link. Thus it appears that this broad band facility can probably be best utilized in ways basically similiar to those used for present day ground facilities. The Telpak approach looks very promising.

The 24-hour system has of course, much less doppler shift but it will have a small residual doppler shift. We don't believe that the doppler shift is an important problem in either one, so that's about a tossup.

Figure 19 indicates how the time parameters of the medium orbit and 24-hour satellite orbit would translate into time dimensions for different data speeds. It's of interest that when transmitting high speed data a considerable number of data blocks are stored, in effect, in the satellite link. The slide shows that some blocks might either be lost or transmitted twice at typical switch from one medium orbit satellite to another.

Figure 20 illustrated how relatively large delay times might effect data transmission. I think the interesting point is what would happen if you have an error. I'm assuming that this data system like a great many of the commercial ones requires a check-back for every block that is sent and a block would be about 8000 bits. Thus in this illustration if there was an error in a block, the station at A would not know it until about 10 blocks later. In this kind of system, this should not be too difficult to handle, because we could number the blocks, by sending just a few extra bits along with each block. The blocks would be identified and so would the responses so if the block number five, for instance, was in error, as received at station B, response number five would indicate this, for station A and it could go back and start sending over again at block number five.

I think the interesting thing here is that it seems to turn out that this is almost a close-up too, between the 24-hour and the medium orbit. It will be necessary to have this response and retransmission anyway in a good many data systems because errors may occur for a variety of causes including the computers themselves sometimes, which require retransmission. This assumes it is the kind of computing problem where you can't just throw away poor data. So, this kind of arrangement would take care of interruptions for any cause, whether it was due to a switch from one satellite to another or something went wrong in a land line or human mistake or anything else.

It is true that the 24-hour satellite system would be a little bit slower on its feet than the medium orbit for data. This might be of importance in some computer problems. I am not enough of a computer man to know just how important this is. I have a feeling that in most problems it would be relatively minor.

So, summing up the comparison, it appears that both the medium orbit and the 24-hour orbit system have advantages and disadvantages. It may well turn out that the ultimate answer would be to have both systems.

One other interesting point in connection though, with a radom orbit multiple satellite system, is that there will be more than one satellite in view during quite a sizeable percentage of the time. For instance, we have found that if we consider a random orbit system to provide 99 percent reliability between here and Europe, there will be a second satellite visible about 90 percent of the time. It would seem that the requirements for TV might be very adequately handled by links which are available about 90 percent of the time.

I think it is also apparent that portions of frequency space in a satellite might be used for either pulse transmission or analog voice tranamission.

There seems to be no reason why different parts of the band could not be used for each through the same satellite. This is aimed at the well known problem of multiple access which is quite important, particularly if satellite systems are used, for communications with some of the lesser developed parts of the world. So, an approach broadly similar to Telpak could provide a flexiable arrangement to exploit either the voice or data capabilities of a given bandwidth through any satellite.

Our Telstar experiments have given preliminary answers to many crucial technical questions but Telstar, it seems to me, might be thought of as step one in this business. Perhaps it should share too with Relay. They are similar in many ways.

To me, though, the most outstanding feature of all the satellite work has been the cooperation between many, many industrial concerns, government agencies, and all sorts of organizations in other nations all over the world.

OVERSEAS TELEPHONE TRAFFIC

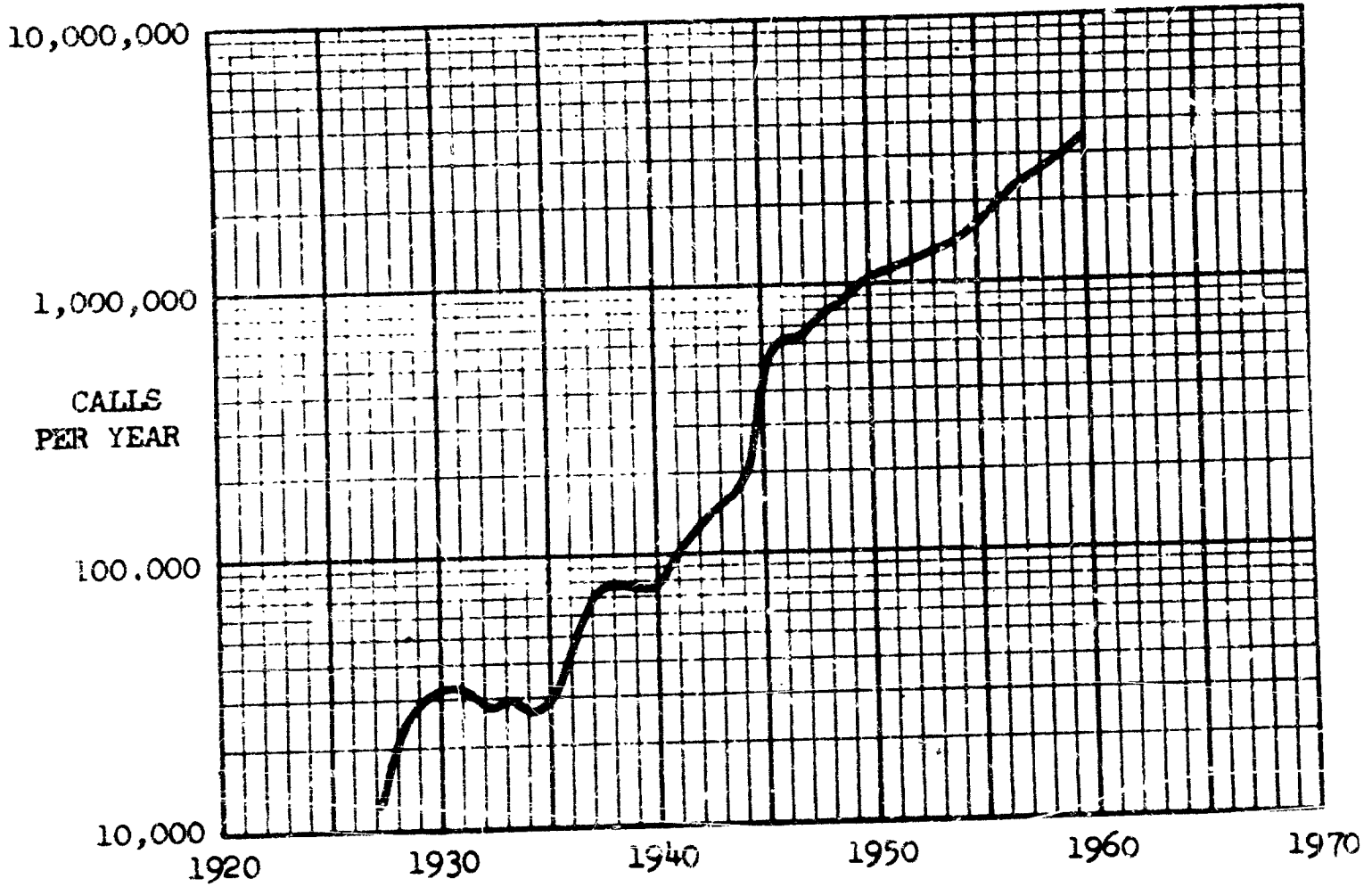

Figure 1

Figure 2

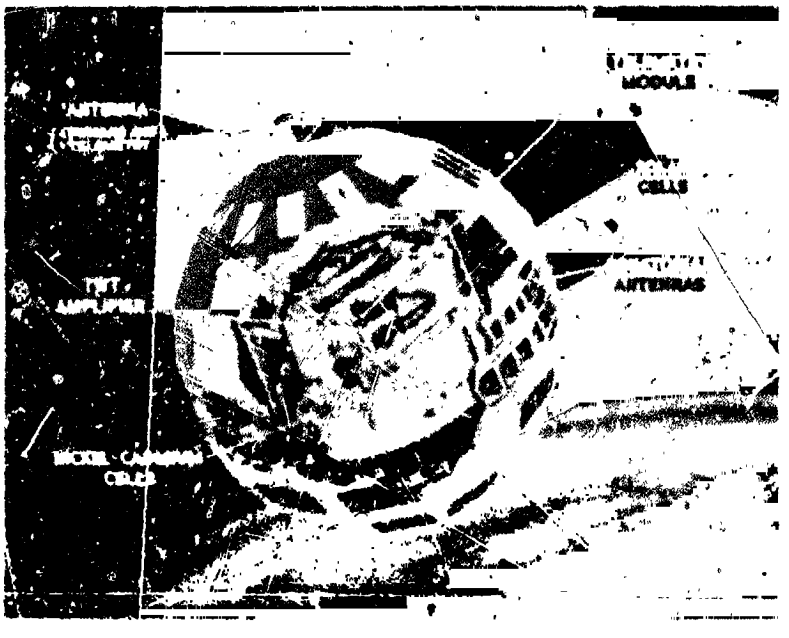

Figure 3

Figure 4

Figure 5

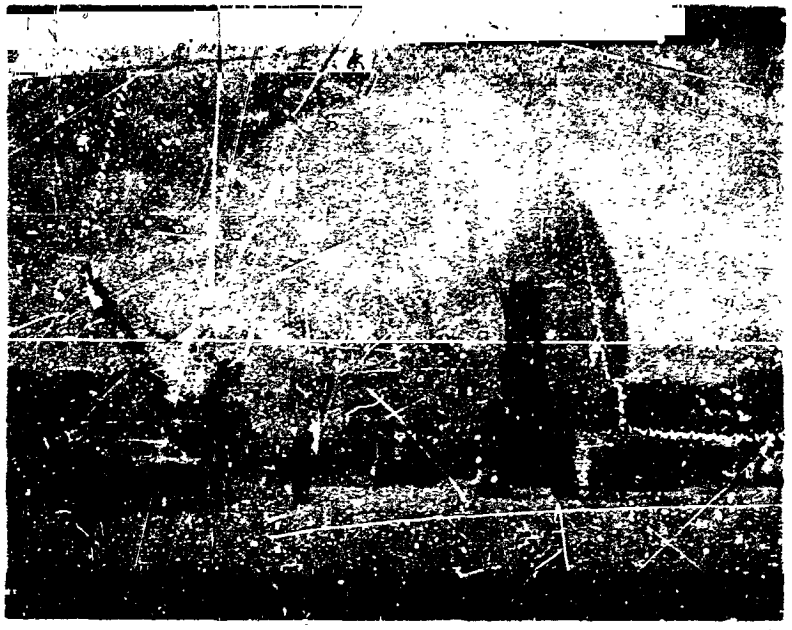

Figure 6

Figure 7

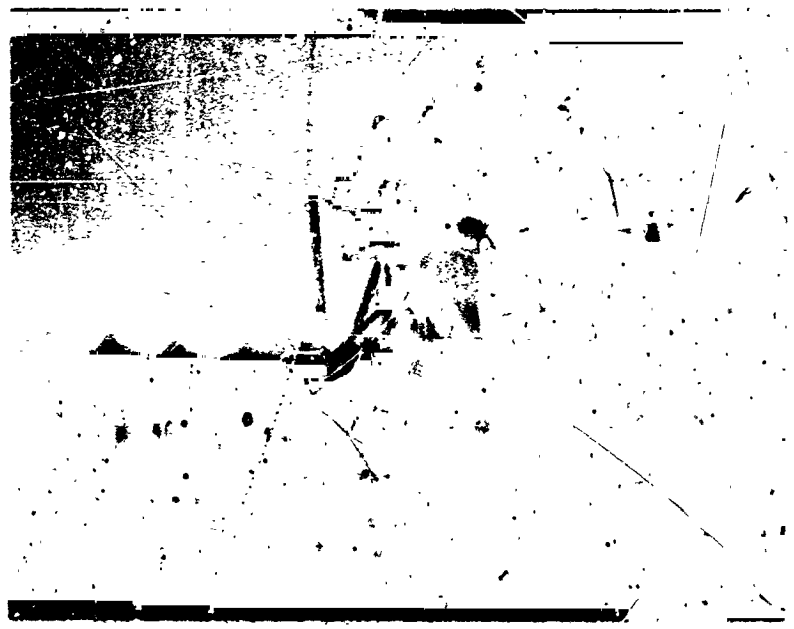

Figure 8

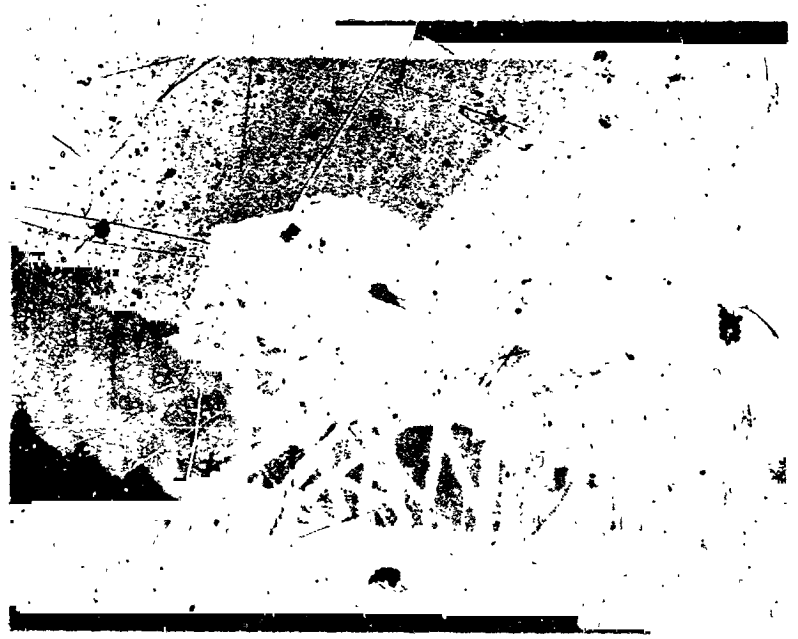

Figure 9

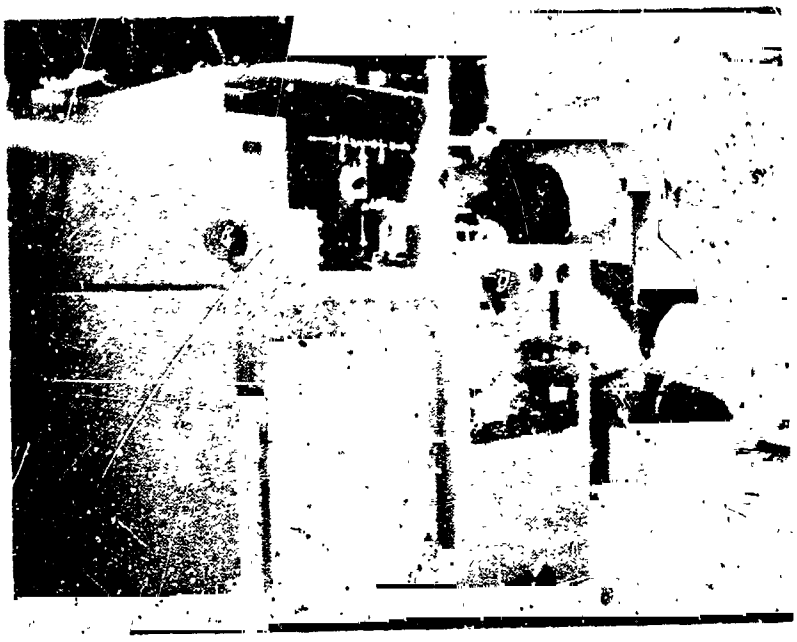

Figure 10

Figure 11

Figure 12

Figure 13

Figure 14

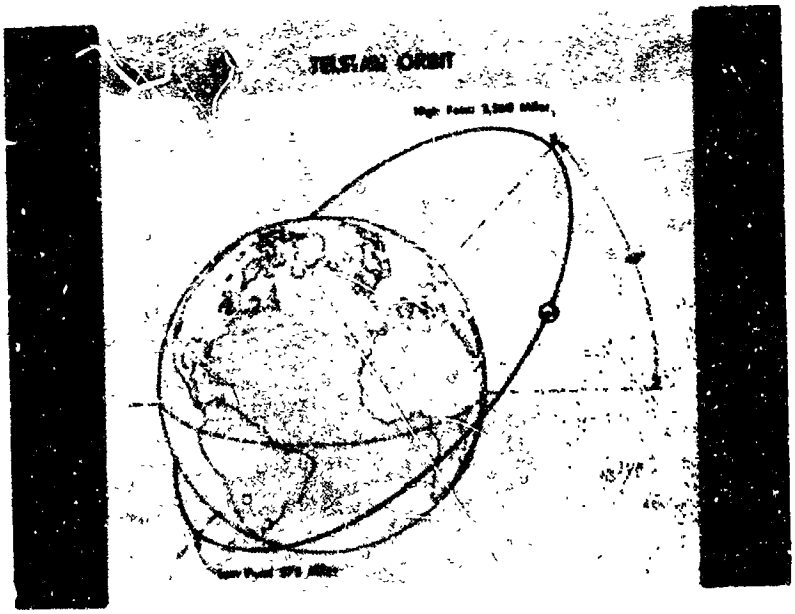

Figure 15

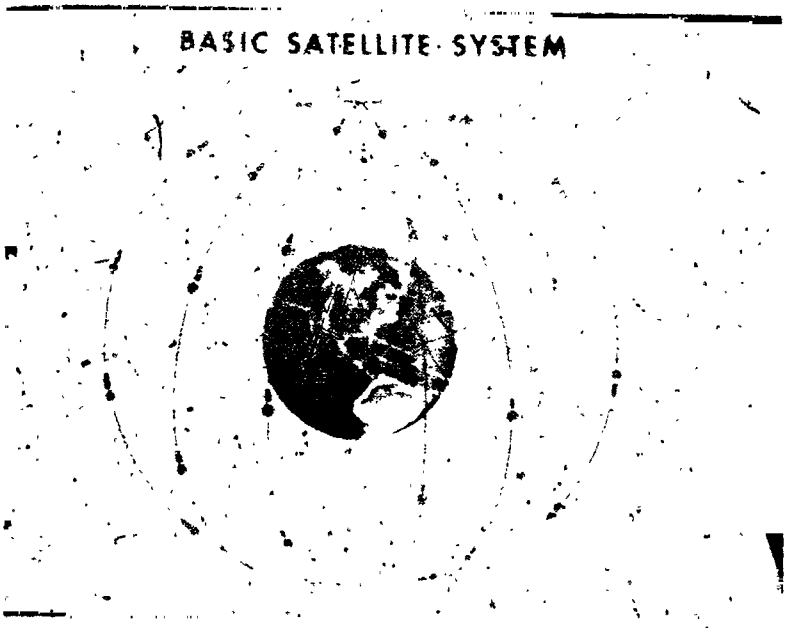

Figure 16

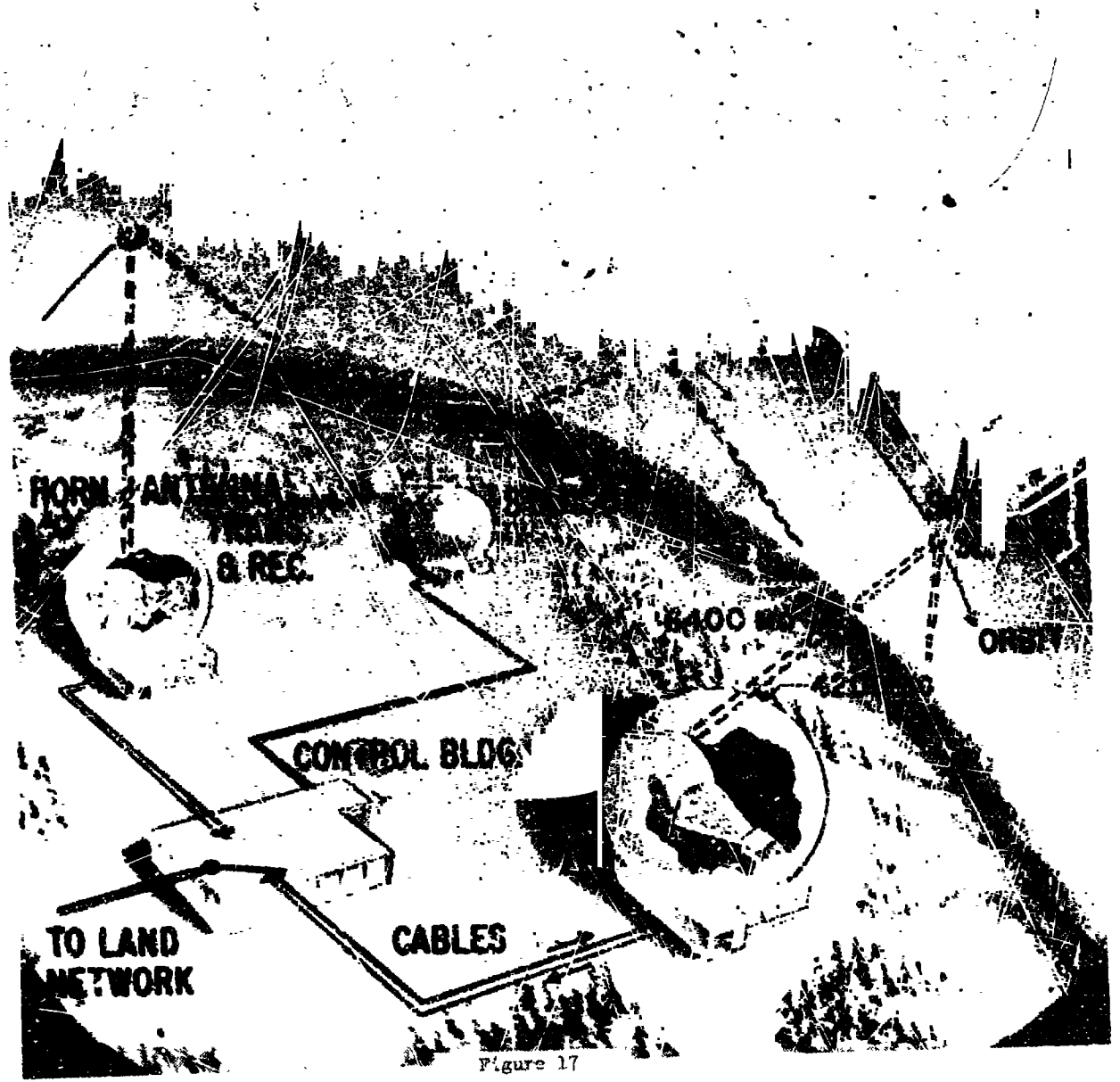

Figure 17

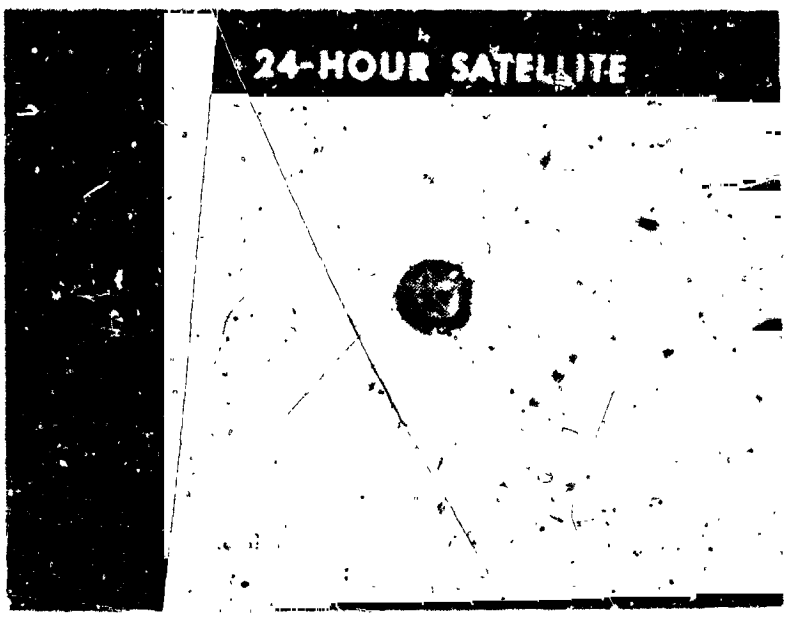

Figure 18

EFFECT OF TIME PARAMETERS
IN DIFFERENT SATELLITE SYSTEMS
ON DATA TRANSMISSION

DATA SYSTEM	MEDIUM ORBIT (95 MS DELAY)	24 HOUR ORBIT (270 MS DELAY)
200 BITS/SEC.		
BITS IN SPACE (ONE WAY)	19	54
2.4 KILOBITS/SEC.		
BITS IN SPACE (ONE WAY)	228	650
MAX. BITS PER SWITCH*	48	-
40.8 KILOBITS/SEC.		
BITS IN SPACE (ONE WAY)	3,880	11,000
BLOCKS IN SPACE (8 KILOBITS -196 MS)	0.48	1.38
MAX. BLOCKS PER SWITCH*	.1	-
875 KILOBITS/SEC.		
BITS IN SPACE (ONE WAY)	83,000	236,000
BLOCKS IN SPACE (8 KILOBITS - 9.1 MS)	10.4	29.5
MAX. BLOCKS PER SWITCH*	2.2	

* MAXIMUM NUMBER OF BITS OR BLOCKS LOST OR SENT TWICE DUE TO 20 MS DELAY JUMP.

Figure 10

SATELLITE SYSTEM USED FOR DATA COMMUNICATION

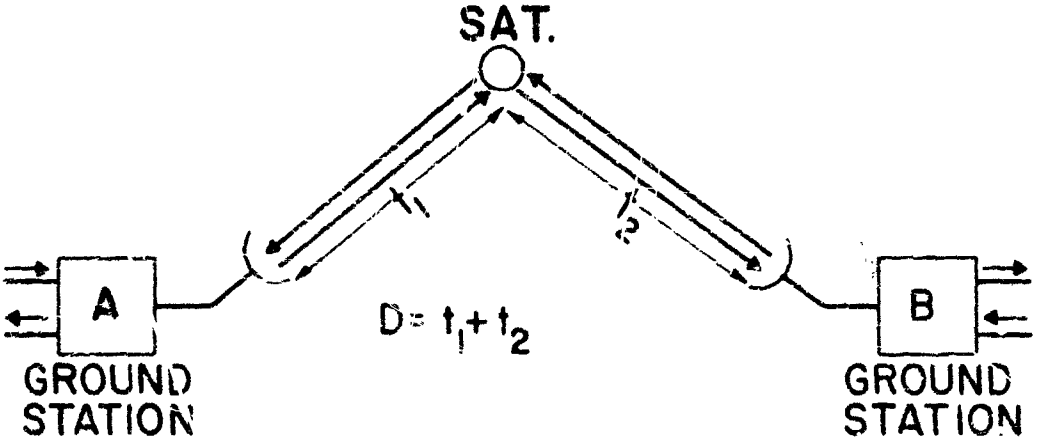

SYSTEM

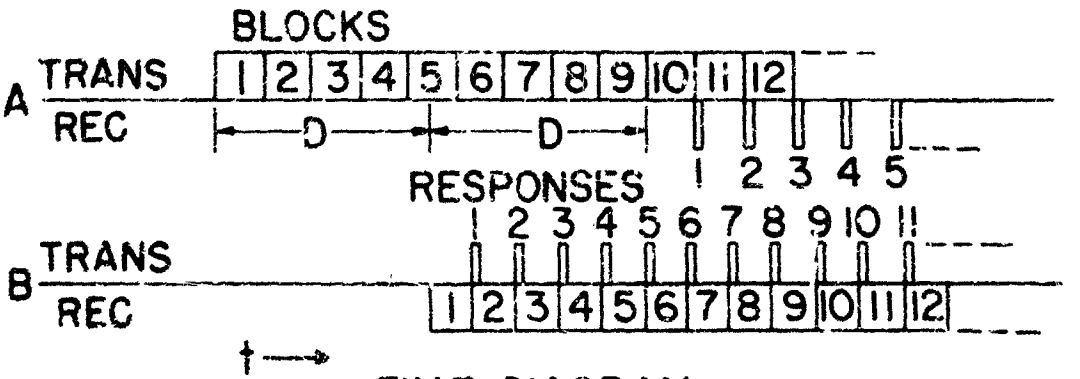

TIME DIAGRAM

TYPICAL BLOCK = 1000 CHARACTERS OF 8 BITS = 8000 BITS

Picture 20